Unit 2 Oscillation and Resonance

(a)

$\omega 0 = 6.283$ $\Gamma = 0.200$

As = 1.000   90°

Resonance Region

135°   Im R   45°

0.2

0.1

Re R

-0.2   -0.1   0.1   0.2

-0.1

-0.2

(b)

0.4

0.3 |R|

Re R

0.2   Im R

0.1

DC Response

-0.1

-0.2

Resonance Response

Resonance Region (FWHM)

$\omega\,(\text{radian/sec})$

5   10   *High* ω *Fall-Off*

0.5   1.5

$\nu\,(\text{Hertz})$ 2

Stimulus Frequency

Resonance Region (FWHM)

W. G. Harter

Oscillation, resonance and wave effects are among the most spectacular in mechanics and physics in general. They are also the keys to our ability to sense our environment and communicate with each other whether by voice, ears, and eyes or by artificial mechanical and electronic devices. It is the quality (in fact, the oscillator *quality* or *finesse* factor Q) of such devices that determines how well they amplify tiny signals and thus the quality of their physics.

Spectral Green's functions and Fourier amplitudes are the mathematical tools for resonance theory in both classical and quantum mechanics. Introduction to these are given along with classical-quantum analogies. This is an important part of physics for it appears that resonance and wave mechanics underlie all of physics and, indeed, our entire existence. So tune in!
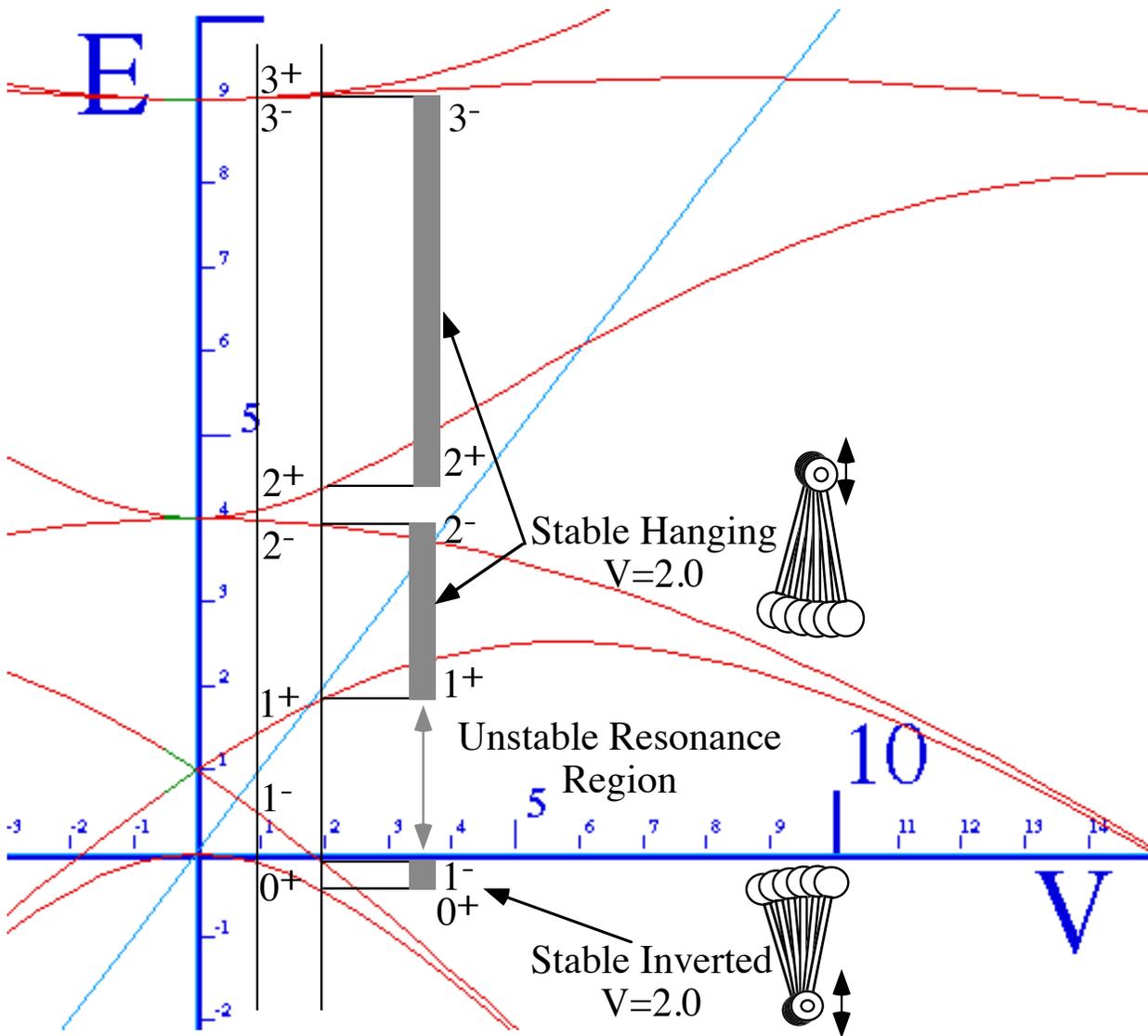
Stability bands of parametric resonance of pendulums
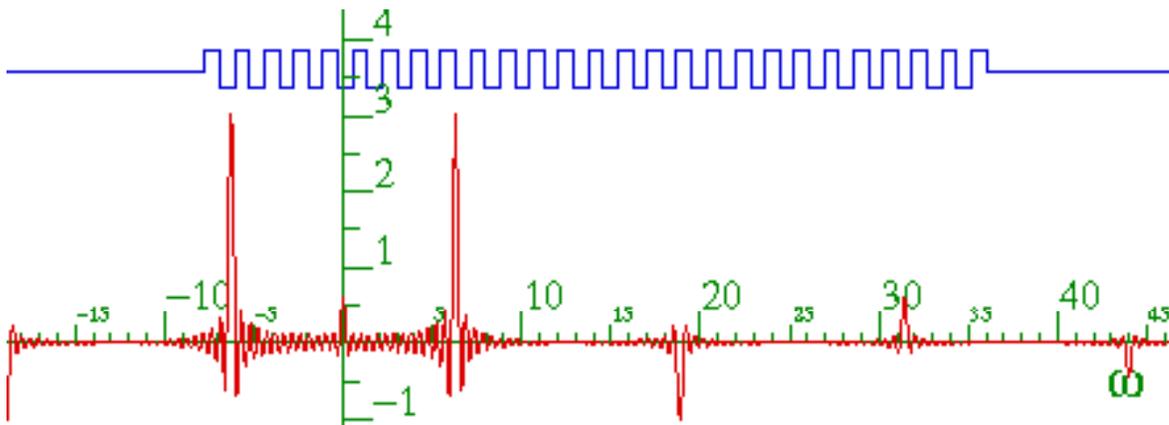
Sudden-cutoff-Fourier-transform of square-wave

-- The Purest Light and a Resonance Hero – Ken Evenson (1932-2002) --

When travelers punch up their GPS coordinates they owe a debt of gratitude to an under sung hero who, alongside his colleagues and students, often toiled 18 hour days deep inside a laser laboratory lit only by the purest light in the universe.

Ken was an "Indiana Jones" of modern physics. While he may never have been called "Montana Ken," such a name would describe a real life hero from Bozeman, Montana, whose extraordinary accomplishments in many ways surpass the fictional characters in cinematic thrillers like *Raiders of the Lost Arc*.

Indeed, there were some exciting real life moments shared by his wife Vera, one together with Ken in a canoe literally inches from the hundred-foot drop-off of Brazil's largest waterfall. But, such outdoor exploits, of which Ken had many, pale in the light of an in-the-lab brilliance and courage that profoundly enriched the world.

Ken is one of few researchers and perhaps the only physicist to be twice listed in the *Guinness Book of Records*. The listings are not for jungle exploits but for his lab's highest frequency measurement and for a speed of light determination that made c many times more precise due to his lab's pioneering work with John Hall in laser resonance and metrology[†].

The meter-kilogram-second (mks) system of units underwent a redefinition largely because of these efforts. Thereafter, the speed of light c was set to $299,792,458 ms^{-1}$. The meter was defined in terms of c, instead of the other way around since his time precision had so far trumped that for distance. Without such resonance precision, the Global Positioning System (GPS), the first large-scale wave space-time coordinate system, would not be possible.

Ken's courage and persistence at the Time and Frequency Division of the Boulder Laboratories in the National Bureau of Standards (now the National Institute of Standards and Technology or NIST) are legendary as are his railings against boneheaded administrators who seemed bent on thwarting his best efforts. Undaunted, Ken's lab painstakingly exploited the resonance properties of metal-insulator diodes, and succeeded in literally counting the waves of near-infrared radiation and eventually visible light itself.

Those who knew Ken miss him terribly. But, his indelible legacy resonates today as ultra-precise atomic and molecular wave and pulse quantum optics continue to advance and provide heretofore unimaginable capability. Our quality of life depends on their metrology through the Quality and Finesse of the resonant oscillators that are the heartbeats of our technology.

Before being taken by Lou Gehrig's disease, Ken began ultra-precise laser spectroscopy of unusual molecules such as HO_2, the radical cousin of the more common H_2O. Like Ken, such radical molecules affect us as much or more than better known ones. But also like Ken, they toil in obscurity, illuminated only by the purest light in the universe.

In 2005 the Nobel Prize in physics was awarded to Glauber, Hall, and Hensch[††] for laser optics and metrology.

† K. M. Evenson, J.S. Wells, F.R. Peterson, B.L. Danielson, G.W. Day, R.L. Barger and J.L. Hall,
Phys. Rev. Letters 29, 1346(1972).
†† *The Nobel Prize in Physics, 2005*. http://nobelprize.org/
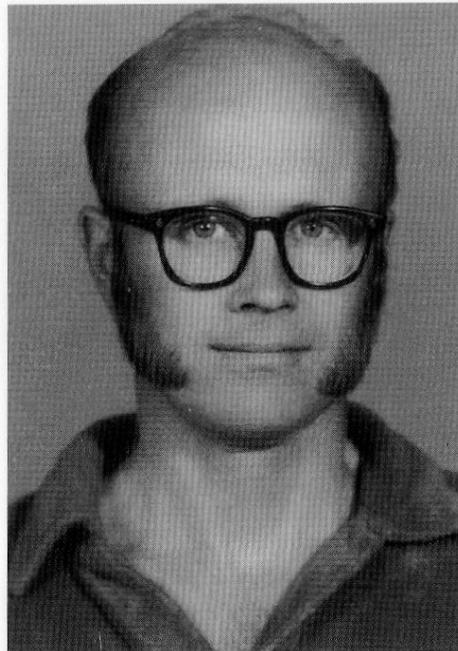
PAULINIA, BRASIL 1976

THE *SPEED OF LIGHT IS*
299,792,458 *METERS PER SECOND!*

Kenneth M. Evenson – 1932-2002

Unit 2. Oscillation and Resonance

Chapter 2.1 Introduction

We begin our development of modern physics with *resonance*, a most important phenomenon or process. One could make the case that resonance is the single most important process in all of physics; without it we are deaf, dumb, blind, and have no telephone, radio, television or computers. Resonant amplification is needed to see or hear, and ever since the invention of the telegraph, our communication technology, power grid and electronics have all needed it, too.

Use of resonance for communication is an obvious classical application, but as introduced in Chapters 4-5, our quantum world lives and breathes resonance for its very existence. Apparently, oscillation is the currency of the universe and resonance is how nature's business is done. Without a good understanding of oscillation, resonance and waves, one should not expect to understand physics deeply if at all.

Much of this book deals with relations and analogies between the older classical mechanics and the newer and more fundamental quantum theory of matter. An important part of this connection begins with a deeper understanding of resonance and resonant transfer of energy. We will introduce some key figures of merit for oscillators such as *quality (Q) factors* and *uncertainty* that also have deep significance in the development of quantum theory. We will also see how the quantum equations of motion (Schrodinger wave equations) are mathematically identical (analogous) to classical Hamiltonian oscillator equations, and how this helps us to appreciate both a little better.

Modern applications of resonance require enormous quality factors; lately *Q* values of millions and billions are possible. As we will see, high quality and low uncertainty are inexorably connected. Without extremely high *Q* there can be no lasers, precision clocks, global positioning system (GPS), or high-speed computers. Indeed, it seems to be the case that the very quality of life for a modern civilization is strongly related to the quality *Q* of the oscillators in its technology.

Two main types of resonance will be discussed. The first and most common classical type is the *linear* or *additive* resonance such as might occur if an oscillating electric **E**-field is applied to a cyclotron orbit . An example of a free linear driven oscillator equation is the following that will be treated first.

$$\ddot{x} + \omega_0^2 x = E_s \cos(\omega_s t) . \tag{2.1.1}$$

In fact, this gives what is known as *cyclotron resonance*. The second type of resonance is known variously as a *nonlinear* or *multiplicative resonance* such as would occur if an oscillating magnetic **B**-field is applied to a cyclotron orbit. It is also called *parametric resonance* because the frequency parameter or spring constant $k=m\omega^2$ is being stimulated. An example of a parametric resonance equation is below where its k-parameter oscillates.

$$\ddot{x} + \left(A + B\cos(\omega_s t) \right) x = 0 \tag{2.1.2}$$

The (2.1.2) form is the one by which resonance occurs in quantum mechanics at the deepest level. However, the (2.1.1) form provides a convenient approximation for much of Nature. So, that is where we will begin.

Chapter 2.2 Linear oscillator response relations

Linear forced-damped-harmonic oscillator satisfy the following classical equation of motion.

$$\frac{d^2 z}{dt^2} + 2\Gamma \frac{dz}{dt} + \omega_0^2 z = a \qquad (2.2.1)$$

Here $a = a(t)$ is an acceleration caused by a stimulating force $F(t) = ma(t)$ (Often $F(t)$ is due to an electric field $E(t): F(t) = eE(t)$.) Coordinate $z = z(t)$ is the response coordinate or amplitude of a particle of mass m and charge e held by a harmonic (linear) restoring force:

$$F_{\text{restore}} = -kz, \quad \left(k = \omega_0^2 m \right), \qquad (2.2.2a)$$

We define the *natural angular frequency* of the oscillator in units of (radian)- Hertz $= s^{-1}$.

$$\omega_0 = \sqrt{\frac{k}{m}} = 2\pi\nu_0 \qquad (2.2.2b)$$

Also included is a "friction" term of the form of a linear damping force:

$$F_{\text{damping}} = -b\frac{dz}{dt}, \quad \left(b = 2\Gamma m \right) \qquad (2.2.3a)$$

Here the *decay constant* is

$$\Gamma = \frac{b}{2m} \qquad (2.2.3b)$$

where b is the frictional damping coefficient.

(a) Complex phasor solutions

For zero stimulus ($a = 0$) one obtains a particular solution to (2.2.1) by letting z be a *complex exponential phasor function*

$$z(t) = z(0)e^{-i\omega t} \qquad (2.2.4a)$$

Euler-DeMoivre's polar-to-Cartesian expansion: $re^{i\phi} = r\cos\phi + i\, r\sin\phi$ expands as follows.

$$
\begin{aligned}
z(t) &= z(0)e^{-i\omega t} \\
&= (A + iB)(\cos\omega t - i\sin\omega t) , \quad \text{where: } A = \text{Re}\, z(0), \text{ and: } B = \text{Im}\, z(0) \qquad (2.2.4b) \\
&= (A\cos\omega t + B\sin\omega t) + i(-A\sin\omega t + B\cos\omega t)
\end{aligned}
$$

Note: either the real or the imaginary part of the complex solution undergo undamped ($\Gamma=0$) oscillator motion introduced in Unit 1 Ch. 8. (Fig. 8.8 thru 8.11.) Two Euler forms of the initial value ($z(0) = re^{i\alpha} = r\cos\alpha + ir\sin\alpha$) let us conveniently derive two forms for the solution in the case of near-zero damping ($\Gamma=0$).

$$
\begin{aligned}
x(t) = \text{Re}\, z(t) &= \text{Re}\left(re^{i\alpha} e^{-i\omega_0 t} \right) \\
&= (r\cos\alpha \,\cos\omega_0 t + r\sin\alpha \,\sin\omega_0 t)
\end{aligned} \qquad (2.2.5a)
$$

$$
\begin{aligned}
x(t) = \text{Re}\, z(t) &= \text{Re}\left(re^{i\alpha - i\omega_0 t} \right) \\
&= r\cos(\omega_0 t - \alpha)
\end{aligned} \qquad (2.2.5a)
$$

Complex arithmetic gives "automatic trig-identities" and is one way it aids analysis of oscillatory phenomena. Also, as noted in Ch. 10 of Unit 1, complex *phasors* provide an oscillator phase space in which real and imaginary parts are proportional to position and momentum (or velocity). A sketch of a phasor diagram is shown in Fig. 2.2.1. Phasor-pairs track 2D oscillator orbits in Ch. 8 of Unit 1 and will do so in Ch. 2.3 of this Unit 2.
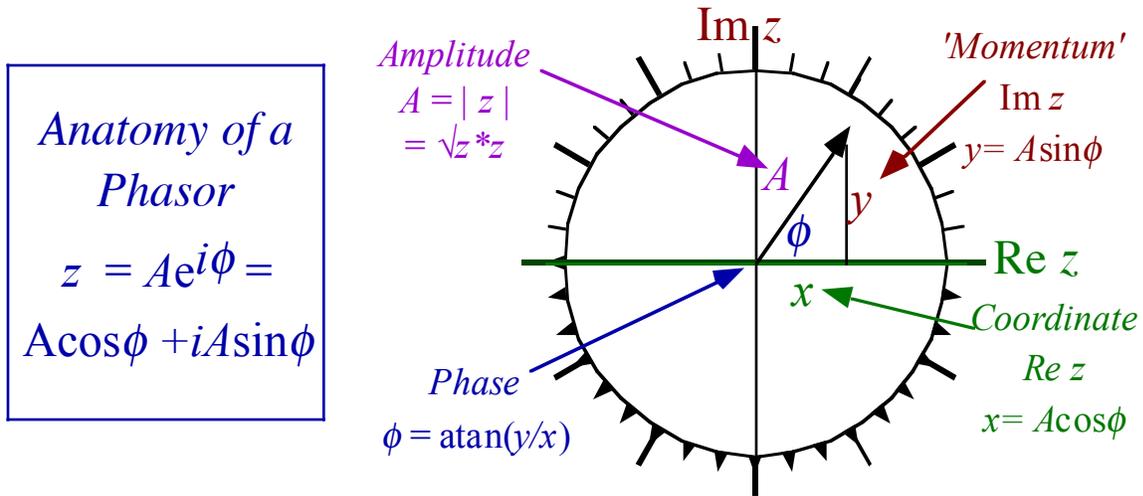
Fig. 2.2.1 Anatomy of a Phasor $z=x+iy=Ae^{i\phi} = A\cos\phi + i\,A\sin\phi$

The oscillator coordinate *x(t)* is the real part of the phasor.

$$x(t) = \text{Re}(Ae^{-i(\omega t-\alpha)}) \; = A\cos(\omega t-\alpha) \qquad\qquad (2.2.6)$$

Choosing a <u>negative</u> imaginary exponential time dependence $e^{-i\omega t}$ makes a phasor rotate <u>clock</u>wise. Also, it makes the imaginary part have the <u>same</u> sign as the instantaneous velocity or momentum since the imaginary part of $e^{-i\omega t}$ is *-sin ω t* with the same sign as the derivative of *cos ω t*.

$$v(t) = \omega\,\text{Im}(Ae^{-i(\omega t-\alpha)}) \; = -\omega A\sin(\omega t-\alpha) \qquad\qquad (2.2.7)$$

So the phasor space is a phase-space with the momentum rescaled by ω so its orbit is circular instead of elliptical. Phasors orbit clockwise just as IHO phase vectors do. Engineers, on the other hand, prefer $e^{+i\omega t}$ phasors with positive or <u>counter</u> clockwise rotation. Perhaps it is right that physicist's phasor turn clockwise since physicists are truly the world's timekeepers. Their legacy ranges from Galileo and Huygens thru the modern ultra precise work begun by Evenson, Hall, and others at the NIST Time and Frequency division.

      An example of a phasor with time plot is in Fig. 2.2.2. The real and imaginary parts are each rotated by 90° so the real part matches the coordinate plot on the right-hand side of the figure. At the instant shown z-coordinate is positive and velocity is negative, corresponding to an instantaneous phase angle of ϕ = -30°.

      Modern calculators have $\boxed{P \leftrightarrow R}$ buttons for converting between polar and rectangular (Cartesian) coordinates. This is aimed mainly at converting between polar form (2.2.4a) and Cartesian form (2.2.4b) or (2.2.6) and (2.2.7). We need to be cognizant of pitfalls in the inverse $R \rightarrow P$ conversion that requires an inverse tangent or arctangent. Let us recommend functions *atan2(y,x)* be used instead of horrible *atan(y/x)* functions. The former, like $\boxed{P \leftrightarrow R}$, always put the angle in the right quadrant. The latter only gets it right sometimes!
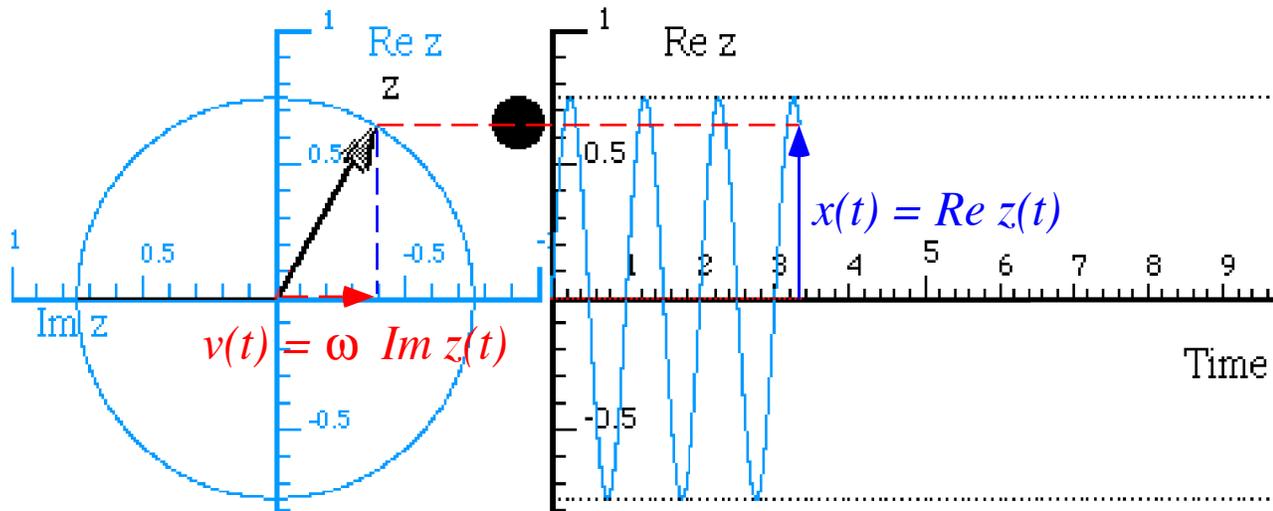
Fig. 2.2.2 Phasor z and corresponding coordinate versus time plot for $\omega_0=2\pi$ and $\Gamma=0$

The oscillator above is a one-Hertz ($v_0=1/s.$ or: $\omega_0 = 2\pi = 6.2832\,rad/s.$) oscillator.

(b) Transient or decaying solutions

The complex phasor $e^{-i\omega \cdot t}$ works for damped oscillation, too. Substituting $e^{-i\omega \cdot t}$ into (2.2.1) gives a quadratic equation for ω . The solutions are complex roots $\omega_\pm$.

$$-\omega^2 - 2i\Gamma\omega + \omega_0^2 = 0, \quad \omega_\pm = -i\Gamma \pm \sqrt{\omega_0^2 - \Gamma^2} \tag{2.28}$$

We choose ω_+ the first root so phase $e^{-i\omega t}$ moves clockwise, as explained before. The resulting $z(t)$ is called a complex *transient solution*, and the real part of this solution is the position $x(t)$.

$$z_{\text{transient}}(t) = z(0)e^{-\Gamma t}e^{-i\omega_\Gamma t} \tag{2.2.9}$$

It oscillates at an angular frequency ω_Γ reduced slightly by .05% from ω_0 due to damping $\Gamma=0.2$.

$$\omega_\Gamma = \sqrt{\omega_0^2 - \Gamma^2} = \omega_0 - \tfrac{1}{2}(\Gamma^2/\omega_0) + ... = 6.2831853 - 0.003183 + .. = 6.280002 + ... = 6.280001 \tag{2.2.10}$$

More important is exponential decay of amplitude $|z(t)|$ by about 95% per time interval $t_{5\%}=15$ sec.

$$t_{5\%} = \frac{3}{\Gamma} = \frac{3}{0.2} = 15 \qquad (2.2.11a) \qquad\qquad t_{4.321\%} = \frac{\pi}{\Gamma} = \frac{\pi}{0.2} = 15.708 \qquad (2.2.11b)$$

An easy-to-recall *5%* approximation is $e^{-3} \cong 0.05$. A more precise one is $e^{-\pi} \cong 0.04321$.

A phase graph and *t*-plot of stimulus-free damped oscillator decay is given in Fig. 2.2.3 with $\omega_0 = 2\pi$ and $\Gamma = 0.2$. This corresponds to a damped one-Hertz (or $\omega_0 = 2\pi = 6.2832\,rad/s.$) oscillator. A damping of $\Gamma=0.2$ reduces its natural frequency only by about 0.05% to 0.9995Hz. Fig. 2.2.3 would need a longer time, about 200 seconds, to magnify such a tiny frequency lag so it could be visible on such a graph. Also, a huge amplitude scale factor, about e^{20}, would be needed to lift the decayed wave off the *z=0* axis.

Instead of *decay rates* we prefer to think of *lifetimes*. For rough estimates we use e^{-3}=5% lifetimes. In precise calculations, use $e^{-\pi}$ = 2.321% lifetime or $\frac{\pi}{\Gamma}$ = 15.708 seconds in (2.2.11b).
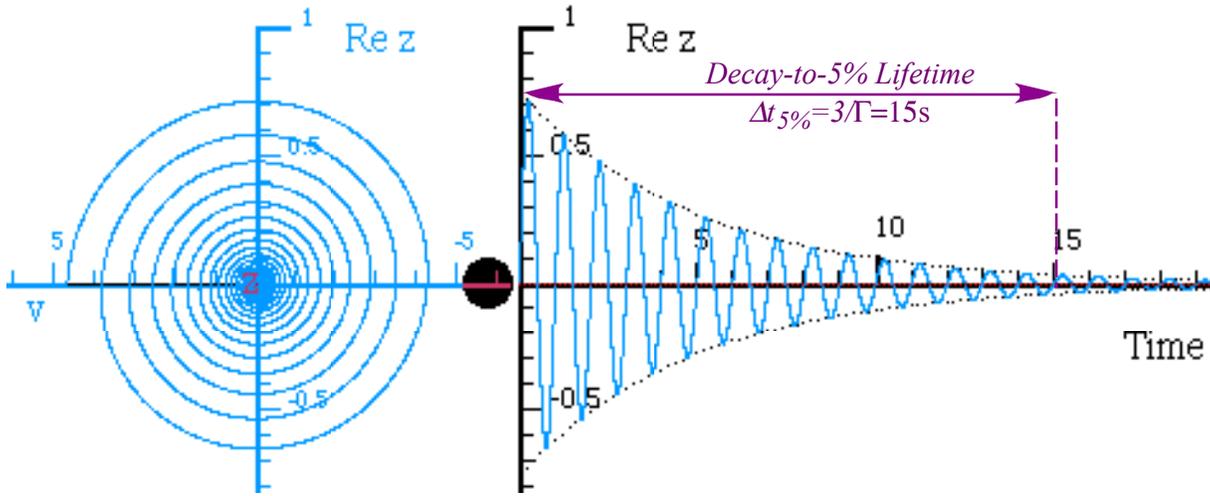
Fig. 2.2.3 Phasor z and corresponding coordinate versus time plot for ω_0=2π *and* Γ=0.2

(c) Lorentz-Green stimulated response function

The complex phasor $e^{-i\omega t}$ is particularly useful for describing resonance or stimulated oscillation. Consider a *monochromatic* (single frequency ω_s) stimulus

$$a(t) = a(0)e^{-i\omega_s t} .\qquad(2.2.12)$$

We postulate a response of the same frequency whose amplitude is proportional to the stimulus.

$$z_{\text{response}}(t) = G_{\omega_0}(\omega_s) a(t)\qquad(2.2.13)$$

The proportionality factor G is supposed to depend upon the stimulus frequency ω_s, the natural frequency ω_0, and damping constant Γ, only. Because the equation is linear and time independent the G-factor should not depend on the amplitude A_s of the stimulus. It may help to think of the oscillator as a 'black box' that responds linearly to input as shown below in Fig. 2.2.4.
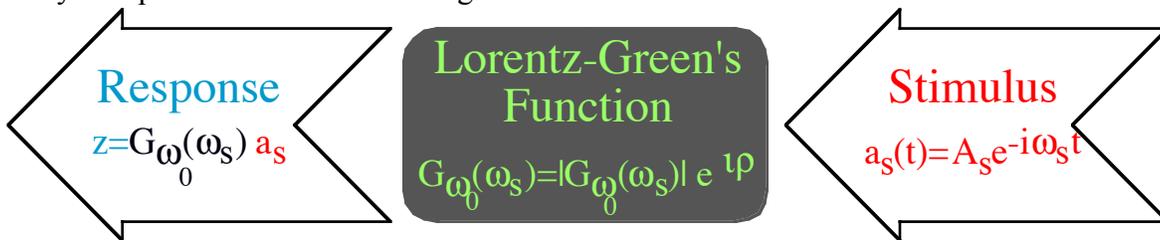
Fig. 2.2.4 Black-box diagram of oscillator response to monochromatic stimulus

Now we substitute z_{response} into the equation of motion (2.2.1) and solve for $G_{\omega_0}(\omega_s)$. The resulting G_{ω_0} is called a complex *Lorentzian response function* or *classical Green's function* of the stimulus frequency ω_s.

$$G_{\omega_0}(\omega_s) = \frac{1}{\omega_0^2 - \omega_s^2 - i2\Gamma\omega_s} = \text{Re}\, G_{\omega_0}(\omega_s) + i\,\text{Im}\, G_{\omega_0}(\omega_s) = \left|G_{\omega_0}(\omega_s)\right|e^{i\rho}\qquad(2.2.14)$$

The Lorentz-Green's function G is a constant amplitude for fixed stimulating frequency ω_s and natural ω_0, so z_{response} is called the *steady-state* stimulated response. The real and imaginary parts of the Green's function are the two parts of the following *Cartesian form* of the Green's function G.

$$\operatorname{Re}G_{\omega_0}(\omega_s)=\frac{\omega_0^2-\omega_s^2}{\left(\omega_0^2-\omega_s^2\right)^2+\left(2\Gamma\omega_s\right)^2} \quad (2.2.15a) \qquad \operatorname{Im}G_{\omega_0}(\omega_s)=\frac{2\Gamma\omega_s}{\left(\omega_0^2-\omega_s^2\right)^2+\left(2\Gamma\omega_s\right)^2} \quad (2.2.15b)$$

Then the magnitude $\left|G_{\omega_0}(\omega_s)\right|$ and polar angle ρ of the *polar form* of G are the following:

$$\left|G_{\omega_0}(\omega_s)\right|=\frac{1}{\sqrt{\left(\omega_0^2-\omega_s^2\right)^2+\left(2\Gamma\omega_s\right)^2}} \quad (2.2.15c) \qquad \rho=\tan^{-1}\left(\frac{\left(2\Gamma\omega_s\right)}{\omega_0^2-\omega_s^2}\right) \quad (2.2.15)\ \text{The}$$

angle ρ is the response *phase lag,* that is, the phase angle by which the response oscillation lags behind the phase $\left(-\omega_s t\right)$ of the stimulating oscillation.

$$z_{\text{response}}(t)=\left|G_{\omega_0}(\omega_s)\right|a(0)e^{-i\left(\omega_s t-\rho\right)} \tag{2.2.15}$$

It may help to visualize stimulus and response phasors as a pair rigidly rotating at rate ω_s. The response phasor lags ρ radians behind the stimulus as shown below in Fig. 2.2.5.
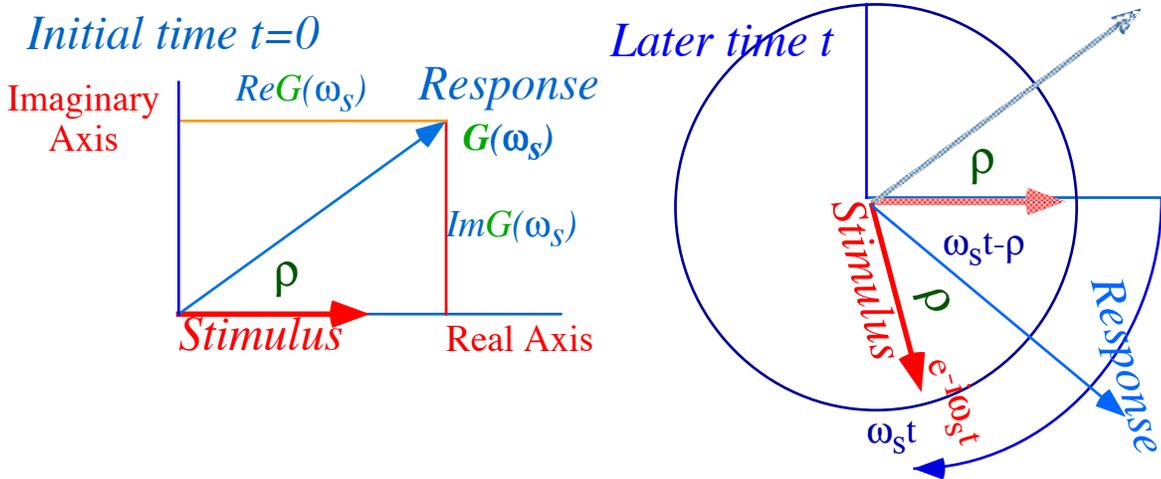
Fig. 2.2.5 Oscillator response and stimulus phasors rotate rigidly at angular rate ω_s.

The real and imaginary parts of G determine the phase lag angle ρ according to (2.2.15d). This angle is a sensitive indicator of the amount of power being delivered during resonance as discussed below.

(d) Lorentzian or Green's function properties

Views of the Lorentz Green's function (2.2.15) are shown in Fig. 2.2.6 for a 1 Hz oscillator with natural angular frequency $\omega_0=2\pi=6.283(\text{radian})/s$ and decay constant $\Gamma=0.2/s$. A complex $G(\omega_s)$ phasor is plotted $\operatorname{Re}G$ vs. $\operatorname{Im}G$ in Fig. 2.2.6a for a range $(0<\omega_s<13)$ of stimulus angular frequency (or $0<\nu_s<2$ Hz of standard frequency). In Fig. 2.2.6b the response R= $G(\omega_s)a_S$ due to three G-function parts $\operatorname{Re}G(\omega_s)$ (blue), $\operatorname{Im}G(\omega_s)$ (green), and $|G(\omega_s)|$ (gray dots) are plotted for the same range.
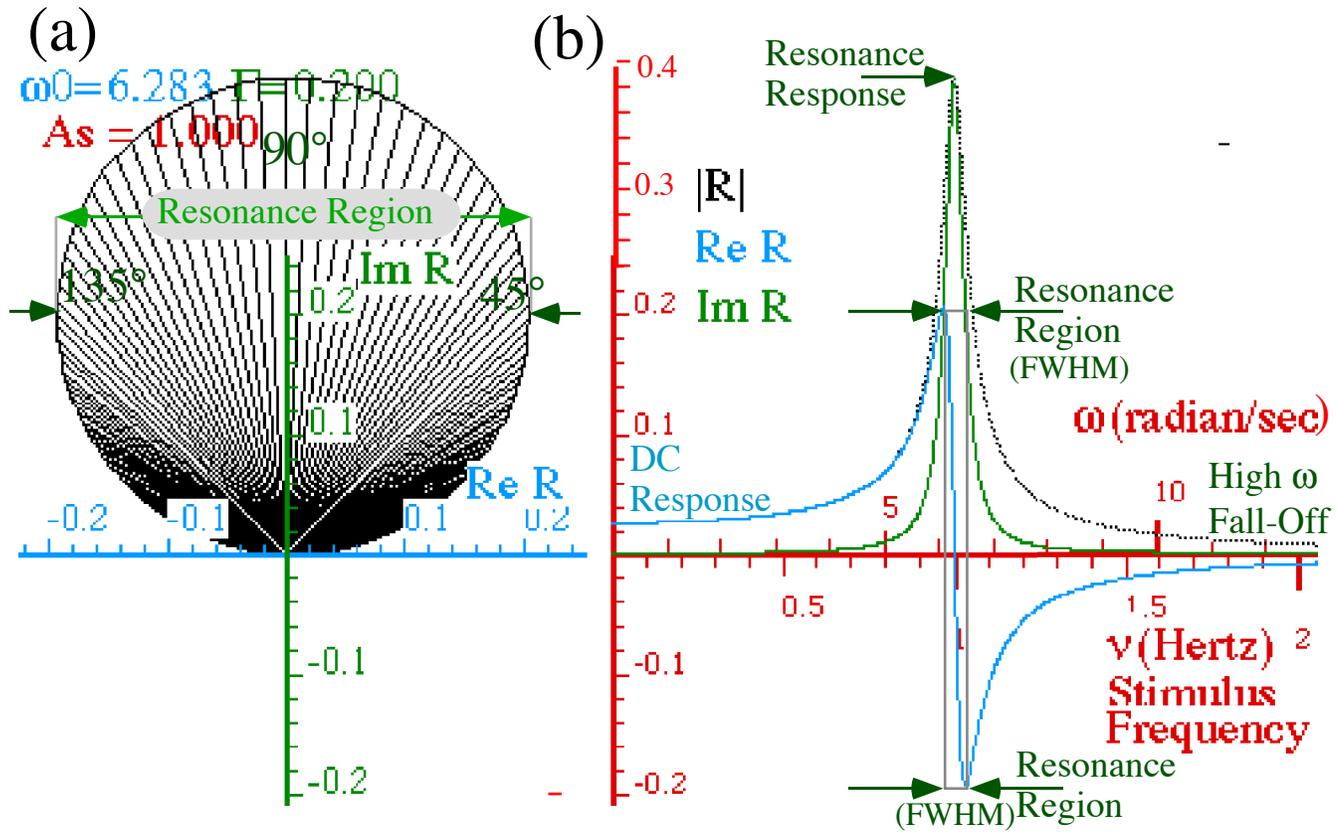
Fig. 2.2.6 Anatomy of oscillator Green-Lorentz response function plots

     The anatomy (mathematical and physical properties) of this function and related terminology are very important for the understanding resonance dynamics. They are presented here in a way that should help you remember key principles. This goes along with Exercises 2.2.3 to 2.2.5.

     The response magnitude $|G(\omega_s)|$ is a dotted curve enveloping the others in Fig. 2.2.6b. It starts at $\omega_s = 0$ small and fairly flat ($\omega_s \ll \omega_0$ is called the *DC response* region.) and peaks near *resonance point* $\omega_s = \omega_0$ and falls to zero for $\omega_s \gg \omega_0$ (*high frequency fall-off*). Real part Re$G(\omega_s)$ dominates in the DC region. Re$G(\omega_s)$ reaches a peak just shy of where it intersects the rising imaginary part Im$G(\omega_s)$. Im$G(\omega_0)$ achieves its peak value near *resonance point* $\omega_s = \omega_0$ where Re$G(\omega_0)=0$ in the center of the *resonance region* between two *Full Width at Half-Maximum* (FWHM) points $\omega_s^{\mathbf{FWHM}}(\pm)=\omega_0\pm\Gamma$ shown in Fig. 2.2.7. These $\omega_s^{\mathbf{FWHM}}(\pm)$ points are near ones that give max or min Re$G(\omega_s)$, half-max Im$G(\omega_s)$, and half-max $|G(\omega_s)|$.

     The ratio of the resonant response $|G(\omega_0)|$ to the DC-response $|G(0)|$ is a very important number. From (2.2.15) we calculate the following (See Exercises 2.2.4 to 2.2.5.).

$$AAF = \frac{\text{Resonant response}}{\text{DC response}} = \frac{\left|G_{\omega_0}(\omega_0)\right|}{\left|G_{\omega_0}(0)\right|} = \frac{1/(2\Gamma\omega_0)}{1/\omega_0^2} = \frac{\omega_0}{2\Gamma} \equiv q \qquad (2.2.16)$$

This ratio is about 15 in Fig. 2.2.7a and 30 in Fig. 2.2.7b. We will call this ratio the *amplitude amplification factor* (AAF) or *angular quality (q) factor* of an oscillator. A *Standard Quality Factor Q=υ₀/2Γ=q/2π* is more commonly known[1] just as standard frequency $\upsilon=\omega/2\pi$ is more common than angular frequancy$\omega=2\pi\upsilon$.
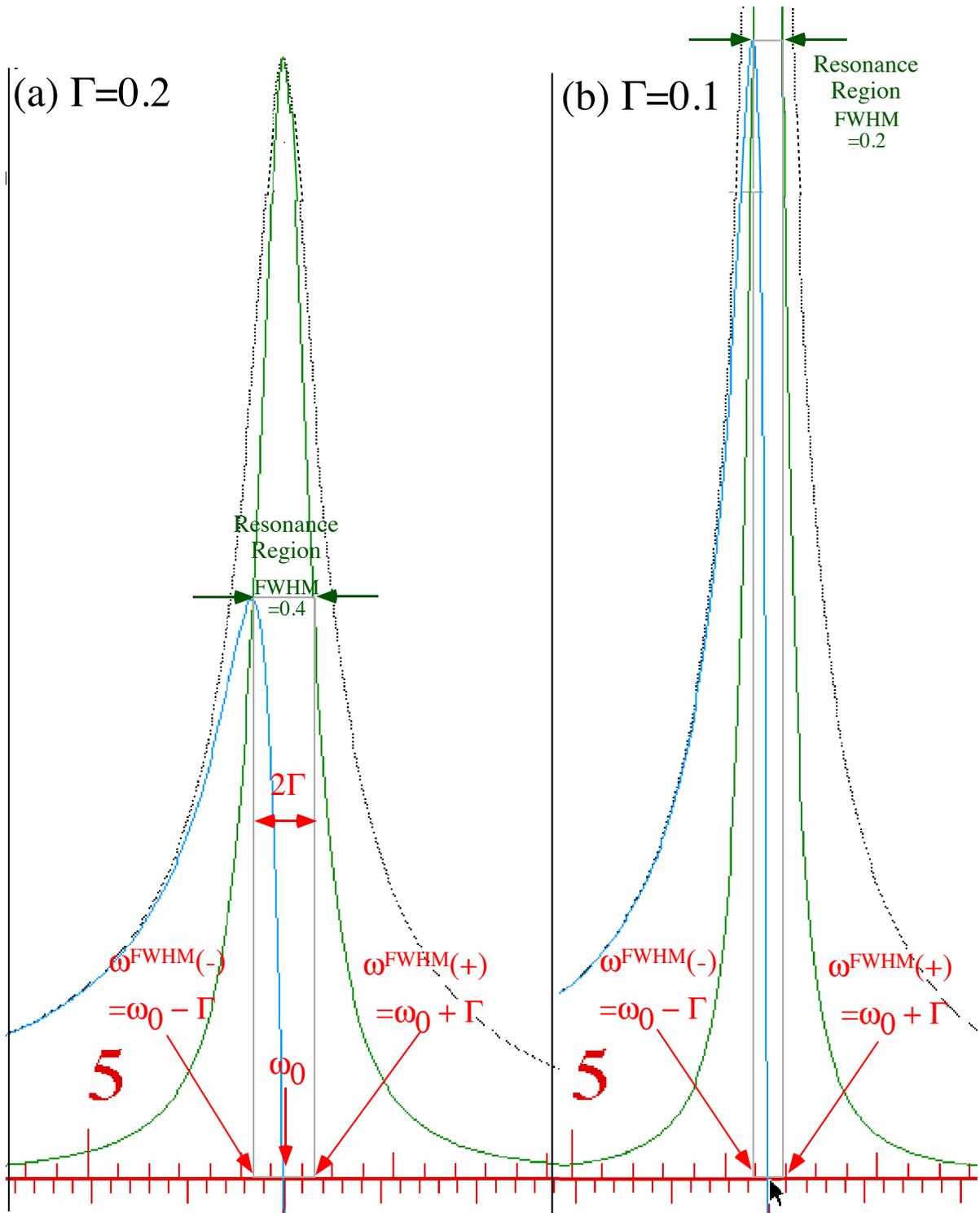
Fig. 2.2.7 Comparing Lorentz-Green resonance region for (a) Γ=0.2 and (b) Γ=0.1. Maximum and minimum points of ReG(ω) *and inflection points of* ImG(ω) *are near region boundaries* $ω^{FWHM}(\pm)=ω_0\pm\Gamma$.

High values for these numbers Q, q, or AAF are good for us as humans in order that we see or hear the tiny optical or acoustical signals. The graphs for $q=15$ and $q=30$ in Fig. 2.2.7 look like impressive peaks or monuments. However, the q of a typical atom or laser resonator is much greater, in fact, <u>millions</u> of times higher and sharper. They are what has given modern physics its sharp teeth!

Resonance peaks are characterized by their width as well as their height. *The Full Width at Half-Maximum* (FWHM) is the stimulus frequency range within which the response is at least 50% of its maximum (resonant) value of $1/(2\Gamma\omega_0)$. At the boundaries of this range the first term $(\omega_0^2 - \omega_s^2)^2$ in the denominator of (2.2.15a-b) equals the second denominator term $(2\Gamma\omega_s)^2$.

$$\left|\left(\omega_0^2 - \omega_s^2\right)\right| = 2\Gamma\omega_s \qquad \text{(For: } \omega_s = \omega_s^{\textbf{FWHM}}(\pm)) \qquad\qquad (2.2.17)$$

If detuning difference $\Delta = \omega_s - \omega_0$ is much less than ω_0 or ω_s we may use a *near-resonant approximation*.

$$\omega_0^2 - \omega_s^2 = (\omega_0 - \omega_s)(\omega_0 + \omega_s)$$
$$\cong (\omega_0 - \omega_s)2\omega_0 \cong (\omega_0 - \omega_s)2\omega_s, \quad \text{for: } \omega_0 \approx \omega_s \qquad\qquad (2.2.18)$$

Then (2.2.17) gives FWHM boundaries at approximately the frequencies $\omega_s^{\textbf{FWHM}}(\pm)$.

$$\omega_s^{\textbf{FWHM}}(\pm) = \omega_0 \pm \Gamma \qquad\qquad (2.2.19a)$$
$$\omega_s^{\textbf{FWHM}}(+) - \omega_s^{\textbf{FWHM}}(-) = 2\Gamma \qquad\qquad (2.2.19b)$$

The FWHM resonance region is seen to have a width of 2Γ that is 0.4 in Fig. 2.2.7a, and centered on ω_0. At $\omega_s^{\textbf{FWHM}}(\pm)$ response $|G(\omega_s)|$ is about 50% of its maximum and its real part (2.2.15a) equals plus-or-minus its imaginary part (2.2.15b). (See Fig. 2.2.6 or Fig. 2.2.7.)

$$\text{Re}\,G_{\omega_0}(\omega_s) \cong \mp \text{Im}\,G_{\omega_0}(\omega_s), \quad (\text{for } \omega_s = \omega_s^{\textbf{FWHM}}(\pm)) \qquad\qquad (2.2.20)$$

So, at the low end $\omega_{(-)}^{\textbf{FWHM}}$ of the resonant region, the phase lag ρ (2.2.10e) is approximately $45°$ (or $\pi/4$), but is $135°$ (or $3\pi/4$) at the high end $\omega_{(+)}^{\textbf{FWHM}}$. (where $\text{Re}G(\omega_s)$ is plotted versus $\text{Im}G(\omega_s)$ in Fig. 2.2.6a.)

$$\rho\left(\omega_s^{\textbf{FWHM}}(\pm)\right) \cong \rho(\omega_0) \pm \pi/4 = \begin{cases} 3\pi/4 & \text{for: } \omega_s = \omega_0 + \Gamma \\ \pi/4 & \text{for: } \omega_s = \omega_0 - \Gamma \end{cases} \qquad\qquad (2.2.21)$$

At exactly the resonance point ($\omega_s = \omega_0$) phase lag is *exactly* $90°$ (or $\pi/2$) by (2.215d).

$$\rho(\omega_0) = \pi/2 \quad (\text{for: } \omega_s = \omega_0) \qquad\qquad (2.2.22)$$

The real part $\text{Re}\,G(\omega_s)$ of Green's function is nearly maximum at the FWHM boundary $\omega_s^{\text{FWHM}}(+)$ and nearly minimum at $\omega_s^{\text{FWHM}}(-)$, as seen in Fig. 2.2.7. The resonant value $\omega_s = \omega_0$ gives exactly zero for $\text{Re}\,G(\omega_s)$ and nearly a maximum for $\text{Im}\,G(\omega_s)$. (See Exercises 2.2.6-7 to compute exact values.)

(e) Oscillator figures of merit: quality factors Q and q=2πQ

To summarize; if an oscillator of a given natural frequency ω_0 has a smaller Γ (or greater q), then it will have greater response to a resonant ($\omega_s = \omega_0$) stimulus. (Recall: $q = \omega_0/2\Gamma$ is the amplification factor (2.2.12).) On the other hand, the resonant width (2Γ) in (2.2.15b) divided by ω_0, i.e., the inverse of q, is the relative error that a stimulus frequency may have and still resonate. So, if you double an oscillator's amplification capability, you will halve its tolerance for frequency error. Larger peak height means proportionally smaller peak width. Compare Fig. 2.2.7a with Fig. 2.2.7b.

Other important quantities are related to q. One is the number of oscillations in the 5% decay time (2.2.10). Natural oscillation frequency (2.2.9) is approximately (for $\Gamma << \omega_0$) $\upsilon_0 = \omega_0 / 2\pi$. Multiplying by $t_{5\%}$ gives a number $n_{5\%}$ of oscillations in a lifetime that decaying oscillator loses 95% of its amplitude.

$$n_{5\%} = \frac{\omega_0}{2\pi} t_{5\%} = \frac{\omega_0 3}{2\pi\Gamma} \cong \frac{\omega_0}{2\Gamma} = q \qquad (2.2.23)$$

For example, it takes about $q = 15$ oscillations to decay to 5% in Fig. 2.2.3. (Here we approximate $\pi = 3$. Better, we use $t_{4.321\%}$ from (2.2.11)). So, angular quality q approximates the number of "heartbeats" in the life of an oscillator. It is interesting to compare q, for your own life expectancy, to that of atoms and molecules.

The most commonly used figure of oscillator merit is the *standard energy quality factor* Q which is defined as the ratio of an oscillator's instantaneous energy content to energy lost each cycle. Since energy is proportional to the square of oscillator amplitude it will decay according to $\left(e^{\Gamma t}\right)^2 = e^{-2\Gamma t}$ i.e., at a rate of 2Γ times the instantaneous energy content. (See Exercise 2.2.8)

$$dE = -2\Gamma E \ .$$

So the relative energy lost during each cycle period $(\tau_0 = 1/\upsilon_0)$ is:

$$\tau_0 \left(\frac{-dE}{E} \right) = \frac{2\Gamma}{\upsilon_0} \equiv 1/Q \ . \qquad (2.2.24)$$

The AAF quantity q was called the *angular* quality factor since *1/q* is the relative loss *(dE/E)* per *radian* of phase while *1/Q* is the relative loss per *cycle* of oscillation

(f) Beats and lifetimes

The quality factor q, decay constant Γ, and lifetime $t_{5\%}$ apply as well to the birth of a resonance as they do to free oscillation decay. Suppose at $t = 0$ a stimulus of constant angular frequency ω_s and constant amplitude $a(0)$ is applied to a 'cold' oscillator $(z(0) = 0)$. Then the sum of two solutions (2.2.8) and (2.2.15) describes the subsequent motion *z(t)*. (Verify!)

$$z(t) = z_{\text{transient}}(t) + z_{\text{response}}(t) \equiv z_{\text{decaying}}(t) + z_{\text{steady state}}(t)$$

$$= Ae^{-\Gamma t}e^{-i\omega_\Gamma t} + G_{\omega_0}(\omega_s)a(0)e^{-i\omega_s t} \qquad (2.2.25a)$$

$$= Ae^{-\Gamma t}e^{-i\omega_\Gamma t} + \left|G_{\omega_0}(\omega_s)\right|a(0)e^{-i(\omega_s t - \rho)} \qquad (2.2.25b)$$

The initial condition $(z(0) = 0)$ demands that the complex transient amplitude A be given by:

$$A = -\left|G_{\omega_0}(\omega_s)\right|a(0)e^{i\rho} \quad (\text{for } z(0) = 0) \qquad (2.2.25c)$$

so A cancels the stimulated response at *t=0*. Then as time progresses, the *transient amplitude* $z_{\text{transient}}(t)$ dies at rate Γ and the solution eventually grows up to the *steady state* $z_{\text{response}}(t)$, alone. An example with a resonant stimulus ($\omega_s = \omega_0 = 2\pi$) is shown below in Fig. 2.2.8.
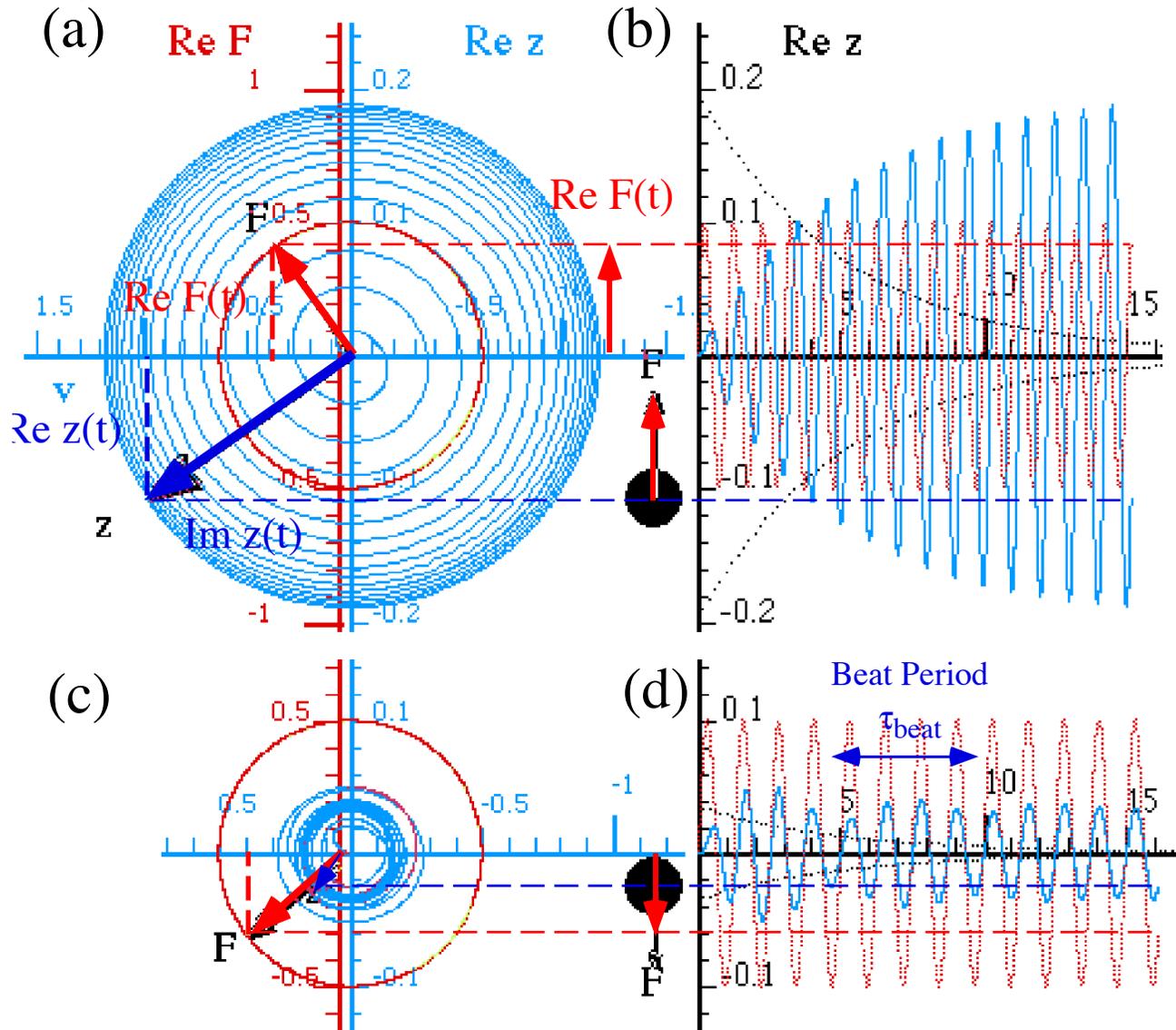
Fig. 2.2.8 On Resonance   *(a)Response z-phasor lags* $\rho=90°$ *behind stimulus F-phasor.*

($\omega_s=\omega_0=2\pi$ and $\Gamma=0.2$).   *(b) Time plots of* Re *z(t) and* Re *F(t)*

Fig. 2.2.8 Below Resonance   *(c)Response z-phasor lags* $\rho=8.05°$ *behind stimulus F-phasor.*

($\omega_s=5.03,\omega_0=2\pi$,$\Gamma=0.2$).   *(d) Time plots of* Re *z(t) and* Re *F(t). Beats are barely visible.*

    The length of time it takes $z(t)$ to approach the steady state oscillation $z_{\text{response}}(t)$ is the same as the time it takes the transient part to die. So, after the 5% lifetime, the solution is mostly, i.e., 95%, steady state response. In Fig. 2.2.8b the transient dies after about $t=15$sec. or about 15 oscillations. The angular quality factor $q=15$ gives the number of oscillations needed for the transient to decay to less than 5% and establish 95% of a

resonance. The outline trace of the hidden transient is shown in Fig. 2.2.8a. It is the same as the outline of the plot in Fig. 2.2.3.

Note that each response oscillation is one-quarter period to the right of its stimulating oscillation in Fig. 2.2.8b, in other words, it *lags* by a quarter period. This is shown more clearly by the phasor diagram in Fig. 2.2.8a where the *z* phasor is behind the stimulus $F = a(0)e^{-i\omega_s t}$ by 90° ($\rho = \pi/2$). This is consistent with (2.2.22). Since the real part of the response vanishes at resonance (Re$G(\omega_0)=0$), the response at $\omega_{s=}\omega_0$ is exactly pure imaginary ($\left|G_{\omega_0}(\omega_0)\right| = \mathrm{Im}\, G_{\omega_0}(\omega_0)$).

A stimulus frequency below resonance causes transient oscillatory *beat modulation*. In Fig. 2.2.8c-d the angular frequency ($\omega_s = 5.026$) of stimulus and steady state response is less than that of the transient ($\omega_\Gamma \cong \omega_0 = 2\pi = 6.28..$). So, the transient phasor $z_{transient}$ turns faster than response phasor $z_{ss\text{-}response}$ by $\omega_0 - \omega_s = 1.25$ radian/s , and it will "2π-lap" the slower phasor every 1.25/(2π) seconds. This lap rate is called the *beat frequency* $\upsilon_{beat}=\omega_{beat}/2\pi$.

$$\upsilon_{\mathrm{beat}} = \left|\upsilon_s - \upsilon_0\right| = \left|\omega_s - \omega_0\right|/(2\pi) = 0.199\, s^{-1} \qquad (2.2.26)$$

The corresponding *beat period* $\tau_{beat} =1/\upsilon_{beat}$ is

$$\tau_{\mathrm{beat}} = 1/\left|\upsilon_s - \upsilon_0\right| = 2\pi/\left|\omega_s - \omega_0\right| = 5.01s \qquad (2.2.27)$$

A beat period of about 5 sec. is seen in Fig. 2.2.8d. Beats are only visible before the transient decays below about 5%. Then the poor *z(t)* phasor has lost 95% of its faster transient part and can no longer "lap" the stimulus *F*-phasor. It is left with only the steady-state response part of (2.2.25a) and forced to "settle down" and lag dutifully at angle ρ behind the all-powerful stimulating *F*-phasor.

In its "younger days" the transient phasor $z_{transient}$ is big enough that the phasor sum *z(t)= $z_{transient}$ + $z_{ss\text{-}response}$* swells up as $z_{transient}$ passes the stimulus F-phasor and $z_{ss\text{-}response}$ but then *z(t)* shrinks as $z_{transient}$ goes on to be opposite $z_{ss\text{-}response}$ and make a node. The interference sum *z(t)* experiences a beat every time $z_{transient}$ laps $z_{ss\ response}$, as shown in Fig. 2.2.10 below.

However, note how much smaller the transient phasor has become just in the time it takes to make a beat. It is "aging" at rate Γ while the steady-state response-phasor $z_{ss\text{-}response}$ is just stuck ρ behind its stimulus *F*-phasor according to *$z_{ss}=G{\cdot}F_{stimulus}$*. Soon *z(t)* falls into *$z_{ss\ response}$* to stay as long as *F_s* lasts.
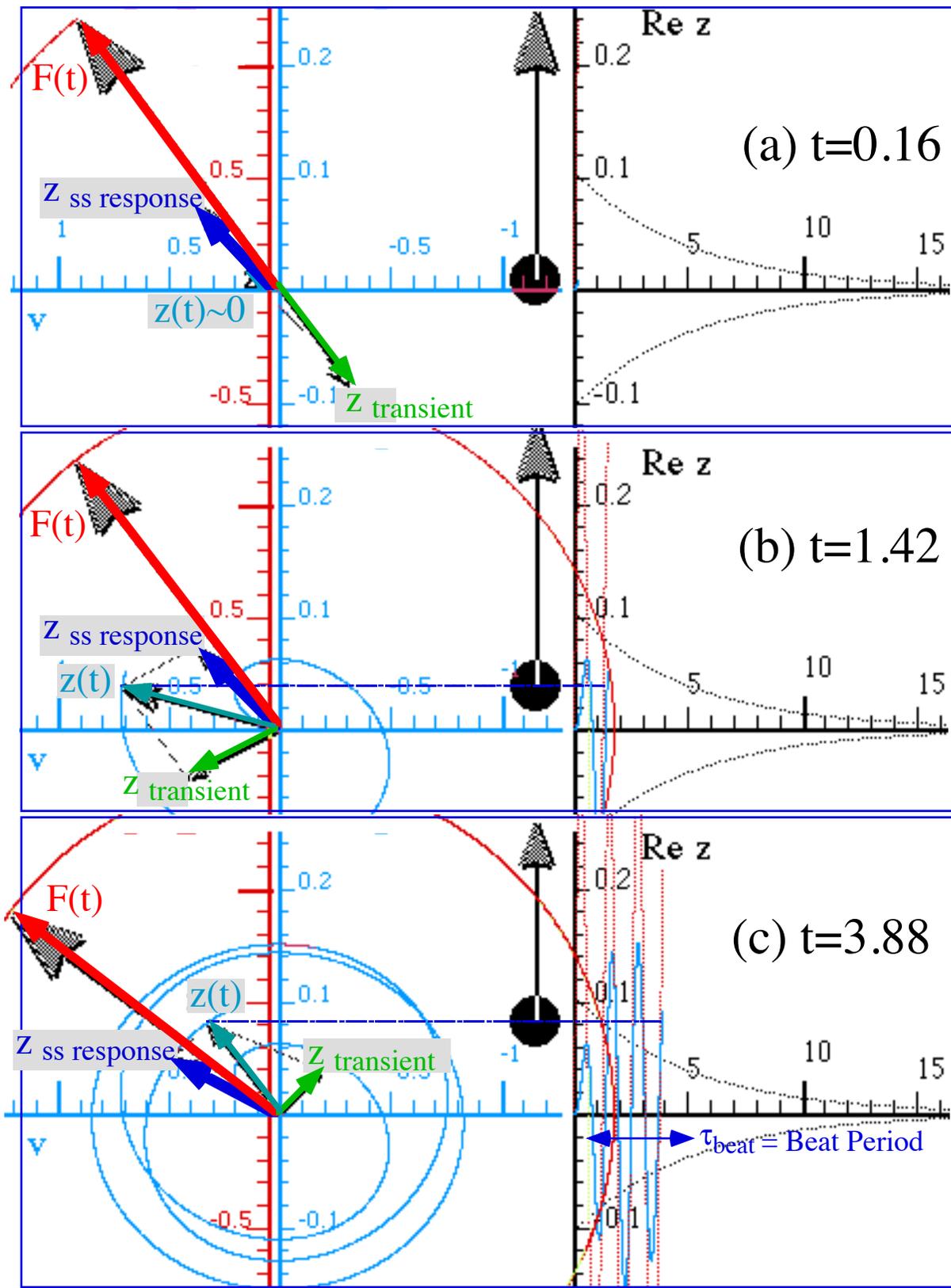
Fig. 2.2.9 Beat formation. Transient phasor $z_{transient}$ catches up with F-phasor and passes it.

By counting the number of beats per second one directly measures the magnitude of the relative *detuning* $v_s - v_0 = \Delta$, but not the sign of Δ. The following example in Fig. 2.2.10 has the stimulus faster than resonance by | Δ|=$0.199s^{-1}$ but with $v_0 - v_s = -0.199/s$, the negative of (2.2.26).
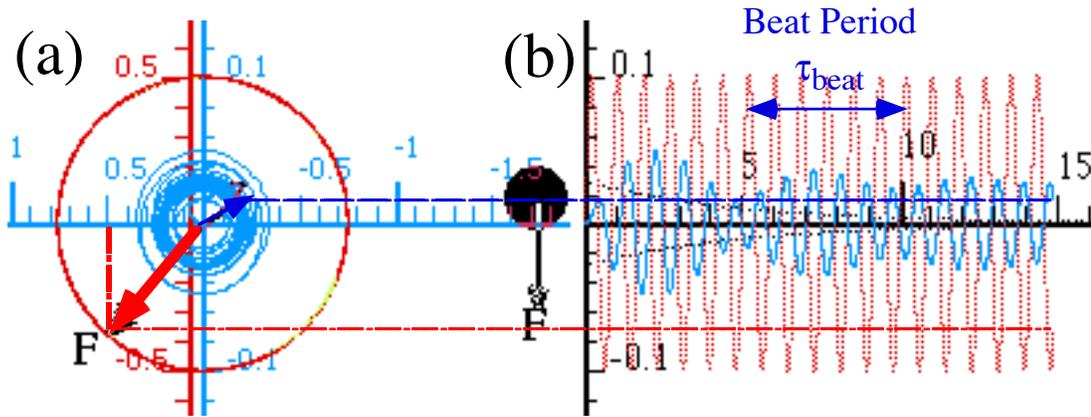
Fig. 2.2.10 Above Resonance (a)Response z-phasor lags ρ=170.2° behind stimulus F-phasor.
(ωₛ=7.53,ω₀=2π ,Γ=0.2).   (b) Time plots of Re *z(t) and* Re *F(t)*

Below is an example with half the detuning ($\omega_0 - \omega_s = -0.63$ and $v_0 - v_s = -0.1$), and so the beats are twice as long or about 10 seconds. As ω_s approaches the resonance region ($\omega_0 \pm \Gamma$) the beat period gets longer still. Finally, τ_{beat} is so long that the poor transient's beating dies below 5% before it can even make a single beat. Such is nearly the case in Fig. 2.2.8d, which looks like a half-beat that has barely come down.
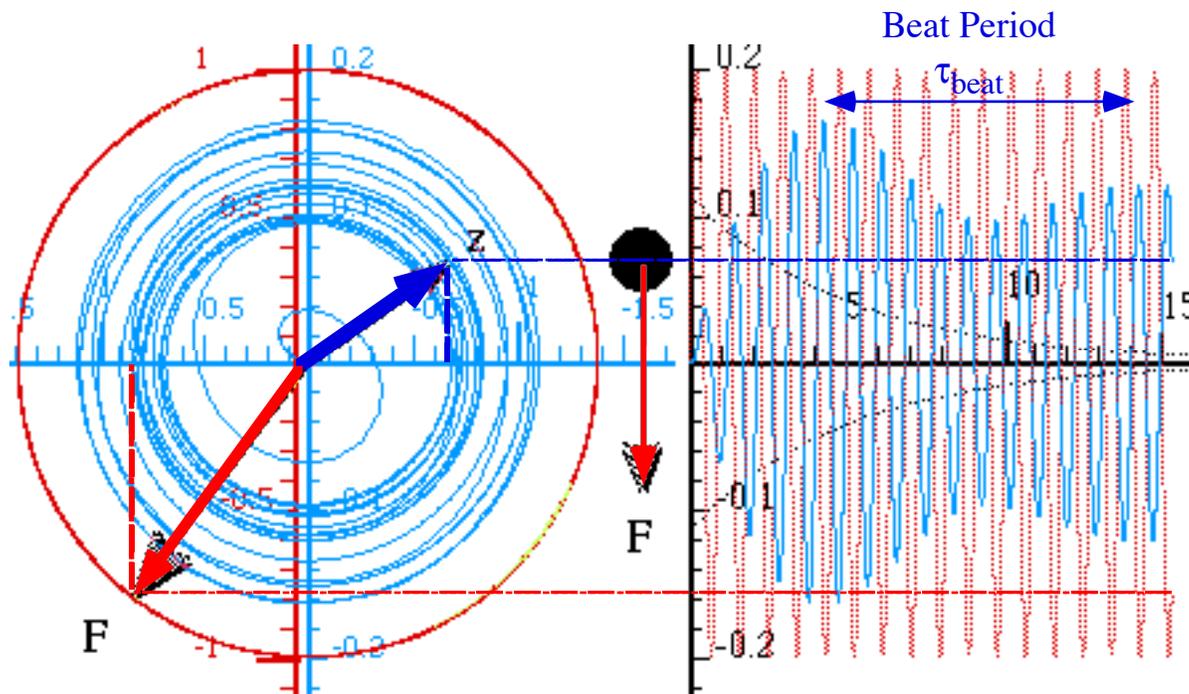
Fig. 2.2.11 Above Resonance (a)Response z-phasor lags ρ=161.6° behind stimulus F-phasor.
(ωₛ=6.91,ω₀=2π ,Γ=0.2).   (b) Time plots of Re *z(t) and* Re *F(t)*

Comparing resonant and non-resonant cases

For the below-resonance case in Fig. 2.2.8c and Fig. 2.2.9, the response phase lag according to (2.2.15d) is $\rho = 0.1405$, so $z_{ss\ response}$ (and eventually $z(t)$ itself) is only *8.05°* behind the stimulus. For the above-resonance case in Fig. 2.2.10, the response $z_{ss\ response}$ and $z(t)$ lag behind by about *180°* ($\rho = 170.2°$). This a the signature of high frequency response $G(\infty)$: it becomes nearly π <u>out of phase</u> with the stimulus. In contrast the low frequency or DC response $G(0)$ is very nearly <u>in phase</u> with the stimulus.

Another difference between high and low frequency response is that high frequency response goes to zero $G(\infty) \sim 1/\omega_S^2 \rightarrow 0$ (as $\omega_S \rightarrow \infty$) but low frequency resonance approaches a constant value, namely

$$DC\ response = G(0) = 1/\omega_0^2. \qquad\qquad (2.2.28)$$

$G(0)$ is just the response due to a static (DC) unit force. For high frequency oscillators, $G(0)$ will be very small, but if you multiply little $G(0)$ by the big angular quality factor ($q = \omega_0/2\Gamma$ is the number of oscillations in the time needed to achieve 95% of a resonance), then the result $1/2\omega_0\Gamma$ is <u>exactly</u> the resonant response amplitude $G(\omega_0)$. (Recall (2.2.23).) In other words, the DC response (2.2.28) is the <u>average amplitude increase which is achieved during each cycle</u> of a unit <u>resonant</u> stimulus <u>before</u> the damping Γ really takes effect.

High-q resonant and non-resonant cases

For very high *q* quality oscillators (very low Γ) the resonant region ($\omega_0 \pm \Gamma$) is so small that it may be considered non-existent. In classical Hamiltonian systems we deal with this limiting case exclusively since damping is zero by definition! Hamiltonian systems are a "transient heaven"; the beats go on forever and the transients never die or even fade away! (To a typical atom first being excited in a laser resonance with a *q* of fifty million, it might seem like transients live forever, too.) For infinite *q* there are only two values for the response phase lag angle: <u>in-phase</u> ($\rho = 0$) and <u>out-of-phase</u> ($\rho = \pi$). The out-of-phase ($\rho = \pi$) occurs <u>above</u> resonance ($\omega_S > \omega_0$) as shown in Fig. 2.2.12a. The in-phase ($\rho = 0$) case occurs <u>below</u> resonance ($\omega_S < \omega_0$) as shown in Fig. 2.2.12c. Exactly at resonance ($\omega_S = \omega_0$) the steady state response and the transient are both infinite and opposite so they cancel each other, and the *z(t)* builds up forever as shown in Fig. 2.2.12b. Each cycle of revolution adds another bit of amplitude equal to the DC response (2.2.28) just as we explained above.

Fig. 2.2.12 Zero damping response ($\omega_0 = 2\pi$, $\Gamma = 0$)   *(Next page)*
(a) Above resonance ($\omega_S = 6.91$)
(b) Resonance ($\omega_S = 6.28$) (Stimulus amplitude reduced to show response.)
(c) Below resonance ($\omega_S = 5.65$)

(a) Above Resonance

Beat Period τ_{beat} = 10

z(t)

Z transient

Z ss response

F(t)

(b) Resonance

Beat Period τ_{beat} = ∞

z(t)

F(t)

Time

(c) Below Resonance

Beat Period τ_{beat} = 10

Z transient

z(t)

F(t)
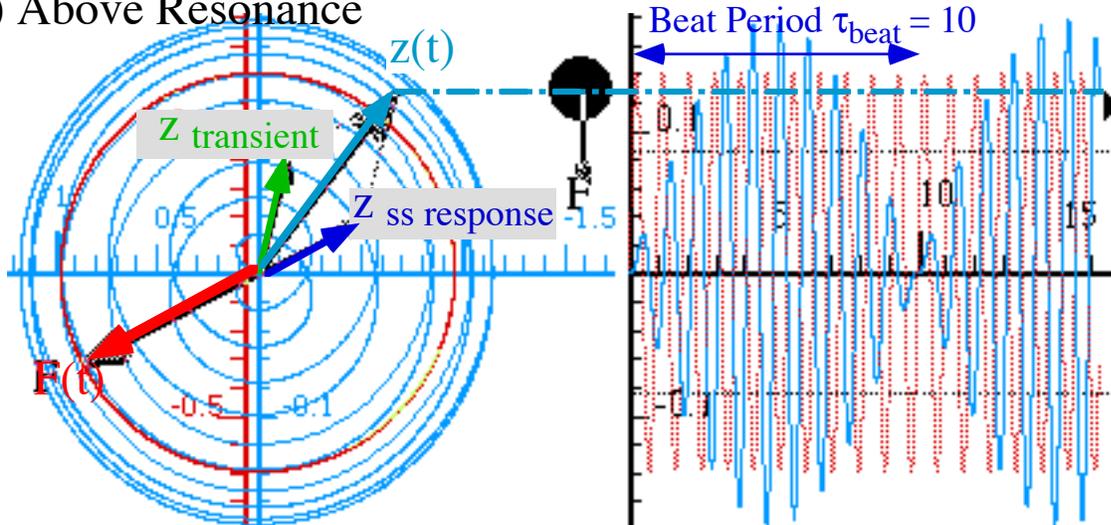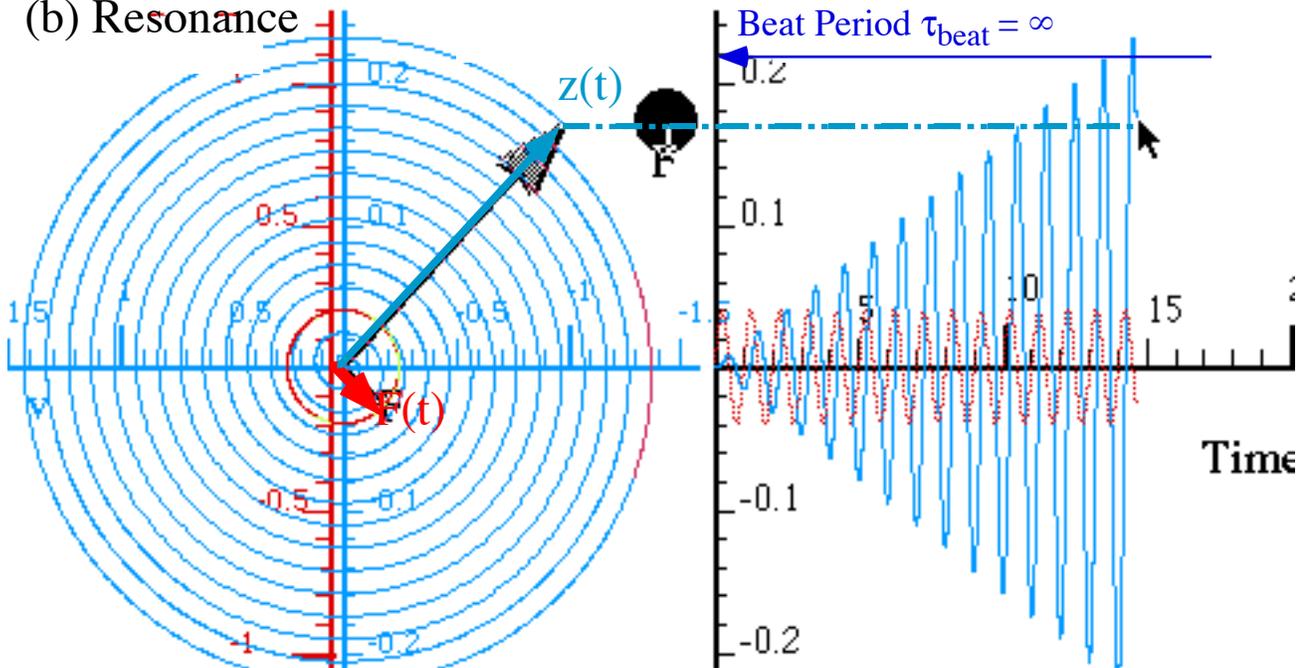
Z ss response
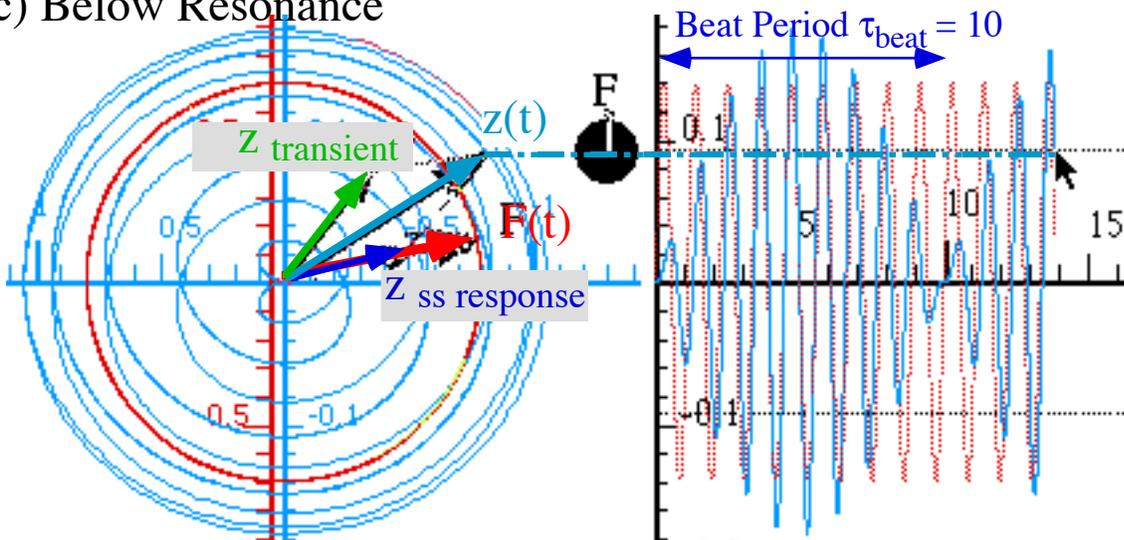
(g) Time and frequency uncertainty relations

Physicists and musicians must deal with oscillators or instruments of moderate *q=10-100*. They may "tune" an oscillator or instrument by detecting the beats between the oscillator and a reference stimulus of much higher *q*. But, how accurately can a finite-*q* oscillator be tuned?

Even if the stimulus is perfect there is a fundamental uncertainty $\Delta\omega$ associated with the oscillator that depends on its decay rate Γ. Suppose you tune the stimulus until you no longer can detect any beats and the tuning is the best it can be. Recall that beats are transient and decay to less than 5% after time $t_{5\%} = 3/\Gamma$. If this time passes before half a beat it is hard to see beats as in Fig. 2.2.8d. Half a beat takes time $\tau_{\text{half-beat}} = \pi / |\omega_s - \omega_0|$. So to see a beat we need $\tau_{\text{half-beat}}$ to be less than $\tau_{5\%}$ or $3/\Gamma$.

$$\pi / |\omega_s - \omega_0| < 3/\Gamma .$$

This means the ω-detuning error is about equal to the decay rate Γ. (Here we approximate π~3.0, again.)

$$|\omega_s - \omega_0| > \Gamma$$

In other words, any detuning less than Γ is becoming undetectable. Total ω uncertainty is ±Γ or twice Γ that is the FWHM width $\Delta\omega = 2\Gamma$ in (2.2.19). Linear frequency uncertainty is $\Delta v = \Delta\omega / 2\pi$.

$$2\Gamma = \Delta\omega = 2\pi{\cdot}\Delta v$$

The *relative frequency uncertainty* $\Delta v / v_0$ is therefore the *inverse* of the angular quality factor *q*.

$$\frac{2\Gamma}{\omega_0} = \frac{\Delta\omega}{\omega_0} = \frac{1}{q} = \frac{\Delta v}{v_0} , \qquad\qquad (2.2.29)$$

If we think of the 5% or 3.321% lifetime of a musical note as its time uncertainty Δt, then $\Delta t \Delta v = 3/\pi \approx 1$

$$\Delta t = t_{5\%} = 3/\Gamma \qquad (2.2.30a) \qquad\qquad \Delta t = t_{4.321\%} = \pi/\Gamma \qquad (2.2.30b)$$

This is a Heisenberg relation: $\Delta t \Delta E \approx h$ if energy *E* is Planck-related to frequency by *E=hv*.

(h) Initial conditions

In general, the transient amplitude $A = |A|e^{i\alpha}$ is a function of the initial conditions $x(0) = x_0 = \mathrm{Re}\, z(0)$ and $v_0 = \dot{x}(0)$ as well as stimulus frequency ω_s and initial acceleration $a(0) = |a(0)|$. See Exercise 2.2.9.

$$\mathrm{Re}\, A = |A|\cos\alpha = x_0 - R\cos\rho \;\; \text{where:} \; R = |G_{\omega_0}(\omega_s)| a(0) \quad \mathrm{Im}\, A = |A|\sin\alpha = \frac{v_0 - \omega_s R\sin\rho + \Gamma(x_0 - R\cos\rho)}{\omega_\Gamma} \;\; (2.2.32)$$

The "cold" oscillator ($x_0=0 =v_0$) of (2.2.25c) is a special case of (2.2.32).

(i) Ideal Lorentz-Green functions and Smith plots

When physicists speak of Lorentzian function they generally mean an ideal version of the *real* Lorentz response (2.2.15) with high-Q near-resonant $\omega_s \to \omega_0$ conditions $\omega_0^2 - \omega_s^2 \cong (\omega_0 - \omega_s)2\omega_s$ of (2.2.18).

$$G_{\omega_0}(\omega_s) = \frac{1}{\omega_0^2 - \omega_s^2 - i2\Gamma\omega_s} \xrightarrow{\omega_s \to \omega_0} \frac{1}{2\omega_s}\frac{1}{\omega_0 - \omega_s - i\Gamma} \approx \frac{1}{2\omega_0}\frac{1}{\Delta - i\Gamma} = \frac{1}{2\omega_0}L(\Delta - i\Gamma) \qquad (2.2.33)$$

A *complex detuning-decay* δ=Δ-iΓ variable δ is defined with the *real detuning* $\Delta = \omega_0 - \omega_s$ defined as before to give an *ideal Lorentzian L(δ)=1/δ* below. Its imaginary part $\Gamma / (\Delta^2 + \Gamma^2)$ is what many call "a Lorentzian." With

$\Delta=0$, it becomes $1/\Gamma$. With $\Gamma=0$, the real part becomes $1/\Delta$. Algebra and geometry of ideal $L(\delta)=1/\delta$ functions is simple as given below, and $1/z$-plots known as *Smith plots* show their geometry in Fig. 2.2.13.

$$L(\Delta - i\Gamma) = \frac{1}{\Delta - i\Gamma} = \operatorname{Re} L + i\operatorname{Im} L = \frac{\Delta}{\Delta^2 + \Gamma^2} + i\frac{\Gamma}{\Delta^2 + \Gamma^2} = |L|^2 \Delta + i|L|^2 \Gamma$$

$$= |L|e^{i\rho} = |L|\cos\rho + i|L|\sin\rho = \frac{\cos\rho}{\sqrt{\Delta^2 + \Gamma^2}} + i\frac{\sin\rho}{\sqrt{\Delta^2 + \Gamma^2}} \quad \text{where:} \ |L| = \frac{1}{\sqrt{\Delta^2 + \Gamma^2}}$$

(2.2.34)

Constant Δ and Γ curves in Fig. 2.2.13 are orthogonal circles of *dipolar coordinates*. Recall Fig. 1.10.11.

$$|L| = \frac{1}{\Delta}\cos\rho \quad (2.2.35a) \qquad\qquad |L| = \frac{1}{\Gamma}\sin\rho \quad (2.2.35b)$$
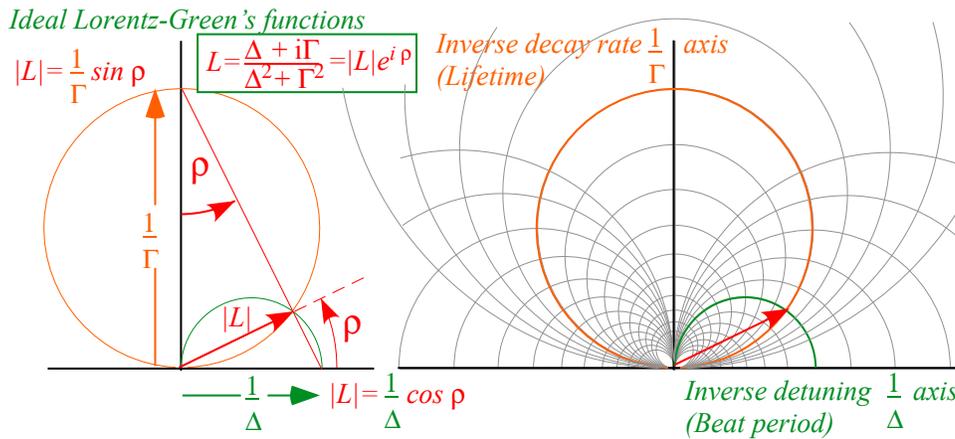
Fig. 2.2.13 Ideal Lorentzian in inverse rate space. (Smith life-time $1/\Gamma$ vs. beat-period $1/\Delta$ coordinates)

A circle of constant decay rate Γ and varying detuning frequency Δ has a diameter of $1/\Gamma$ along the vertical of the inverse frequency space in Fig. 2.2.13. As detuning approaches zero (perfect tuning) the polar phase-lag angle angle ρ approaches $\pi/2$ and the inverse detuning or beat-period $1/\Delta$ approaches infinity.

There appears to be circle of constant decay rate $\Gamma=0.2$ in Fig. 2.2.6, however, it cannot be a perfect circle, particularly in the DC region around origin. Ideal Lorentzian (2.2.34), unlike the real one, has no DC response. As decay rate Γ increases the $1/\Gamma$ circle shrinks and becomes distorted by its DC "flat" at $\omega=0$ as shown by a rather low quality *(Q=1/4)*-example having $\Gamma=2.0$ and $\omega=2\pi$ in Fig. 2.2.14 below.
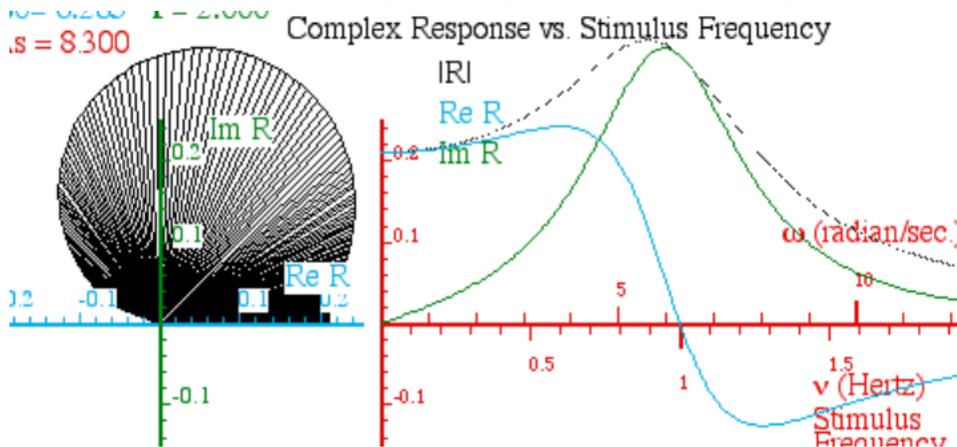
Fig. 2.2.14 Highly damped Lorentz-Green function plots with $\Gamma=2.0$ and $\omega=2\pi$.

Exercises for Ch. 2.2: Oscillator G-functions of Forced Damped Harmonic Oscillator (FDHO)

Exercise 2.2.4 DC G-response of FDHO

DC response $G_{\omega_0}(0)$ is the amplitude caused by a unit acceleration $(a=1)$ at zero stimulus frequency. This may be confusing since there is no acceleration at zero frequency. A clearer definition of $G_{\omega_0}(0)$ is the response due to a static *force* of magnitude $F = ma = m$ acting on mass m. Use this to show that the value of $G_{\omega_0}(0)$ is consistent with the spring force equation (2.2.2) and Hooke's Law.

Exercise 2.2.5 Resonant G-response of FDHO

Resonant response $G_{\omega_0}(\omega_0)$ is the amplitude caused by a unit acceleration amplitude $(|a(t)|=1)$ or force amplitude $(|F(t)|=m)$ at resonance $(\omega_s = \omega_0)$. Compute the value of $G_{\omega_0}(\omega_0)$ and show it is consistent with drag force equation (2.2.3), and that all work done by F is wasted by friction.

Exercise 2.2.6 The "standard" Lorentzian

In physics literature a standard Lorentzian function generally means a form $L(\Delta) = A/(\Delta^2 + A^2)$ with constant A. If one uses the *near-resonant approximation* (*NRA* is (2.2.18)) then $L(\Delta)$ or its derivative results from exact G-equations (2.2.15).

(a) Use *NRA* (2.2.18) to reduce (2.2.15a-d) to a standard Lorentzian function of the detuning parameter $\Delta = \omega_s - \omega_0$.

(b) Show that *NRA* for complex response $G = \text{Re}\,G + i\,\text{Im}\,G$ gives an arc of a circle in the complex plane for constant Γ and variable detuning Δ. How does this circle deviate from what appears to be a circle in Fig. 2.2.6? (Consider higher Γ values for which *NRA* breaks down.) Fixed Δ and varying Γ give what curve? Explain and do a ruler-and-compass construction of plots of *NRA* Lorentz Green functions $\text{Re}\,G_{\omega_0}(\omega_s)$, $\text{Im}\,G_{\omega_0}(\omega_s)$, and $|G_{\omega_0}(\omega_s)|$.
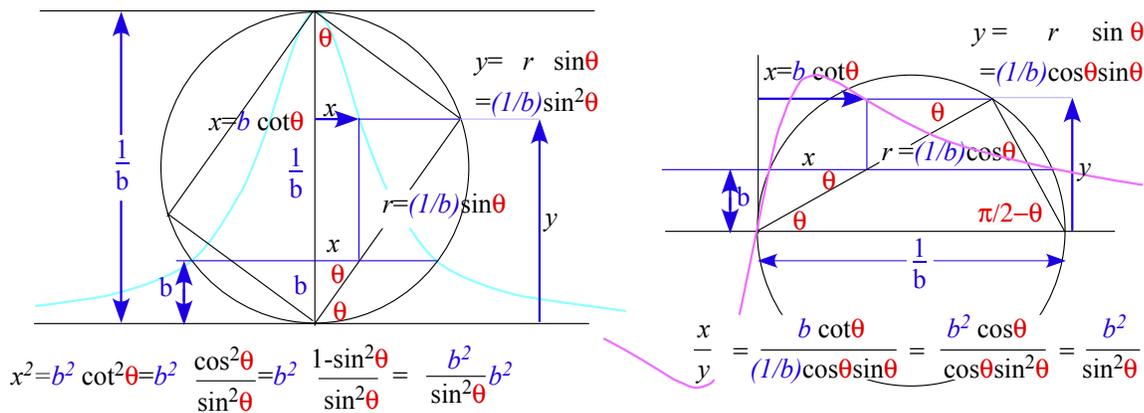
Exercise 2.2.7 Max and min G-values

Derive equations for the extreme values for the response function or function related to G as asked below.
For part (a) *only* use *near-resonant approximation* (*NRA*): See preceding Ex. 2.2.6.

(a) Find ω_s values which give maxima for: $\text{Re}\,G_{\omega_0}(\omega_s)$, $\text{Im}\,G_{\omega_0}(\omega_s)$, and $|G_{\omega_0}(\omega_s)|$.

(b) Do (a) for *exact* $G_{\omega_0}(\omega_s)$. Exact plots by calculator help check these answers.

(c) Find exact ω_s value(s) that maximize peak KE of responding oscillator.

(First show total $KE=1/2\ m\omega^2 x^2$ for oscillation of amplitude x.)

Exercise 2.2.8 Lifetimes
Compare the number of heartbeats in your lifetime (assuming you live to a ripe old age of 100 years) to the number of oscillations in atomic and molecular lifetimes given below. (First, estimate your own angular quality factor q.)

Typical atomic <u>energy</u> decay time is $t_{5\%} = 3/\Gamma = 3.4 \times 10^{-8}$ s for a green spectral 600Thz line. Compute atomic q and Q.

Exercise 2.2.9 Initializing
Derive the initial transient components Re A *and* Im A in terms of initial values $x_0 = x(0)$, $v_0 = \dot{x}(0)$ of stimulated FDHO, response

magnitude $R = \left| G_{\omega_0}(\omega_s) \right|$, initial stimulus $a(0) = |a|e^{i\alpha}$, Γ, ω_Γ, and ρ.
(Check that your total solution (2.2.25) does satisfy the initial conditions.)

Exercise 2.2.10 Wiggling Old-Main lamp posts
Let a static force of $10N$ on a lamp post cause it to bend $1cm$. Upon release it vibrates at $1Hz$ for a minute before its amplitude dies to less than $0.05cm$. Estimate ω_0, Γ, and q and how much it bends 1 minute after a $1Hz$ *oscillating* force of $\pm 1N$ starts. What is the bending after 2 minutes? Do this *quickly* by *reasoning* using q-factor properties and 5% mnemonics. (Points-off for too much algebra!)

Exercise 2.2.11 Timing is everything! (A formula to remember)
(a) Let oscillating force $F(t)=F_s\cos\omega t$ act on a mass whose response $x(t)=G\cos(\omega t-\rho)$ also is frequency ω but with a amplitude G and a phase lag of ρ. Derive a formula for the work loop integral $\oint F\ dx$ for exactly one period of oscillation. Discuss how result relates to work done against friction in a *FDHO*. (Recall Ex. 2.2.5.)
(b) Let oscillation x_1 and x_2 each have amplitude A but x_1 lags x_2 by phase ρ. Show by geometry that the x_1 vs. x_2 path is an ellipse of major axis $a=A\sqrt{2}\cos(\rho/2)$ and $b=A\sqrt{2}\sin(\rho/2)$ and area $W=$____. Compare this W to loop work derived in part (a).

---
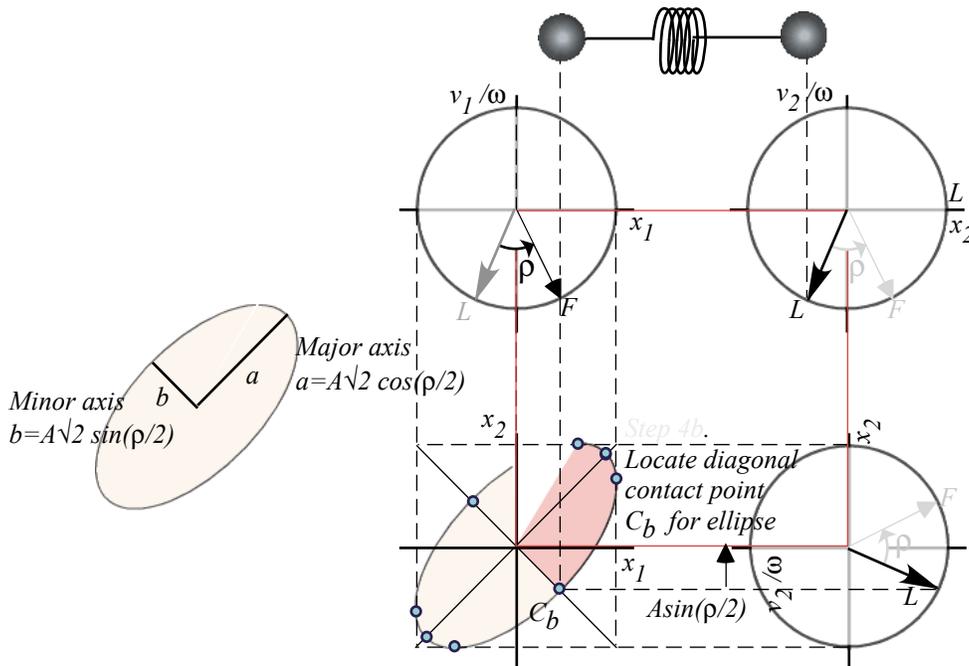
[1] Peter W. Milonni, private communication.

Chapter 2.3 Coupled Oscillators: Eigenvalues and Eigenvectors

The Lorentz theory of preceding Ch 2.2 may be generalized to derive the spectral response of coupled oscillators. Variations of this will be used throughout the following sections. First we will consider coupled oscillator system consisting of two masses shown in Fig. 2.3.1. It is analogous to coupled pendulum pairs in Fig. 2.3.2 or to a single 2-dimensional oscillator in Fig. 2.3.3. The latter was introduced in Ch. 8 of Unit 1.
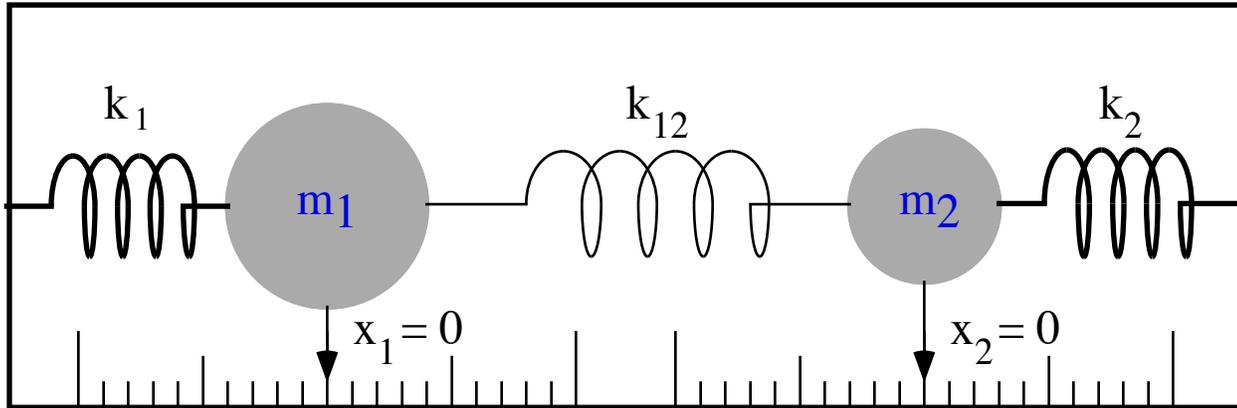
Fig. 2.3.1 Two 1-dimensional coupled oscillators
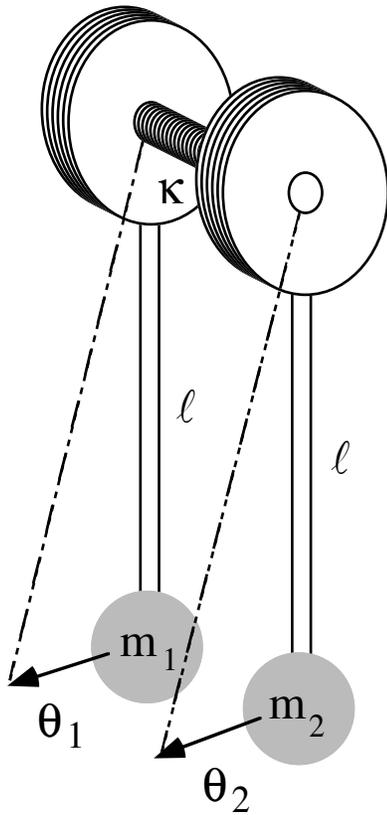
Fig. 2.3.2 Coupled pendulums
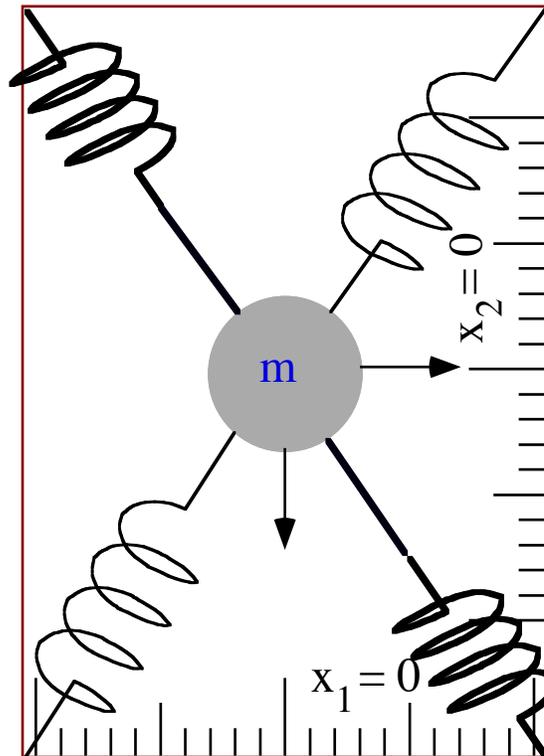
Fig. 2.3.3 One 2-dimensional coupled oscillator

(a) Equations of motion

Linear (Hooke's law) spring forces in Newton or Lagrange equations of motion for the system in Fig. 2.3.1 are gradients of a sum of Hooke-Law potential energies $V = \Sigma \ \frac{1}{2} k (\Delta L)^2$ for each spring.

$$V = \frac{1}{2} k_1 x_1^2 + \frac{1}{2} k_2 x_2^2 + \frac{1}{2} k_{12} (x_1 - x_2)^2$$

$$V = \frac{1}{2} (k_1 + k_{12}) x_1^2 - k_{12} x_1 x_2 + \frac{1}{2} (k_2 + k_{12}) x_2^2 \tag{2.3.1}$$

Kinetic energy is simply a sum of squares of velocities.

$$T = \frac{1}{2} m_1 \dot{x}_1^2 + \frac{1}{2} m_2 \dot{x}_2^2$$

The resulting dynamic equations are the following:

$$\frac{d}{dt}\left(\frac{\partial T}{\partial \dot{x}_1}\right) = m_1 \ddot{x}_1 = F_1 = -\frac{\partial V}{\partial x_1} = -(k_1 + k_{12}) x_1 + k_{12} x_2$$

$$\frac{d}{dt}\left(\frac{\partial T}{\partial \dot{x}_2}\right) = m_2 \ddot{x}_2 = F_2 = -\frac{\partial V}{\partial x_2} = k_{12} x_1 - (k_2 + k_{12}) x_2 \tag{2.3.2}$$

Similar equations can be derived for the torsion coupled pendulum system in Fig. 2.3.2 for small angles. $\left(\sin\theta_j \cong \theta_j \text{ if } \theta_j \ll 1\right)$ The torsion spring constant is κ .

$$m_1 \ell^2 \ddot{\theta}_1 = -m_1 g\ell \sin\theta_1 - \kappa\theta_1 + \kappa\theta_2 \cong -m_1 g\ell\theta_1 - \kappa\theta_1 + \kappa\theta_2$$

$$m_2 \ell^2 \ddot{\theta}_2 = \kappa\theta_1 - m_2 g\ell \sin\theta_2 - \kappa\theta_2 \cong \kappa\theta_1 - m_2 g\ell\theta_2 - \kappa\theta_2 \tag{2.3.3}$$

For large angles, the equation has a non-linear 'sine-gordon' form. The small-angle approximation yields an equation identical to (2.3.2) with $x_j = \theta_j$ and

$$k_1 = \frac{g}{l} + \frac{\kappa}{l^2} = k_2 \qquad\qquad k_{12} = \frac{\kappa}{l^2} . \tag{2.3.4}$$

(b) Matrix equation and reciprocity symmetry

A matrix form of the equation of motion is the following:

$$\begin{pmatrix} m_1 \ddot{x}_1 \\ m_2 \ddot{x}_2 \end{pmatrix} = -\begin{pmatrix} \kappa_{11} & \kappa_{12} \\ \kappa_{21} & \kappa_{22} \end{pmatrix} \begin{pmatrix} x_1 \\ x_2 \end{pmatrix} \tag{2.3.5a}$$

where we define diagonal force matrix components.

$$\kappa_{11} = k_1 + k_{11}, \quad \kappa_{22} = k_2 + k_{22} \tag{2.3.5b}$$

Off-diagonal force constants are minus the original coupling constant in Fig. 2.3.1 and equation (2.3.1).

$$k_{12} = -\kappa_{12} = -\kappa_{21} = k_{21} \tag{2.3.5c}$$

Off-diagonal symmetry of force matrices is mandatory for conservative potentials, according to *Reciprocity Relations* such as the following:

$$k_{12} = \frac{\partial F_1}{\partial x_2} = -\frac{\partial^2 V}{\partial x_2 \partial x_1} = -\frac{\partial^2 V}{\partial x_1 \partial x_2} = \frac{\partial F_2}{\partial x_1} = k_{21} \tag{2.3.5d}$$

This depends on either order of partial differentiation giving the same result.

(c) Rescaling and symmetrization

Suppose we replace each coordinate (x_1, x_2) with appropriately rescaled coordinates $(q_1 = s_1 x_1, q_2 = s_2 x_2)$. This can be used to symmetrize the mass factors on the $\ddot{q}_j$ terms.

$$-\frac{m_1}{s_1}\ddot{q}_1 = \kappa_{11}\frac{q_1}{s_1} + \kappa_{12}\frac{q_2}{s_2} \qquad\qquad -\ddot{q}_1 = \frac{\kappa_{11}}{m_1}q_1 + \frac{\kappa_{12}s_1}{m_1 s_2}q_2 \equiv K_{11}q_1 + K_{12}q_2$$

$$-\frac{m_2}{s_2}\ddot{q}_2 = \kappa_{12}\frac{q_1}{s_1} + \kappa_{22}\frac{q_2}{s_2} \qquad (2.3.6) \qquad -\ddot{q}_2 = \frac{\kappa_{12}s_2}{m_2 s_1}q_1 + \frac{\kappa_{22}}{m_2}q_2 \equiv K_{21}q_1 + K_{22}q_2 \qquad (2.3.7)$$

The resulting mass-symmetrized equations can be made to have reciprocity symmetry, too if new constants K_{ij} satisfy the following. The pseudo-reciprocity relations require a special scale factor ratio (2.3.8d) below.

$$K_{21} = \frac{\kappa_{12}s_2}{m_2 s_1} = K_{12} = \frac{\kappa_{12}s_1}{m_1 s_2} = \frac{-k_{12}}{\sqrt{m_1 m_2}} \qquad K_{11} = \frac{\kappa_{11}}{m_1} = \frac{k_1 + k_{12}}{m_1} \qquad K_{22} = \frac{\kappa_{22}}{m_2} = \frac{k_2 + k_{12}}{m_2} \qquad \frac{s_2}{s_1} = \sqrt{\frac{m_2}{m_1}}$$

$$(2.3.8a) \qquad\qquad\qquad (2.3.8b) \qquad\qquad\qquad (2.3.8c) \qquad\qquad\qquad (2.3.8d)$$

Caution is recommended since forced symmetry may lead to unphysical results.

(d) Impedance operators and general oscillation equations

There are other coefficients besides the mass-symmetrized spring force constant matrix K_{ij}.

$$K_{ij} = K_{ji} \qquad\qquad\qquad (2.3.9)$$

A general linear equation may also have a resistive or frictional *damping coefficient matrix* R_{ij}, and an inductive or *inertial coefficient matrix* L_{ij}, as well as *stimulus components* $f_i(t)$ as in the following general equation for two coupled damped and stimulated oscillators.

$$\begin{pmatrix} L_{11} & L_{12} \\ L_{21} & L_{22} \end{pmatrix}\begin{pmatrix} \ddot{q}_1 \\ \ddot{q}_2 \end{pmatrix} + \begin{pmatrix} R_{11} & R_{12} \\ R_{21} & R_{22} \end{pmatrix}\begin{pmatrix} \dot{q}_1 \\ \dot{q}_2 \end{pmatrix} + \begin{pmatrix} K_{11} & K_{12} \\ K_{21} & K_{22} \end{pmatrix}\begin{pmatrix} q_1 \\ q_2 \end{pmatrix} = \begin{pmatrix} f_1(t) \\ f_2(t) \end{pmatrix}. \qquad (2.3.10a)$$

It is often the case that the reciprocity relations hold for all impedance matrices, as well as they do for potential force and acceleration components. (But don't count on it!)

$$L_{ij} = L_{ji}, \qquad R_{ij} = R_{ji} \qquad\qquad\qquad (2.3.10b)$$

The equations can be written using *Dirac matrix notation* $Z_{ij} = \langle i|\mathbf{Z}|j\rangle$ for each impedance matrix element, *Dirac bra-ket notation* $q_j = \langle j|q\rangle$ for each coordinate, and $f_j(t) = \langle j|f(t)\rangle$ for each component of the stimulus $(i, j = 1, 2)$. (See the review of Dirac bra-ket notation in Appendix 3.A below.)

$$\sum_{j=1}^{2}\langle i|\mathbf{L}|j\rangle\langle j|\ddot{q}\rangle + \langle i|\mathbf{R}|j\rangle\langle j|\dot{q}\rangle + \langle i|\mathbf{K}|j\rangle\langle j|q\rangle = \langle i|f(t)\rangle \qquad (2.3.10c)$$

Removing bra $\langle i|$ and using completeness relation $(\Sigma|j\rangle\langle j| = \mathbf{1})$ yields an abstract operator equations of motion.

$$\mathbf{L}|\ddot{q}\rangle + \mathbf{R}|\dot{q}\rangle + \mathbf{K}|q\rangle = |f(t)\rangle \quad \text{or:} \quad \mathbf{L}\cdot\ddot{\mathbf{q}} + \mathbf{R}\cdot\dot{\mathbf{q}} + \mathbf{K}\cdot\mathbf{q} = \mathbf{f}(t) \qquad (2.3.10d)$$

In electric circuits, capacitance C_{ij}^{-1} is the spring matrix K_{ij} and $\dot{\mathbf{q}} = \mathbf{I}$ is current flow of charge $\mathbf{q}$.

$$\mathbf{L}\cdot\dot{\mathbf{I}} + \mathbf{R}\cdot\mathbf{I} + \mathbf{C}^{-1}\int\mathbf{I}\,dt = \mathbf{V}_{emf}(t) \qquad (2.3.10e)$$

This is a combination of laws of *Faraday* $(\mathbf{V} = \mathbf{L}\cdot\dot{\mathbf{I}})$, *Ohm* $(\mathbf{V} = \mathbf{R}\cdot\mathbf{I})$, and *Gauss* $(\mathbf{V} = \mathbf{C}\cdot\mathbf{q} = \mathbf{C}\cdot\int\mathbf{I}\,dt)$.

Appendix 3.A Review of Dirac Bra-ket Notation

Dirac bra-ket notation is not just for quantum mechanics; it is used for all types of linear algebra. A bra-ket $\langle a|b \rangle$ indicates a *scalar product* (This is **a·b** in the older Gibbs notation.)

$$\langle a|b \rangle = \bar{\mathbf{a}} \bullet \vec{\mathbf{b}} = \begin{pmatrix} a_1 & a_2 & \cdots & a_n \end{pmatrix} \bullet \begin{pmatrix} b_1 \\ b_2 \\ \vdots \\ b_n \end{pmatrix} = \sum_k a_k b_k \text{ of a } \textit{column} \text{ or } \textit{ket vector } |b \rangle = \vec{\mathbf{b}} = \begin{pmatrix} b_1 \\ b_2 \\ \vdots \\ b_n \end{pmatrix} \quad (2.A.1)$$

with a *row* or *bra vector* $\langle a| = \bar{\mathbf{a}} = \begin{pmatrix} a_1 & a_2 & \cdots & a_n \end{pmatrix}$. Expansion of a vector in terms of a complete set of unit vectors $\mathbf{e_1}, \mathbf{e_2}, \cdots, \mathbf{e_n}$ in Gibbs notation is

$$\bar{\mathbf{a}} = a_1 \bar{\mathbf{e}}_1 + a_2 \bar{\mathbf{e}}_2 + \cdots + a_n \bar{\mathbf{e}}_n \qquad \text{or else} \quad \vec{\mathbf{b}} = b_1 \bar{\mathbf{e}}_1 + b_2 \bar{\mathbf{e}}_2 + \cdots + b_n \bar{\mathbf{e}}_n$$

In Dirac notation we write this as

$$\langle a| = a_1 \langle 1| + a_2 \langle 2| + \cdots + a_n \langle n| \quad \text{or else} \quad |b \rangle = b_1 |1 \rangle + b_2 |2 \rangle + \cdots + b_n |n \rangle \quad (2.A.2)$$

Scalar product *orthonormality* of unit bras $\{\langle 1|, \langle 2|, \cdots \langle n|\}$ with kets $\{|1 \rangle, |2 \rangle, \cdots |n \rangle\}$ is required.

$$\langle j|k \rangle = \delta_{jk} = \begin{cases} 1 & \text{if j=k} \\ 0 & \text{if j} \neq \text{k} \end{cases} \quad (2.A.3)$$

It implies that each bra or ket component is itself a bra-ket scalar product.

$$\langle a|1 \rangle = a_1, \ \langle a|2 \rangle = a_2, \cdots \langle a|n \rangle = a_n \quad \text{or else,} \quad \langle 1|b \rangle = b_1, \ \langle 2|b \rangle = b_2, \cdots \langle n|b \rangle = b_n . \quad (2.A.4)$$

This in turn implies what is called *completeness* of the unit bases $\{|1 \rangle, |2 \rangle, \cdots |n \rangle\}$ and $\{\langle 1|, \langle 2|, \cdots \langle n|\}$.

$$\langle a| = \langle a|1 \rangle\langle 1| + \langle a|2 \rangle\langle 2| + \cdots + \langle a|n \rangle\langle n| \quad \text{or else,} \quad |b \rangle = |1 \rangle\langle 1|b \rangle + |2 \rangle\langle 2|b \rangle + \cdots + |n \rangle\langle n|b \rangle \quad (2.A.5)$$

The scalar product (2.A.1) is the following in full Dirac notation.

$$\langle a|b \rangle = \langle a|1 \rangle\langle 1|b \rangle + \langle a|2 \rangle\langle 2|b \rangle + \cdots + \langle a|n \rangle\langle n|b \rangle = \Sigma \langle a|k \rangle\langle k|b \rangle \quad (2.A.6)$$

If $\{|\bar{1} \rangle, |\bar{2} \rangle, \cdots |\bar{n} \rangle\}$ is another set of n-base vectors that is orthonormal then it must be complete, too.

$$\langle \bar{m}|\bar{n} \rangle = \delta_{mn} = \begin{cases} 1 & \text{if m=n} \\ 0 & \text{if m} \neq \text{n} \end{cases} \quad \text{implies: } \langle j|k \rangle = \langle j|\bar{1} \rangle\langle \bar{1}|k \rangle + \langle j|\bar{2} \rangle\langle \bar{2}|k \rangle + \cdots + \langle j|\bar{n} \rangle\langle \bar{n}|k \rangle \quad (2.A.7)$$

The n-by-n matrix of scalar products between these two bases are called *transformation matrices*.

$$\text{Transformation } \mathbf{T}: \begin{pmatrix} \langle 1|\bar{1} \rangle & \langle 1|\bar{2} \rangle & \cdots & \langle 1|\bar{n} \rangle \\ \langle 2|\bar{1} \rangle & \langle 2|\bar{2} \rangle & \cdots & \langle 2|\bar{n} \rangle \\ \vdots & \vdots & \ddots & \vdots \\ \langle n|\bar{1} \rangle & \langle n|\bar{2} \rangle & \cdots & \langle n|\bar{n} \rangle \end{pmatrix} \qquad \text{Inverse } \mathbf{T^{-1}}: \begin{pmatrix} \langle \bar{1}|1 \rangle & \langle \bar{1}|2 \rangle & \cdots & \langle \bar{1}|n \rangle \\ \langle \bar{2}|1 \rangle & \langle \bar{2}|2 \rangle & \cdots & \langle \bar{2}|n \rangle \\ \vdots & \vdots & \ddots & \vdots \\ \langle \bar{n}|1 \rangle & \langle \bar{n}|2 \rangle & \cdots & \langle \bar{n}|n \rangle \end{pmatrix} \quad (2.A.8)$$

The matrix product $\mathbf{TT^{-1}}$ is a unit matrix according to (2.A.6) and (2.A.7) and so is $\mathbf{T^{-1}T}$. (Prove!)

$$\mathbf{TT^{-1} = 1 = T^{-1}T} \quad (2.A.9)$$

$\mathbf{T}$ maps each ket into the corresponding "barred" ket, while $\mathbf{T^{-1}}$ maps bras similarly.

$$\mathbf{T}|1 \rangle = |\bar{1} \rangle, \ \mathbf{T}|2 \rangle = |\bar{2} \rangle, \cdots \mathbf{T}|n \rangle = |\bar{n} \rangle \text{ , and } \langle 1|\mathbf{T^{-1}} = \langle \bar{1}|, \ \langle 2|\mathbf{T^{-1}} = \langle \bar{2}|, \cdots \langle n|\mathbf{T^{-1}} = \langle \bar{n}|$$

So: $\langle 1|\mathbf{T}|1 \rangle = \langle 1|\bar{1} \rangle, \ \langle 1|\mathbf{T}|2 \rangle = \langle 1|\bar{2} \rangle$, etc., and $\langle 1|\mathbf{T^{-1}}|1 \rangle = \langle \bar{1}|1 \rangle, \ \langle 2|\mathbf{T^{-1}}|1 \rangle = \langle \bar{2}|1 \rangle$, etc. are the *transformation operator matrix components*. (Prove: $\langle 1|\mathbf{T}|1 \rangle = \langle \bar{1}|\mathbf{T}|\bar{1} \rangle, \ \langle 1|\mathbf{T}|2 \rangle = \langle \bar{1}|\mathbf{T}|\bar{2} \rangle$, etc.)

(e) Change of basis and eigenstate equations

It is always possible to introduce a new ket-basis $\{|\varepsilon_1\rangle, |\varepsilon_2\rangle\}$ that is a linear combination of the old basis $\{|1\rangle, |2\rangle\}$ and similarly for the bra-vectors. (See Appendix 3.B *Review of Change of Basis*)

$$|\varepsilon_k\rangle = \Sigma |j\rangle\langle j|\varepsilon_k\rangle, \quad \langle\varepsilon_k| = \Sigma\langle\varepsilon_k|j\rangle\langle j| \tag{2.3.11}$$

Then new coordinates $\{q_{\varepsilon_1}, q_{\varepsilon_2}\}$ will be the bra-combination of the old $\{q_1, q_2\}$. See Appendix (2.B.5).

$$q_{\varepsilon_k} \equiv \langle\varepsilon_k|q\rangle = \Sigma\langle\varepsilon_k|j\rangle\langle j|q\rangle = \Sigma\langle\varepsilon_k|j\rangle q_j \tag{2.3.12}$$

The equation of motion in the new basis is the same form as (2.3 10c) only it uses new bra-kets.

$$\sum_{k=1}^{2}\left[\langle\varepsilon_j|\mathbf{L}|\varepsilon_k\rangle\langle\varepsilon_k|\ddot{q}\rangle + \langle\varepsilon_j|\mathbf{R}|\varepsilon_k\rangle\langle\varepsilon_k|\dot{q}\rangle + \langle\varepsilon_j|\mathbf{K}|\varepsilon_k\rangle\langle\varepsilon_k|q\rangle\right] = \langle\varepsilon_j|f(t)\rangle \tag{2.3.13}$$

Here the new impedance components $\langle\varepsilon_j|\mathbf{Z}|\varepsilon_k\rangle$ are obtained from the old $\langle j|\mathbf{Z}|k\rangle$ using a basis transformation matrix $\langle\varepsilon_j|j\rangle$ and its inverse $\langle k|\varepsilon_k\rangle$. (See Appendix (2.B.6).)

$$\langle\varepsilon_j|\mathbf{Z}|\varepsilon_k\rangle = \sum_j\sum_k \langle\varepsilon_j|j\rangle\langle j|\mathbf{Z}|k\rangle\langle k|\varepsilon_k\rangle \tag{2.3.14}$$

A basis change is very helpful if all the impedance $\mathbf{Z}$-operators $\mathbf{L}$, $\mathbf{R}$, and $\mathbf{K}$ can be simultaneously *diagonalized*, so each $\mathbf{Z}$ is reduced to numbers only on its diagonal (*eigenvalues*) as described in (2.C.2).

$$\langle\varepsilon_j|\mathbf{Z}|\varepsilon_k\rangle = Z_k\delta_{jk} \tag{2.3.14}$$

Such is always possible for a frictionless coupled oscillator for which the resistance operator is zero $(\mathbf{R} = \mathbf{0})$ and the inertial operator is a unit matrix $(\mathbf{L} = \mathbf{1})$. Matrices $\mathbf{1}$ and $\mathbf{0}$ are invariant to a change of basis that diagonalizes a symmetric acceleration matrix $(\mathbf{K} = \mathbf{K}^\dagger)$ and such $\mathbf{K}$ are always diagonalizable.

In an eigenbasis $\{|\varepsilon_1\rangle, |\varepsilon_2\rangle\}$ in which (2.3.14) holds, the equations (2.3.13) decouple into two separate stimulated damped harmonic oscillator equations.

$$L_1\langle\varepsilon_1|\ddot{q}\rangle + R_1\langle\varepsilon_1|\dot{q}\rangle + K_1\langle\varepsilon_1|q\rangle = \langle\varepsilon_1|f(t)\rangle$$
$$L_2\langle\varepsilon_2|\ddot{q}\rangle + R_2\langle\varepsilon_2|\dot{q}\rangle + K_2\langle\varepsilon_2|q\rangle = \langle\varepsilon_2|f(t)\rangle \tag{2.3.15a}$$

If inertial eigenvalues $(L_k \neq 0)$ are non-zero then two equations of standard form (2.2.1) result.

$$\ddot{q}_{\varepsilon_1} + 2\Gamma_1\dot{q}_{\varepsilon_1} + \omega_0^2(\varepsilon_1)q_{\varepsilon_1} = a_{\varepsilon_1}(t) = \langle\varepsilon_1|a(t)\rangle$$
$$\ddot{q}_{\varepsilon_2} + 2\Gamma_2\dot{q}_{\varepsilon_2} + \omega_0^2(\varepsilon_2)q_{\varepsilon_2} = a_{\varepsilon_2}(t) = \langle\varepsilon_2|a(t)\rangle \tag{2.3.15b}$$

The decay constants Γ_k and eigenfrequencies $\omega_0(\varepsilon_k)$ are related to impedance eigenvalues.

$$2\Gamma_k = R_k/L_k \quad (2.3.15c) \qquad\qquad \omega_0^2(\varepsilon_k) = K_k/L_k \qquad (2.3.15d)$$

Accelerating stimuli are combinations of the f_1 and f_2, or a_1 and a_2 using transformation (2.3.12).

$$a_{\varepsilon_k}(t) = \frac{\langle\varepsilon_k|f\rangle}{L_k} = \frac{\sum_j\langle\varepsilon_k|j\rangle f_j(t)}{L_k} = \sum_j\langle\varepsilon_k|j\rangle a_j(t) \tag{2.3.15e}$$

Appendix 3.B Review of Change-of-Basis Transformations

First we find the effect of the transformation on the unit ket vectors. Consider a rotational transformation $\mathbf{T}=\mathbf{R}(\phi)$ that takes each Cartesian ket $\{|x\rangle,|y\rangle\}$ and maps it into a new rotated basis $\{|\bar{x}\rangle = \mathbf{T}|x\rangle, |\bar{y}\rangle = \mathbf{T}|y\rangle\}$ given by the following and shown in Fig. 2.B-1.

$$\{|\bar{x}\rangle = \mathbf{T}|x\rangle = \cos\phi|x\rangle + \sin\phi|y\rangle, \qquad |\bar{y}\rangle = \mathbf{T}|y\rangle = -\sin\phi|x\rangle + \cos\phi|y\rangle\} \quad (2.B.1)$$
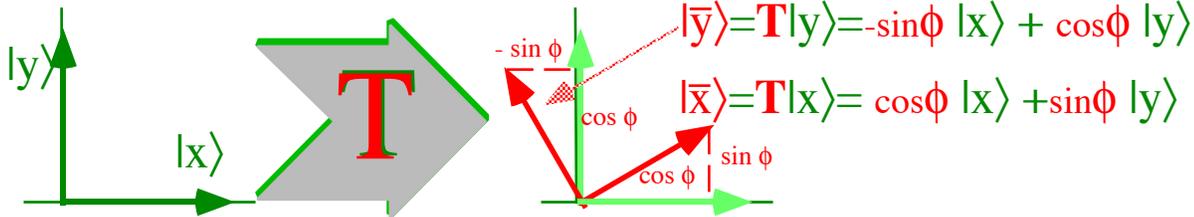
Fig. 2.B.1 Transformation $\mathbf{T}$ *maps unit kets into rotated ones*

Dotting (2.B.1) by bra $\langle x|$ and then by bra $\langle y|$ gives the four transformation matrix components.

$$\begin{pmatrix} \langle x|\bar{x}\rangle & \langle x|\bar{y}\rangle \\ \langle y|\bar{x}\rangle & \langle y|\bar{y}\rangle \end{pmatrix} = \begin{pmatrix} \langle x|\mathbf{T}|x\rangle & \langle x|\mathbf{T}|y\rangle \\ \langle y|\mathbf{T}|x\rangle & \langle y|\mathbf{T}|y\rangle \end{pmatrix} = \begin{pmatrix} \cos\phi & -\sin\phi \\ \sin\phi & \cos\phi \end{pmatrix} \quad (2.B.2)$$

The bras transform inversely to preserve orthonormality $\langle j|k\rangle = \delta_{jk} = \langle \bar{j}|\bar{k}\rangle$.

$$\{\langle\bar{x}| = \langle x|\mathbf{T}^{-1} = \langle x|\cos\phi + \langle y|\sin\phi, \qquad \langle\bar{y}| = \langle y|\mathbf{T}^{-1} = -\langle x|\sin\phi + \langle y|\cos\phi\} \quad (2.B.3)$$

Now it is a simple matter to derive the transformation rules for components of any ket vector $|\Psi\rangle$ that lives in this ket space. Remember that $|\Psi\rangle$ does not move. It is just expressed in two equivalent ways. (In other words, it has two "aliases" as shown below.)

$$|\Psi\rangle = |x\rangle\langle x|\Psi\rangle + |y\rangle\langle y|\Psi\rangle = |\bar{x}\rangle\langle\bar{x}|\Psi\rangle + |\bar{y}\rangle\langle\bar{y}|\Psi\rangle \quad (2.B.4)$$

Fig. 2.B.2 Same vector $|\Psi\rangle$ *with different coordinates*

Dot $\langle\bar{x}|$ in (2.B.3) on the right by $|\Psi\rangle$ or (2.B.4) on the left by $\langle\bar{x}|$ or $\langle\bar{y}|$ to get new coordinates.

$$\langle\bar{x}|\Psi\rangle = \langle\bar{x}|x\rangle\langle x|\Psi\rangle + \langle\bar{x}|y\rangle\langle y|\Psi\rangle = \cos\phi\langle x|\Psi\rangle - \sin\phi\langle y|\Psi\rangle$$
$$\langle\bar{y}|\Psi\rangle = \langle\bar{y}|x\rangle\langle x|\Psi\rangle + \langle\bar{y}|y\rangle\langle y|\Psi\rangle = \sin\phi\langle x|\Psi\rangle + \cos\phi\langle y|\Psi\rangle \quad (2.B.5)$$

The same expansion done twice gives a transformation of matrix operator components $\langle m|\mathbf{O}|n\rangle$.

$$\langle\bar{m}|\mathbf{O}|\bar{n}\rangle = \sum_m \sum_n \langle\bar{m}|m\rangle\langle m|\mathbf{O}|n\rangle\langle n|\bar{n}\rangle \quad (2.B.6)$$

In matrix form this is $\langle\bar{\mathbf{O}}\rangle = \langle\mathbf{TOT}^{-1}\rangle$. It is called a *similarity transformation*.

Appendix 3.C Review of Eigensolutions and Diagonalization

The *eigenvectors* $\{|\varepsilon_1\rangle, |\varepsilon_2\rangle, \cdots |\varepsilon_n\rangle\}$ of a matrix operator $\mathbf{M}$ are the most convenient basis for dealing with $\mathbf{M}$. An eigenvector $|\varepsilon_k\rangle$ of $\mathbf{M}$ is in a direction that is left unchanged by $\mathbf{M}$, that is

$$\mathbf{M}|\varepsilon_k\rangle = \varepsilon_k |\varepsilon_k\rangle, \quad \text{or:} \quad (\mathbf{M} - \varepsilon_k \mathbf{1})|\varepsilon_k\rangle = \mathbf{0}, \qquad (2.C.1)$$

where ε_k is the *eigenvalue* associated with that eigenvector $|\varepsilon_k\rangle$ direction. A change of basis to $\{|\varepsilon_1\rangle, |\varepsilon_2\rangle, \cdots |\varepsilon_n\rangle\}$ is called *diagonalization*. If $|\varepsilon_k\rangle$ are orthonormal by (2.A.3) then (2.C.1) is

$$\begin{pmatrix} \langle\varepsilon_1|\mathbf{M}|\varepsilon_1\rangle & \langle\varepsilon_1|\mathbf{M}|\varepsilon_2\rangle & \cdots & \langle\varepsilon_1|\mathbf{M}|\varepsilon_n\rangle \\ \langle\varepsilon_2|\mathbf{M}|\varepsilon_1\rangle & \langle\varepsilon_2|\mathbf{M}|\varepsilon_2\rangle & \cdots & \langle\varepsilon_2|\mathbf{M}|\varepsilon_n\rangle \\ \vdots & \vdots & \ddots & \vdots \\ \langle\varepsilon_n|\mathbf{M}|\varepsilon_1\rangle & \langle\varepsilon_n|\mathbf{M}|\varepsilon_2\rangle & \cdots & \langle\varepsilon_n|\mathbf{M}|\varepsilon_n\rangle \end{pmatrix} = \begin{pmatrix} \varepsilon_1 & 0 & \cdots & 0 \\ 0 & \varepsilon_2 & \cdots & 0 \\ \vdots & \vdots & \ddots & \vdots \\ 0 & 0 & \cdots & \varepsilon_n \end{pmatrix}. \qquad (2.C.2)$$

The first step in finding solutions to (2.C.1) is to solve or factor the *secular equation*

$$\det|\mathbf{M} - \varepsilon\mathbf{1}| = 0 = (-1)^n \left(\varepsilon^n + a_1\varepsilon^{n-1} + a_2\varepsilon^{n-2} + \ldots + a_{n-1}\varepsilon + a_n\right) \qquad (2.C.3)$$

where: $a_1 = -Trace\mathbf{M}, \cdots, a_k = (-1)^k \sum \text{diagonal k-by-k minors of } \mathbf{M}, \cdots, a_n = (-1)^n \det|\mathbf{M}|$

The secular equation has *n*-factors, one for each eigenvalue.

$$\det|\mathbf{M} - \varepsilon\mathbf{1}| = 0 = (-1)^n (\varepsilon - \varepsilon_1)(\varepsilon - \varepsilon_2)\cdots(\varepsilon - \varepsilon_n) \qquad (2.C.4)$$

If each ε in (2.C.4) is replaced by $\mathbf{M}$ and each ε_k by $\varepsilon_k \mathbf{1}$ then the following matrix equation results.

$$\mathbf{0} = (\mathbf{M} - \varepsilon_1\mathbf{1})(\mathbf{M} - \varepsilon_2\mathbf{1})\cdots(\mathbf{M} - \varepsilon_n\mathbf{1}) \qquad (2.C.5)$$

This is obviously true if $\mathbf{M}$ has the diagonal form (2.C.2). (But, that is circular logic since one needs to *prove* the diagonal form.) (2.C.4) is known as the *Hamilton-Cayley equation* or *theorem*.

To obtain eigenvectors we construct *projection operators* $\mathbf{p}_j$ by replacing j^{th} factor from (2.C.5) by unit matrix ($\mathbf{1}$) as follows. (Assume <u>distinct</u> eigenvalues $\varepsilon_1 \neq \varepsilon_2 \neq \ldots$ here.)

$$\mathbf{p}_1 = (\quad \mathbf{1} \quad)(\mathbf{M} - \varepsilon_2\mathbf{1})\cdots(\mathbf{M} - \varepsilon_n\mathbf{1})$$
$$\mathbf{p}_2 = (\mathbf{M} - \varepsilon_1\mathbf{1})(\quad \mathbf{1} \quad)\cdots(\mathbf{M} - \varepsilon_n\mathbf{1})$$
$$\vdots \qquad\qquad\qquad (2.C.6)$$
$$\mathbf{p}_n = (\mathbf{M} - \varepsilon_1\mathbf{1})(\mathbf{M} - \varepsilon_2\mathbf{1})\cdots(\quad \mathbf{1} \quad) \quad \text{or:} \quad \mathbf{p}_k = \prod_{j \neq k} (\mathbf{M} - \varepsilon_j\mathbf{1})$$

Each operator $\mathbf{p}_k$ has the delightful property that it contains <u>ket eigenvectors</u> $|\varepsilon_k\rangle$ in its <u>columns</u> and <u>bra eigenvectors</u> $\langle\varepsilon_k|$ in its <u>rows</u>, that is, the $\mathbf{p}_k$ solve the original eigenvector equation (2.C.1).

$$(\mathbf{M} - \varepsilon_k \mathbf{1}) \mathbf{p}_k = \mathbf{0} \quad \text{or:} \quad \mathbf{M} \mathbf{p}_k = \varepsilon_k \mathbf{p}_k = \mathbf{p}_k \mathbf{M} \qquad (2.C.7)$$

We may normalize $\mathbf{p}_k$ operators to make the *idempotent projection operators* $\mathbf{P}_k$ defined by

$$\mathbf{P}_k = \frac{\prod_{j \neq k} (\mathbf{M} - \varepsilon_j\mathbf{1})}{\prod_{j \neq k} (\varepsilon_k - \varepsilon_j)} = |\varepsilon_k\rangle\langle\varepsilon_k| \quad \text{where:} \quad \mathbf{P}_j\mathbf{P}_k = \delta_{jk} \mathbf{P}_k, \text{ and } \mathbf{P}_1 + \mathbf{P}_2 + \ldots + \mathbf{P}_n = \mathbf{1} \qquad (2.C.8)$$

for <u>distinct</u> eigenvalues. The *projection ortho-completeness relations* are given in (2.C.8).

(f) Quadratic forms

The matrix form for potential (2.3.1) is a *quadratic form* first defined in Ch. 2 and Ch. 9 of Unit 1.

$$V = \sum_{i=1}^{2} \sum_{j=1}^{2} \frac{1}{2} x_i K_{ij} x_j = \frac{1}{2} \mathbf{x} \cdot \mathbf{K} \cdot \mathbf{x} \tag{2.3.16}$$

(Recall spring matrix K_{ij} .) Dirac notation for Cartesian coordinates $\langle j|x\rangle \equiv x_j$ gives V as follows.

$$V = \sum_{i=1}^{2} \sum_{j=1}^{2} \frac{1}{2} \langle x|i\rangle\langle i|\mathbf{K}|j\rangle\langle j|x\rangle = \frac{1}{2}\langle x|\mathbf{K}|x\rangle . \tag{2.3.17}$$

If eigenvectors $\{|\varepsilon_1\rangle,|\varepsilon_2\rangle\}$ of $\mathbf{K}$ replace Cartesian bases $\{|1\rangle,|2\rangle\}$ then $\mathbf{K}$ is diagonal ($\langle\varepsilon_i|\mathbf{K}|\varepsilon_j\rangle = \delta_{ij} K_j$).

$$V = \sum_{i=1}^{2} \sum_{j=1}^{2} \frac{1}{2} \langle x|\varepsilon_i\rangle\langle\varepsilon_i|\mathbf{K}|\varepsilon_j\rangle\langle\varepsilon_j|x\rangle = \frac{1}{2}\langle x|\mathbf{K}|x\rangle = \frac{1}{2}\mathbf{x} \cdot \mathbf{K} \cdot \mathbf{x} \tag{2.3.18}$$

This simplifies V to a diagonal sum of squares of *normal coordinates* $q_{\varepsilon_j} \equiv \langle x|\varepsilon_i\rangle$.

$$V = \sum_{i=1}^{2} \sum_{j=1}^{2} \frac{1}{2} q_{\varepsilon_i} \delta_{ij} K_j q_{\varepsilon_j} = \frac{1}{2} \sum_{j=1}^{2} K_j q_{\varepsilon_j}^2 = \frac{1}{2}(K_1 q_1^2 + K_2 q_2^2) \tag{2.3.19}$$

For constant V these are equations for elliptical level curves in the valley shown in Fig. 2.3.4 and 3.3.5.
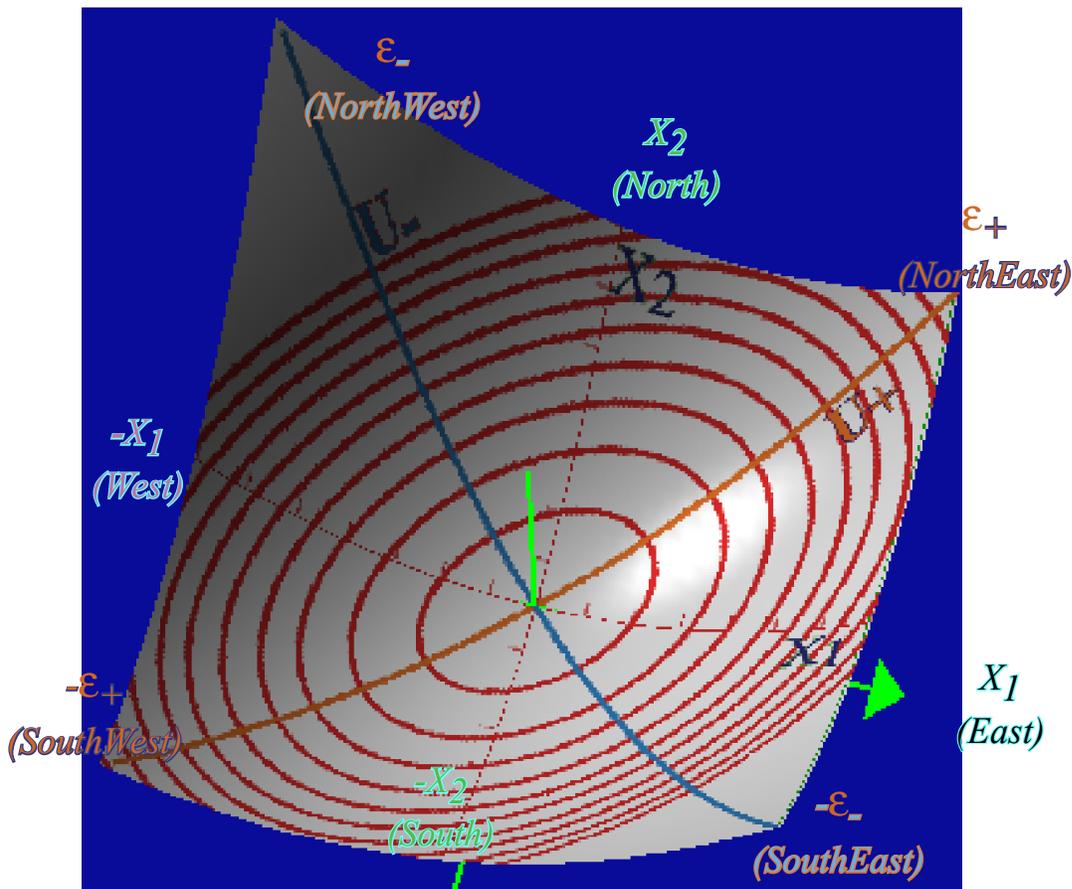
Fig. 2.3.4 Plot of potential function V(x₁,x₂) showing elliptical V(x₁,x₂)=const. level curves.

The concentric ellipses are topographical lines *V=const.* for an elliptical paraboloid that is like a "ski-bowl" with major (North-East) and minor (South-East) axes along eigenvectors $\{|\varepsilon_1\rangle = |\varepsilon_+\rangle, |\varepsilon_2\rangle = |\varepsilon_-\rangle\}$ of $\mathbf{K}$.
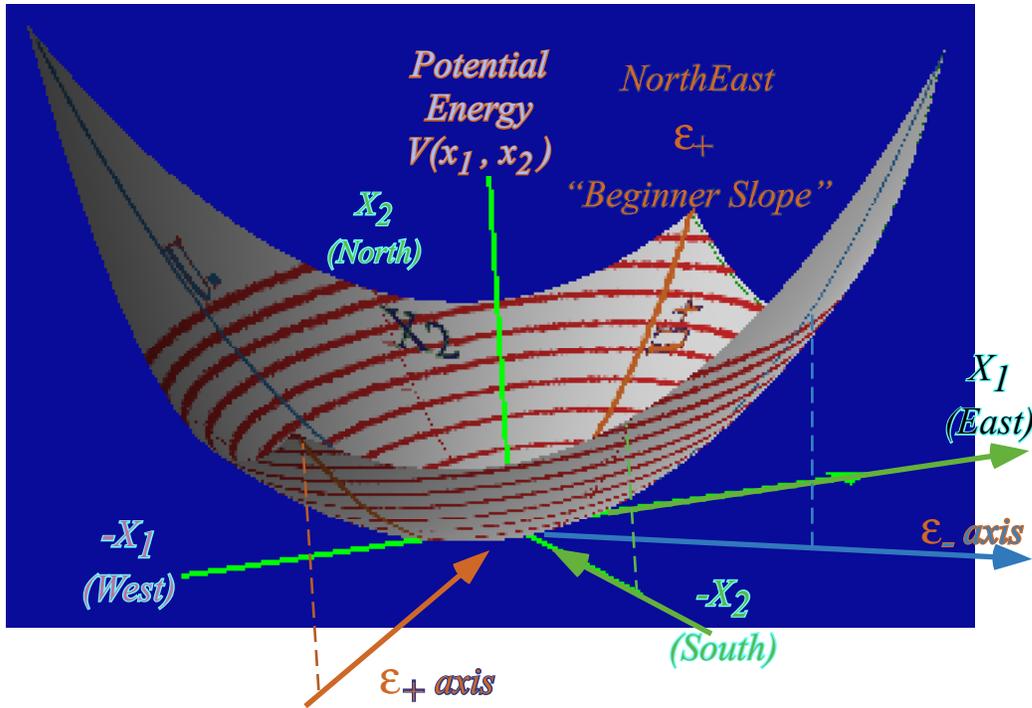
Fig. 2.3.5 Topography lines of potential function $V(x_1,x_2)$ and orthogonal ε_+ and ε_- normal mode slopes

One can visualize coupled oscillator motion by imagining a mass sliding in the elliptical bowl in Fig. 2.3.5. A mass moves on a straight line if it is dropped on the major $\varepsilon_1 = \varepsilon_+$ axis ("Beginner Slope") or on the minor $\varepsilon_2 = \varepsilon_-$ axis ("Advanced Slope") of the ellipses. It will go back and forth on an eigenvector axis forever since the force gradient is always along the axis. The frequency of oscillation $\omega_0(\varepsilon_1)$ for major axis is lower than $\omega_0(\varepsilon_2)$ for the minor axis since the potential slope is least along ε_1 and greatest along ε_2. In fact, the eigenvectors represent extreme values for a quadratic form expression.

$$\frac{\langle x|\mathbf{K}|x\rangle}{\langle x|x\rangle} = \begin{cases} \text{is minimum for } |x\rangle = |\varepsilon_1\rangle \\ \text{is maximum for } |x\rangle = |\varepsilon_2\rangle \end{cases} \tag{2.3.20}$$

Eigenvalues of $\mathbf{K} = \begin{pmatrix} K_{11} & K_{12} \\ K_{12} & K_{22} \end{pmatrix} = \begin{pmatrix} (k_1 + k_{12})/m_1 & -k_{12}/\sqrt{m_1 m_2} \\ -k_{12}/\sqrt{m_1 m_2} & (k_2 + k_{12})/m_2 \end{pmatrix}$ are solutions to secular equation (2.C.3)

$$K^2 - (Trace\,\mathbf{K})K + \det |\mathbf{K}| = 0 \tag{2.3.21}$$

$$K_1 = \left(K_{11} + K_{22} - \sqrt{(K_{11} - K_{22})^2 + 4K_{12}^2} \right)/2, \qquad K_2 = \left(K_{11} + K_{22} + \sqrt{(K_{11} - K_{22})^2 + 4K_{12}^2} \right)/2.$$

The normal mode eignevectors are then given from (2.C.6) and (2.C.7).

$$|\varepsilon_1\rangle = \begin{pmatrix} K_{11} - K_2 \\ K_{12} \end{pmatrix} / norm(1) \quad (2.3.22b) \qquad |\varepsilon_2\rangle = \begin{pmatrix} K_{11} - K_1 \\ K_{12} \end{pmatrix} / norm(2) \quad (2.3.22b)$$

The two normal coordinates oscillate independently of each other according to (2.3.15b). Each parabolic ε_1 section of the $V(\varepsilon_1, \varepsilon_2)$ paraboloid has the same shape regardless of its ε_2 coordinate and *visa-versa*. So the force f_1 along ε_1 direction depends only on coordinate ε_1 and not on ε_2 and *visa-versa* for f_2.

(g) Normal coordinates and modes

We consider an example of a frictionless oscillator (2.3.2) with equal masses $m_1 = 1 = m_2$ and spring constants $k_1 = 7 - 3\sqrt{3}$, $k_2 = 13 - 3\sqrt{3}$, and $k_{12} = 3\sqrt{3}$. With $\mathbf{L} = 1$ and $\mathbf{R} = 0$ we are left with only the spring constant matrix $\mathbf{K}$ to diagonalize. Using (2.3.8-9) we find $\mathbf{K}$. (See Exercise 2.3.3)

$$\mathbf{K} = \begin{pmatrix} K_{11} & K_{12} \\ K_{12} & K_{22} \end{pmatrix} = \begin{pmatrix} 7 & -3\sqrt{3} \\ -3\sqrt{3} & 13 \end{pmatrix} \qquad (2.3.23)$$

The secular equation $K^2 - 20K + 64 = 0$ has as roots eigenvalues K_k and squared eigenfrequencies $\omega_0(\varepsilon_k)^2$

$$K_1 = \omega_0^2(\varepsilon_1) = 4, \quad K_2 = \omega_0^2(\varepsilon_2) = 16, \qquad (2.3.14)_{\text{Example}}$$

with eigenbra vectors

$$\langle \varepsilon_1 | = \begin{pmatrix} \sqrt{3}/2 & 1/2 \end{pmatrix}, \quad \langle \varepsilon_2 | = \begin{pmatrix} -1/2 & \sqrt{3}/2 \end{pmatrix} \qquad (2.3.11)_{\text{Example}}$$

From this we derive *normal coordinates* $\left(q_{\varepsilon_1} = \langle \varepsilon_1 | x \rangle, q_{\varepsilon_2} = \langle \varepsilon_2 | x \rangle \right)$ in terms of old $\left(x_1 = \langle 1 | x \rangle, x_2 = \langle 2 | x \rangle \right)$.

$$q_{\varepsilon_1} = \frac{\sqrt{3}}{2} x_1 + \frac{1}{2} x_2 = \langle \varepsilon_1 | x \rangle$$

$$q_{\varepsilon_2} = -\frac{1}{2} x_1 + \frac{\sqrt{3}}{2} x_2 = \langle \varepsilon_2 | x \rangle \qquad (2.3.12)_{\text{Example}}$$

The old coupled equations of motion need to be uncoupled by normal mode transformation.

$$\begin{pmatrix} \ddot{x}_1 \\ \ddot{x}_2 \end{pmatrix} + \begin{pmatrix} 7 & -3\sqrt{3} \\ -3\sqrt{3} & 13 \end{pmatrix} \begin{pmatrix} x_1 \\ x_2 \end{pmatrix} = \begin{pmatrix} a_1 \\ a_2 \end{pmatrix}, \qquad (2.3.25)$$

They are uncoupled equations in new coordinates and with new stimulus components $a_{\varepsilon_j} = \langle \varepsilon_j | a \rangle$,

$$\ddot{q}_{\varepsilon_1} + 4 q_{\varepsilon_1} = \langle \varepsilon_1 | a \rangle = a_{\varepsilon_1}$$

$$\ddot{q}_{\varepsilon_2} + 16 q_{\varepsilon_2} = \langle \varepsilon_2 | a \rangle = a_{\varepsilon_2}. \qquad (2.3.15b)_{\text{Example}}$$

The stimulus transformation is the same as the coordinate transformation (2.13.12) above.

$$a_{\varepsilon_1} = \langle \varepsilon_1 | a \rangle = \langle \varepsilon_1 | 1 \rangle a_1 + \langle \varepsilon_1 | 2 \rangle a_2 = \frac{\sqrt{3}}{2} a_1 + \frac{1}{2} a_2$$

$$a_{\varepsilon_2} = \langle \varepsilon_2 | a \rangle = \langle \varepsilon_2 | 1 \rangle a_1 + \langle \varepsilon_2 | 2 \rangle a_2 = -\frac{1}{2} a_1 + \frac{\sqrt{3}}{2} a_2. \qquad (2.3.15d)_{\text{Example}}$$

In the absence of stimuli $\left(a_1 = 0 = a_2 \right)$, equations $(2.3.15)_{\text{Example}}$ predict simple harmonic motions in two orthogonal directions $| \varepsilon_1 \rangle$ and $| \varepsilon_2 \rangle$ that are called *normal modes* of vibration.

$$| x(t) \rangle = q_{\varepsilon_1}(t) | \varepsilon_1 \rangle + q_{\varepsilon_2}(t) | \varepsilon_2 \rangle, \text{ where: } q_{\varepsilon_k}(t) = A_k \cos \left(\omega(\varepsilon_k) t + \alpha_k \right) \qquad (2.3.26)$$

The coordinates $\left(q_{\varepsilon_1}, q_{\varepsilon_2} \right)$ along these directions are called *normal coordinates* and their axes are drawn in Fig. 2.3.3. They lie along eigenvector directions tipped at 30°:

$$| \varepsilon_1 \rangle = \frac{\sqrt{3}}{2} | 1 \rangle + \frac{1}{2} | 2 \rangle, \quad | \varepsilon_2 \rangle = -\frac{1}{2} | 1 \rangle + \frac{\sqrt{3}}{2} | 2 \rangle. \qquad (2.3.27)$$

ω1 = 2
ω2 = 4
Θ = 30°

k12 = -5.1961524
k22 =   13
k11 =   7
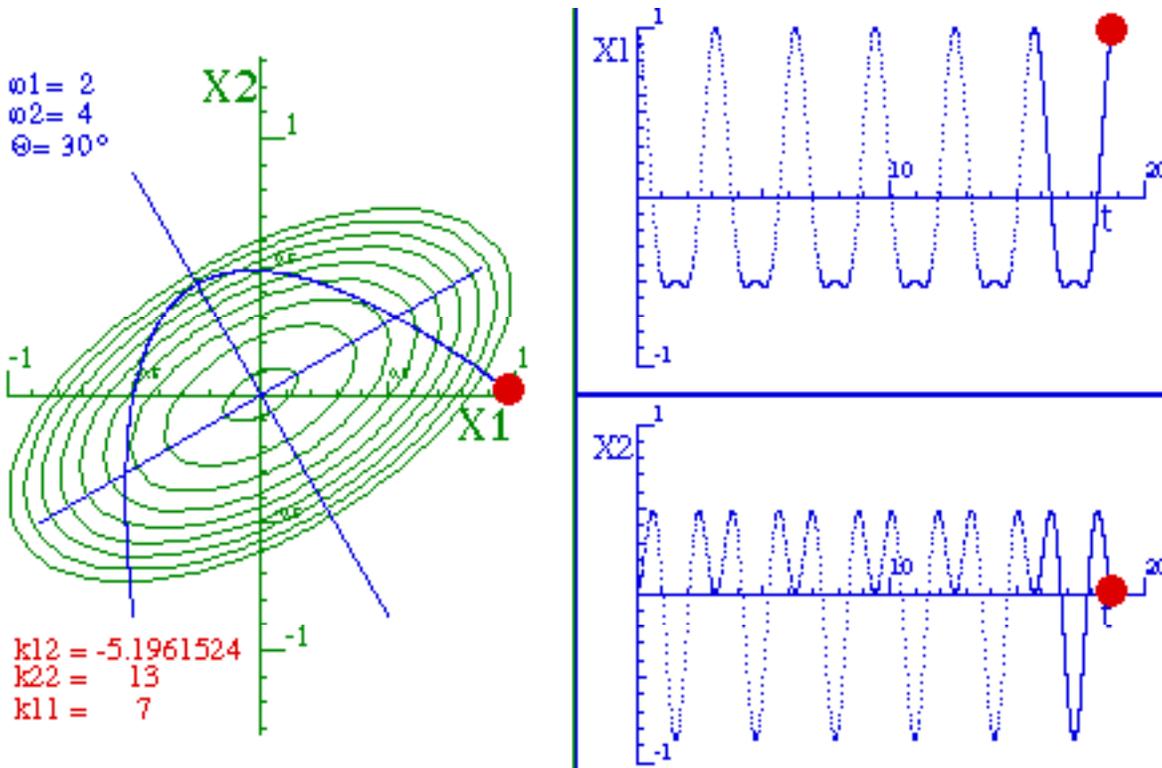
Fig. 2.3.6 Normal coordinate axes, coupled oscillator trajectories and equipotential (V=const.) ovals for an integral 1:2 eigenfrequency ratio (ω₀(ε₁)=2.0, ω₀(ε₂)= 4.0) and zero initial velocity.

In this example, the eigenfrequency is $\omega_0(\varepsilon_1) = \sqrt{K_1} = 2.0$ for q_{ε_1} oscillations and $\omega_0(\varepsilon_2) = \sqrt{K_2} = 4.0$ for

q_{ε_2} oscillation for a ratio of exactly 2:1 between $\omega_0(\varepsilon_1)$ and $\omega_0(\varepsilon_2)$. Because of this, the trajectory in $\left(q_{\varepsilon_1}, q_{\varepsilon_2} \right)$

space executes two oscillations in the q_{ε_2} direction for every one q_{ε_1} oscillation as shown in Fig. 2.3.6. The

initial values which give this trajectory are $\left(x_1(0) = 1, x_2(0) = 0 \right)$ for the primitive coordinates, and ($q_{\varepsilon_1}(0) = \sqrt{3}/2$,

$q_{\varepsilon_2}(0) = -1/2$) for the normal coordinates. The initial velocities are assumed zero, here. Then each normal

coordinate oscillates simply and independently of the other. Time parametric equations for the resulting normal

coordinate oscillation are as follows:

$$\left(q_{\varepsilon_1}(t) = \frac{\sqrt{3}}{2} \cos 2t, \quad q_{\varepsilon_2}(t) = -\frac{1}{2} \cos 4t \right). \tag{2.3.28a}$$

From $\cos 2x = 2\cos^2 x - 1$ one derives the parabolic trajectory seen in Fig. 2.3.6.

$$q_{\varepsilon_2} = -\frac{1}{2} 2\cos^2 2t + \frac{1}{2} = -\frac{4}{3} q_{\varepsilon_1}^2 + \frac{1}{2} \tag{2.3.28b}$$

Trajectories generated by two normal modes having rational frequency ratios are called *Lissajous figures.* If the

ratio is an integer (and $\dot{q}_j(0) = 0$) the trajectories are given by simple polynomials such as (2.3.28). These are

closely related to *Chebyshev* polynomials. (See Exercise 2.3.4) For non-zero initial velocity the trajectory

makes a loop as shown in Fig. 2.3.7. But, it is still a *closed* or *periodic* trajectory. It always returns home exactly

with a precise period *(2π/ω₁=π here.).*
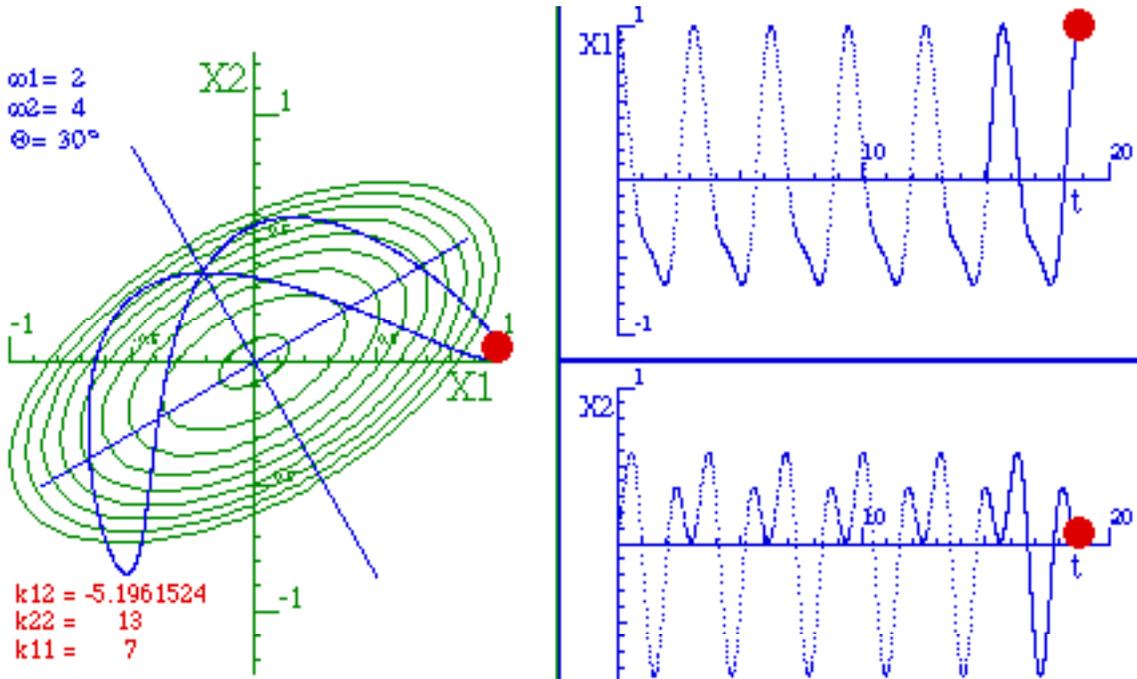
Fig. 2.3.7 Same as Fig. 2.3.6 with non-zero initial velocity.

Now we change k_{11} from 7 to 6.876. The mode trajectories weave a complex pattern that densely fills a rectangle aligned with the normal coordinate axes as shown in Fig. 2.3.8.
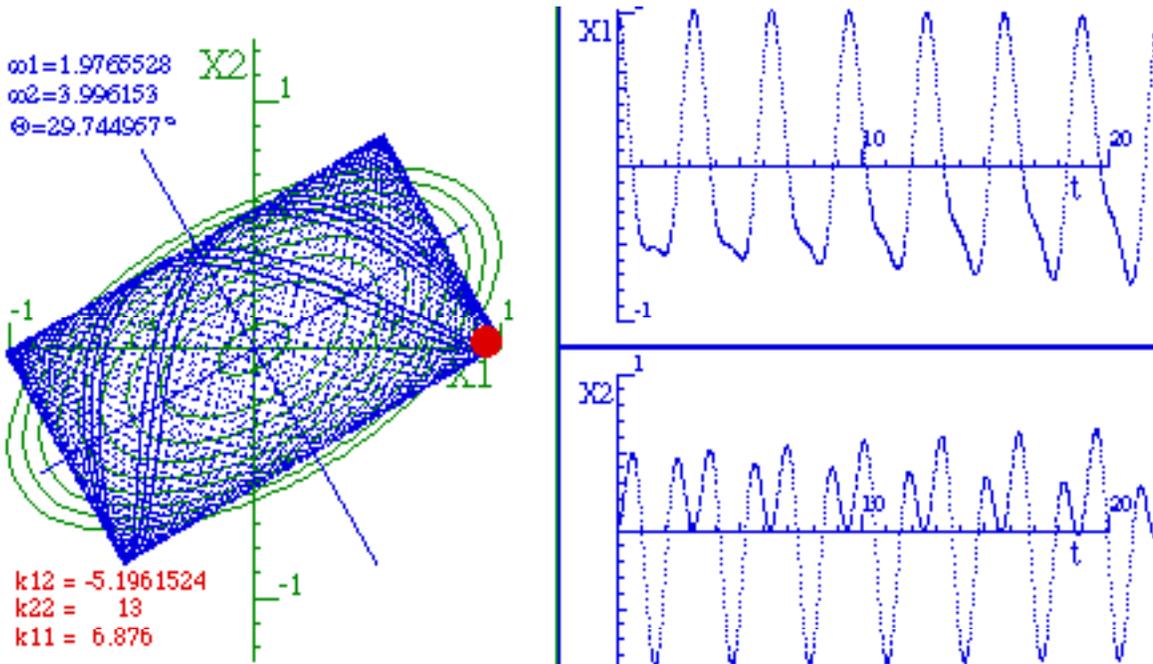
Fig. 2.3.8 Like Fig. 2.3.6 but has irrational $\omega_2:\omega_1=2.0218..$ratio due to changing k_{11} slightly.

This is an example of a more typical *open* or *quasi-periodic* trajectory. The usual coupled oscillator trajectory lacks integral or rational frequency ratios so it may not ever quite return to the same coordinate or phase point. It almost returns after each π sec. but not quite! Instead, it evolves through a series of shapes including ones that

temporarily resemble the parabola seen in Fig. 2.3.6 and then the loop seen in Fig. 2.3.7. If you wait long enough you can find it repeating itself to an arbitrary degree of accuracy. This so-called *Poincare period* will be discussed later.

First, we must discuss *beat periods*. With more nearly equal eigenfrequencies, the time plot of $x_1(t)$ and $x_2(t)$ exhibit obvious *beating* or *modulation* as seen in Fig. 2.3.9 below.
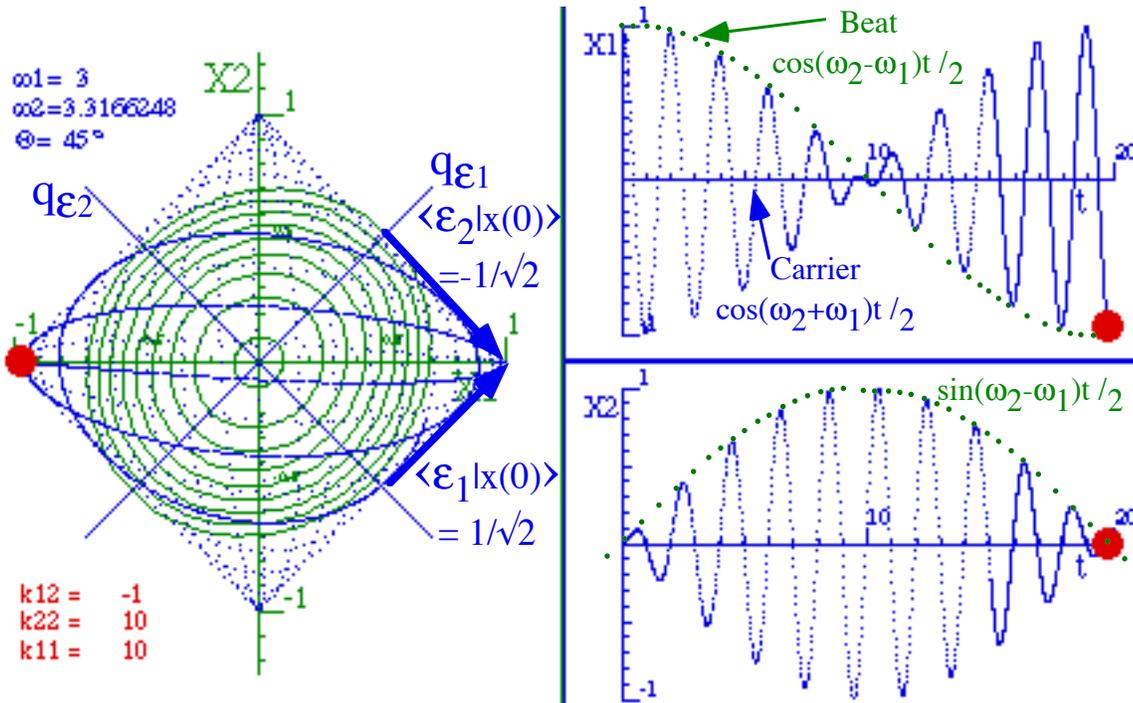
Fig. 2.3.9 Beats in weakly coupled symmetric oscillators with equal mode magnitudes.

The acceleration matrix for this example is $\mathbf{K} = \begin{pmatrix} K_{11} & K_{12} \\ K_{12} & K_{22} \end{pmatrix} = \begin{pmatrix} 10 & -1 \\ -1 & 10 \end{pmatrix}$ $(2.3.9)_{\text{Example 2}}$

Its eigenvalues K_k and squared eigenfrequencies $\omega_0(\varepsilon_k)^2$ are

$$K_1 = \omega_0^2(\varepsilon_1) = 9, \quad K_2 = \omega_0^2(\varepsilon_2) = 11,$$ $(2.3.14)_{\text{Example 2}}$

with eigenbra vectors located at $\pm 45°$ relative to x_1 and x_2 axes as seen in Fig. 2.3.7.

$$\langle\varepsilon_1| = \begin{pmatrix} 1/\sqrt{2} & 1/\sqrt{2} \end{pmatrix}, \quad \langle\varepsilon_2| = \begin{pmatrix} 1/\sqrt{2} & -1/\sqrt{2} \end{pmatrix}$$ $(2.3.11)_{\text{Example 2}}$

Let us use complex normal coordinates $\left(q_{\varepsilon_1}(t) = \langle\varepsilon_1|x(t)\rangle, \ q_{\varepsilon_2}(t) = \langle\varepsilon_2|x(t)\rangle\right)$ to describe the motion in the Fig. 2.3.9. Each coordinate is an independent phasor rotating at its assigned eigenfrequency $\omega_1 = \omega_0(\varepsilon_1) = 3$ or $\omega_2 = \omega_0(\varepsilon_2) = \sqrt{11} = 3.3166$, respectively.

$$\left(q_{\varepsilon_1}(t) = \langle\varepsilon_1|x(t)\rangle = \langle\varepsilon_1|x(0)\rangle e^{-i\omega_1 t}, \ q_{\varepsilon_2}(t) = \langle\varepsilon_2|x(t)\rangle = \langle\varepsilon_2|x(0)\rangle e^{-i\omega_2 t}\right)$$ $(2.3.29)$

The resulting coordinate vector is, by completeness (2.A.5),

$$|x(t)\rangle = |\varepsilon_1\rangle\langle\varepsilon_1|x(t)\rangle + |\varepsilon_2\rangle\langle\varepsilon_2|x(t)\rangle = |\varepsilon_1\rangle\langle\varepsilon_1|x(0)\rangle e^{-i\omega_1 t} + |\varepsilon_2\rangle\langle\varepsilon_2|x(0)\rangle e^{-i\omega_2 t}$$ $(2.3.30a)$

In vector notation

$$|x(t)\rangle = |\varepsilon_1\rangle \ \langle\varepsilon_1|x(0)\rangle e^{-i\omega_1 t} + \ |\varepsilon_2\rangle \ \langle\varepsilon_2|x(0)\rangle e^{-i\omega_2 t}$$

$$\begin{pmatrix} x_1(t) \\ x_2(t) \end{pmatrix} = \begin{pmatrix} 1/\sqrt{2} \\ 1/\sqrt{2} \end{pmatrix}\langle\varepsilon_1|x(0)\rangle e^{-i\omega_1 t} + \begin{pmatrix} -1/\sqrt{2} \\ 1/\sqrt{2} \end{pmatrix}\langle\varepsilon_2|x(0)\rangle e^{-i\omega_2 t} \tag{2.3.30b}$$

The initial coordinates ($x_1(0)=1$ and $x_2(0)=0$) for Fig. 2.3.9 give initial normal coordinates

$$\left(q_{\varepsilon_1}(0)=\langle\varepsilon_1|x(0)\rangle=1/\sqrt{2}, \ q_{\varepsilon_2}(0)=\langle\varepsilon_2|x(0)\rangle=-1/\sqrt{2} \right) \tag{2.3.30c}$$

Let us use the *expo-trig relation* $e^{ia} \pm e^{ib} = e^{i(a+b)/2} (e^{i(a-b)/2} \pm e^{-i(a-b)/2})$ so each component factors.

$$\begin{pmatrix} x_1(t) \\ x_2(t) \end{pmatrix} = \begin{pmatrix} \dfrac{e^{-i\omega_1 t} + e^{-i\omega_2 t}}{2} \\ \dfrac{e^{-i\omega_1 t} - e^{-i\omega_2 t}}{2} \end{pmatrix} = \dfrac{e^{-i\frac{(\omega_1+\omega_2)}{2}t}}{2}\begin{pmatrix} e^{-i\frac{(\omega_1-\omega_2)}{2}t} + e^{i\frac{(\omega_1-\omega_2)}{2}t} \\ e^{-i\frac{(\omega_1-\omega_2)}{2}t} - e^{i\frac{(\omega_1-\omega_2)}{2}t} \end{pmatrix} = e^{-i\frac{(\omega_1+\omega_2)}{2}t}\begin{pmatrix} \cos\dfrac{(\omega_2-\omega_1)t}{2} \\ i\sin\dfrac{(\omega_2-\omega_1)t}{2} \end{pmatrix} \tag{2.3.30d}$$

The factors $\cos(\omega_2-\omega_2)t/2$ and $i\sin(\omega_2-\omega_2)t/2$ above are slow *beat waves* seen on top and bottom of Fig. 2.3.9. Each long beat contains shorter *carrier waves* $e^{-i(\omega_1+\omega_2)t/2}$ with a higher frequency

$$\omega_{\text{carrier}}=(\omega_2+\omega_1)/2 \ (=3.156 \sim 1/2\,Hz \text{ in Fig. 2.3.7}) \tag{2.3.31}$$

that is the <u>average</u> of the two eigenfrequencies. The carriers suffer *amplitude modulation (AM)* with a lower frequency that is the <u>difference</u> of the two eigenfrequencies,

$$\omega_{\text{beat}}=\omega_2-\omega_1 \ (=0.3166 \sim 1/20\,Hz \text{ in Fig. 2.3.7}) \tag{2.3.32}$$

That is about 10 carrier waves per beat, as seen in Fig. 2.3.9 and in Fig. 2.3.10 below.
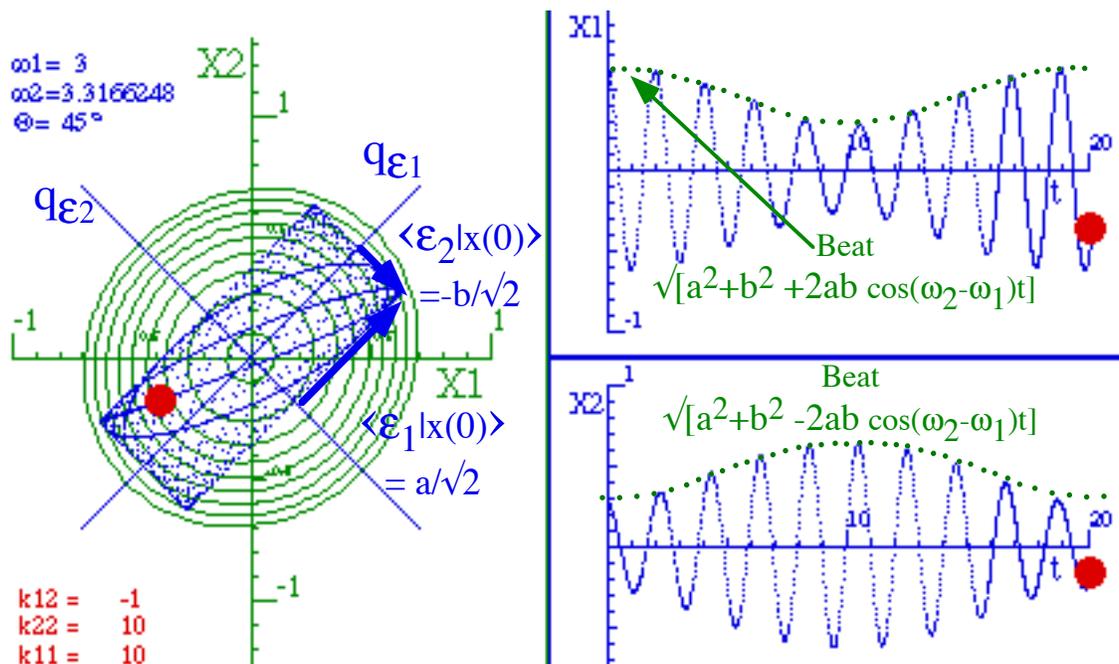
Fig. 2.3.10 Same as Fig. 2.3.9 but mode-1 magnitude a/√2 is greater than b/√2 for mode-2.

Note we use $(\omega_2-\omega_1)$ not $(\omega_2-\omega_1)/2$ for ω_{beat}. The latter is the frequency of a *double beat* or two groups that would be seen if Fig. 2.3.9 ran another 20 sec. Fig. 2.3.10 shows why ω_{beat} is used instead of $\omega_{\text{beat}}/2$. The coordinates factor only for equal mode amplitudes. Otherwise we have

$$
\begin{pmatrix} x_1(t) \\ x_2(t) \end{pmatrix} = \begin{pmatrix} \dfrac{ae^{-i\omega_1 t} + be^{-i\omega_2 t}}{2} \\[2mm] \dfrac{ae^{-i\omega_1 t} - be^{-i\omega_2 t}}{2} \end{pmatrix} = \begin{pmatrix} \dfrac{\sqrt{a^2 + b^2 + 2ab\cos(\omega_1 - \omega_2)t}}{2} \quad e^{i\Omega_1 t} \\[2mm] \dfrac{\sqrt{a^2 + b^2 - 2ab\cos(\omega_1 - \omega_2)t}}{2} \quad e^{i\Omega_2 t} \end{pmatrix}
\tag{2.3.33}
$$

Here the amplitude factor oscillates at $(\omega_2 - \omega_1)$ not $(\omega_2 - \omega_1)/2$ while the phase factors $e^{i\Omega t}$ vary the carrier frequency from high to low when the amplitude goes through a minimum. Compare Fig. 2.3.9 where the carrier is a constant frequency of about 1 Hz. to Fig. 2.3.10 or 3.3.11 below where the carrier frequency slows down at the beat minimum.
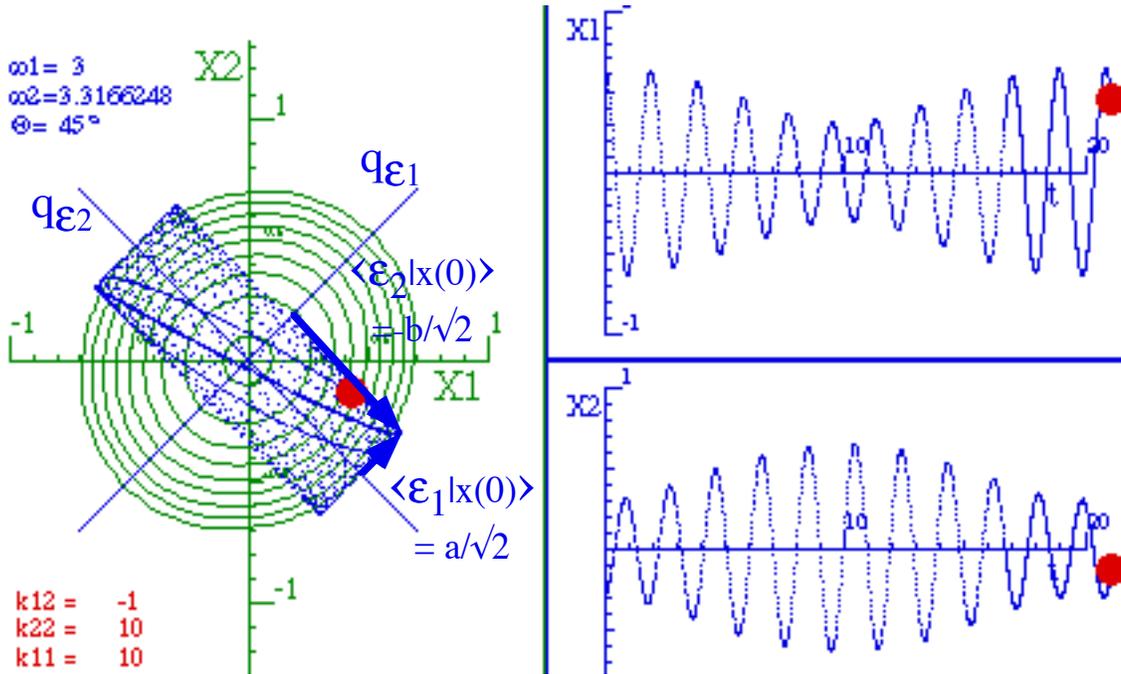
Fig. 2.3.11 Same as Fig. 2.3.9 but mode-1 magnitude $a/\sqrt{2}$ is less than $b/\sqrt{2}$ for mode-2.

The coordinate $|x\rangle$ is a combination (2.3.26) of two normal coordinate vectors $|\varepsilon_1\rangle$ and $|\varepsilon_2\rangle$ or normal modes. Pure normal modes oscillate at eigenfrequencies $\omega_1 = \omega_0(\varepsilon_1)$ or $\omega_2 = \omega_0(\varepsilon_2)$, as shown in Fig. 2.3.12 a and b respectively. Combinations of the modes such as Figs. 3.3.9-11 have beats that go up and down at their *relative* angular velocity, i.e. the difference (2.3.32). The *beat period* is 2π over ω_{beat} or about 20 in Figs. 3.3.9-11 above.

$$
\tau_{\text{beat}} = 2\pi / \omega_{\text{beat}} = 2\pi / |\omega_2 - \omega_1| \quad (= 19.85 \text{ in Fig. 2.3.9})
\tag{2.3.34}
$$

Beats seen in these figures are similar to the beats between stimulus and response seen in Fig. 2.2.8 and described by (2.2.21).

(a) Lower frequency symmetric mode

ω1= 3
ω2=3.3166248
Θ= 45°

k12 =   -1
k22 =   10
k11 =   10
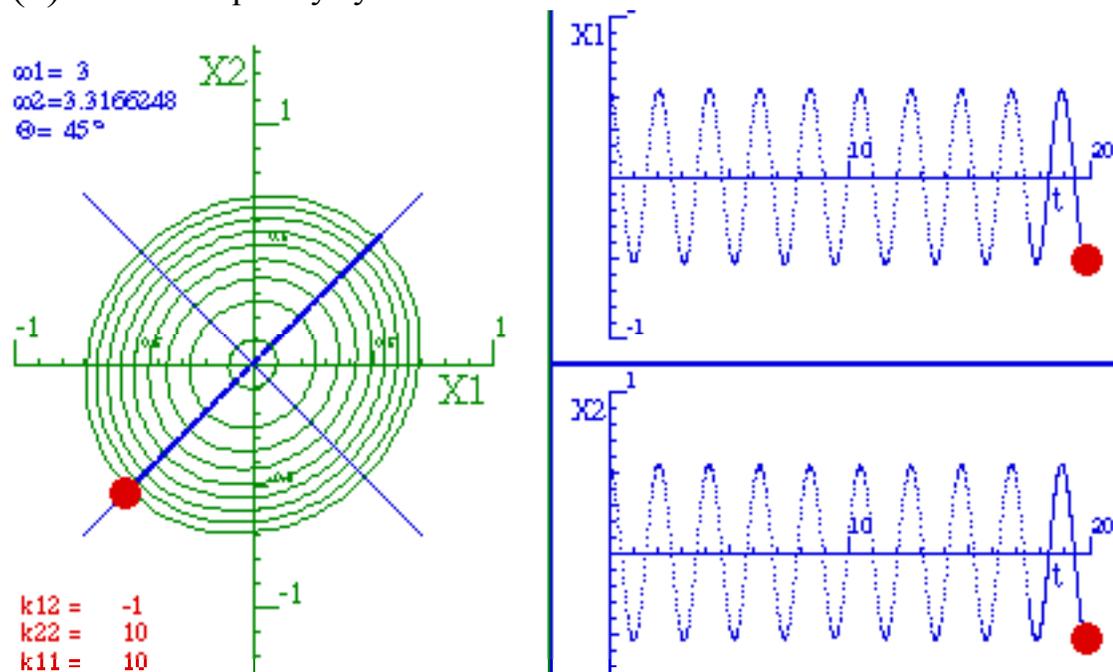
(b) Higher frequency anti symmetric mode

ω1= 3
ω2=3.3166248
Θ= 45°

k12 =   -1
k22 =   10
k11 =   10
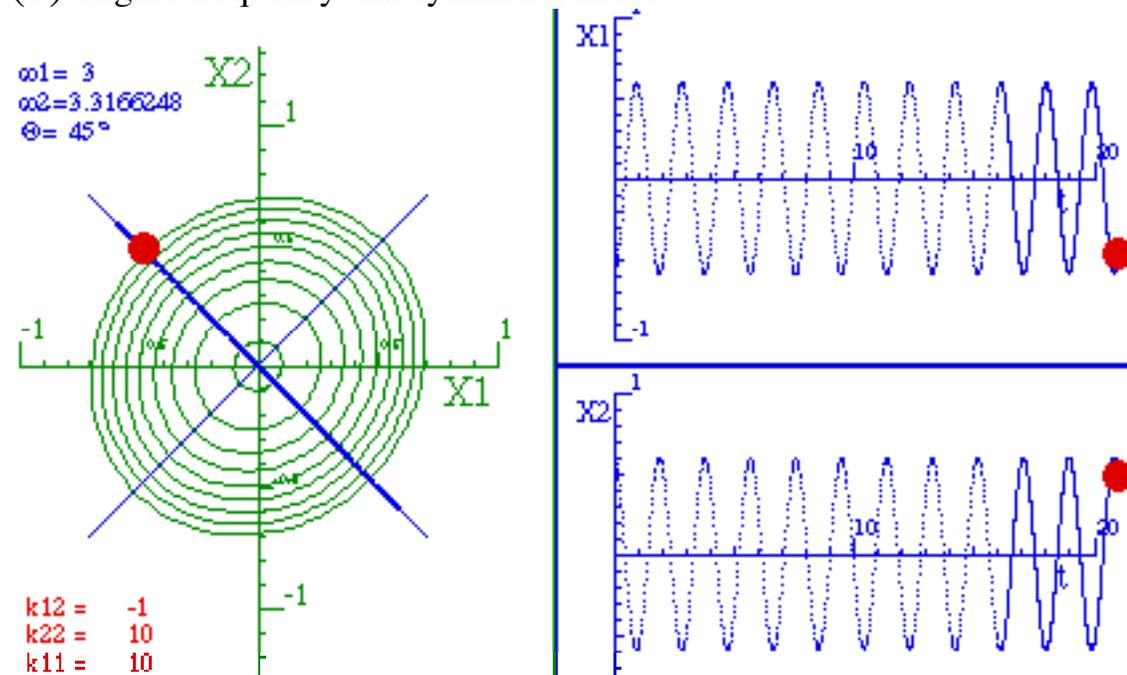
Fig. 2.3.12 Normal modes for symmetric coupled oscillators

Note that pure modes move along major or minor axes of the elliptical equipotential curves. If the oscillators are symmetric ($K_{11}=K_{22}$) these axes are at exactly ±45° as in Fig. 2.3.12. (If the mode frequencies are close in value the equipotential curves are nearly circular.) For general asymmetric oscillators the equipotentials have arbitrary inclination.

(h) Poincare periods and orbit closure

Beat periods (2.3.34) or frequencies (2.3.32) depend on the differences *(ω_2-ω_1)* of eigen-frequencies. However, many of the finer properties of the dynamics depend upon the ratios ω_2 /ω_1 of the frequencies. What distinguishes closed orbits like the one in Fig. 2.3.7 from those in subsequent Figs. 3.3.8-11 has to do with the *rationality* of the ratio ω_2 /ω_1 . To assess the rationality of any number we approximate it using successive levels of *continued fractions*.

$$\alpha = n_0 + \cfrac{1}{n_1 + \cfrac{1}{n_2 + \cfrac{1}{n_3 + \cfrac{1}{n_4 + \cfrac{1}{\ddots}}}}} \tag{2.3.35}$$

Then we compare how closely each level approximates the number. If any level gives the number α exactly then α is perfectly rational, that is, an integral ratio $\alpha = m/n$. Otherwise, it depends upon how close α is to a given integral fraction *m/n* and how small are the integers *m* and *n*. Consider, as our first example, the number π = 3.1415926..., and the following recipe for getting n_k .

$A_0 = \alpha = 3.14159265...$

$A_1 = \dfrac{1}{A_0 - n_0} = 7.06...$

$A_2 = \dfrac{1}{A_1 - n_1} = 15.99...$

$A_3 = \dfrac{1}{A_2 - n_2} = 1.003...$

$n_0 = INT(A_0) = 3$

$n_1 = INT(A_1) = 7$

$n_2 = INT(A_2) = 15$

$n_3 = INT(A_3) = 1$

$\pi \cong \quad = 3.000..$

$\pi \cong 3 + \dfrac{1}{7} = \dfrac{22}{7} = 3.1428$

$\pi \cong 3 + \cfrac{1}{7 + \cfrac{1}{15}} = \dfrac{333}{106} = 3.141509$

$\pi \cong 3 + \cfrac{1}{7 + \cfrac{1}{15 + 1}} = \dfrac{355}{113} = 3.14159292$

The first level approximation of 22/7 is within 0.0013 of π, and the second level approximation 333/106 is within 0.00008 of π, and so on. A larger integer n_k means a better *k-th* level approximation to α. A zero or infinite n_k terminates (2.3.35) which makes α perfectly rational. If higher level- *k* is needed to get a desired degree of approximation to α, then α is less rational. Consider the *Golden Mean G=*$(1+\sqrt{5})/2=1.618...$

$A_0 = G = 1.618033989...$

$A_1 = \dfrac{1}{A_0 - n_0} = 1.6180...$

$A_2 = \dfrac{1}{A_1 - n_1} = 1.6180...$

$A_3 = \dfrac{1}{A_2 - n_2} = 1.6180...$

$n_0 = INT(A_0) = 1$

$n_1 = INT(A_1) = 1$

$n_2 = INT(A_2) = 1$

$n_3 = INT(A_3) = 1$

$G \cong \quad = 1.000..$

$G \cong 1 + \dfrac{1}{1} = \dfrac{2}{1} = 2.000$

$G \cong 1 + \cfrac{1}{1 + \cfrac{1}{1}} = \dfrac{3}{2} = 1.500$

$G \cong 1 + \cfrac{1}{1 + \cfrac{1}{1 + 1}} = \dfrac{5}{3} = 1.666...$

G is clearly less rational than π. Its first and second levels are off by 0.4 and 0.12 respectively. In fact *G* is often called the <u>most irrational number</u> since each level integer n_k is 1,the smallest it can be. (If an n_k is 0, the series terminates as a rational.) The sequence (1, 2, 3, 5, 8, 13, ...,f_k =f_{k-1} +f_{k-2} , ...) of *G* fraction parts is called a *Fibonacci sequence* . This sequence is often seen in nature because nature is irrational by nature!

A closed or periodic orbit requires that the amplitudes of the form in (2.3.33) or

$$z = a\, e^{i\omega_1 t} + b\, e^{i\omega_2 t}$$

will be exactly the same at some time $t = \tau_p$ as they were at $t = 0$. The first time this happens is when both of the following two equations hold

$$\omega_1\, \tau_p = n_1\, 2\pi \quad \underline{and} \quad \omega_2\, \tau_p = n_2\, 2\pi \tag{2.3.36}$$

for integers n_1, $n_2 = 1, 2, ...$that are relatively prime. The time is called the Poincare' recurrence period

$$\tau_p = n_1\, 2\pi\, /\omega_1 = n_2\, 2\pi\, /\omega_2 \tag{2.3.37}$$

This implies that eigenfrequency ratio is perfectly rational <u>reduced</u> fraction.

$$\omega_1 / \omega_2 = n_1 / n_2 \tag{2.3.38}$$

The beat period (2.3.34) is

$$\tau_{beat} = 2\pi / |\omega_2 - \omega_1| = \tau_p / |n_2 - n_1| \tag{2.3.39}$$

which is an integral fraction of the Poincare period which it must be to have perfect periodicity.

Below are some examples. The arrow indicates the Poincare period in each case.
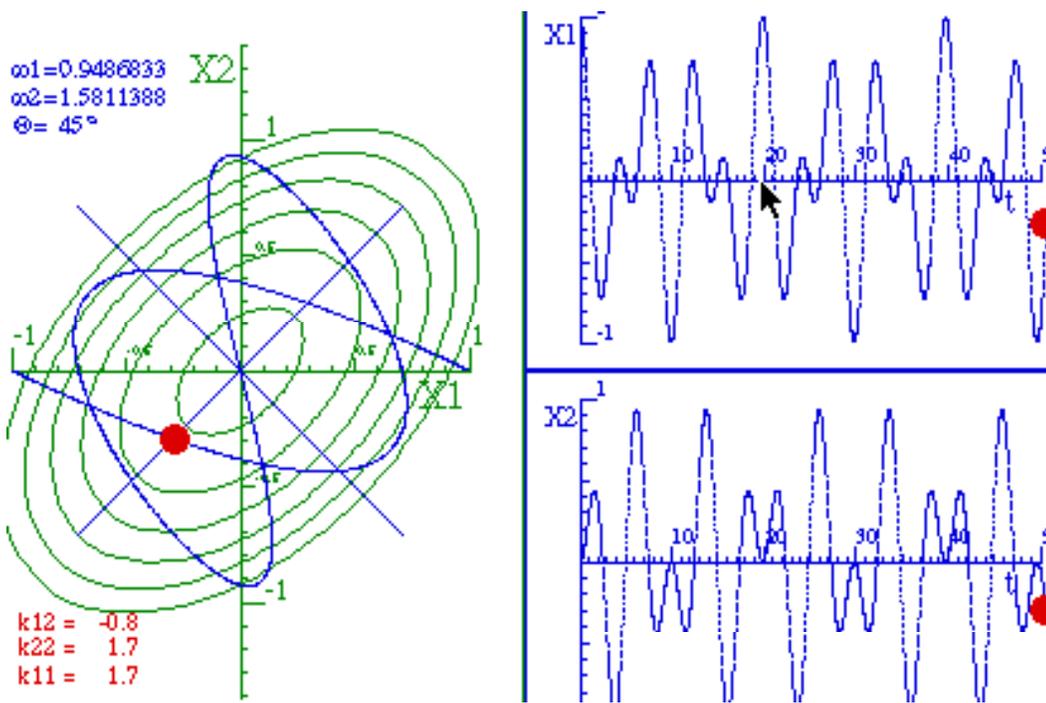
Fig. 2.3.13 Ratio of eigenfrequencies: 3:5 . Two beats per Poincare' period.

$\omega_1 = 1.5811388$
$\omega_2 = 2.2135944$
$\Theta = 45°$

$k12 = -1.3$
$k22 = 3.7$
$k11 = 3.7$
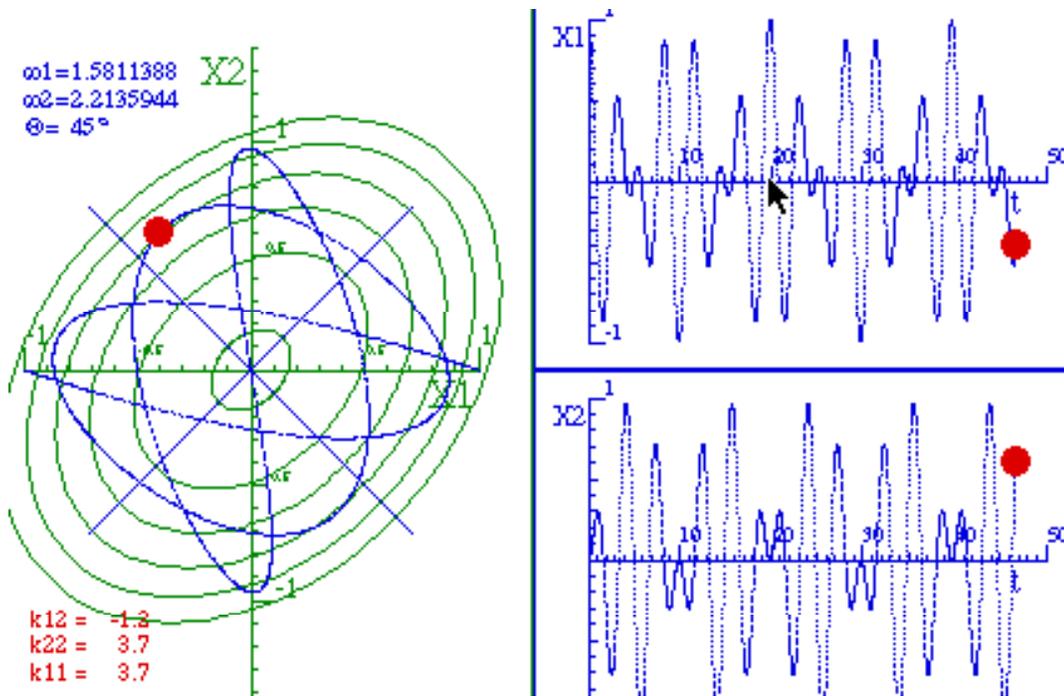
Fig. 2.3.14 Ratio of eigenfrequencies: 7:5 . Two beats per Poincare' period.

$\omega_1 = 1.5811388$
$\omega_2 = 2.5298221$
$\Theta = 45°$

$k12 = -1.95$
$k22 = 4.45$
$k11 = 4.45$
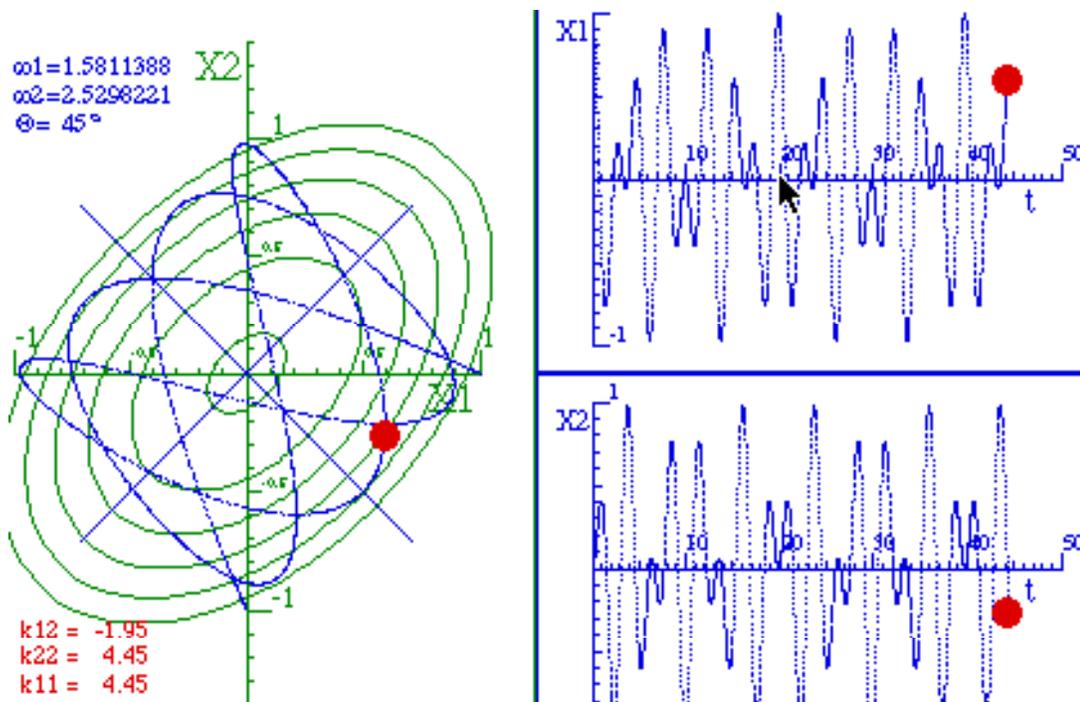
Fig. 2.3.15 Ratio of eigenfrequencies: 8:5 . Three beats per Poincare' period.

Characterizing resonances: Chaos or not?

Resonance between a pair of frequencies ω_1 and ω_2 is described first by their sum or carrier frequency $\omega_1 + \omega_2$ and their difference or beat frequency $\omega_1 - \omega_2$ in the expo-trig relation used in (2.3.30). Here it has just been shown that the product $\omega_1 \cdot \omega_2$ and ratio ω_1 / ω_2 are important, too, for the detailed shape of the waveforms.

The latter are important in the study of non-linear and chaotic oscillators. The effect of higher order potentials is to generate harmonics and sub-harmonics. If the ratio ω_1/ω_2 is composed of small integers as in Fig. 2.3.7 then the harmonics may add tremendous resonances, while a less rational case like Fig. 2.3.8 is less likely to do so. So it is the symmetric and rational cases that are most susceptible to the ravages of classical oscillator chaos.

Exercises for Ch. 2.3, Ch. 2.4, and Ch. 2.5 Coupled oscillators
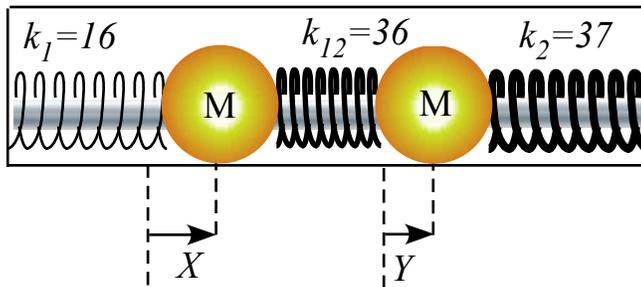
1a. Two identical mass $M=1kg$ blocks slide friction-free on a rod and are connected by springs $k_1=16N\cdot m^{-1}$ and $k_2=37N\cdot m^{-1}$ to ends of a box and coupled to each other by spring $k_{12}=36N\cdot m^{-1}$.
Write Lagrangian equations of motion.
Solve for eigenmodes and eigenfrequencies of system and plot their directions on an X,Y-graph. Use spectral decomposition methods of Appendix 3.C to derive eigensolution projectors.
Given initial conditions ($X(0)=1,Y(0)=0$), plot the resulting path in the XY-plane. Show algebraically that it is a parabola.

1b. Decompose the spring **K**-matrix for problem 1 into an **H**-matrix where $\mathbf{K}=\mathbf{H}^2$ as in (2.4.8).
Give the resulting **H**-matrix as an *(A,B,C,D)* combination of **1**, σ_A, σ_B, and σ_C as in (2.4.9).
Find the resulting Ω-whirl vector or "crank" in *(A,B,C)*–space as in (2.4.10).
For *(X(0)=1,Y(0)=0)* find the initial **S**-state vector or "spin" in *(A,B,C)*–space as in (2.4.16). Show its evolution by Ω as in Fig. 2.4.2.

2. Do the exercises 1a and 1b for a system with two identical springs $k_1=4N\cdot m^{-1}=k_2$ and $M=1kg$ masses coupled to each other by spring $k_{12}=30N\cdot m^{-1}$. Show it is a *B*-type system. Does *(X(0)=1,Y(0)=0)* also give a parabola? If not, what curve or function?

3. Let three identical $M=1kg$ masses slide on a circular friction-free rod and be coupled by three identical $k=4N\cdot m^{-1}$ springs. Show that the resulting **K**-matrix can be written as a combination of three matrices that commute, satisfy $\mathbf{r}^{3m}=\mathbf{1}$, and have 3rd-roots-of-unity eigenvalues $e^{im2\pi/3}=\{1,e^{i2\pi/3},e^{-i2\pi/3}\}$.

$$\mathbf{r}^0=\mathbf{1}=\begin{pmatrix}1&0&0\\0&1&0\\0&0&1\end{pmatrix}\ ,\ \mathbf{r}^1=\mathbf{r}=\begin{pmatrix}0&0&1\\1&0&0\\0&1&0\end{pmatrix}\ ,\ \mathbf{r}^2=\mathbf{r}\cdot\mathbf{r}=\begin{pmatrix}0&1&0\\0&0&1\\1&0&0\end{pmatrix}\ \text{Note:}\ \begin{matrix}\mathbf{r}|1\rangle=|2\rangle\\ \mathbf{r}|2\rangle=|3\rangle\\ \mathbf{r}|3\rangle=|1\rangle\end{matrix}\ ,i.e.,\ \mathbf{r}\begin{pmatrix}1\\ \cdot\\ \cdot\end{pmatrix}=\begin{pmatrix}\cdot\\1\\ \cdot\end{pmatrix},\text{etc.}$$

Obtain a spectral decomposition of $\mathbf{r}^m$ and use it to get a **K**-matrix spectral decomposition, as well. Make a table of eigen modes and their frequencies and show they are also linear combinations of 3rd-roots $e^{im2\pi/3}$.

4. Do exercise 3 for four identical spring-*k*-coupled masses.

Chapter 2.4 Classical Oscillators and Quantum Analogs

A fundamental equation of quantum dynamics, namely *Schrodinger's equation,* is related to that of classical coupled oscillators. Consider, for example the simplest quantum system: the *two-level atom* or a *spin-1/2* particle. The equation has a general form (2.4.1a) that for 2-levels uses 2-D arrays (2.4.1b-c).

$$i\hbar\frac{\partial}{\partial t}|\Psi(t)\rangle = \mathbf{H}|\Psi(t)\rangle \qquad (2.4.1a)$$

$\mathbf{H}$ is a 2-by-2 Hermitian $\left(\mathbf{H}^\dagger = \mathbf{H}\right)$ matrix operator and Dirac ket $|\Psi\rangle$ is a 2-D complex vector.

$$\mathbf{H} = \begin{pmatrix} A & B - iC \\ B + iC & D \end{pmatrix} \qquad (2.4.1b) \qquad |\Psi\rangle = \begin{pmatrix} \Psi_1 \\ \Psi_2 \end{pmatrix} = \begin{pmatrix} x_1 + ip_1 \\ x_2 + ip_2 \end{pmatrix} = \begin{pmatrix} a_1 \\ a_2 \end{pmatrix} \qquad (2.4.1c)$$

Separating real and imaginary parts of the amplitudes (2.4.1c) lets us convert the complex 2D equation (2.4.1a) into twice as many real differential equations. The results are as follows.

$$\begin{aligned} \dot{x}_1 &= Ap_1 + Bp_2 - Cx_2 \\ \dot{x}_2 &= Bp_1 + Dp_2 + Cx_1 \end{aligned} \quad (2.4.2a) \qquad\qquad \begin{aligned} \dot{p}_1 &= -Ax_1 - Bx_2 - Cp_2 \\ \dot{p}_2 &= -Bx_1 - Dx_2 + Cp_1 \end{aligned} \quad (2.4.2b)$$

A classical analog of Schrodinger dynamics

The same equations arise from the following classical coupled oscillator Hamiltonian in which x_j and p_j are canonical coordinate and momentum pairs, respectively.

$$H_c = \frac{A}{2}\left(p_1^2 + x_1^2\right) + B\left(x_1 x_2 + p_1 p_2\right) + C\left(x_1 p_2 - x_2 p_1\right) + \frac{D}{2}\left(p_2^2 + x_2^2\right) \qquad (2.4.3a)$$

Hamilton's equations of motion are the following. (Recall (4.12.5) or (2.12.10).)

$$\begin{aligned} \dot{x}_1 &= \frac{\partial H_c}{\partial p_1} = Ap_1 + Bp_2 - Cx_2 \\ \dot{x}_2 &= \frac{\partial H_c}{\partial p_2} = Bp_1 + Dp_2 + Cx_1 \end{aligned} \quad (2.4.3b) \qquad \begin{aligned} \dot{p}_1 &= -\frac{\partial H_c}{\partial x_1} = -\left(Ax_1 + Bx_2 + Cp_2\right) \\ \dot{p}_2 &= -\frac{\partial H_c}{\partial x_2} = -\left(Bx_1 + Dx_2 - Cp_1\right) \end{aligned} \quad (2.4.3c)$$

Note that these are identical to Schrodinger's equations (2.4.2).

To see a connection with conventional second order coupled oscillator equations (4.3.7), we differentiate the $\dot{x}_j$ equations (2.4.3b) and substitute the $\dot{p}_j$ expressions (2.4.3c). (Note: Canonical momentum here is <u>not</u> the usual $p_j = m\dot{x}_j$. See Exercise 2.4.1.)

$$\begin{aligned} \ddot{x}_1 &= A\dot{p}_1 + B\dot{p}_2 - C\dot{x}_2 \\ &= -A\left(Ax_1 + Bx_2 + Cp_2\right) - B\left(Bx_1 + Dx_2 - Cp_1\right) - C\left(Bp_1 + Dp_2 + Cx_1\right) \\ &= -\left(A^2 + B^2 + C^2\right)x_1 - \left(AB + BD\right)x_2 - C\left(A + D\right)p_2 \end{aligned} \qquad (2.4.4a)$$

$$\begin{aligned} \ddot{x}_2 &= B\dot{p}_1 + D\dot{p}_2 + C\dot{x}_1 \\ &= -B\left(Ax_1 + Bx_2 + Cp_2\right) - D\left(Bx_1 + Dx_2 - Cp_1\right) + C\left(Ap_1 + Bp_2 - Cx_2\right) \\ &= -\left(AB + BD\right)x_1 - \left(B^2 + D^2 + C^2\right)x_2 + C\left(A + D\right)p_1 \end{aligned} \qquad (2.4.4b)$$

Setting Schrodinger parameter C to zero reduces (2.4.4) to coupled oscillator equations (2.3.5) or (2.3.7).

$$-\ddot{x}_1 = K_{11}x_1 + K_{12}x_2 \tag{2.4.5a}$$

$$-\ddot{x}_2 = K_{21}x_1 + K_{22}x_2 \tag{2.4.5b}$$

Spring force matrix components K_{mn} are related below to **H**-matrix parameters A, B, and D.

$$K_{11} = A^2 + B^2, \qquad\qquad K_{12} = AB + BD,$$

$$K_{21} = AB + BD, \qquad\qquad K_{22} = B^2 + D^2. \tag{2.4.6}$$

The eigenfrequencies for the Schrodinger equation (2.4.1) with $(C \equiv 0)$ are squares of the eigenvalues of

the **K**-matrix in (2.4.5). (See Exercise 2.4.2.) This is quickly seen in the case $A = D$ and $C=0$ where the quantum Hamiltonian matrix (2.4.1b) has a super-symmetric form.

$$\mathbf{H} = \begin{pmatrix} A & B \\ B & A \end{pmatrix} \tag{2.4.7a}$$

This Hamiltonian matrix has the following eigenvalues.

$$\varepsilon_1 = A + B, \qquad\qquad \varepsilon_2 = A - B. \tag{2.4.7b}$$

For the same parameters $A = D$, B, and $C=0$, the classical acceleration matrix is super-symmetric, too.

$$\mathbf{K} = \begin{pmatrix} A^2 + B^2 & 2AB \\ 2AB & A^2 + B^2 \end{pmatrix} = \begin{pmatrix} A & B \\ B & A \end{pmatrix}\begin{pmatrix} A & B \\ B & A \end{pmatrix} = \mathbf{H}^2 \tag{2.4.8a}$$

A is the matrix square of **H** so the classical acceleration eigenvalues are squares of quantum eigenvalues.

$$K_1 = (A + B)^2, \qquad\qquad K_2 = (A - B)^2. \tag{2.4.8b}$$

Quantum dynamics differs from classical dynamics in a few important ways. First, the classical equations are *second* order differential equations so eigenvalues give *squared* frequencies as in (2.4.8b) rather than frequencies as in (2.4.7b). Also, stimuli for quantum dynamics enter multiplicatively by varying **H** components A, B, C, or D. Quantum equation $i|\dot{\Psi}\rangle = \mathbf{H}|\Psi\rangle$ is *always homogeneous*, i.e. $i|\dot{\Psi}\rangle - \mathbf{H}|\Psi\rangle = 0$ is *always zero* unlike classical $|\ddot{x}\rangle + \mathbf{K}|x\rangle = |a\rangle$. Finally, parameter C corresponds to classical cyclotron or Coriolis effects. It gives circular cyclotron orbits if the others are zero. This is discussed later on.

ABCD Symmetry operator analysis and U(2) spinors

Let us decompose the Hamiltonian operator **H** in (2.4.1) into four *ABCD symmetry operators* that are so labeled to provide helpful dynamic mnemonics and symmetry names (as well as colorful analogies).

$$\begin{pmatrix} A & B - iC \\ B + iC & D \end{pmatrix} = A\begin{pmatrix} 1 & 0 \\ 0 & 0 \end{pmatrix} + B\begin{pmatrix} 0 & 1 \\ 1 & 0 \end{pmatrix} + C\begin{pmatrix} 0 & -i \\ i & 0 \end{pmatrix} + D\begin{pmatrix} 0 & 0 \\ 0 & 1 \end{pmatrix} = A\mathbf{e}_{11} + B\boldsymbol{\sigma}_B + C\boldsymbol{\sigma}_C + D\mathbf{e}_{22}$$

$$= \frac{A-D}{2}\begin{pmatrix} 1 & 0 \\ 0 & -1 \end{pmatrix} + B\begin{pmatrix} 0 & 1 \\ 1 & 0 \end{pmatrix} + C\begin{pmatrix} 0 & -i \\ i & 0 \end{pmatrix} + \frac{A+D}{2}\begin{pmatrix} 1 & 0 \\ 0 & 1 \end{pmatrix}$$

$$\tag{2.4.9a}$$

$$\mathbf{H} = \frac{A-D}{2}\,\boldsymbol{\sigma}_A \quad + B\,\boldsymbol{\sigma}_B \quad + C\,\boldsymbol{\sigma}_C \quad + \frac{A+D}{2}\,\boldsymbol{\sigma}_0$$

The $\{\sigma_1, \sigma_A, \sigma_B, \sigma_C\}$ are best known as *Pauli-spin operators* $\{\sigma_1 = \sigma_0, \sigma_B = \sigma_X, \sigma_C = \sigma_Y, \sigma_A = \sigma_Z\}$ but ones quite like them were discovered a century earlier by Hamilton who was looking to generalize complex numbers to 3-dimensional space. Hamilton's *quaternions* {**1, i, j, k**} are related as follows to the *ABCD* or *ZXY0* operators. (He carved them into a bridge in Dublin in 1843, though, not in technicolor.)

$$\{\sigma_1=\mathbf{1}=\sigma_0, \; i\sigma_B=\mathbf{i}=i\sigma_X, \; i\sigma_C=\mathbf{j}=i\sigma_Y, \; i\sigma_A=\mathbf{k}=i\sigma_Z\} \tag{2.4.9b}$$

Note: $\mathbf{i}^2=\mathbf{j}^2=\mathbf{k}^2=\mathbf{-1}$. Each squares to *negative*-**1** like imaginary number $i^2=-1$. Pauli's form removes the imaginary i so each σ_μ squares to *positive* **1** ($\sigma_X^2=\sigma_Y^2=\sigma_Z^2=+1$) and each belongs to a cyclic C_2 group.

We'll consider each C_2 symmetry $C_2{}^A=\{\mathbf{1},\sigma_A\}$, $C_2{}^B=\{\mathbf{1},\sigma_B\}$, and $C_2{}^C=\{\mathbf{1},\sigma_C\}$ in turn. They are labeled as *A (Asymmetric-diagonal)*, *B (Bilateral-balanced)*, or *C (Chiral-circular)* symmetry, respectively. Each is an archetype of dynamics and symmetry. The systems in Ch. 3.3 belong to *A-to-B* cases in Fig. 2.4.1 below.
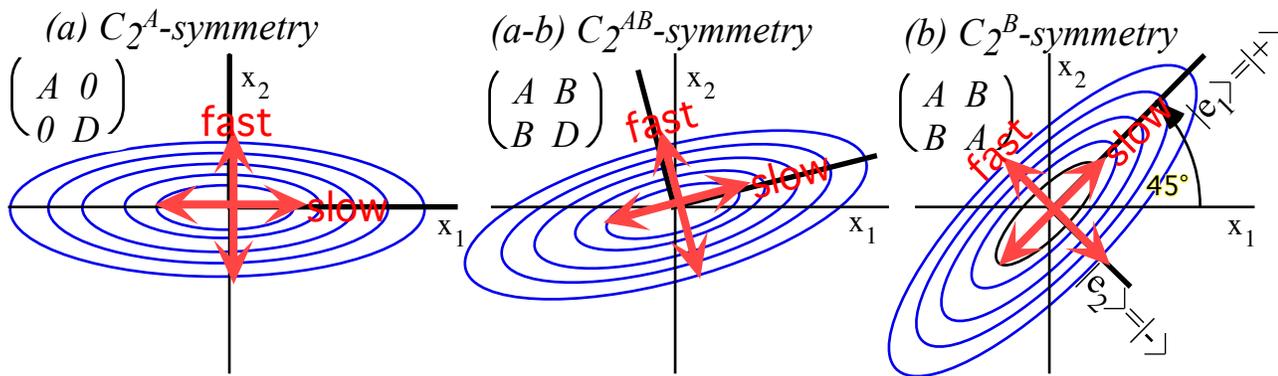

Fig. 2.4.1 Potentials for (a) $C_2{}^A$-asymmetric-diagonal, (ab) $C_2{}^{AB}$-mixed , (b) $C_2{}^B$-bilateral U(2)system.

A secret to Hamilton's Hamiltonian decomposition (2.4.9) lies in how it can solve the fundamental 1st order $i|\dot\Psi\rangle - \mathbf{H}|\Psi\rangle = 0$ equation (2.4.1) by evaluating and (*most* important!) *visualizing* matrix-exponent solutions.

$$\left|\Psi(t)\right\rangle = e^{-i\mathbf{H}\cdot t}\left|\Psi(0)\right\rangle \tag{2.4.10a}$$

Hamilton generalized Euler's expansion $e^{-i\Omega t}=\cos\Omega t - i\sin\Omega t$ so a matrix exponential becomes powerful.

$$e^{-i\mathbf{H}\cdot t} = e^{-i\left(\begin{smallmatrix} A & B-iC \\ B+iC & D \end{smallmatrix}\right)\cdot t} = e^{-i\frac{A-D}{2}\left(\begin{smallmatrix} 1 & 0 \\ 0 & -1 \end{smallmatrix}\right)\cdot t - iB\left(\begin{smallmatrix} 0 & 1 \\ 1 & 0 \end{smallmatrix}\right)\cdot t - iC\left(\begin{smallmatrix} 0 & -i \\ i & 0 \end{smallmatrix}\right)\cdot t - i\frac{A+D}{2}\left(\begin{smallmatrix} 1 & 0 \\ 0 & 1 \end{smallmatrix}\right)\cdot t}$$

$$= e^{-i\boldsymbol{\sigma}\bullet\boldsymbol{\Omega}\cdot t/2} e^{-i\Omega_0\cdot t} \quad \text{where: } \boldsymbol{\Theta}=\boldsymbol{\Omega}\cdot t = \begin{pmatrix} \Omega_A \\ \Omega_B \\ \Omega_C \end{pmatrix}\cdot t = \begin{pmatrix} A-D \\ 2B \\ 2C \end{pmatrix}\cdot t \text{ and: } \Omega_0 = \frac{A+D}{2} \tag{2.4.10b}$$

Each matrix $\mathbf{H}$ has a rotation *crank vector* $\boldsymbol{\Theta}=\boldsymbol{\Omega}\cdot t$ that dots with quaternions to solve (2.4.1). $\boldsymbol{\Omega}$ is a 3D *ABC*-or *XYZ* -space whirl rate like ω described in Ch. 3.11c. Hamilton generalized a *2D* complex phasor rotation $e^{-i\Omega t}=\cos\Omega t - i\sin\Omega t$ and he did this by first generalizing the imaginary number $i=\sqrt{-1}$ as described below.

(a) How spinors and quaternions *work*

Symmetry relations make spinors σ_X,σ_Y, and σ_Z or quaternions $\mathbf{i}=-i\sigma_X$, $\mathbf{j}=-i\sigma_Y$, and $\mathbf{k}=-i\sigma_Z$ powerful. Each σ_X squares to one (unit matrix $\mathbf{1}=\sigma_X\cdot\sigma_X$) and each quaternion squares to minus-one ($-\mathbf{1}=\mathbf{i}\cdot\mathbf{i}=\mathbf{j}\cdot\mathbf{j}$, *etc.*) just like $i=\sqrt{-1}$. This is true even for spinor components based on *any* unit vector $\hat{\mathbf{a}}=(a_X,a_Y,a_Z)$ for which $\hat{\mathbf{a}}\bullet\hat{\mathbf{a}}=1=a_X^2+a_Y^2+a_Z^2$. To see this just try it out on any $\hat{\mathbf{a}}$ -component: $\sigma_a=\boldsymbol{\sigma}\bullet\hat{\mathbf{a}}=a_X\sigma_X+a_Y\sigma_Y+a_Z\sigma_Z$.

$$\sigma_a^2 = (\boldsymbol{\sigma} \bullet \hat{\mathbf{a}})(\boldsymbol{\sigma} \bullet \hat{\mathbf{a}}) = (a_X \sigma_X + a_Y \sigma_Y + a_Z \sigma_Z)(a_X \sigma_X + a_Y \sigma_Y + a_Z \sigma_Z)$$

$$
\begin{array}{lll}
\quad a_X \sigma_X a_X \sigma_X & +a_X \sigma_X a_Y \sigma_Y & +a_X \sigma_X a_Z \sigma_Z \qquad a_X a_X \sigma_X \sigma_X \quad +a_X a_Y \sigma_X \sigma_Y \quad +a_X a_Z \sigma_X \sigma_Z \\
= +a_Y \sigma_Y a_X \sigma_X & +a_Y \sigma_Y a_Y \sigma_Y & +a_Y \sigma_Y a_Z \sigma_Z \;=\; +a_Y a_X \sigma_Y \sigma_X \quad +a_Y a_Y \sigma_Y \sigma_Y \quad +a_Y a_Z \sigma_Y \sigma_Z \\
\quad +a_Z \sigma_Z a_X \sigma_X & +a_Z \sigma_Z a_Y \sigma_Y & +a_Z \sigma_Z a_Z \sigma_Z \qquad +a_Z a_X \sigma_Z \sigma_X \quad +a_Z a_Y \sigma_Z \sigma_Y \quad +a_Z a_Z \sigma_Z \sigma_Z
\end{array}
$$

To finish we need another symmetry property called *anti-commutation*: $\sigma_X \sigma_Y = -\sigma_Y \sigma_X$, *etc.* (Check this!) Put this together with unit squares $\mathbf{1} = \sigma_X^2$, *etc.* Then all off-diagonal terms cancel so that $\mathbf{1} = \sigma_a^2$, too.

$$\sigma_a^2 = (\boldsymbol{\sigma} \bullet \hat{\mathbf{a}})(\boldsymbol{\sigma} \bullet \hat{\mathbf{a}}) = (a_X \sigma_X + a_Y \sigma_Y + a_Z \sigma_Z)(a_X \sigma_X + a_Y \sigma_Y + a_Z \sigma_Z)$$

$$
\begin{array}{lll}
\quad a_X^2 \mathbf{1} & +a_X a_Y \sigma_X \sigma_Y & +a_X a_Z \sigma_X \sigma_Z \\
= -a_X a_Y \sigma_X \sigma_Y & +a_Y^2 \mathbf{1} & +a_Y a_Z \sigma_Y \sigma_Z \qquad = (a_X^2 + a_Y^2 + a_Z^2)\mathbf{1} = \mathbf{1} \\
\quad -a_X a_Z \sigma_X \sigma_Z & -a_Y a_Z \sigma_Y \sigma_Z & +a_Z^2 \mathbf{1}
\end{array}
$$

(2.4.11)

Finally, that anti-commutation relation is cyclic: $\sigma_X \sigma_Y = i\sigma_Z = -\sigma_Y \sigma_X$, $\sigma_Z \sigma_X = i\sigma_Y = -\sigma_X \sigma_Z$, and $\sigma_Y \sigma_Z = i\sigma_X = -\sigma_Z \sigma_Y$. So, σ-products do dot • *and* cross× products. (ε-products do× in (4.11.22).)

$$\sigma_a \sigma_b = (\boldsymbol{\sigma} \bullet \mathbf{a})(\boldsymbol{\sigma} \bullet \mathbf{b}) = (a_X \sigma_X + a_Y \sigma_Y + a_Z \sigma_Z)(b_X \sigma_X + b_Y \sigma_Y + b_Z \sigma_Z)$$

$$
\begin{array}{llll}
\quad a_X b_X \mathbf{1} & +a_X b_Y \sigma_X \sigma_Y & -a_X b_Z \sigma_Z \sigma_X & +i(a_Y b_Z - a_Z b_Y)\sigma_X \\
= -a_Y b_X \sigma_X \sigma_Y & +a_Y b_Y \mathbf{1} & +a_Y b_Z \sigma_Y \sigma_Z \;=\; (a_X b_X + a_Y b_Y + a_Z b_Z)\mathbf{1} & +i(a_Z b_X - a_X b_Z)\sigma_Y \\
\quad +a_Z b_X \sigma_Z \sigma_X & -a_Z b_X \sigma_Y \sigma_Z & +a_Z b_Z \mathbf{1} & +i(a_X b_Y - a_Y b_X)\sigma_Z
\end{array}
$$

(2.4.12a)

To see this we write the product in Gibbs notation. (Where do you think Gibbs *got* his {**i,j,k**} notation!)

$$\sigma_a \sigma_b = (\boldsymbol{\sigma} \bullet \mathbf{a})(\boldsymbol{\sigma} \bullet \mathbf{b}) = \quad (\mathbf{a} \bullet \mathbf{b})\mathbf{1} \quad + \quad i(\mathbf{a} \times \mathbf{b}) \bullet \boldsymbol{\sigma} \tag{2.4.12b}$$

Complex numbers $A = A_x + iA_y$ do a similar thing if you *-multiply them as follows. (Recall (1.10.29).)

$$
\begin{aligned}
A * B &= (A_X + iA_Y) * (B_X + iB_Y) = (A_X - iA_Y)(B_X + iB_Y) \\
&= (A_X B_X + A_Y B_Y) + i(A_X B_Y - A_Y B_X) = (\mathbf{A} \bullet \mathbf{B}) + i(\mathbf{A} \times \mathbf{B})
\end{aligned}
\tag{2.4.13}
$$

The results are just the *2D* versions of dot and cross products. Hamilton's idea was to generalize to three dimensions and even four dimensions. (Lorentz relativity transformations are done by spinors, too!) So finally Hamilton is able to generalize Euler's complex rotation operators $e^{+i\varphi}$ and $e^{-i\varphi}$. (Recall (1.10.17).)

$$
\begin{aligned}
e^{-i\varphi} = 1 + (-i\varphi) + \frac{1}{2!}(-i\varphi)^2 + \frac{1}{3!}(-i\varphi)^3 + \frac{1}{4!}(-i\varphi)^4 \cdots &= \quad [1 \qquad -\frac{1}{2!}\varphi^2 \qquad +\frac{1}{4!}\varphi^4 \cdots] = \quad [\cos\varphi] \\
&\qquad -i(\varphi \qquad +\frac{1}{3!}\varphi^3 \qquad \cdots) \qquad -i(\sin\varphi)
\end{aligned}
$$

Euler's series is the result of the binomial series definition of the exponential growth function e^{rt}.

$$e^{rt} = \lim_{N \to \infty}(1 + \frac{rt}{N})^N = \lim_{N \to \infty}(1 + N\frac{rt}{N} + \frac{N(N-1)}{2!}\left(\frac{rt}{N}\right)^2 + \frac{N(N-1)(N-2)}{3!}\left(\frac{rt}{N}\right)^3 + \ldots)$$

Euler's identity works because even powers of *(-i)* are ±*1* and odd powers of *(-i)* are ±*i*. That is how $-i\sigma_a$ works, too. Hamilton replaces *(-i)* with $-i\sigma_a$ in an $e^{-i\varphi}$ power series to get a sequence of terms

$$(-i\sigma_a)^0 = +\mathbf{1}, \; (-i\sigma_a)^1 = -i\sigma_a, \; (-i\sigma_a)^2 = -\mathbf{1}, \; (-i\sigma_a)^3 = +i\sigma_a, \; (-i\sigma_a)^4 = +\mathbf{1}, \; (-i\sigma_a)^5 = -i\sigma_a, etc.$$

This allows Hamilton to generalize Euler's $e^{-i\varphi}$ rotation to $e^{-i\boldsymbol{\sigma}_a \varphi}$ for any $\sigma_a = (\boldsymbol{\sigma} \bullet \mathbf{a}) = a_X \sigma_X + a_Y \sigma_Y + a_Z \sigma_Z$.

$$e^{-i\varphi} = \mathbf{1}\cos\varphi \; - \; i \sin\varphi \qquad \text{generalizes to:} \quad e^{-i\boldsymbol{\sigma}_a \varphi} = \mathbf{1}\cos\varphi \; - \; i\,\boldsymbol{\sigma}_a \sin\varphi$$

Below are $\sigma_A = \sigma_Z$ and $\sigma_C = \sigma_Y$ rotations and a σ_a-rotation around a general *3D* whirl axis $\hat{\boldsymbol{\omega}} = \hat{\boldsymbol{\Theta}}_a = \hat{\mathbf{a}}$.

$$e^{-i(\sigma_A)\varphi_A} = \quad \mathbf{1} \quad \cos\varphi_A \; - \; i \; (\sigma_A) \; \sin\varphi_A = \mathbf{R}(\varphi_A)$$

<div align="center">(2.4.14a)</div>

$$e^{-i\begin{bmatrix} 1 & 0 \\ 0 & -1 \end{bmatrix}\varphi_A} = \begin{pmatrix} 1 & 0 \\ 0 & 1 \end{pmatrix}\cos\varphi_A - i\begin{pmatrix} 1 & 0 \\ 0 & -1 \end{pmatrix}\sin\varphi_A$$

$$= \begin{pmatrix} \cos\varphi_A - i\sin\varphi_A & 0 \\ 0 & \cos\varphi_A - i\sin\varphi_A \end{pmatrix} = \begin{pmatrix} e^{-i\varphi_A} & 0 \\ 0 & e^{i\varphi_A} \end{pmatrix}$$

$$e^{-i(\sigma_C)\varphi_C} = \quad \mathbf{1} \quad \cos\varphi_C - i \; (\sigma_C) \; \sin\varphi_C = \mathbf{R}(\varphi_C)$$

<div align="center">(2.4.14c)</div>

$$e^{-i\begin{bmatrix} 0 & -i \\ i & 0 \end{bmatrix}\varphi_C} = \begin{pmatrix} 1 & 0 \\ 0 & 1 \end{pmatrix}\cos\varphi_C - i\begin{pmatrix} 0 & -i \\ i & 0 \end{pmatrix}\sin\varphi_C$$

$$= \begin{pmatrix} \cos\varphi_C & -\sin\varphi_C \\ \sin\varphi_C & \cos\varphi_C \end{pmatrix}$$

$$e^{-i\sigma_a\varphi_a} = e^{-i(\sigma\bullet\hat{a})\varphi_a} = \mathbf{1}\cos\varphi_a - i \; (\sigma\bullet\hat{a})\sin\varphi_a \qquad\qquad (2.4.14b)$$

We now see that *3D* (*ABC*) rotations are by an angle $\Theta_a = 2\varphi_a$ that is *twice* the angle φ_a in *2D* space $\{x_1, x_2\}$.

The "mysterious" factors of 2

A factor of 2 or $\frac{1}{2}$ relates φ_a-rotation of *2D* oscillator variables $\{x_1, x_2\}$ to *3D* vector rotation Θ_a in *ZXY* or *ABC*-space. *3D* vector $\hat{a}$ defines a combination $\sigma_a = a_A\sigma_A + a_B\sigma_B + a_C\sigma_C$ of *operators* $\sigma_A, \sigma_B, \sigma_C$ to be rotated by 2-by-2 matrices (2.4.15) acting *twice*, fore and aft^{-1}(as operators do in (4.B.6)) by *twice* the *2D* angle φ_a.

$$\mathbf{R}(\varphi_C) \quad \cdot \quad \sigma_A \quad \cdot \quad \mathbf{R}^{-1}(\varphi_C)$$

$$= \begin{pmatrix} \cos\varphi_C & -\sin\varphi_C \\ \sin\varphi_C & \cos\varphi_C \end{pmatrix}\begin{pmatrix} 1 & 0 \\ 0 & -1 \end{pmatrix}\begin{pmatrix} \cos\varphi_C & \sin\varphi_C \\ -\sin\varphi_C & \cos\varphi_C \end{pmatrix}$$

$$= \begin{pmatrix} \cos^2\varphi_C - \sin^2\varphi_C & 2\sin\varphi_C\cos\varphi_C \\ 2\sin\varphi_C\cos\varphi_C & \sin^2\varphi_C - \cos^2\varphi_C \end{pmatrix}$$

$$= \begin{pmatrix} 1 & 0 \\ 0 & -1 \end{pmatrix}\cos 2\varphi_C + \begin{pmatrix} 0 & 1 \\ 1 & 0 \end{pmatrix}\sin 2\varphi_C$$

$$= \quad \sigma_A \; \cos 2\varphi_C + \; \sigma_B \; \sin 2\varphi_C$$

$$\mathbf{R}(\varphi_C) \quad \cdot \quad \sigma_B \quad \cdot \quad \mathbf{R}^{-1}(\varphi_C)$$

$$= \begin{pmatrix} \cos\varphi_C & -\sin\varphi_C \\ \sin\varphi_C & \cos\varphi_C \end{pmatrix}\begin{pmatrix} 0 & 1 \\ 1 & 0 \end{pmatrix}\begin{pmatrix} \cos\varphi_C & \sin\varphi_C \\ -\sin\varphi_C & \cos\varphi_C \end{pmatrix}$$

$$= \begin{pmatrix} -2\sin\varphi_C\cos\varphi_C & \cos^2\varphi_C - \sin^2\varphi_C \\ \cos^2\varphi_C - \sin^2\varphi_C & 2\sin\varphi_C\cos\varphi_C \end{pmatrix}$$

$$= \begin{pmatrix} -1 & 0 \\ 0 & 1 \end{pmatrix}\sin 2\varphi_C + \begin{pmatrix} 0 & 1 \\ 1 & 0 \end{pmatrix}\cos 2\varphi_C$$

$$= \; -\sigma_A \; \sin 2\varphi_C + \; \sigma_B \; \cos 2\varphi_C$$

So the *2D* rotation φ_a angle must be exactly $\frac{1}{2}$ the *3D* angle Θ_a of rotation. When a spin axis goes from *up-A* to *down-A* that is a rotation by $\Theta_C = \pi$ or *180°* in *ZXY* or *ABC*-space, but only by $\varphi_C = \pi/2$ or *90°* in spinor space $\{x_1, x_2\}$. State $|\uparrow\rangle$ of spin *up-Z* and the state $|\downarrow\rangle$ of spin *down-Z* are orthogonal kets *90°* apart. This analogy to a *2D*$\{x_1, x_2\}$-oscillator underlies spin $\frac{1}{2}$. So, *3D crank* <u>*vector*</u> $\vec{\Theta}$ and *spin* <u>*operator*</u> $\mathbf{S}$ are defined for *3D ZXY* or *ABC*-space with a ratio $\frac{1}{2}$ or 2 between Θ_a and $\varphi_a = \frac{1}{2}\Theta_a$ or between $\mathbf{S}$ and $\sigma = 2\mathbf{S}$.

$$e^{-i\sigma\bullet\vec{\varphi}} = e^{-i\sigma\bullet\vec{\Theta}/2} = e^{-i\mathbf{S}\bullet\vec{\Theta}} = \mathbf{1}\cos\frac{\Theta}{2} - i \; (\sigma\bullet\hat{\Theta})\sin\frac{\Theta}{2} = \begin{pmatrix} \cos\dfrac{\Theta}{2} - i\hat{\Theta}_A\sin\dfrac{\Theta}{2} & (-i\hat{\Theta}_B - \hat{\Theta}_C)\sin\dfrac{\Theta}{2} \\ (-i\hat{\Theta}_B + \hat{\Theta}_C)\sin\dfrac{\Theta}{2} & \cos\dfrac{\Theta}{2} + i\hat{\Theta}_A\sin\dfrac{\Theta}{2} \end{pmatrix}$$

<div align="right">(2.4.15a)</div>

$$\text{2D angle}: \varphi = \tfrac{1}{2}\Theta \qquad\qquad \text{3D Crank vector}: \vec{\Theta} = \Theta\hat{\Theta} = 2\varphi_a\hat{a} = 2\vec{\varphi} \qquad\qquad \text{2D spin matrix}: \mathbf{S} = \tfrac{1}{2}\sigma$$

<div align="center">(2.4.15b)   (2.4.15c)   (2.4.15d)</div>

Eighty years after Hamilton (1924) comes Pauli and Jordan spin $\mathbf{S} = \frac{\hbar}{2}\sigma$ with its *half-quantum* factor $\frac{\hbar}{2}$.

2D polarization and 3D Stokes vector S

In 1862 George Stokes found an application of Hamilton's mathematics to optical polarization that has a *2D* complex oscillator space $\{E_1, E_2\}$ analogous to Ψ-space $\{a_1, a_2\} = \{x_1 + ip_1, x_2 + ip_2\}$ in (2.4.1c). He gave 3 *Stokes vector components* S_a that wonderfully define polarization ellipses, *2D* HO orbits, and spin $\frac{1}{2}$ states.

$$\textit{Asymmetry } S_A = \frac{1}{2}\left(a|\sigma_A|a\right) = \frac{1}{2}\begin{pmatrix} a_1^* & a_2^* \end{pmatrix} \begin{pmatrix} 1 & 0 \\ 0 & -1 \end{pmatrix} \begin{pmatrix} a_1 \\ a_2 \end{pmatrix} = \frac{1}{2}\left[a_1^* a_1 - a_2^* a_2 \right] = \frac{1}{2}\left[x_1^2 + p_1^2 - x_2^2 - p_2^2 \right] \text{ (2.4.16a)}$$

$$\textit{Balance } \quad S_B = \frac{1}{2}\left(a|\sigma_B|a\right) = \frac{1}{2}\begin{pmatrix} a_1^* & a_2^* \end{pmatrix} \begin{pmatrix} 0 & 1 \\ 1 & 0 \end{pmatrix} \begin{pmatrix} a_1 \\ a_2 \end{pmatrix} = \frac{1}{2}\left[a_1^* a_2 + a_2^* a_1 \right] = \left[p_1 p_2 + x_1 x_2 \right] \quad \text{(2.4.16b)}$$

$$\textit{Chirality } \quad S_C = \frac{1}{2}\left(a|\sigma_C|a\right) = \frac{1}{2}\begin{pmatrix} a_1^* & a_2^* \end{pmatrix} \begin{pmatrix} 0 & -i \\ i & 0 \end{pmatrix} \begin{pmatrix} a_1 \\ a_2 \end{pmatrix} = \frac{-i}{2}\left[a_1^* a_2 - a_2^* a_1 \right] = \left[x_1 p_2 - x_2 p_1 \right] \quad \text{(2.4.16c)}$$

Components of real *3D* spin-vector $S = (S_A, S_B, S_C)$ label orbit *states* in 4D phase space (x_1, p_1, x_2, p_2) just as real components of *3D* whirl-vector $\Omega = (\Omega_A, \Omega_B, \Omega_C)$ label 4D matrix *operators* **H** that whirl these states.
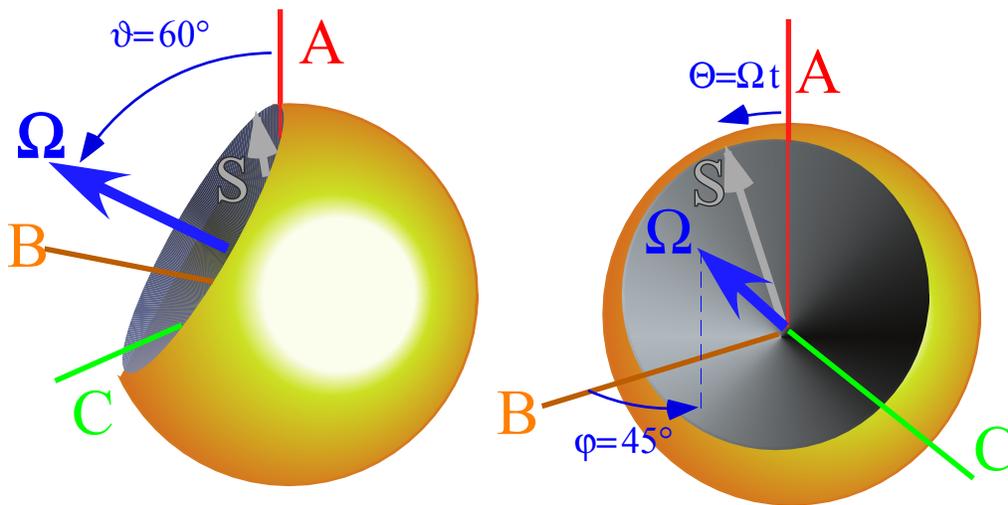
Fig. 2.4.2 Two views of Hamilton crank vector $\Omega(\varphi, \vartheta)$ whirling Stokes state vector S in ABC-space.

Matrix **H** cranks S around rotation axis $\Theta = \Omega \cdot t$ according to (2.4.15) at whirl rate Ω as Fig. 2.4.2 depicts.

$$\Omega = |\Omega| = \sqrt{\Omega_A^2 + \Omega_B^2 + \Omega_C^2} \tag{2.4.17}$$

Length of $\Theta = (\Theta_A, \Theta_B, \Theta_C) = \Omega \cdot t = (\Omega_A \cdot t, \Omega_B \cdot t, \Omega_C \cdot t)$ grows at a constant rate Ω but its direction is fixed if the constants (A, B, C, D) or $(\Omega_A = A - D, \Omega_B = 2B, \Omega_C = 2C)$ in **H** are in fact constant. The Ω-whirl direction is given by polar coordinates (φ, ϑ) that we call *Darboux angles* after the inventor of ω-whirl vectors. The spin S-vector has polar coordinates, too, so designated in the next section by *Euler angles* (α, β).

Fixed points: A port in the storm of action

It helps to look at Fig. 2.4.2 as a phase space analogous to that of harmonic oscillators. Points on **H** 's whirl vector Ω are stable fixed points for state spin-S where it can rest and not be whirled. It still twists if S could do so. Such a twist is in the 0th-overall average angular phase rate $\Omega_0 = (A+D)/2$ in (2.4.10). The S-states for which S

aligns $(\alpha,\beta)=(\varphi,\vartheta)$ or anti-aligns $(\alpha,\pi-\beta)=(\varphi,\vartheta)$ are called own-states or *eigenstates* of **H**. This gives a nice quick computational aid later.

The S_a-terms in (2.4.16) are the same as the parts of the classical Hamiltonian H_c in (2.4.3a).

$$H_c = \frac{A}{2}\left(p_1^2 + x_1^2\right) + B\left(x_1 x_2 + p_1 p_2\right) + C\left(x_1 p_2 - x_2 p_1\right) + \frac{D}{2}\left(p_2^2 + x_2^2\right) \qquad (2.4.3a)_{repeated}$$

Rearranging the A and D terms lends a classical action form $\dot{q}^m p_m = \boldsymbol{\omega} \cdot \mathbf{J} = \boldsymbol{\Omega} \cdot \mathbf{S}$ to the expression of H_c.

$$H_c = \frac{A-D}{2}\left[\frac{x_1^2 + p_1^2 - x_2^2 - p_2^2}{2}\right] + B\left[p_1 p_2 + x_1 x_2\right] + C\left[x_1 p_2 - x_2 p_1\right] + \frac{1}{2}\frac{A+D}{2}\left[p_1^2 + x_1^2 + p_2^2 + x_2^2\right]$$

$$= \frac{1}{2}\Omega_A\left[S_A\right] \qquad\qquad + \frac{1}{2}\Omega_B\left[S_B\right] \qquad + \frac{1}{2}\Omega_C\left[S_C\right] \qquad\qquad + \frac{1}{2}\Omega_0 \ \left[I\right]$$

$$(2.4.18a)$$

Contrast this with the quantum spin matrix operator form for **H**=**Ω•S+$\Omega_0$1** given by (2.4.9) thru (2.4.15).

$$\begin{pmatrix} A & B-iC \\ B+iC & D \end{pmatrix} = \left[A-D\right]\begin{pmatrix} \frac{1}{2} & 0 \\ 0 & -\frac{1}{2} \end{pmatrix} + 2B\begin{pmatrix} 0 & \frac{1}{2} \\ \frac{1}{2} & 0 \end{pmatrix} + 2C\begin{pmatrix} 0 & -\frac{i}{2} \\ \frac{i}{2} & 0 \end{pmatrix} + \frac{A+D}{2}\begin{pmatrix} 1 & 0 \\ 0 & 1 \end{pmatrix} \qquad (2.4.18b)$$

$$\mathbf{H} = \quad \Omega_A \quad \mathbf{S}_A \quad + \Omega_B \ \mathbf{S}_B \quad + \Omega_C \ \mathbf{S}_C \quad + \ \Omega_0 \ \mathbf{1}$$

Classical S_a-magnitude is $I/2 = \sqrt{S_A^2 + S_B^2 + S_C^2}$ but the matrix forms give: $\mathbf{S}_A^2 + \mathbf{S}_B^2 + \mathbf{S}_C^2 = \frac{3}{4}\mathbf{1}$.

(b) Oscillator states by spinor rotation

Sophus Lie sought to define classical dynamics in terms of transformation operators. The preceding (2.4.10) and (2.4.15) let us do this for a *2D* oscillator by relating it to a *3D* spinning body. All states $|a\rangle = \binom{a_1}{a_2}$ of a *2D* oscillator or *3D* body are defined by rotation **R** of an initial *2D* state $|1\rangle = \binom{1}{0}$ or *3D* vector $\mathbf{S}(1) = (0,0,1)$.

$$|a\rangle = \begin{pmatrix} a_1 \\ a_2 \end{pmatrix} = \mathbf{R}(a)|1\rangle = \left\langle e^{-i\boldsymbol{\sigma}\bullet\vec{\phi}}a \right\rangle_{2\times2} \begin{pmatrix} 1 \\ 0 \end{pmatrix} \quad (2.4.19a) \qquad \mathbf{S}(a) = \begin{pmatrix} S_A(a) \\ S_B(a) \\ S_C(a) \end{pmatrix} = \mathbf{R}(a)\bullet\mathbf{S}(1) = \left\langle e^{-i\mathbf{S}\bullet\vec{\Theta}} \right\rangle_{3\times3} \begin{pmatrix} 0 \\ 0 \\ 1 \end{pmatrix} \quad (2.4.19b)$$

3D rotation **R** has 3 parameters $(\Theta_A, \Theta_B, \Theta_C)$ or else 3 *Euler angles* (α,β,γ) as shown in Fig. 2.4.3. That can define a *2D* oscillator's 4 phase variables (x_1, p_1, x_2, p_2) if energy is conserved. Else, we need to include an *intensity amplitude* $I^{1/2} = A$ with the 3 rotation angles. Euler's *ZYZ* or *ACA* rotation of 1st-state $|1\rangle$ gives state $|a\rangle = \mathbf{R}_a|1\rangle$ of spin *S* with 2 polar angles (α,β) and a *phase factor* $e^{-i\frac{\gamma}{2}}$ with phase $-\gamma/2$.

$$|a\rangle = \mathbf{R}(\alpha\beta\gamma)|1\rangle \qquad \textit{(Euler's definition of any state } |a\rangle \textit{)} \qquad (2.4.20a)$$

$$= \mathbf{R}[\alpha \text{ about } Z]\cdot\mathbf{R}[\beta \text{ about } Y]\cdot\mathbf{R}[\gamma \text{ about } Z]|\uparrow\rangle \qquad \textit{(Using matrix } \mathbf{R}(\alpha/2) \textit{ of (2.4.14a) and } \mathbf{R}(\beta/2) \textit{ of (2.4.14c))}$$

$$= \begin{pmatrix} e^{-i\frac{\alpha}{2}} & 0 \\ 0 & e^{i\frac{\alpha}{2}} \end{pmatrix} \begin{pmatrix} \cos\frac{\beta}{2} & -\sin\frac{\beta}{2} \\ \sin\frac{\beta}{2} & \cos\frac{\beta}{2} \end{pmatrix} \begin{pmatrix} e^{-i\frac{\gamma}{2}} & 0 \\ 0 & e^{i\frac{\gamma}{2}} \end{pmatrix} \begin{pmatrix} A \\ 0 \end{pmatrix} = \begin{pmatrix} e^{-i\frac{\alpha+\gamma}{2}}\cos\frac{\beta}{2} & -e^{-i\frac{\alpha-\gamma}{2}}\sin\frac{\beta}{2} \\ e^{i\frac{\alpha-\gamma}{2}}\sin\frac{\beta}{2} & e^{i\frac{\alpha+\gamma}{2}}\cos\frac{\beta}{2} \end{pmatrix} \begin{pmatrix} A \\ 0 \end{pmatrix} = A \begin{pmatrix} e^{-i\frac{\alpha}{2}}\cos\frac{\beta}{2} \\ e^{i\frac{\alpha}{2}}\sin\frac{\beta}{2} \end{pmatrix} e^{-i\frac{\gamma}{2}} = \begin{pmatrix} x_1 + ip_1 \\ x_2 + ip_2 \end{pmatrix}$$

Real x_k and imaginary p_k parts of phasor variables $a_k = x_k + ip_k$ are functions of all 3 Euler angles (α,β,γ) and A.

$$x_1 = A\cos(\alpha+\gamma)/2\cdot\cos\beta/2 \qquad\qquad x_2 = A\cos(\alpha-\gamma)/2\cdot\sin\beta/2 \qquad\qquad (2.4.20b)$$

$$p_1 = -A\sin(\alpha+\gamma)/2\cdot\cos\beta/2 \qquad\qquad p_2 = A\sin(\alpha-\gamma)/2\cdot\sin\beta/2 \qquad\qquad (2.4.20c)$$

But, the 3 components (2.4.16) of spin vector *S* depend on only 2 polar angles (α,β) and *I* as in Fig. 2.4.3.

$$S_A = \frac{1}{2}\left[x_1^2 + p_1^2 - x_2^2 - p_2^2\right] = \frac{I}{2}[\cos^2\frac{\beta}{2} - \sin^2\frac{\beta}{2}] = \frac{I}{2}\cos\beta \qquad (2.4.21a)$$

$$S_B = \left[p_1 p_2 + x_1 x_2\right] = I\left[-\sin\frac{\alpha+\gamma}{2}\sin\frac{\alpha-\gamma}{2} + \cos\frac{\alpha+\gamma}{2}\cos\frac{\alpha-\gamma}{2}\right]\cos\frac{\beta}{2}\sin\frac{\beta}{2} = \frac{I}{2}\cos\alpha\sin\beta \qquad (2.4.21b)$$

$$S_C = \left[x_1 p_2 - x_2 p_1\right] = I\left[\cos\frac{\alpha+\gamma}{2}\sin\frac{\alpha-\gamma}{2} - \cos\frac{\alpha-\gamma}{2}\cdot-\sin\frac{\alpha+\gamma}{2}\right]\cos\frac{\beta}{2}\sin\frac{\beta}{2} = \frac{I}{2}\sin\alpha\sin\beta \qquad (2.4.21c)$$

Intensity factor $I = A^2$ is called a *norm* and is unity $(I=1=A)$ for quantum states. Here it is the total *action* of classical oscillators. Spin (S_A, S_B, S_C) is independent of phase $-\gamma/2$. Action I is independent of γ, β, and α.

$$\textit{Action} = 2S_0 = (a|\mathbf{1}|a) = \left[x_1^2 + p_1^2 + x_2^2 + p_2^2\right] = I[\cos^2\frac{\beta}{2} + \sin^2\frac{\beta}{2}] = I = \textit{Intensity} \qquad (2.4.21d)$$

According to (2.4.18 a,b,c) action is twice the spin magnitude: $I/2 = \sqrt{S_A^2 + S_B^2 + S_C^2}$.

Let a *2D elliptic orbit* of frequency ω have amplitudes A_1 and A_2, and phase shifts ρ_1 and $\rho_2 = -\rho_1$.

$$x_1 = A_1\cos(\omega t + \rho_1) \qquad\qquad x_2 = A_2\cos(\omega t - \rho_1) \qquad\qquad (2.4.22a)$$

$$p_1 = -A_1\sin(\omega t + \rho_1) \qquad\qquad p_2 = -A_2\sin(\omega t - \rho_1) \qquad\qquad (2.4.22b)$$

This is a case of (2.4.20). Euler angles (α,β,γ) and action amplitude A are set to match (2.4.22) as follows.

$$\alpha = 2\rho_1 \qquad \tan\beta/2 = A_2/A_1 \qquad \gamma = 2\omega\cdot t \qquad A^2 = A_1^2 + A_2^2 \qquad (2.4.22c)$$

This example is used to show how the Stokes-Hamilton formulas expose orbital geometry and dynamics.

S_Z Original
Spin State $|1\rangle$
S $= |\uparrow\rangle$

S_X S_Y

(2) Rotate by β
around Y

β

S

(1) Rotate by γ
around Z

γ

S

γ

(3) Rotate by α
around Z

S_Z

α

S

β

S

S_Y

$S_X =$
$S\cos\alpha\sin\beta$

$S_Y = S\sin\alpha\sin\beta$

β

S

$S_Z = S\cos\beta$

γ

α

General Spin State
$|\Psi\rangle = \mathbf{R}(\alpha\beta\gamma)|\uparrow\rangle$
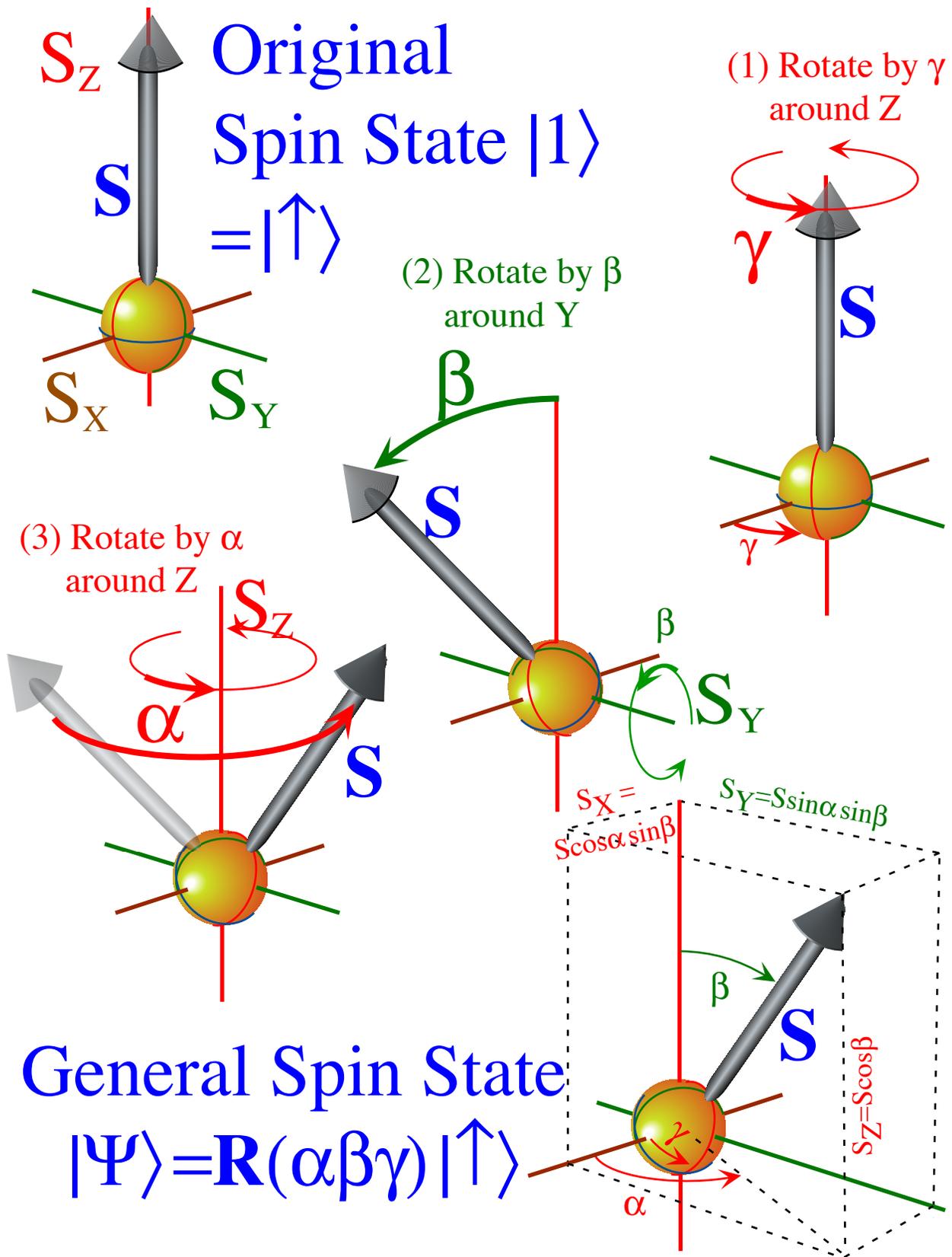
Fig. 2.4.3 The operational definition of Euler (αβγ)-angle coordinates is applied to a unit spin-state.

The A-view in {x₁,x₂}-basis

The orbit (2.4.22) has angles $\alpha_A=\rho_1-\rho_2=2\rho_1$, $\beta_A=2\tan^{-1}A_2/A_1$, and $\gamma_A=\omega t/2$ with intensity $I=A^2=A_1^2+A_2^2$.

$$\begin{pmatrix} a_1 \\ a_2 \end{pmatrix} = A \begin{pmatrix} e^{-i\alpha_A/2}\cos\frac{\beta_A}{2} \\ e^{+i\alpha_A/2}\sin\frac{\beta_A}{2} \end{pmatrix} e^{-i\omega t} = A \begin{pmatrix} \left(\cos(\omega t+\frac{\alpha_A}{2})-i\sin(\omega t+\frac{\alpha_A}{2})\right)\cos\frac{\beta_A}{2} \\ \left(\cos(\omega t-\frac{\alpha_A}{2})-i\sin(\omega t-\frac{\alpha_A}{2})\right)\sin\frac{\beta_A}{2} \end{pmatrix} = \begin{pmatrix} x_1+ip_1 \\ x_2+ip_2 \end{pmatrix} \quad (2.4.23)$$

Fig. 2.4.3 shows an ellipse (2.4.22) next to its *ABC* space **S**-vector (2.4.21) for *A* or *Z*-axis Euler angles

$\alpha=\alpha_A=\rho_1-\rho_2=2\rho_1=60°$ (2.4.24a) $\beta=\beta_A=2\tan^{-1}A_2/A_1=60°$ (2.4.24b) $\gamma_A=\omega t/2$.   (2.4.24c)

Cartesian-x_1x_2 axes in Fig. 2.4.3a map onto $\pm A$ or Z -axis in Fig. 2.4.3b. Azimuth angle-α_A off the *B*-axis is the phase lag between $a_1=e^{-i\alpha/2}|a_1|$ and $a_2=e^{+i\alpha/2}|a_2|$ in (2.4.23). Note projected A_1 or A_2 box contact points in Fig. 2.4.2a. Contact points go to the box diagonal for $\alpha_A=0°$ or the other diagonal for $\alpha_A=180°$, or the box x_k-axes for $\alpha_A=\pm90°$. Polar β_A angle of **S** from *A*-or-*z*-axis is the angle between ellipse box diagonals in Fig. 2.4.2a. An orbit with $\beta_A=0°(180°)$ is $x_1(x_2)$-polarized. Circular orbits have $\beta_A=\pm90°=\alpha_A$.
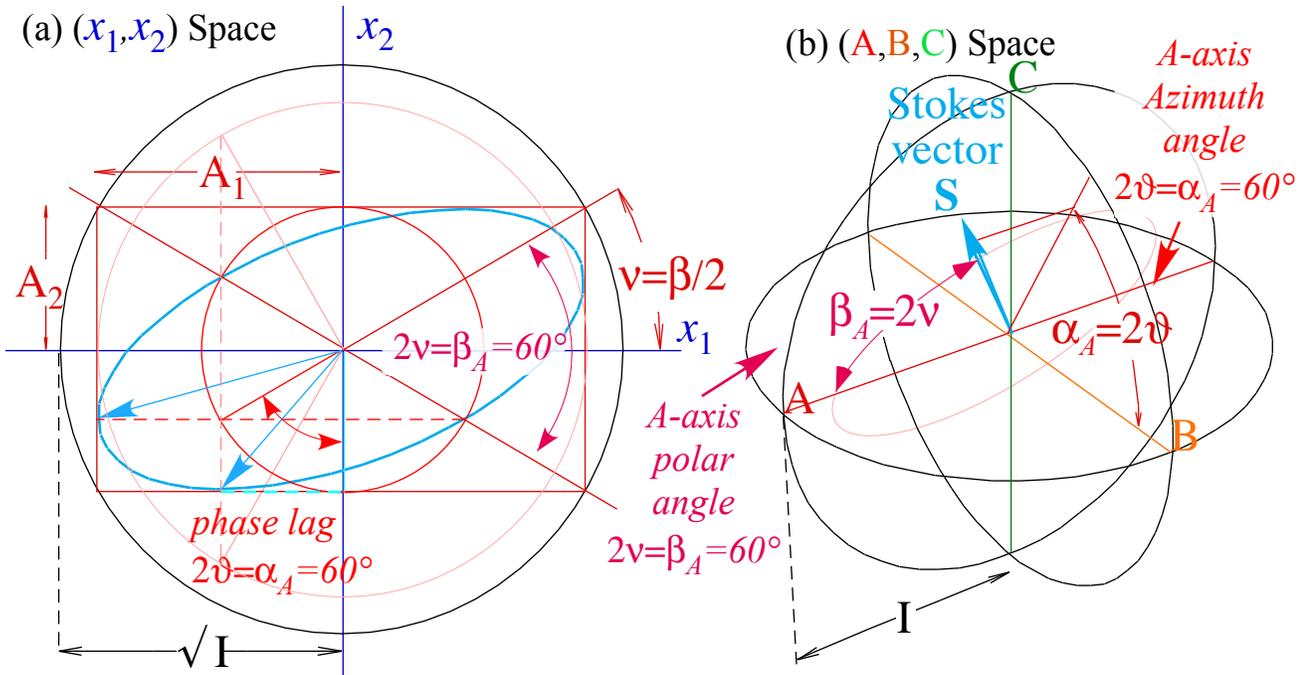
Fig. 2.4.3 Polarization described by (a) plane-x_1x_2 bases and (b) A-axis polar angles of Stokes vector.

Converting an *A*-based set (2.4.20) of Stokes parameters into a *C*-based one or into a *B*-based one is simply a matter of cyclic permutation of *A*, *B*, and *C* polar formulas as follows.

Asymmetry $S_A=\dfrac{I}{2}\cos\beta_A$ $=\dfrac{I}{2}\sin\alpha_B\sin\beta_B=\dfrac{I}{2}\cos\alpha_C\sin\beta_C$ (2.4.25a)

Balance $S_B=\dfrac{I}{2}\cos\alpha_A\sin\beta_A=\dfrac{I}{2}\cos\beta_B$ $=\dfrac{I}{2}\sin\alpha_C\sin\beta_C$ (2.4.25b)

Circularity $S_C=\dfrac{I}{2}\sin\alpha_A\sin\beta_A$ $=\dfrac{I}{2}\cos\alpha_B\sin\beta_B=\dfrac{I}{2}\cos\beta_C$ (2.4.25 c)

To find the *C*-axis polar angle β_C in terms of *A*-axis angles α_A and β_A, we use (2.4.25 c).

The C-view in {xR,xL}-basis

The same orbit can be expressed in right and left circular polarization $\{x_R, x_L\}$-bases using angles $(\alpha_C, \beta_C, \gamma_C)$.

$$\begin{pmatrix} a_R \\ a_L \end{pmatrix} = A \begin{pmatrix} e^{-i\alpha_C/2}\cos\frac{\beta_C}{2} \\ e^{+i\alpha_C/2}\sin\frac{\beta_C}{2} \end{pmatrix} e^{-i\frac{\gamma_C}{2}} = \begin{pmatrix} x_R + ip_R \\ x_R + ip_R \end{pmatrix} \tag{2.4.26}$$

Angles (α_C, β_C) are found quickly using (2.4.25). C-axial polar angle β_C uses (2.4.25c). See β_C in Fig. 2.4.4b.

$$\sin\alpha_A \sin\beta_A = \cos\beta_C \qquad \text{or:} \quad \beta_C = ACS(\sin\alpha_A \sin\beta_A) = ACS(\frac{\sqrt{3}}{2}\cdot\frac{\sqrt{3}}{2}) = 41.4° \tag{2.4.27}$$

C-axis azimuth angle α_C relates to A-axis angles α_A and β_A by (2.4.25a) and (2.4.25b). See α_C in Fig. 2.4.4b.

$$\frac{\cos\alpha_A \sin\beta_A}{\cos\beta_A} = \tan\alpha_C \quad \text{or:} \quad \alpha_C = ATN2(\cos\alpha_A \sin\beta_A / \cos\beta_A) = ATN2(\frac{1}{2}\cdot\frac{\sqrt{3}}{2} / \frac{1}{2}) = 40.9° \tag{2.4.28}$$

Half the azimuth angle α_C turns is the ellipse tipping angle $\varphi = \alpha_C/2$, and half –polar-elevation $2\psi = \pi/2 - \beta_C$ is the ellipse diagonal half-angle ψ as seen in Fig. 2.4.4a. Recall, *2D* angles are $\frac{1}{2}$ the corresponding *3D* ones.
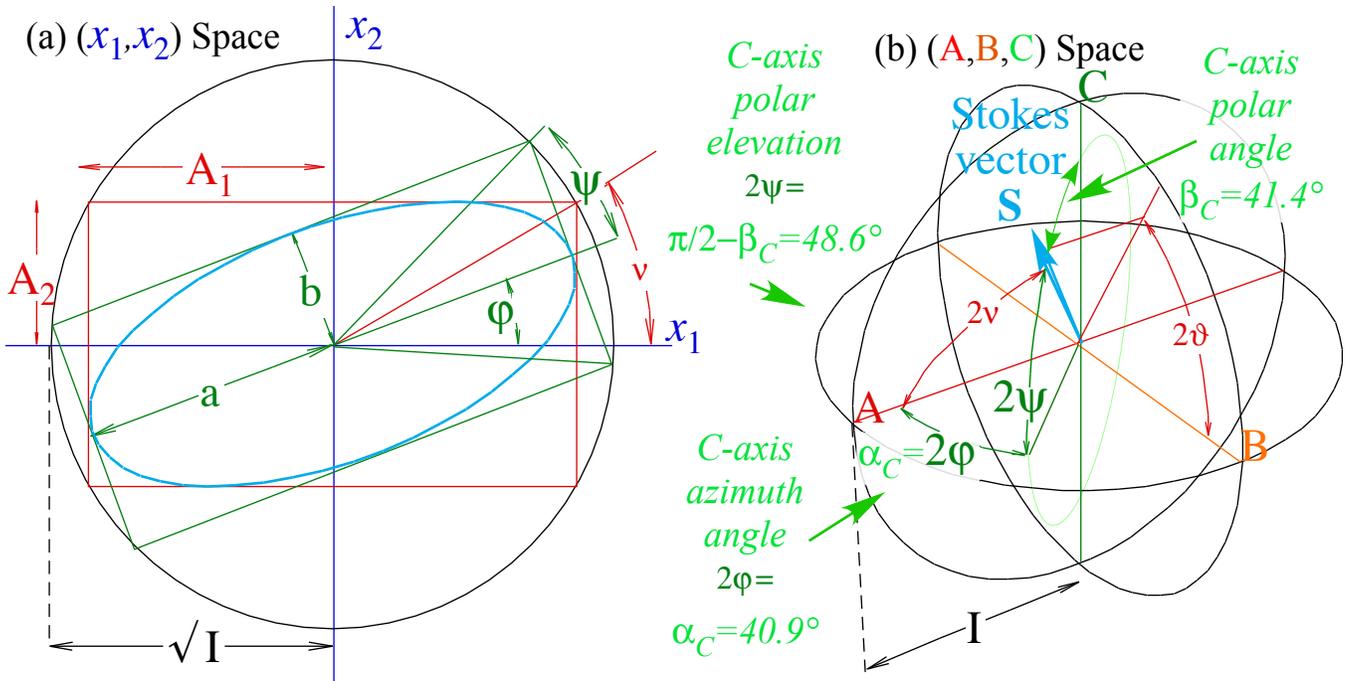
Fig. 2.4.4 Polarization described by (a) circular-RL bases and (b) C-axis polar angles of Stokes vector.

A 90° B –rotation $\mathbf{R}(\pi/4)|x_1\rangle = |x_R\rangle$ of axis A into C gets $(\alpha_C, \beta_C, \gamma_C)$ from $(\alpha_A, \beta_A, \gamma_A)$ all at once.

$$\begin{pmatrix} \cos\frac{\pi}{4} & i\sin\frac{\pi}{4} \\ i\sin\frac{\pi}{4} & \cos\frac{\pi}{4} \end{pmatrix}\begin{pmatrix} x_1+ip_1 \\ x_2+ip_2 \end{pmatrix} = \frac{\sqrt{2}}{2}\begin{pmatrix} 1 & i \\ i & 1 \end{pmatrix}\begin{pmatrix} Ae^{-i\alpha_A/2}\cos\frac{\beta_A}{2} \\ Ae^{+i\alpha_A/2}\sin\frac{\beta_A}{2} \end{pmatrix}e^{-i\frac{\gamma_A}{2}} = \begin{pmatrix} Ae^{-i\alpha_C/2}\cos\frac{\beta_C}{2} \\ Ae^{+i\alpha_C/2}\sin\frac{\beta_C}{2} \end{pmatrix}e^{-i\frac{\gamma_C}{2}} = \begin{pmatrix} x_R+ip_R \\ x_R+ip_R \end{pmatrix} \tag{2.4.29}$$

Circular polarization is the more natural for applications that involve *chirality* or "handedness" associated with magnetic fields or Coriolis rotational effects. Then the C-axis becomes the "special z-one" as indicated in Fig. 2.4.5.

(a)
Stokes Vector
ABC-Space

(b)
Polarization
xy-Space
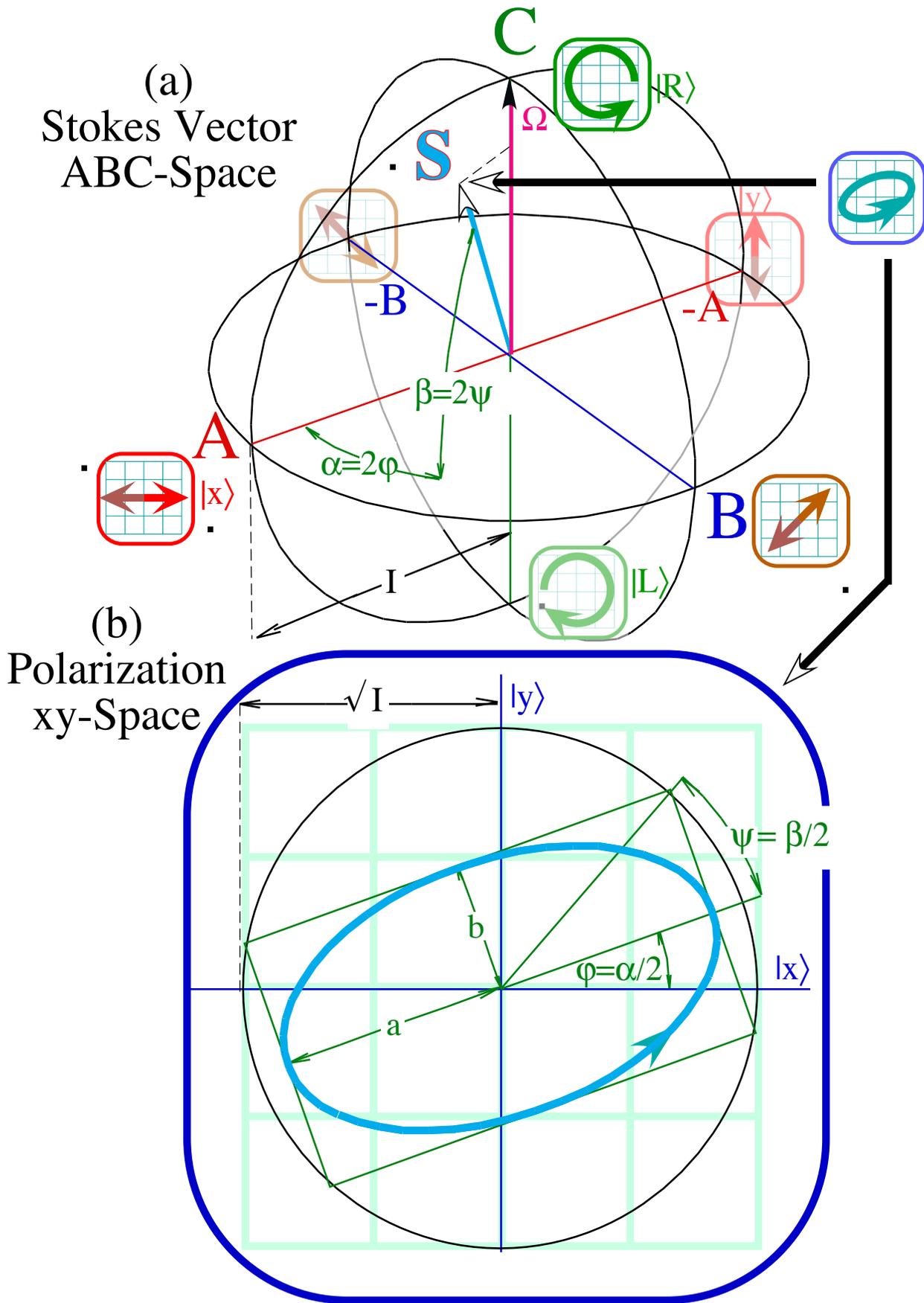
Fig. 2.4.5 Polarization variables (a) Stokes real-vector space (ABC) (b) Complex xy-spinor-space (x_1, x_2).

(c) How spinors give eigensolutions *(Gone in 60 seconds!)*

Can you write down all eigensolutions to the following **H** -matrix in 60 seconds?

$$\mathbf{H} = \begin{pmatrix} 10 + 4\cos\dfrac{\pi}{3} & 4\cos\dfrac{\pi}{4}\sin\dfrac{\pi}{3} - i4\sin\dfrac{\pi}{4}\sin\dfrac{\pi}{3} \\ 4\cos\dfrac{\pi}{4}\sin\dfrac{\pi}{3} + i4\sin\dfrac{\pi}{4}\sin\dfrac{\pi}{3} & 10 - 4\cos\dfrac{\pi}{3} \end{pmatrix} = \begin{pmatrix} 12 & \sqrt{6}(1-i) \\ \sqrt{6}(1+i) & 8 \end{pmatrix}$$

We're not just asking for eigen*values* in 60 minutes, but *all* eigen*solutions*, vectors *and* values, in *60 seconds flat*! If you know your spinors, it's as easy as π . Here they are.

$\underline{eigenvalue - 1}$

$$\omega_{\uparrow} = 10 + \sqrt{\left(\frac{12-8}{2}\right)^2 + \left(\sqrt{6}\right)^2 + \left(\sqrt{6}\right)^2}$$

$$= 10 + 4 = 14$$

$\underline{eigenvector - 1}$

$$\left|\uparrow\right\rangle = \begin{pmatrix} e^{-i\frac{\pi}{8}}\cos\dfrac{\pi}{6} \\ e^{+i\frac{\pi}{8}}\sin\dfrac{\pi}{6} \end{pmatrix} = \begin{pmatrix} 1 \\ e^{i\frac{\pi}{4}}\dfrac{\sqrt{3}}{3} \end{pmatrix} e^{-i\frac{\pi}{8}}\dfrac{\sqrt{3}}{2}$$

$\underline{eigenvalue - 2}$

$$\omega_{\downarrow} = 10 - \sqrt{\left(\frac{12-8}{2}\right)^2 + \left(\sqrt{6}\right)^2 + \left(\sqrt{6}\right)^2}$$

$$= 10 - 4 = 6$$

$\underline{eigenvector - 2}$

$$\left|\downarrow\right\rangle = \begin{pmatrix} -e^{-i\frac{\pi}{8}}\sin\dfrac{\pi}{6} \\ e^{+i\frac{\pi}{8}}\cos\dfrac{\pi}{6} \end{pmatrix} = \begin{pmatrix} -e^{i\frac{\pi}{4}}\dfrac{\sqrt{3}}{3} \\ 1 \end{pmatrix} e^{-i\frac{\pi}{8}}\dfrac{\sqrt{3}}{2}$$

The trick: Get the **H** crank vector $\vec{\Omega}$ polar angles of azimuth φ , polar ϑ , and rate Ω . Here $\Omega = 8$.

$$\vec{\Omega} = [(A-D), 2B, 2C] = \Omega[\cos\vartheta, \cos\varphi\sin\vartheta, \sin\varphi\sin\vartheta] \quad \text{where:} \quad \Omega = \sqrt{(A-D)^2 + (2B)^2 + (2C)^2} \quad (2.4.30a)$$

$$\mathbf{H} = \begin{pmatrix} \dfrac{A+D}{2} + \dfrac{\Omega}{2}\cos\vartheta & \dfrac{\Omega}{2}\cos\varphi\sin\vartheta - i\dfrac{\Omega}{2}\sin\varphi\sin\vartheta \\ \dfrac{\Omega}{2}\cos\varphi\sin\vartheta + i\dfrac{\Omega}{2}\sin\varphi\sin\vartheta & \dfrac{A+D}{2} - \dfrac{\Omega}{2}\cos\vartheta \end{pmatrix} = \begin{pmatrix} A & B-iC \\ B+iC & D \end{pmatrix} \quad (2.4.30b)$$

Eigenstate $\left|\uparrow\right\rangle$ spin vector $\vec{s}$ has Euler angles of azimuth $\alpha = \varphi$, pole $\beta = \vartheta$, and any phase $(\text{let:}\gamma = 0)$.

$$\left|\uparrow\right\rangle = \begin{pmatrix} e^{-i\frac{\alpha}{2}}\cos\dfrac{\beta}{2} \\ e^{+i\frac{\alpha}{2}}\sin\dfrac{\beta}{2} \end{pmatrix} e^{-i\frac{\gamma}{2}} = \begin{pmatrix} e^{-i\frac{\varphi}{2}}\cos\dfrac{\vartheta}{2} \\ e^{+i\frac{\varphi}{2}}\sin\dfrac{\vartheta}{2} \end{pmatrix} \qquad \left|\downarrow\right\rangle = \begin{pmatrix} e^{-i\frac{\alpha}{2}}\cos\dfrac{\beta}{2} \\ e^{+i\frac{\alpha}{2}}\sin\dfrac{\beta}{2} \end{pmatrix} e^{-i\frac{\gamma}{2}} = \begin{pmatrix} -e^{-i\frac{\varphi}{2}}\sin\dfrac{\vartheta}{2} \\ e^{+i\frac{\varphi}{2}}\cos\dfrac{\vartheta}{2} \end{pmatrix} \quad (2.4.30c)$$

$$\text{has eigenvalue: } \omega_{\uparrow} = \dfrac{A+D}{2} + \dfrac{\Omega}{2} \qquad\qquad \text{has eigenvalue: } \omega_{\downarrow} = \dfrac{A+D}{2} - \dfrac{\Omega}{2}$$

Eigenstate $\left|\downarrow\right\rangle$ with spin vector $-\vec{s}$ has same azimuth $\alpha = \varphi$, flipped pole $\beta = \vartheta \pm \pi$, and arbitrary phase $\gamma/2$.

It doesn't get much easier! You just line up state spin vector- $\vec{s}$ angles (α, β) and (φ, ϑ) of Hamiltonian

crank vector to get the first (spin-up) eigenstate, and then stick $\vec{s}$ the other way to get an orthogonal (spin-down)

eigenstate. But, don't goof the **H** angles. Use *atan2* or $Rct \rightleftharpoons Pol$.

$$\varphi = atan2(C, B) \quad [\tan^{-1}(C / B) \text{ is unreliable}] \qquad\qquad \vartheta = atan2(2\sqrt{B^2 + C^2}, A - D)$$

Simple arc-functions like *arctan(C/B)* are unreliable due to their multi-valued quadrant ambiguity.

(d) How spinors give time evolution

Can you just as quickly write down the evolution operator of that Hamiltonian?

$$\mathbf{U}(0,t)=e^{-i\mathbf{H}t/\hbar}=e^{-i\begin{pmatrix}12 & \sqrt{6}(1-i)\\ \sqrt{6}(1+i) & 8\end{pmatrix}t/\hbar}=\begin{pmatrix}? & ?\\ ? & ?\end{pmatrix}$$

A formal exponential is pretty useless unless you expand it using the **H** -crank $\vec{\Omega}$ in (2.4.15c).

$$e^{-i(\sigma\bullet\vec{\Omega}t)/2}=e^{-i\mathbf{S}\bullet\vec{\Omega}t}=\mathbf{1}\cos\frac{\Omega t}{2}-i\,(\sigma\bullet\hat{\Omega})\sin\frac{\Omega t}{2}$$

This is the $e^{-i\mathbf{S}\bullet\vec{\Theta}}$ formula (2.4.15a) with whirl rate-times-time $\vec{\Omega}t=\vec{\Theta}$ replacing turn-axis vector $\vec{\Theta}$.

$$\mathbf{U}(0,t)=e^{-i(\sigma\bullet\vec{\Omega}t)/2}=\mathbf{1}\cos\frac{\Omega t}{2}-i\,(\sigma\bullet\hat{\Omega})\sin\frac{\Omega t}{2}\qquad\left(\begin{array}{c}\text{The overall phase factor }e^{-i\frac{A+D}{2}t}\\ \text{may be attached later. (Or ignored)}\end{array}\right)\qquad(2.4.31a)$$

(The *unit* crank vector $\hat{\Omega}=[(A-D),2B,2C]/\Omega=[\cos\vartheta,\cos\varphi\sin\vartheta,\sin\varphi\sin\vartheta]$ is also *unit* $\hat{\Theta}$.)

$$\mathbf{U}(0,t)=\quad\mathbf{1}\quad\cos\frac{\Omega t}{2}-i\,(\quad\sigma_A\quad\cos\vartheta+\quad\sigma_B\quad\cos\varphi\sin\vartheta+\quad\sigma_C\quad\sin\varphi\sin\vartheta)\sin\frac{\Omega t}{2}$$

$$=\begin{pmatrix}1 & 0\\ 0 & 1\end{pmatrix}\cos\frac{\Omega t}{2}-i\,\left(\begin{pmatrix}1 & 0\\ 0 & -1\end{pmatrix}\cos\vartheta+\begin{pmatrix}0 & 1\\ 1 & 0\end{pmatrix}\cos\varphi\sin\vartheta+\begin{pmatrix}0 & -i\\ i & 0\end{pmatrix}\sin\varphi\sin\vartheta\right)\sin\frac{\Omega t}{2}$$

$$(2.4.31b)$$

Sum this all into a single matrix and you get a useful general evolution operator.

$$\mathbf{U}(0,t)=\begin{pmatrix}\cos\frac{\Omega t}{2}-i\cos\vartheta\sin\frac{\Omega t}{2} & -i(\cos\varphi-i\sin\varphi)\sin\vartheta\sin\frac{\Omega t}{2}\\[2mm] -i(\cos\varphi-i\sin\varphi)\sin\vartheta\sin\frac{\Omega t}{2} & \cos\frac{\Omega t}{2}+i\cos\vartheta\sin\frac{\Omega t}{2}\end{pmatrix}$$

$$=\begin{pmatrix}\cos\frac{\Omega t}{2}-i\cos\vartheta\sin\frac{\Omega t}{2} & -ie^{-i\varphi}\sin\vartheta\sin\frac{\Omega t}{2}\\[2mm] -ie^{+i\varphi}\sin\vartheta\sin\frac{\Omega t}{2} & \cos\frac{\Omega t}{2}+i\cos\vartheta\sin\frac{\Omega t}{2}\end{pmatrix}=\begin{pmatrix}\cos\frac{\Omega t}{2}-i\hat{\Omega}_A\sin\frac{\Omega t}{2} & -i\left(\hat{\Omega}_B-i\hat{\Omega}_C\right)\sin\frac{\Omega t}{2}\\[2mm] -i\left(\hat{\Omega}_B+i\hat{\Omega}_C\right)\sin\frac{\Omega t}{2} & \cos\frac{\Omega t}{2}+i\hat{\Omega}_A\sin\frac{\Omega t}{2}\end{pmatrix}$$

$$(2.4.31c)$$

Our numerical crank rate is $\Omega=8$. Our *unit* crank rate vector $\hat{\Omega}$ fills in the numbers for $\mathbf{U}(0,t)$.

$$\hat{\Omega}=\frac{[(12-8),2\sqrt{6},2\sqrt{6}]}{\Omega}=\left[\frac{1}{2},\frac{\sqrt{6}}{4},\frac{\sqrt{6}}{4}\right]=[\cos\vartheta,\cos\varphi\sin\vartheta,\sin\varphi\sin\vartheta]=[\hat{\Omega}_A,\hat{\Omega}_B,\hat{\Omega}_C]$$

$$\mathbf{U}(0,t)=\begin{pmatrix}\cos 4t-i\frac{1}{2}\sin 4t & -i(1-i)\frac{\sqrt{6}}{4}\sin 4t\\[2mm] -i(1+i)\frac{\sqrt{6}}{4}\sin 4t & \cos 4t+i\frac{1}{2}\sin 4t\end{pmatrix}$$

Starting from any initial state like $\left|\Psi(0)\right\rangle=\begin{pmatrix}1\\ 0\end{pmatrix}$ we compute what it will be at time t.

$$\left|\Psi(t)\right\rangle=\mathbf{U}(0,t)\left|\Psi(0)\right\rangle=\begin{pmatrix}\cos 4t-i\frac{1}{2}\sin 4t & -i(1-i)\frac{\sqrt{6}}{4}\sin 4t\\[2mm] -i(1+i)\frac{\sqrt{6}}{4}\sin 4t & \cos 4t+i\frac{1}{2}\sin 4t\end{pmatrix}\begin{pmatrix}1\\ 0\end{pmatrix}=\begin{pmatrix}\cos 4t-i\frac{1}{2}\sin 4t\\[2mm] (1-i)\frac{\sqrt{6}}{4}\sin 4t\end{pmatrix}$$

B-Type Oscillation: Simple examples of balanced beats

Resonant beats in Fig. 4.3.9 are super-positions of a 0°-in-phase mode (○→ ○→) of slower frequency ω_{slow} and a 180°-out-of-phase mode (○→ ←○) of faster frequency ω_{fast}. Transverse 0°-in-phase modes $\left(\begin{array}{c}○→\\○→\end{array}\right)$ and 180°-out-of-phase modes $\left(\begin{array}{c}○→\\←○\end{array}\right)$ belong to complex amplitude vectors $e^{-i\omega_{slow}t}\left(\begin{array}{c}1\\1\end{array}\right)$ and $e^{-i\omega_{fast}t}\left(\begin{array}{c}1\\-1\end{array}\right)$, respectively.

Let's add them half-and-half or 50-50. (We let slow and fast phases be $s=-\omega_{slow}t$ and $f=-\omega_{fast}t$.)

$$\left(\begin{array}{c}a_1^{50-50}\\a_2^{50-50}\end{array}\right)=\frac{1}{2}e^{-i\omega_{slow}t}\left(\begin{array}{c}1\\1\end{array}\right)+\frac{1}{2}e^{-i\omega_{fast}t}\left(\begin{array}{c}1\\-1\end{array}\right)=\frac{1}{2}e^{is}\left(\begin{array}{c}1\\1\end{array}\right)+e^{if}\left(\begin{array}{c}1\\-1\end{array}\right)=\frac{1}{2}\left(\begin{array}{c}e^{is}+e^{if}\\e^{is}-e^{if}\end{array}\right)\quad(2.4.32)$$

We could write the complex numbers in Cartesian form: $e^{is}=\cos s+i\sin s$ and $e^{if}=\cos f+i\sin f$.

$$\left(\begin{array}{c}a_1^{50-50}\\a_2^{50-50}\end{array}\right)=\frac{1}{2}\left(\begin{array}{c}e^{is}+e^{if}\\e^{is}-e^{if}\end{array}\right)=\frac{1}{2}\left(\begin{array}{c}\cos s+i\sin s+\cos f+i\sin f\\\cos s+i\sin s-\cos f-i\sin f\end{array}\right)=\frac{1}{2}\left(\begin{array}{c}(\cos s+\cos f)+i[\sin s+\sin f]\\(\cos s-\cos f)+i[\sin s-\sin f]\end{array}\right)=\left(\begin{array}{c}X_1+iP_1\\X_2+iP_2\end{array}\right)$$

Cartesian $X_1=Re\,a_1$, $P_1=Im\,a_1$, $X_2=Re\,a_2$, $P_2=Im\,a_2$ are then given. A factored polar form is better:

$$\left(\begin{array}{c}a_1^{50-50}\\a_2^{50-50}\end{array}\right)=\frac{1}{2}\left(\begin{array}{c}e^{is}+e^{if}\\e^{is}-e^{if}\end{array}\right)=\frac{1}{2}\left(\begin{array}{c}e^{i\frac{s+f}{2}}(e^{i\frac{s-f}{2}}+e^{-i\frac{s-f}{2}})\\e^{i\frac{s+f}{2}}(e^{i\frac{s-f}{2}}-e^{-i\frac{s-f}{2}})\end{array}\right)=\left(\begin{array}{c}e^{i\frac{s+f}{2}}\cos\frac{s-f}{2}\\e^{i\frac{s+f}{2}}i\sin\frac{s-f}{2}\end{array}\right)\quad\text{where:}\quad\begin{array}{c}\cos A=\frac{e^{iA}+e^{-iA}}{2}\\[6pt]i\sin A=\frac{e^{iA}-e^{-iA}}{2}\end{array}$$

Note: this trick easily gives four *sin-cos* identities like $\cos\frac{s+f}{2}\cos\frac{s-f}{2}=\frac{1}{2}(\cos s+\cos f)$. Now we factor out overall phase and compute the (get real!) Stokes vector $\mathbf{S}=(S_A,S_B,S_C)$ as functions of time.

$$\left(\begin{array}{c}a_1^{50-50}\\a_2^{50-50}\end{array}\right)=e^{i\frac{s+f}{2}}\left(\begin{array}{c}\cos\frac{s-f}{2}\\i\sin\frac{s-f}{2}\end{array}\right)=e^{i\frac{s+f}{2}}\left(\begin{array}{c}\cos\frac{\Delta}{2}\\i\sin\frac{\Delta}{2}\end{array}\right)\quad\text{gives the following where: }\Delta=s-f=-\left(\omega_{fast}-\omega_{slow}\right)t.$$

$$S_A=\left(\begin{array}{cc}\cos\frac{\Delta}{2}&i\sin\frac{\Delta}{2}\end{array}\right)^*\left(\begin{array}{cc}1&0\\0&-1\end{array}\right)\left(\begin{array}{c}\cos\frac{\Delta}{2}\\i\sin\frac{\Delta}{2}\end{array}\right)=\left(\begin{array}{cc}\cos\frac{\Delta}{2}&-i\sin\frac{\Delta}{2}\end{array}\right)\left(\begin{array}{c}\cos\frac{\Delta}{2}\\-i\sin\frac{\Delta}{2}\end{array}\right)=\cos^2\frac{\Delta}{2}-\sin^2\frac{\Delta}{2}=\cos\Delta=\cos(s-f)$$

$$S_B=\left(\begin{array}{cc}\cos\frac{\Delta}{2}&i\sin\frac{\Delta}{2}\end{array}\right)^*\left(\begin{array}{cc}0&1\\1&0\end{array}\right)\left(\begin{array}{c}\cos\frac{\Delta}{2}\\i\sin\frac{\Delta}{2}\end{array}\right)=\left(\begin{array}{cc}\cos\frac{\Delta}{2}&-i\sin\frac{\Delta}{2}\end{array}\right)\left(\begin{array}{c}i\sin\frac{\Delta}{2}\\\cos\frac{\Delta}{2}\end{array}\right)=i\cos\frac{\Delta}{2}\sin\frac{\Delta}{2}-i\sin\frac{\Delta}{2}\cos\frac{\Delta}{2}=0$$

$$S_C=\left(\begin{array}{cc}\cos\frac{\Delta}{2}&i\sin\frac{\Delta}{2}\end{array}\right)^*\left(\begin{array}{cc}0&-i\\i&0\end{array}\right)\left(\begin{array}{c}\cos\frac{\Delta}{2}\\i\sin\frac{\Delta}{2}\end{array}\right)=\left(\begin{array}{cc}\cos\frac{\Delta}{2}&-i\sin\frac{\Delta}{2}\end{array}\right)\left(\begin{array}{c}\sin\frac{\Delta}{2}\\i\cos\frac{\Delta}{2}\end{array}\right)=\cos\frac{\Delta}{2}\sin\frac{\Delta}{2}+\sin\frac{\Delta}{2}\cos\frac{\Delta}{2}=\sin\Delta=\sin(s-f)$$

It is a B-axial rotation of Stokes vector $\mathbf{S}=(S_A,S_B,S_C)=(\cos\Delta,0,\sin\Delta)$ past $\pm$A and $\pm$C-axes as in Fig. 2.4.6.

The angular frequency $|\Delta| = |\omega_{fast} - \omega_{slow}|$ of the rotation is called a *beat frequency* . In quantum theory it is the *Rabi rotation frequency* or the *NMR precession frequency* in spin resonance that Rabi pioneered. It is simply the relative angular velocity between two phasors having a race around the clock. It is twice that of the half-difference $|\Delta/2| = |\omega_{fast} - \omega_{slow}|/2$ seen in phasor space. That mysterious factor of *1/2* discussed after (2.4.14) appears again and makes us sharpen our view of space and time.
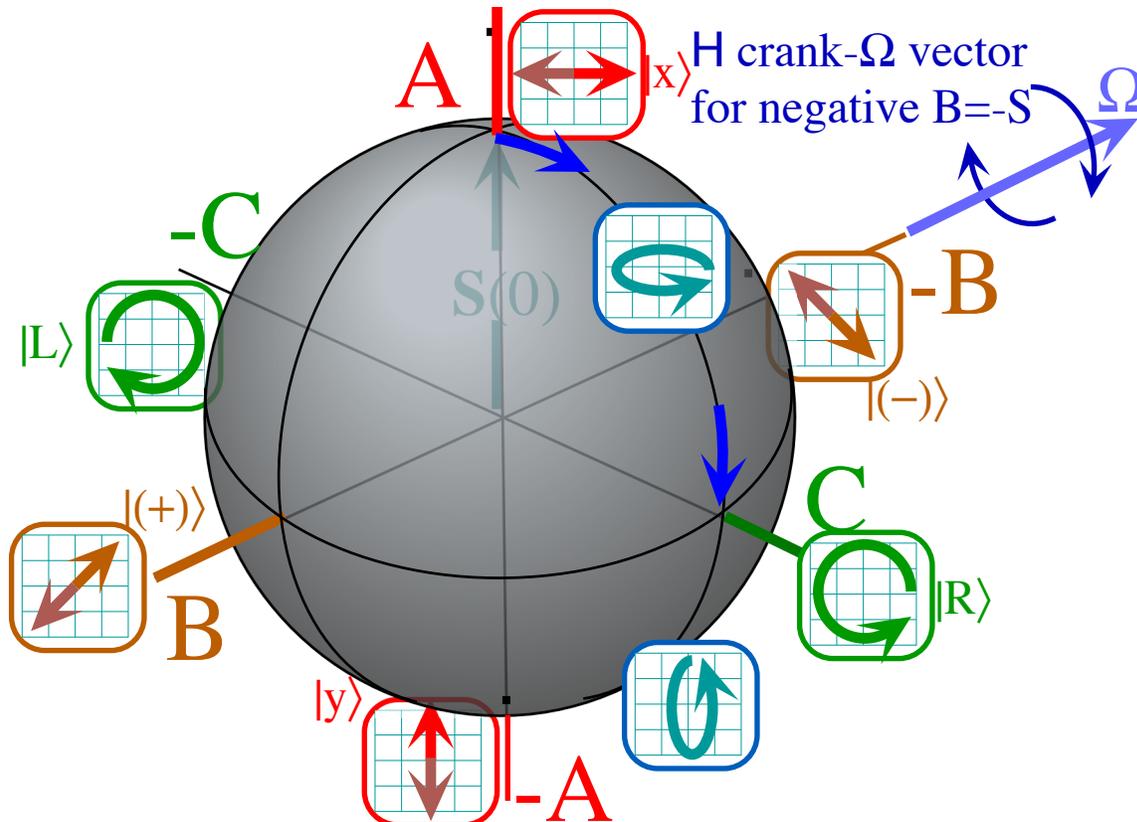
*Fig. 2.4.6 Time evolution of a B-type beat. **S**-vector rotates from A to C to -A to -C and back to A.*

For example if you follow the rotation in the $X_1 = Re\ a_1$, $P_1 = Im\ a_1$, $X_2 = Re\ a_2$, $P_2 = Im\ a_2$ space you will see that one rotation by 360° in ABC-space is only half way back to the starting line, and another 360° rotation (either way) is needed in ABC-space to get a full 360° rotation in phasor xy-space. That is, a rotation of 720° or 0° in the Stokes ABC-space is needed to return to where they started in *xy*-space.

Points that are separated by 180° in ABC-vector-space map onto phasor (2D-spinor) base vectors that are only 90° apart since in *xy*-space $|x\rangle$ and $|y\rangle$ are orthogonal. So a 180° separation in *xy*-space, that is, a 180° phase factor $e^{\pm i\pi} = -1$, maps onto the *same* Stokes-vector in ABC space. Another way to see this strange phase shift is to look at a C-rotation that happens in Circular polarization environments, or in a Cyclotron oscillator, or in the presence of a Coriolis or Chiral force of Earth rotation. (Notice all the C's including Complex that are used to describe the circular case.) The Fig. 2.4.7 shows how *+x*-polarization returns first to *–x*-polarization, that is 180° out of phase and needs another 360° rotation around the C-axis to really be back to *+x*-polarization. The

xy-spinor rotates by half the angle its Stokes vector turns in ABC-space so xy-oscillation vector returns to the North pole "pointing backwards" with a 180° phase shift.

*Fig. 2.4.7 Time evolution of a C-type beat. **S**-vector rotates from A to B to -A to -B and back to A.*

Exercise 2.4.1

The example given in (2.4.32) was a perfect 50-50 combination of the balanced ±45°polarization B-modes as repeated here.

$$\begin{pmatrix} a_1^{50-50} \\ a_2^{50-50} \end{pmatrix} = \frac{1}{2}e^{-i\omega_{slow}t}\begin{pmatrix} 1 \\ 1 \end{pmatrix} + \frac{1}{2}e^{-i\omega_{fast}t}\begin{pmatrix} 1 \\ -1 \end{pmatrix} = \frac{1}{2}e^{is}\begin{pmatrix} 1 \\ 1 \end{pmatrix} + \frac{1}{2}e^{if}\begin{pmatrix} 1 \\ -1 \end{pmatrix} = \frac{1}{2}\begin{pmatrix} e^{is} + e^{if} \\ e^{is} - e^{if} \end{pmatrix}$$

It starts at time *t=0* in the x-polarization state $\begin{pmatrix} 1 \\ 0 \end{pmatrix}$ goes through circular polarization and then y-polarization and so on.

What if, instead, we start at time *t=0* in the x-tipped-at-angle-ψ-polarization state $\begin{pmatrix} \cos\psi \\ \sin\psi \end{pmatrix}$?

_____

Find the combination of ±45°polarization B-mode vectors $\begin{pmatrix} 1 \\ 1 \end{pmatrix}/\sqrt{2}$, $\begin{pmatrix} 1 \\ -1 \end{pmatrix}/\sqrt{2}$ for intial state and it's initial Stokes vector.

Let the B-mode base vectors oscillate as they did in Fig. 2.4.6 and calculate how the Stokes vector of this initially (tipped-at-angle-ψ)-polarization state evolves vs. time *t*. To compare with an earlier phasor construction take $\omega_{slow}=1$ and $\omega_{fast}=2$.

Sketch or describe the results in ABC-space <u>and</u> xy-space for intial angles ψ=15°, 30°, 45°.

Solutions to ψ-state dynamics

ψ-polarization state $\begin{pmatrix} \cos\psi \\ \sin\psi \end{pmatrix}$ is an (a_+, a_-) combination of B-unit vectors $|+\rangle = \begin{pmatrix} \frac{1}{\sqrt{2}} \\ \frac{1}{\sqrt{2}} \end{pmatrix}$ and $|-\rangle = \begin{pmatrix} \frac{1}{\sqrt{2}} \\ \frac{-1}{\sqrt{2}} \end{pmatrix}$.

$|\psi\rangle = a_+|+\rangle + a_-|-\rangle$ is represented by $\begin{pmatrix} \cos\psi \\ \sin\psi \end{pmatrix} = a_+ \begin{pmatrix} \frac{1}{\sqrt{2}} \\ \frac{1}{\sqrt{2}} \end{pmatrix} + a_- \begin{pmatrix} \frac{1}{\sqrt{2}} \\ \frac{-1}{\sqrt{2}} \end{pmatrix}$ with components (a_+, a_-) in A-basis.

$$a_+ = \langle +|\psi\rangle = \begin{pmatrix} \frac{1}{\sqrt{2}} & \frac{1}{\sqrt{2}} \end{pmatrix}\begin{pmatrix} \cos\psi \\ \sin\psi \end{pmatrix} = \frac{\cos\psi + \sin\psi}{\sqrt{2}}, \quad a_- = \langle -|\psi\rangle = \begin{pmatrix} \frac{1}{\sqrt{2}} & \frac{-1}{\sqrt{2}} \end{pmatrix}\begin{pmatrix} \cos\psi \\ \sin\psi \end{pmatrix} = \frac{\cos\psi - \sin\psi}{\sqrt{2}}.$$

It helps to factor the sum $\cos\psi + \sin\psi$ using relations $\cos\psi = \frac{1}{2}(e^{i\psi} + e^{-i\psi})$ and $\sin\psi = \frac{-i}{2}(e^{i\psi} - e^{-i\psi})$

$$a_+ = \frac{\cos\psi + \sin\psi}{\sqrt{2}} = \frac{1}{2}\frac{e^{i\psi} + e^{-i\psi}}{\sqrt{2}} - \frac{i}{2}\frac{e^{i\psi} - e^{-i\psi}}{\sqrt{2}} = \frac{1}{2}\frac{(1-i)e^{i\psi} + (1+i)e^{-i\psi}}{\sqrt{2}}$$

$$a_- = \frac{\cos\psi - \sin\psi}{\sqrt{2}} = \frac{1}{2}\frac{e^{i\psi} + e^{-i\psi}}{\sqrt{2}} + \frac{i}{2}\frac{e^{i\psi} - e^{-i\psi}}{\sqrt{2}} = \frac{1}{2}\frac{(1+i)e^{i\psi} + (1-i)e^{-i\psi}}{\sqrt{2}}$$

The polar forms $\frac{(1+i)}{\sqrt{2}} = e^{i\pi/4}$ and $\frac{(1-i)}{\sqrt{2}} = e^{-i\pi/4}$ let you factor the sums. (Here we define: β=2ψ−π/2.)

$$a_+ = \frac{1}{2}(e^{-i\pi/4}e^{i\psi} + e^{i\pi/4}e^{-i\psi}) = \frac{1}{2}(e^{i(\psi-\pi/4)} + e^{-i(\psi-\pi/4)}) = \cos(\psi - \pi/4) = \cos\frac{\beta}{2}$$

$$a_- = \frac{1}{2}(e^{i\pi/4}e^{i\psi} + e^{-i\pi/4}e^{-i\psi}) = \frac{1}{2}(e^{i(\psi+\pi/4)} + e^{-i(\psi+\pi/4)}) = \cos(\psi + \pi/4) = -\sin\frac{\beta}{2}$$

Each component oscillates at its assigned mode frequency.

$$\begin{pmatrix} a_1^{(\psi)}(t) \\ a_2^{(\psi)}(t) \end{pmatrix} = a_+ e^{-i\omega_{slow}t}\begin{pmatrix} \frac{1}{\sqrt{2}} \\ \frac{1}{\sqrt{2}} \end{pmatrix} + a_- e^{-i\omega_{fast}t}\begin{pmatrix} \frac{1}{\sqrt{2}} \\ \frac{-1}{\sqrt{2}} \end{pmatrix} = \cos\frac{\beta}{2}e^{is}\begin{pmatrix} \frac{1}{\sqrt{2}} \\ \frac{1}{\sqrt{2}} \end{pmatrix} - \sin\frac{\beta}{2}e^{if}\begin{pmatrix} \frac{1}{\sqrt{2}} \\ \frac{-1}{\sqrt{2}} \end{pmatrix} = \frac{1}{\sqrt{2}}\begin{pmatrix} \cos\frac{\beta}{2}e^{is} - \sin\frac{\beta}{2}e^{if} \\ \cos\frac{\beta}{2}e^{is} + \sin\frac{\beta}{2}e^{if} \end{pmatrix}$$

We simplify using B-unit vectors and define $\bar{\beta} = -\beta$ that turns out to be the B-axis polar angle $\bar{\beta} \equiv \beta_B$.

$$\begin{pmatrix} a_+^{(\psi)}(t) \\ a_-^{(\psi)}(t) \end{pmatrix} = a_+ e^{-i\omega_{slow}t}\begin{pmatrix} 1 \\ 0 \end{pmatrix} + a_- e^{-i\omega_{fast}t}\begin{pmatrix} 0 \\ 1 \end{pmatrix} = \cos\frac{\beta}{2}e^{is}\begin{pmatrix} 1 \\ 0 \end{pmatrix} - \sin\frac{\beta}{2}e^{if}\begin{pmatrix} 0 \\ 1 \end{pmatrix} = \begin{pmatrix} e^{is}\cos\frac{\beta}{2} \\ -e^{if}\sin\frac{\beta}{2} \end{pmatrix} = \begin{pmatrix} e^{is}\cos\frac{\bar{\beta}}{2} \\ e^{if}\sin\frac{\bar{\beta}}{2} \end{pmatrix}$$

The idea is to make it more like the standard form (A.11). The overall phase *(s+f)/2* is factored out.

$$\begin{pmatrix} a_+^{(\psi)}(t) \\ a_-^{(\psi)}(t) \end{pmatrix} = \begin{pmatrix} e^{is}\cos\frac{\bar{\beta}}{2} \\ e^{if}\sin\frac{\bar{\beta}}{2} \end{pmatrix} = e^{i\frac{(s+f)}{2}}\begin{pmatrix} e^{i\frac{(s-f)}{2}}\cos\frac{\bar{\beta}}{2} \\ e^{-i\frac{(s-f)}{2}}\sin\frac{\bar{\beta}}{2} \end{pmatrix} = e^{i\frac{(s+f)}{2}}\begin{pmatrix} e^{-i\frac{\bar{\alpha}}{2}}\cos\frac{\bar{\beta}}{2} \\ e^{+i\frac{\bar{\alpha}}{2}}\sin\frac{\bar{\beta}}{2} \end{pmatrix} \quad \text{where: } \bar{\alpha} = f - s \equiv \alpha_B$$

Standard (α,β)-forms yield **S**-vectors with azimuth-α and polar angle-β in σ-operator quad-forms.

The quadratic forms of the operators $\sigma_B = \begin{pmatrix} 0 & 1 \\ 1 & 0 \end{pmatrix}$, $\sigma_C = \begin{pmatrix} 0 & -i \\ i & 0 \end{pmatrix}$, and $\sigma_A = \begin{pmatrix} 1 & 0 \\ 0 & -1 \end{pmatrix}$ give three S-components in terms of their polar

angles $(\bar{\alpha}, \bar{\beta})$. However, the $\bar{\beta}$ angle refers to the B-axis and $\bar{\alpha}$ to the C-axis.

$$\begin{pmatrix} e^{-i\frac{\bar{\alpha}}{2}}\cos\frac{\bar{\beta}}{2} & e^{i\frac{\bar{\alpha}}{2}}\sin\frac{\bar{\beta}}{2} \end{pmatrix}^{*} \begin{pmatrix} 1 & 0 \\ 0 & -1 \end{pmatrix} \begin{pmatrix} e^{-i\frac{\bar{\alpha}}{2}}\cos\frac{\bar{\beta}}{2} \\ e^{i\frac{\bar{\alpha}}{2}}\sin\frac{\bar{\beta}}{2} \end{pmatrix} = \begin{pmatrix} e^{i\frac{\bar{\alpha}}{2}}\cos\frac{\bar{\beta}}{2} & e^{-i\frac{\bar{\alpha}}{2}}\sin\frac{\bar{\beta}}{2} \end{pmatrix} \begin{pmatrix} e^{-i\frac{\bar{\alpha}}{2}}\cos\frac{\bar{\beta}}{2} \\ -e^{i\frac{\bar{\alpha}}{2}}\sin\frac{\bar{\beta}}{2} \end{pmatrix} = \cos^2\frac{\bar{\beta}}{2}-\sin^2\frac{\bar{\beta}}{2} \qquad = \cos\bar{\beta}$$

$$\begin{pmatrix} e^{-i\frac{\bar{\alpha}}{2}}\cos\frac{\bar{\beta}}{2} & e^{i\frac{\bar{\alpha}}{2}}\sin\frac{\bar{\beta}}{2} \end{pmatrix}^{*} \begin{pmatrix} 0 & 1 \\ 1 & 0 \end{pmatrix} \begin{pmatrix} e^{-i\frac{\bar{\alpha}}{2}}\cos\frac{\bar{\beta}}{2} \\ e^{i\frac{\bar{\alpha}}{2}}\sin\frac{\bar{\beta}}{2} \end{pmatrix} = \begin{pmatrix} e^{i\frac{\bar{\alpha}}{2}}\cos\frac{\bar{\beta}}{2} & e^{-i\frac{\bar{\alpha}}{2}}\sin\frac{\bar{\beta}}{2} \end{pmatrix} \begin{pmatrix} e^{i\frac{\bar{\alpha}}{2}}\sin\frac{\bar{\beta}}{2} \\ e^{-i\frac{\bar{\alpha}}{2}}\cos\frac{\bar{\beta}}{2} \end{pmatrix} = \left(e^{i\bar{\alpha}}+e^{-i\bar{\alpha}}\right)\cos\frac{\bar{\beta}}{2}\sin\frac{\bar{\beta}}{2} = \cos\bar{\alpha}\sin\bar{\beta}$$

$$\begin{pmatrix} e^{-i\frac{\bar{\alpha}}{2}}\cos\frac{\bar{\beta}}{2} & e^{i\frac{\bar{\alpha}}{2}}\sin\frac{\bar{\beta}}{2} \end{pmatrix}^{*} \begin{pmatrix} 0 & -i \\ i & 0 \end{pmatrix} \begin{pmatrix} e^{-i\frac{\bar{\alpha}}{2}}\cos\frac{\bar{\beta}}{2} \\ e^{i\frac{\bar{\alpha}}{2}}\sin\frac{\bar{\beta}}{2} \end{pmatrix} = \begin{pmatrix} e^{i\frac{\bar{\alpha}}{2}}\cos\frac{\bar{\beta}}{2} & e^{-i\frac{\bar{\alpha}}{2}}\sin\frac{\bar{\beta}}{2} \end{pmatrix} \begin{pmatrix} -ie^{i\frac{\bar{\alpha}}{2}}\sin\frac{\bar{\beta}}{2} \\ ie^{-i\frac{\bar{\alpha}}{2}}\cos\frac{\bar{\beta}}{2} \end{pmatrix} = \left(e^{i\bar{\alpha}}+e^{-i\bar{\alpha}}\right)\cos\frac{\bar{\beta}}{2}\sin\frac{\bar{\beta}}{2} = \sin\bar{\alpha}\sin\bar{\beta}$$
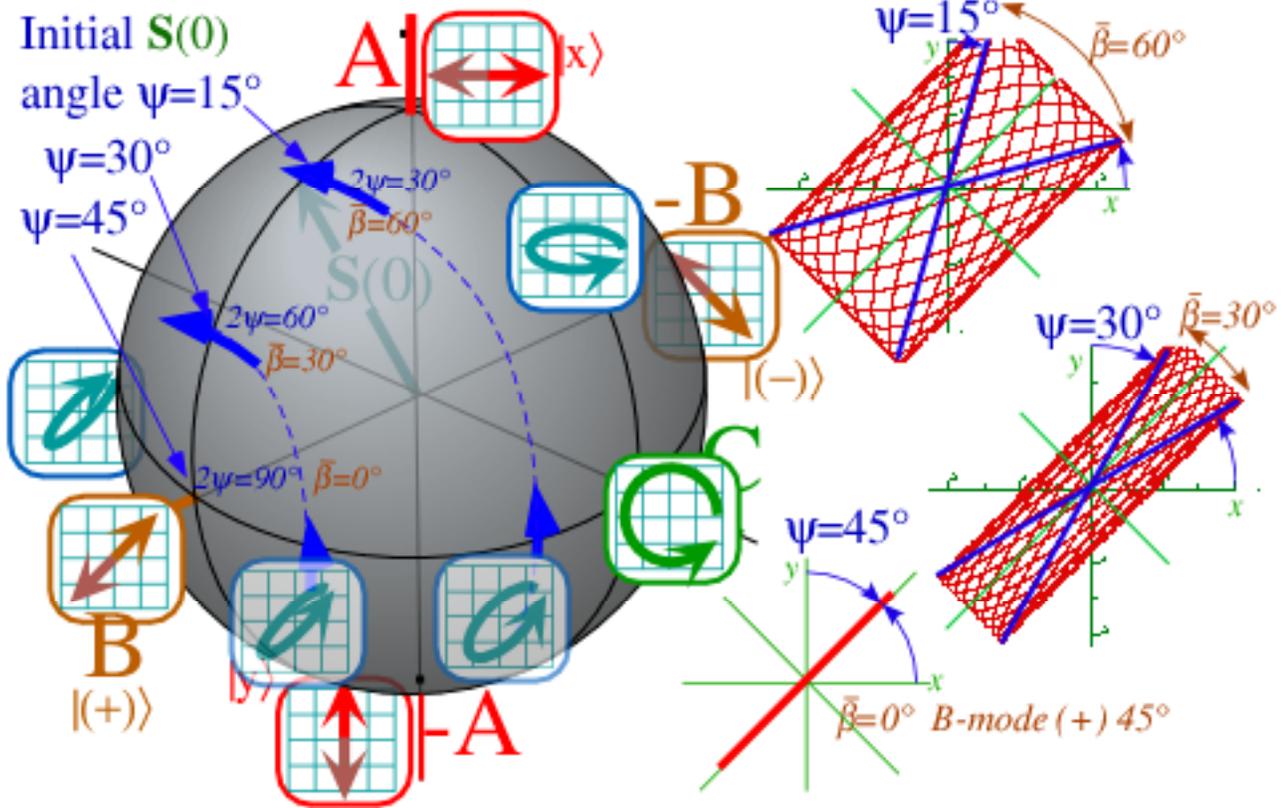
Fig. B.3 Spin vector being rotated around B-axis during beats. The ψ-45° case is fixed on B-axis.

How spinors give rotation products

Now we find the product $\mathbf{R}_a \mathbf{R}_b$ of rotation $\mathbf{R}_a$ by crank-axis $\vec{\Theta}_a = \hat{\Theta}_a \Theta_a$ following $\mathbf{R}_b$ by axis $\vec{\Theta}_b = \hat{\Theta}_b \Theta_b$.

$$\mathbf{R}_a(\mathbf{\Theta}_a) \cdot \mathbf{R}_b(\mathbf{\Theta}_b) = e^{-i(\sigma \bullet \vec{\Theta}_a)/2} e^{-i(\sigma \bullet \vec{\Theta}_b)/2} = (\mathbf{1}\cos\frac{\Theta_a}{2} \quad - \quad i\,(\sigma \bullet \hat{\Theta}_a)\sin\frac{\Theta_a}{2})\,(\mathbf{1}\cos\frac{\Theta_b}{2} \quad - \quad i\,(\sigma \bullet \hat{\Theta}_b)\sin\frac{\Theta_b}{2}) = \mathbf{R}_{ab}(\mathbf{\Theta}_{ab})$$

$$=(\mathbf{1}\cos\frac{\Theta_a}{2}\cos\frac{\Theta_b}{2} - i\,(\sigma \bullet \hat{\Theta}_a)\sin\frac{\Theta_a}{2}\cos\frac{\Theta_b}{2} - i\,(\sigma \bullet \hat{\Theta}_b)\cos\frac{\Theta_a}{2}\sin\frac{\Theta_b}{2} - (\sigma \bullet \hat{\Theta}_a)(\sigma \bullet \hat{\Theta}_b)\sin\frac{\Theta_a}{2}\sin\frac{\Theta_b}{2})$$

$$=\mathbf{1}\left(\cos\frac{\Theta_a}{2}\cos\frac{\Theta_b}{2} - (\hat{\Theta}_a \bullet \hat{\Theta}_b)\sin\frac{\Theta_a}{2}\sin\frac{\Theta_b}{2} \right) - i\,\sigma \bullet \left[\hat{\Theta}_a \sin\frac{\Theta_a}{2}\cos\frac{\Theta_b}{2} + \hat{\Theta}_b \cos\frac{\Theta_a}{2}\sin\frac{\Theta_b}{2} + (\hat{\Theta}_a \times \hat{\Theta}_b)\sin\frac{\Theta_a}{2}\sin\frac{\Theta_b}{2} \right]$$

$$=\mathbf{1}\left(\qquad\qquad \cos\frac{\Theta_{ab}}{2} \qquad\qquad \right) - i\,\sigma \bullet \left[\qquad\qquad \hat{\Theta}_{ab}\sin\frac{\Theta_{ab}}{2} \qquad\qquad \right]$$

By equating the first two (expressions) you find the product crank angle Θ_{ab}. Then you can equate the second two [expressions] and get the direction $\hat{\Theta}_{ab}$ of the product crank vector.

(e) Relation of Lorentz oscillators to Schrodinger classical analog

      Lorentz theory was concerned with the atomic spectral frequencies. For each spectral line, Lorentz presupposed another one of his oscillators. The discovery of quantum theory lets us associate each spectral line with a *transition* between a pair of energy levels. Each spectral frequency is a *difference* between two eigenfrequencies $\omega(\varepsilon_1)$ and $\omega(\varepsilon_2)$, i.e.,

$$\omega(1 \leftrightarrow 2\ \text{transition}) = |\omega(\varepsilon_1) - \omega(\varepsilon_2)|,$$

where energy values are proportional to corresponding quantum frequencies by *Planck's constant* $(\hbar = 1.054572 \times 10^{-34} J \cdot s)$. The energy level eigenvalues for the transition pair are $\varepsilon_1 = \hbar\omega(\varepsilon_1)$ and $\varepsilon_2 = \hbar\omega(\varepsilon_2)$ while the observed spectral energy is just the difference between energy levels.

$$\Delta\mathrm{E} = |\varepsilon_1 - \varepsilon_2| = \hbar\omega(1 \leftrightarrow 2\ \text{transition}) = \hbar|\omega(\varepsilon_1) - \omega(\varepsilon_2)| \qquad (2.4.10)$$

      It is not possible to directly observe the individual level frequencies $\omega(\varepsilon_j)$ of any quantum system. Quantum energy eigenstates $|\varepsilon_1\rangle$ or "quantum normal modes" are asleep, motionless, dead to the world; indeed they are called *stationary states*. Eigenstates of (2.4.1) only have phase time dependence, i.e.,

$$\langle j|\varepsilon_k(t)\rangle = e^{-i\omega(\varepsilon_k)t}\langle j|\varepsilon_k(0)\rangle. \qquad (2.4.11)$$

To get state probability one takes the absolute square ($|\ |^2$) which kills the phase factor. So all pure state eigenstate probability factors are motionless or time independent.

$$\left|\langle j|\varepsilon_k(t)\rangle\right|^2 = \langle j|\varepsilon_k(0)\rangle^* \langle j|\varepsilon_k(0)\rangle = \left|\langle j|\varepsilon_k(0)\rangle\right|^2 = \text{constant}. \qquad (2.4.12)$$

      Only by mixing two or more states of differing energy do we actually get observable motion. This is analogous to mixing two normal modes as in (4.3.16) which gives a modulation oscillation or *beat* frequency.

$$\omega_{\text{beat}}(\text{mode 1 plus mode 2}) = |\omega(\varepsilon_1) - \omega(\varepsilon_2)|$$

(Recall Fig. 4.3.4.) The beat frequency is analogous to the *transition frequency* in (2.4.10). All Lorentz oscillations are the result of 'beating' between eigenstates belonging to two different energy levels.

Exercises for Ch. 4 Classical-quantum oscillator analogs

Chapter 2.5 Wave resonance in cyclic symmetry

One gains insight into Fourier analysis by framing it in finite discrete domains. Here we will generalize normal mode analysis of Ch. 2.3 and Ch. 2.4 using spectral decomposition of nth-order cyclic C_n symmetry groups and introduce a powerful techniques used in classical and quantum physics. Then Ch. 2.6 thru 2.8 treat Fourier analysis of Green's functions, continuous spectral analysis, and parametric resonance.

(a) *A 3D-oscillator with cyclic C₃ symmetry*

Ch. 2.4 introduced the B-type or *bilateral-balanced* symmetry of a coupled 2D oscillator with equivalent parts, that is, equal masses $(m_1=m_2)$ and spring $(k_1=k_2)$ couplings. Such systems are described by a doubly symmetric Hamiltonian matrix $\mathbf{H}$ or spring-constant matrix $\mathbf{K}=\mathbf{H}^2$ as in (2.4.8a), and either matrix is a simple expansion (2.4.9) of a unit matrix $\mathbf{1}$ and a Hamilton-Pauli reflection matrix σ_B.

$$\mathbf{H} = \begin{pmatrix} A & B \\ B & A \end{pmatrix} = A\begin{pmatrix} 1 & 0 \\ 0 & 1 \end{pmatrix} + B\begin{pmatrix} 0 & 1 \\ 1 & 0 \end{pmatrix} \quad \begin{matrix} (4.4.7a) \\ (4.4.9a) \\ repeated \end{matrix} \qquad \mathbf{K}=\mathbf{H}^2 = \begin{pmatrix} A^2+B^2 & 2AB \\ 2AB & A^2+B^2 \end{pmatrix} \qquad (2.5.1)$$

$$= A\cdot\mathbf{1} \quad + B\cdot\sigma_B \qquad\qquad\qquad = (A^2+B^2)\cdot\mathbf{1} \quad + 2AB\cdot\sigma_B$$

This is based on reflection symmetry σ_B defined by $(\sigma_B)^2=\mathbf{1}$ or the following C_2 group product table.

$$\begin{array}{c|cc} C_2 & \mathbf{1} & \sigma_B \\ \hline \mathbf{1} & \mathbf{1} & \sigma_B \\ \sigma_B & \sigma_B & \mathbf{1} \end{array} \qquad (2.5.2)$$

Now we generalize (2.5.2) for a 3D oscillator with 3-fold cyclic symmetry shown in Fig. 2.5.1 based on 3-fold $\pm120°$ rotations $\mathbf{r}=\mathbf{r}^1$ and $(\mathbf{r})^2=\mathbf{r}^2=\mathbf{r}^{-1}$ defined by $(\mathbf{r})^3=\mathbf{r}^3=\mathbf{1}$ or a C_3 **g†g-*product-table*** in (2.5.3) that pairs each operator $\mathbf{g}$ in the 1st row with its inverse $\mathbf{g}^\dagger=\mathbf{g}^{-1}$ in the 1st column so all unit $\mathbf{1}=\mathbf{g}^{-1}\mathbf{g}$ lie on diagonal.

$$\begin{array}{c|ccc} C_3 & \mathbf{r}^0=\mathbf{1} & \mathbf{r}^1=\mathbf{r}^{-2} & \mathbf{r}^2=\mathbf{r}^{-1} \\ \hline \mathbf{r}^0=\mathbf{1} & \mathbf{1} & \mathbf{r}^1 & \mathbf{r}^2 \\ \mathbf{r}^2=\mathbf{r}^{-1} & \mathbf{r}^2 & \mathbf{1} & \mathbf{r}^1 \\ \mathbf{r}^1=\mathbf{r}^{-2} & \mathbf{r}^1 & \mathbf{r}^2 & \mathbf{1} \end{array} \qquad (2.5.3a)$$

A C_3 $\mathbf{H}$-matrix is then constructed directly from the **g†g**-table and so is each $\mathbf{r}^p$-matrix representation.

$$\mathbf{H} = \begin{pmatrix} r_0 & r_1 & r_2 \\ r_2 & r_0 & r_1 \\ r_1 & r_2 & r_0 \end{pmatrix} = r_0\begin{pmatrix} 1 & 0 & 0 \\ 0 & 1 & 0 \\ 0 & 0 & 1 \end{pmatrix} + r_1\begin{pmatrix} 0 & 1 & 0 \\ 0 & 0 & 1 \\ 1 & 0 & 0 \end{pmatrix} + r_2\begin{pmatrix} 0 & 0 & 1 \\ 1 & 0 & 0 \\ 0 & 1 & 0 \end{pmatrix} \qquad (2.5.3b)$$

$$= r_0\cdot\mathbf{1} \qquad + r_1\cdot\mathbf{r}^1 \qquad + r_2\cdot\mathbf{r}^2$$

Each $\mathbf{H}$-matrix coupling constant $\{r_0, r_1, r_2\}$ is related respectively to an operator $\{\mathbf{r}^0, \mathbf{r}^1, \mathbf{r}^2\}$ that transmits a particular force or current as labeled in Fig. 2.5.1a. This particular $\mathbf{H}$-matrix is *self-conjugate* ($\mathbf{H}^\dagger=\mathbf{H}$) and has time reversal symmetry provided $\{r_0, r_1, r_2\}$ satisfy conjugation relations.

$$r_0^* = r_0 \quad (2.5.4a) \qquad\qquad r_1^* = r_2 \quad (2.5.4b) \qquad\qquad r_2^* = r_1 \quad (2.5.4c)$$

$\mathbf{H}$ has reflection-parity symmetry C_{3v} if the parameters r_1 and r_2 are also real and equal $(r_1=r=r_2=r^*)$.
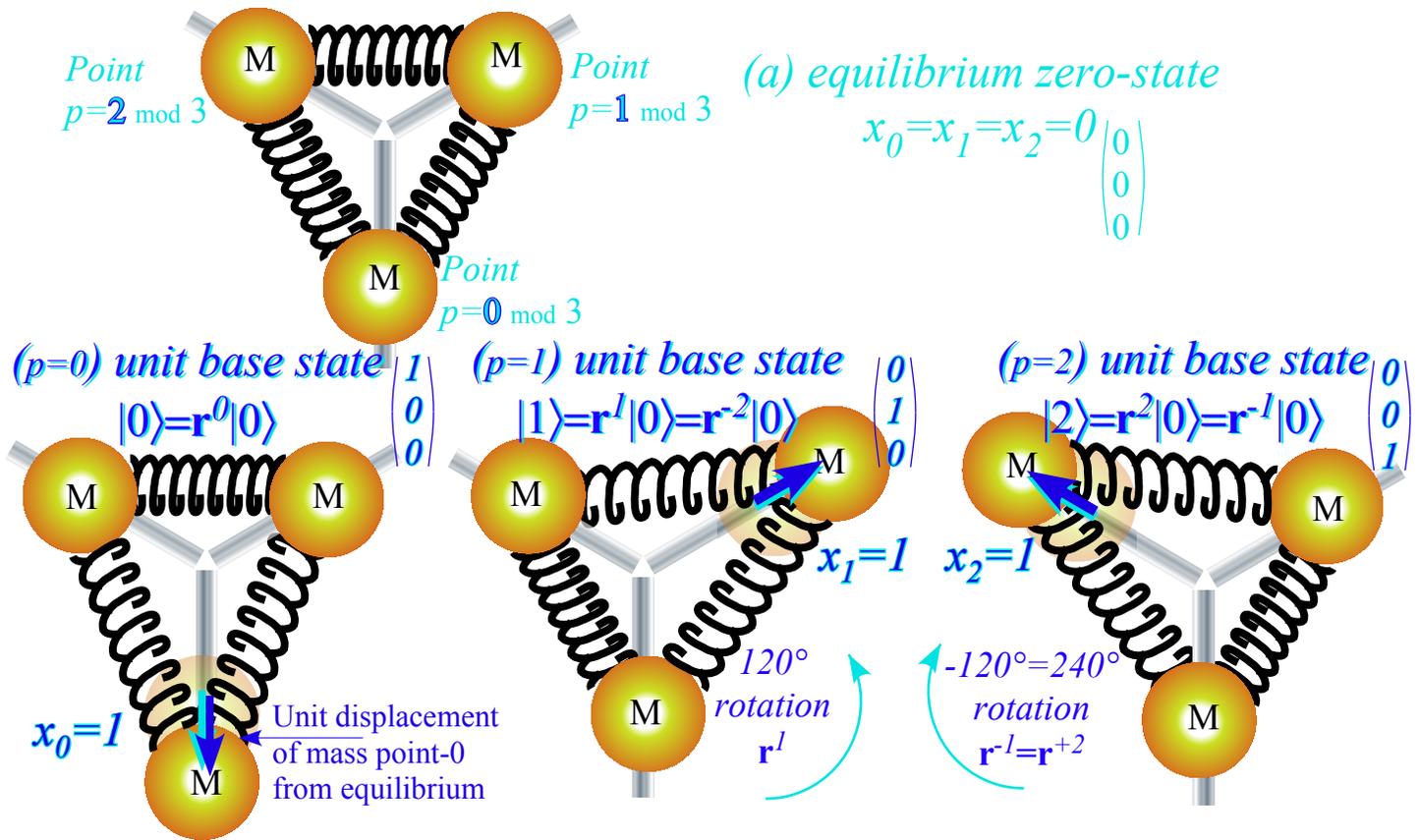
Fig. 2.5.1(a) C₃-symmetric coupled oscillator in equilibrium and unit-displacement base states p=0,1, and 2.

(b) C₃ Spectral resolution: 3ʳᵈ roots of unity

We can spectrally resolve **H** if we resolve **r** since is **H** a combination (2.5.3b) of powers $\mathbf{r}^p$. The **r**-symmetry gives a cubic $\mathbf{r}^3=\mathbf{1}$, or $\mathbf{r}^3-\mathbf{1}=\mathbf{0}$ that resolves to factors involve three *3ʳᵈ roots of unity* $\rho_m=e^{im2\pi/3}$.

$$\mathbf{1}=\mathbf{r}^3 \text{ implies}: \ \ \mathbf{0}=\mathbf{r}^3-\mathbf{1}=(\mathbf{r}-\rho_0\mathbf{1})(\mathbf{r}-\rho_1\mathbf{1})(\mathbf{r}-\rho_2\mathbf{1}) \text{ where}: \ \rho_m=e^{im\frac{2\pi}{3}} \tag{2.5.5a}$$

By (2.C.7) there is an idempotent projector $\mathbf{P}^{(m)}$ such that $\mathbf{r}\cdot\mathbf{P}^{(m)}=\rho_m\mathbf{P}^{(m)}$ for each eigenvalue ρ_m of **r**, and the three of them are *orthonormal* ($\mathbf{P}^{(m)}\mathbf{P}^{(n)}=\delta_{mn}\mathbf{P}^{(m)}$) and sum to unit **1** by the *completeness* relation in (2.C.8).

$$\mathbf{r}\cdot\mathbf{P}^{(m)}=\rho_m\mathbf{P}^{(m)} \qquad (2.5.5b) \qquad\qquad \mathbf{1} = \quad \mathbf{P}^{(0)} + \quad \mathbf{P}^{(1)} + \quad \mathbf{P}^{(2)} \qquad (2.5.5c)$$

$$\rho_0=e^{i0}=1, \qquad \rho_1=e^{i\frac{2\pi}{3}}, \quad \rho_2=e^{-i\frac{2\pi}{3}}, \qquad\qquad \mathbf{r} = \rho_0\ \mathbf{P}^{(0)} + \rho_1\ \mathbf{P}^{(1)} + \rho_2\ \mathbf{P}^{(2)} \qquad (2.5.5d)$$

$$(\rho_0)^2=1, \qquad (\rho_1)^2=\rho_2, \ \ (\rho_2)^2=\rho_1, \qquad\qquad \mathbf{r}^2=(\rho_0)^2\mathbf{P}^{(0)}+(\rho_1)^2\mathbf{P}^{(1)}+(\rho_2)^2\mathbf{P}^{(2)} \qquad (2.5.5e)$$

The last two expressions for **r** and $\mathbf{r}^2$ result if **r** acts once and twice on (2.5.5c) using (2.5.5b).

Projector $\mathbf{P}^{(m)}$ can be derived in terms of **1**, **r** and $\mathbf{r}^2$ using (2.C.8), but there is an easier way since they are orthogonal by (2.C.7). Just conjugate each ρ_{mp} to ρ^*_{mp} in (2.5.5) and multiply by factor $\frac{1}{3}$. Its square root normalizes eigenbra vectors $\langle(m)_3|=\langle0|\mathbf{P}^{(m)}/\sqrt{\frac{1}{3}}$ listed below and in Fig. 2.5.2 of $\mathbf{r}^p$ and **H** or **K**.

$$P^{(0)} = \tfrac{1}{3}(r^0 + r^1 + r^2) = \tfrac{1}{3}(1 + r^1 + r^2)$$

$$P^{(1)} = \tfrac{1}{3}(r^0 + \rho_1^* r^1 + \rho_2^* r^2) = \tfrac{1}{3}(1 + e^{-i2\pi/3} r^1 + e^{+i2\pi/3} r^2) \quad \text{implies:}$$

$$P^{(2)} = \tfrac{1}{3}(r^0 + \rho_2^* r^1 + \rho_1^* r^2) = \tfrac{1}{3}(1 + e^{+i2\pi/3} r^1 + e^{-i2\pi/3} r^2)$$

$$\langle (0_3)| = \langle 0|P^{(0)}\sqrt{3} = \sqrt{\tfrac{1}{3}}(\ 1 \quad 1 \quad 1 \ )$$

$$\langle (1_3)| = \langle 0|P^{(1)}\sqrt{3} = \sqrt{\tfrac{1}{3}}(\ 1 \ \ e^{-i2\pi/3} \ \ e^{+i2\pi/3}) \quad (2.5.6)$$

$$\langle (2_3)| = \langle 0|P^{(2)}\sqrt{3} = \sqrt{\tfrac{1}{3}}(\ 1 \ \ e^{+i2\pi/3} \ \ e^{-i2\pi/3})$$

We simply use r^p operators to define coordinate bases in Fig. 2.5.1 and their eigen-projectors. This then gives bra or ket eigenvectors of Hamiltonian matrix **H** or spring matrix $K = H^2$.

Modular arithmetic of mode momentum m vs. position point p

There are two distinct types of "quantum" numbers. One is $p=0,1,$ or 2 that is *power p* of operator r^p that defines each oscillator's *position point p* in Fig. 2.5.1. The other is $m=0,1,$ or 2 that is the *mode momentum m* of the waves sketched in Fig. 2.5.2. Each number follows *modular arithmetic* with sums or products taken as an *integer-modulo-3* that is always $0,1,$ or 2. For example, for $m=2$ and $p=2$ the number $(\rho_m)^p = (e^{im2\pi/3})^p$ is $e^{imp\cdot 2\pi/3} = e^{i4\cdot 2\pi/3} = e^{i1\cdot 2\pi/3} e^{i2\pi} = e^{i2\pi/3} = \rho_1$. That is, (*2-times-2*) mod 3 is not 4 but 1 (4 mod $3=1$), the remainder of 4 divided by 3. Thus, $(\rho_2)^2 = \rho_1$. Also, 5 mod $3=2$ so $(\rho_1)^5 = \rho_2$, and 6 mod $3=0$ so $(\rho_1)^6 = \rho_0$. Other examples: -1 mod $3=2$ $[(\rho_1)^{-1} = (\rho_{-1})^1 = \rho_2]$ and -2 mod $3=1$. The trick is to imagine walking around the ring in Fig. 2.5.1 and reading off the address points $p = \dots$ *0, 1, 2, 0, 1, 2, 0, 1, 2, 0, 1, 2,*.... If you just count the number of points without doing p mod 3 your count is: ...*-3,-2,-1, 0, 1, 2, 3, 4, 5, 6, 7, 8,*.... The mod 3 count is applied to *both* momentum number m *and* point number p since $e^{imp2\pi/3}$ must always equal $e^{i(mp \bmod 3)2\pi/3}$.

$$(\rho_m)^p = (e^{im2\pi/3})^p = e^{imp\cdot 2\pi/3} = \rho_{mp} = e^{i(mp \bmod 3)2\pi/3} = \rho_{mp \bmod 3} \qquad (2.5.6)$$
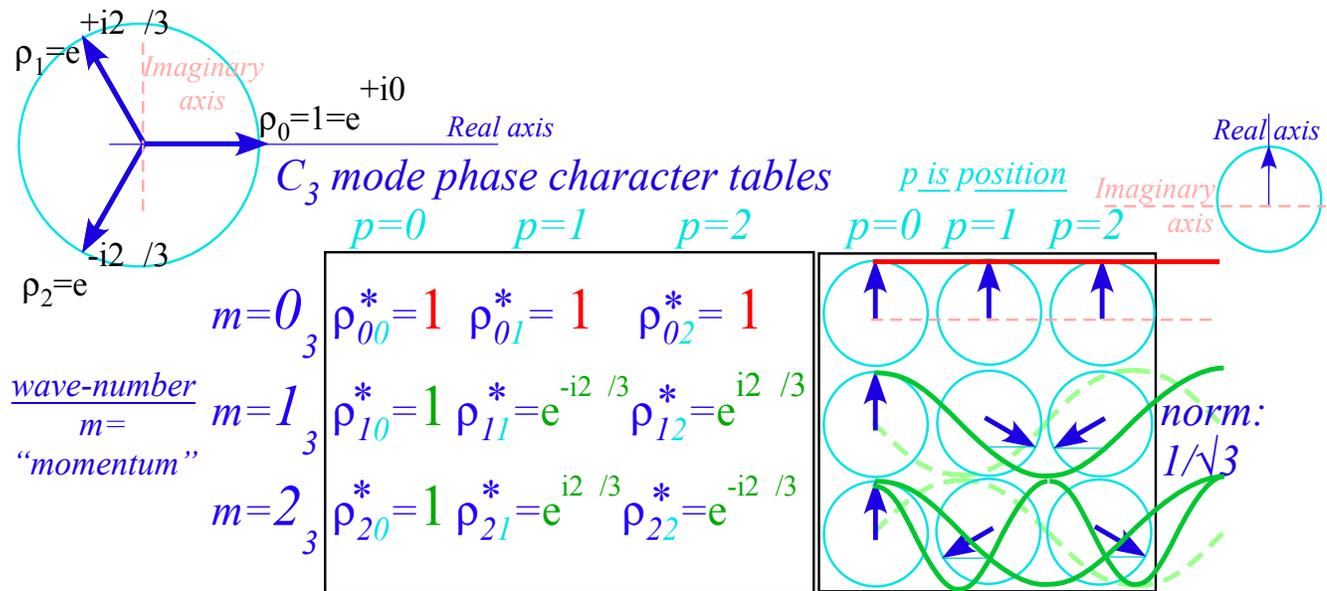
Fig. 2.5.2 C_3 coupled oscillator moving-wave normal mode states $m=0,1,$ and 2 in terms of 3rd roots of 1.

Eigenvalues and wave dispersion functions

H (or **K**) matrix eigenvalues of eigenbra $\langle (m)_3|$ or ket $|(m)_3\rangle$ in Fig. 2.5.2 are sums of eigenvalues $\langle m|r^p|m\rangle = (\rho_m)^p = (e^{im2\pi/3})^p = e^{imp\cdot 2\pi/3}$ of r^p according to (2.5.3b). C_{3v} cases (2.5.4) are treated. $(r_1 = r = r_2 = r^*)$

$$\langle m|\mathbf{H}|m\rangle = \langle m|r_0\mathbf{r}^0 + r_1\mathbf{r}^1 + r_2\mathbf{r}^2|m\rangle = r_0 e^{i0(m)\frac{2\pi}{3}} + r_1 e^{i1(m)\frac{2\pi}{3}} + r_2 e^{i2(m)\frac{2\pi}{3}}$$

$$= r_0 e^{i0(m)\frac{2\pi}{3}} + r(e^{i2\frac{m\pi}{3}} + e^{-i2\frac{m\pi}{3}}) = r_0 + 2r\cos(2\tfrac{m\pi}{3}) = \begin{cases} r_0 + 2r & \text{(for } m=0) \\ r_0 - r & \text{(for } m=\pm1) \end{cases}$$

H-values: $\begin{pmatrix} r_0 & r & r \\ r & r_0 & r \\ r & r & r_0 \end{pmatrix}\begin{pmatrix} 1 \\ e^{i2\frac{m\pi}{3}} \\ e^{-i2\frac{m\pi}{3}} \end{pmatrix} = \left(r_0 + 2r\cos(2\tfrac{m\pi}{3})\right)\begin{pmatrix} 1 \\ e^{i2\frac{m\pi}{3}} \\ e^{-i2\frac{m\pi}{3}} \end{pmatrix}$ **K**-values: $\begin{pmatrix} K & -k & -k \\ -k & K & -k \\ -k & -k & K \end{pmatrix}\begin{pmatrix} 1 \\ e^{i2\frac{m\pi}{3}} \\ e^{-i2\frac{m\pi}{3}} \end{pmatrix} = \left(K - 2k\cos(2\tfrac{m\pi}{3})\right)\begin{pmatrix} 1 \\ e^{i2\frac{m\pi}{3}} \\ e^{-i2\frac{m\pi}{3}} \end{pmatrix}$

H eigenvalues for $m=\pm1$ (that is, $m=1$ and $m=2$) are degenerate and distinct from the $m=0$ level. Also, **K** matrix eigenfrequencies are square roots of **K**-eigenvalues. The $m=\pm1$ degeneracy allows us to combine conjugate *moving wave* pairs into real sine-and-cosine *standing wave* pairs as shown below. The **K**-eigenfrequency for $k_0=2k$ is $\omega = \sqrt{2k - 2k\cos(2\tfrac{\pi m}{3})} = 2\sqrt{k}\,|\sin(4\tfrac{\pi m}{3})|$ shown by a right hand side plot in Fig. 2.5.3.

Moving eigenwave	Standing eigenwaves		H − eigenfrequencies	K − eigenfrequencies
$|(+1)_3\rangle = \frac{1}{\sqrt{3}}\begin{pmatrix} 1 \\ e^{+i2\pi/3} \\ e^{-i2\pi/3} \end{pmatrix}$	$|c_3\rangle = \frac{|(+1)_3\rangle + |(-1)_3\rangle}{\sqrt{2}} = \frac{1}{\sqrt{6}}\begin{pmatrix} 2 \\ -1 \\ -1 \end{pmatrix}$		$r_0 + 2r\cos(2\tfrac{m\pi}{3})$ $= r_0 - r$	$\sqrt{k_0 - 2k\cos(2\tfrac{m\pi}{3})}$ $= \sqrt{k_0 + k}$
$|(-1)_3\rangle = \frac{1}{\sqrt{3}}\begin{pmatrix} 1 \\ e^{-i2\pi/3} \\ e^{+i2\pi/3} \end{pmatrix}$	$|s_3\rangle = \frac{|(+1)_3\rangle - |(-1)_3\rangle}{i\sqrt{2}} = \frac{1}{\sqrt{2}}\begin{pmatrix} 0 \\ +1 \\ -1 \end{pmatrix}$		$r_0 + 2r\cos(\tfrac{-2m\pi}{3})$ $= r_0 - r$	$\sqrt{k_0 - 2k\cos(2\tfrac{m\pi}{3})}$ $= \sqrt{k_0 + k}$
	$|(0)_3\rangle = \frac{1}{\sqrt{3}}\begin{pmatrix} 1 \\ 1 \\ 1 \end{pmatrix}$		$r_0 + 2r$	$\sqrt{k_0 - 2k}$
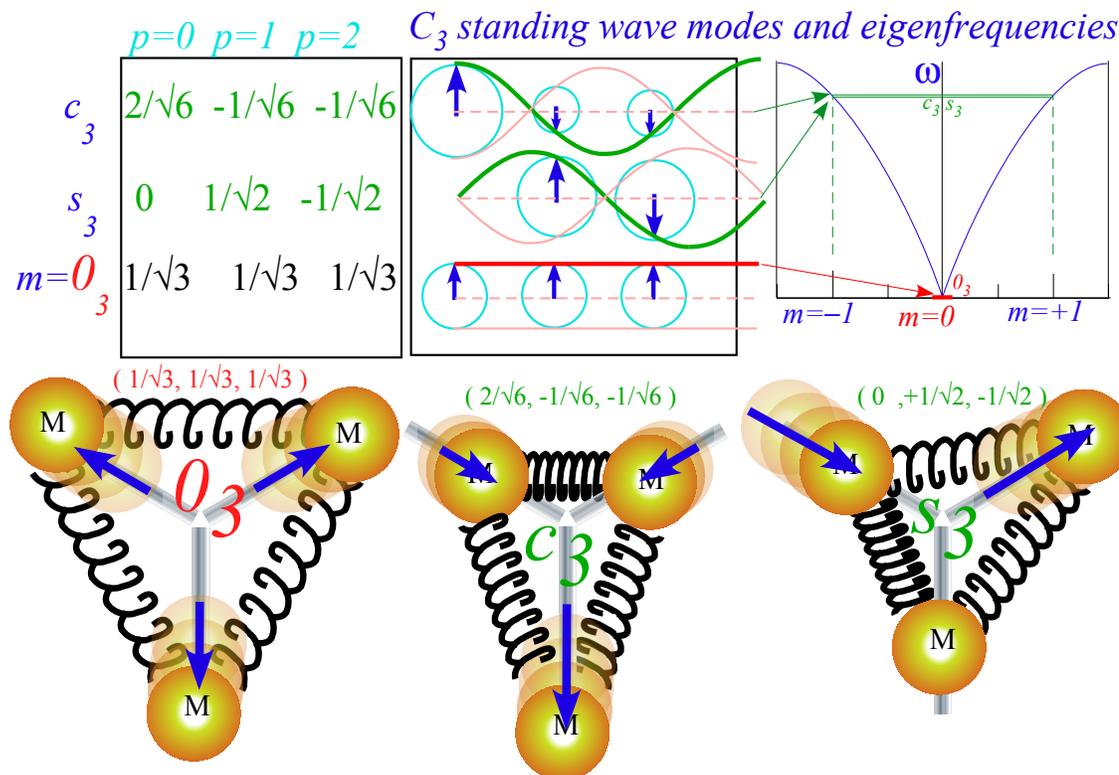
Fig. 2.5.3 C₃ coupled oscillator standing-wave normal mode states.

Real standing wave phasors are either *in* phase *(ρ=0)* or else completely *out* of phase *(ρ=±π)*. They must therefore be completely current-free states and are called *quenched* waves.

(a) Shower-Curtain Models

What if we hook up *N* oscillators in a ring? Let's imagine rings of *N* masses in Fig. 2.5.4 like lead weights at the bottom of a shower curtain. An *N*-dimensional **K** matrix like (2.5.10b) gives forces F_m.

$$-\begin{pmatrix} F_0 \\ F_1 \\ F_2 \\ F_3 \\ F_4 \\ \vdots \\ F_{N-1} \end{pmatrix} = \begin{pmatrix} K & -k_{12} & . & . & . & \cdots & -k_{12} \\ -k_{12} & K & -k_{12} & . & . & \cdots & . \\ . & -k_{12} & K & -k_{12} & . & \cdots & . \\ . & . & -k_{12} & K & -k_{12} & \cdots & . \\ . & . & . & -k_{12} & K & \cdots & . \\ \vdots & \vdots & \vdots & \vdots & \vdots & \ddots & -k_{12} \\ -k_{12} & . & . & . & . & -k_{12} & K \end{pmatrix} \bullet \begin{pmatrix} x_0 \\ x_1 \\ x_2 \\ x_3 \\ x_4 \\ \vdots \\ x_{N-1} \end{pmatrix} \quad \text{where:} \quad \begin{array}{l} K = k + 2k_{12} \\[6pt] k = \dfrac{Mg}{\ell} \\[6pt] (\cdot) = 0 \end{array} \qquad (2.5.12)$$

Each mass-*M* connects through a k_{12} spring to its two nearest neighbors. The mass at origin coordinate x_0 connects to x_1 on its right and x_{N-1} on its left. Then the first mass to the right of origin with coordinate x_1 connects to x_2 on its right and x_1 on its left, and so on around the loop. If all in (2.5.12) are fixed except x_0 (Let x_0 vary but fix $0=x_1=x_2=...x_{N-1}$) then x_0 has its pendulum oscillation frequency $\omega = \sqrt{\frac{k}{M}} = \sqrt{\frac{g}{\ell}}$ plus that of two k_{12}-springs connecting it to fixed neighbors with restoring force $-F_0=Kx_0 = (k+2k_{12})x_0$ from (2.5.12).
This circular *shower curtain model* may be solved using complex arithmetic and symmetry arguments.

We now use symmetry to find eigenvectors $\mathbf{u}_m$ of the **K**-matrix in (2.5.12) for which $\mathbf{K}\bullet\mathbf{u}_m=k_m\mathbf{u}_m$. The $\mathbf{u}_m$ give directions in **u**-space that are invariant to spring-force matrix **K** and thus don't change in time.
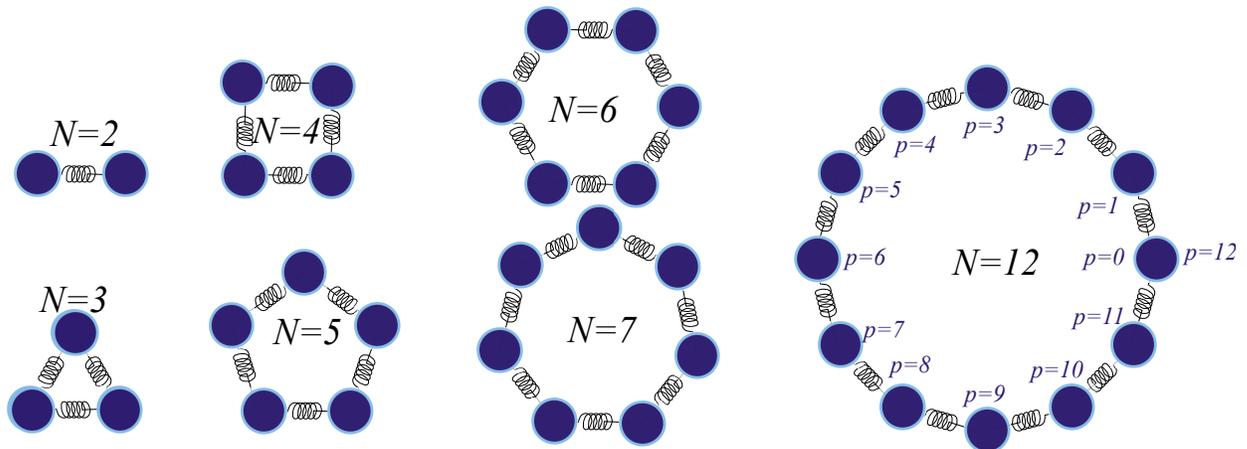
Fig. 2.5.4 N-Coupled Pendulums. (Viewed from above.)

N^{th} *Roots of unity*

The eigenvectors and eigenvalues of the *N*-by-*N*-matrix **K** (2.5.12) are made of the complex N^{th}-*roots of unity*, that are solutions to the equation $x^N=1$. The 2-mass solutions of (2.5.1) use 2nd roots ±1 of 1. Euler's exponential leads to the Nth roots of $1=e^{2\pi i}$, that is, exactly *N different* solutions to $x^N= e^{2\pi i}$.

$$x^N = 1 = e^{2\pi i} \quad \text{implies}: x = \left(e^{2\pi i}\right)^{\frac{1}{N}} = e^{\frac{2\pi i}{N}} \quad \text{and}: \quad x^m = e^{\frac{2\pi i}{N}m} \quad \text{satisfies}: \left(x^m\right)^N = 1 \qquad (2.5.13)$$

Square, cubic, quartic, quintic(5th), hexaic (6th), and duodecaic (12th) roots of 1 are plotted in Fig. 2.5.5. They form regular polygons whose vertices are powers $(\psi_N)^m$ of a *fundamental N^{th} root* $\psi_N = e^{2\pi i/N}$.

Fig. 2.5.5 N^{th}-Roots of Unity. Collections of Fourier coefficients for discrete N=2,3,4,5,6.7, and 12.

We'll use N=12 since it's easy to picture clock numerals. Note that *0* and *12 o'clock* share a point (ψ_{12}) $^0 = e^{i0} = (e^{i2\pi/12})^{12} = (\psi_{12})^{12}$ as do $(\psi_{12})^{-1} = (\psi_{12})^{11}$, and $(\psi_{12})^{-2} = (\psi_{12})^{10}$, and so on down to the *6 o'clock* point $(\psi_{12})^{-6} = -1 = (\psi_{12})^6$. Real axis (*6 and 12 o'clock*) is horizontal in Fig. 2.5.5 but vertical in later Fig. 2.5.6.

(b) Solving shower curtain models by symmetry

Eigenvectors of *rotate-shuffle-ops* **r** and **r**$^{-1}$ are also eigenvectors of **K**-matrix (2.5.12).

$$\mathbf{K} = K \cdot \mathbf{1} - k_{12} \cdot \mathbf{r} - k_{12} \cdot \mathbf{r}^{-1} \quad \text{where}: \quad \mathbf{1} = \text{unit matrix} \text{, and}: \qquad (2.5.14a)$$

So let's find vectors $\mathbf{u}_m = (x_0, x_1, x_2, x_3, ...)$ that are the same after a rotate-shuffle except for a factor f_m.

$$\mathbf{r}^{-1} \cdot \mathbf{u}_m = \mathbf{r}^{-1}(x_0, x_1, x_2, x_3, ...) = (x_1, x_2, x_3, x_4, ...) = f_m (x_0, x_1, x_2, x_3, ...) = f_m \mathbf{u}_m \qquad (2.5.14c)$$

Factors f_m will be the desired eigenvalues for **r**$^{-1}$, **r** *and* by (2.18.14a) for **K**, too.

The N=2 eigenvector $\mathbf{u}_+ = (1,1)$ in (2.3.30) gives us a clue for N=12. Fig. 2.5.6(g) shows pendulums swinging together in the $(m_{12}) = 0_{12}$ wave with phasor x_p set to 0th-root $(\psi_{12}) = 1$. The π-out-of-phase wave $(m_{12}) = 6_{12}$ has x_p set to the pth power of 6th-root $(\psi_{12}) = -1$, analogous to (2.3.30) vector $\mathbf{u}_- = (1,-1)$.

$$\mathbf{u}_0 = (1,1,1,1,1,1,...) \quad (2.5.15a) \qquad\qquad \mathbf{u}_6 = (1,-1,1,-1,1,-1,...) \qquad (2.5.15b)$$

To understand general $\mathbf{u}_m$ eigenvectors consider the $(m_{12}) = 1_{12}$ and 2_{12} vectors plotted in Fig. 2.5.6(g).

$x_p:$	x_0	x_1	x_2	x_3	x_4	x_5	x_6	x_7	x_8	x_9	x_{10}	x_{11}	x_{12}
$\mathbf{u}_1 =$	(1	$e^{ik_1 1}$	$e^{ik_1 2}$	$e^{ik_1 3}$	$e^{ik_1 4}$	$e^{ik_1 5}$	$e^{ik_1 6}$	$e^{-ik_1 5}$	$e^{-ik_1 4}$	$e^{-ik_1 3}$	$e^{-ik_1 2}$	$e^{-ik_1 1}$	1)
$\mathbf{u}_2 =$	(1	$e^{ik_1 2}$	$e^{ik_1 4}$	$e^{ik_1 6}$	$e^{ik_1 8}$	$e^{ik_1 10}$	1	$e^{ik_1 2}$	$e^{ik_1 4}$	$e^{ik_1 6}$	$e^{ik_1 8}$	$e^{ik_1 10}$	1)

$$e^{ik_1} = e^{2\pi i/12}$$
$$e^{i12k_1} = 1$$

Each phasor in wave $\mathbf{u}_1$ leads the phasor to the left of it by 1-hour. Clocks are set *12 o'clock, 1 o'clock, 2 o'clock, 3 o'clock, 4 o'clock, 5 o'clock,* and so on for <u>one</u> complete *12 hr.* day going around the "world."

Each phasor in wave $\mathbf{u}_2$ leads the phasor to the left of it by 2-hours. Clocks are set *12 o'clock, 2 o'clock, 4 o'clock, 6 o'clock, 8 o'clock, 10 o'clock,* and so on for <u>two</u> complete *12 hr.* days going around the loop. This means the $\mathbf{u}_{\pm m}$ eigenvalues of the shuffle-ops $\mathbf{r}^{-1}$ and $\mathbf{r}$ are the *single-step phase-factor* $f_m = e^{\pm ik_1 m}$.

$$\mathbf{r}^{-1} \bullet \mathbf{u}_m = e^{ik_1 m}\mathbf{u}_m \qquad (2.5.16a) \qquad\qquad \mathbf{r} \bullet \mathbf{u}_m = e^{-ik_1 m}\mathbf{u}_m \qquad (2.5.16b)$$

Here $k_1 = 2\pi/N = 2\pi/12$. The **K**-matrix has the same eigenvalue and frequency for a $\mathbf{u}_{+m}$ wave as for $\mathbf{u}_{-m}$.

$$\mathbf{K} \bullet \mathbf{u}_m = \left[K\mathbf{1} - k_{12}\left(\mathbf{r}^{-1} + \mathbf{r}\right)\right] \bullet \mathbf{u}_m = \left[K - k_{12}\left(e^{ik_1 m} + e^{-ik_1 m}\right)\right]\mathbf{u}_m = \left[K - 2k_{12}\cos k_1 m\right]\mathbf{u}_m \qquad (2.5.16c)$$

This gives the *wave* or *spectral dispersion function*. An $\omega(k) = \omega_m$ is the key to wave theory.

$$\omega_m = \sqrt{\frac{K - 2k_{12}\cos k_1 m}{M}} = \sqrt{\frac{k + 2k_{12} - 2k_{12}\cos(2\pi m / N)}{M}} \qquad (2.5.17)$$

Linear wave motions, velocity, and spreading (dispersion) are ruled by dispersion functions of some kind. The K-pendulum dispersion function ω_m above is a good example and is plotted with others in Fig. 2.5.9.

An $\omega(k)$ plot is a graph of *per-time* (frequency ω) versus *per-space* (wavevector k). In other words it is a *per-space-time* graph. These *"winks-vs-kinks"* functions determine wave physics as shown in Sec. (d).

If we compare binary *(N=2)* oscillators with *(N=3)* models in Fig. 2.5.1 thru *(N=12)* "clocktane" models in Fig. 2.5.3 we see base-3 or modulo-3 labels $(m)_3$ introduced in connection with (2.5.8) are analogous to binary base-2 labels of $m=(0)_2$ *(symmetric)* and $m=(1)_2$ *(anti-symmetric)* in Fig. 2.3.12.

Higher *N* wave labeling approaches a continuum. The $\mathbf{K} = k(2\mathbf{1} - \mathbf{r} - \mathbf{r}^{-1})$ matrix (2.5.14a) is closely related to a 2nd *finite-difference* matrix that approaches a 2nd *x*-derivative operator $\frac{\partial^2}{\partial t^2}$.

1st derivative: $\dfrac{\partial y}{\partial x} \approx \dfrac{y(x + \Delta x) - y(x)}{(\Delta x)}$ 　　　　2nd derivative: $\dfrac{\partial^2 y}{\partial x^2} \approx \dfrac{y(x + \Delta x) - 2y(x) + y(x - \Delta x)}{(\Delta x)^2}$

$$\begin{pmatrix} \cdot & \cdot & \cdot & \cdot & \cdot & \cdot \\ \cdot & 1 & -1 & \cdot & \cdot & \cdot \\ \cdot & \cdot & 1 & -1 & \cdot & \cdot \\ \cdot & \cdot & \cdot & 1 & -1 & \cdot \\ \cdot & \cdot & \cdot & \cdot & 1 & \cdot \\ \cdot & \cdot & \cdot & \cdot & \cdot & \cdot \end{pmatrix} \begin{pmatrix} \cdot \\ y_1 \\ y_2 \\ y_3 \\ y_4 \\ \cdot \end{pmatrix} = \begin{pmatrix} \cdot \\ y_1 - y_0 \\ y_2 - y_1 \\ y_3 - y_2 \\ y_4 - y_3 \\ \cdot \end{pmatrix} \qquad -\begin{pmatrix} \cdot & \cdot & \cdot & \cdot & \cdot & \cdot \\ -1 & 2 & -1 & \cdot & \cdot & \cdot \\ \cdot & -1 & 2 & -1 & \cdot & \cdot \\ \cdot & \cdot & -1 & 2 & -1 & \cdot \\ \cdot & \cdot & \cdot & -1 & 2 & \cdot \\ \cdot & \cdot & \cdot & \cdot & \cdot & \cdot \end{pmatrix} \begin{pmatrix} \cdot \\ y_1 \\ y_2 \\ y_3 \\ y_4 \\ \cdot \end{pmatrix} = \begin{pmatrix} \cdot \\ y_0 - 2y_1 + y_2 \\ y_1 - 2y_2 + y_3 \\ y_2 - 2y_3 + y_4 \\ y_3 - 2y_4 + y_5 \\ \cdot \end{pmatrix}$$

H and **K** matrix equations are finite-difference versions of quantum and classical wave equations.

$$i\frac{\partial}{\partial t}|\psi\rangle = (H - E)|\psi\rangle \quad \textbf{(H-\textit{matrix equation})} \qquad\qquad -\frac{\partial^2}{\partial t^2}|y\rangle = \mathbf{K}|y\rangle \qquad \textbf{(K-\textit{matrix equation})}$$

$$i\frac{\partial}{\partial t}|\psi\rangle = \left(-r\frac{\partial^2}{\partial x^2} - E\right)|\psi\rangle \quad \textit{(Scrodinger equation)} \qquad -\frac{\partial^2}{\partial t^2}|y\rangle = -k\frac{\partial^2}{\partial x^2}|y\rangle \qquad \textit{(Classical wave equation)}$$

Because the latter has a 2nd time derivative (acceleration $\mathbf{a=\ddot{y}}$ in Newton's $\mathbf{F}=m\mathbf{a}$ equal to Hooke's $\mathbf{F=-K\cdot y}$) the frequency values of classical wave modes are *square roots* of the $\mathbf{K}$-matrix eigenvalues , but quantum wave frequencies are simply proportional to $\mathbf{H}$-matrix eigenvalues as was noted in (2.5.11).
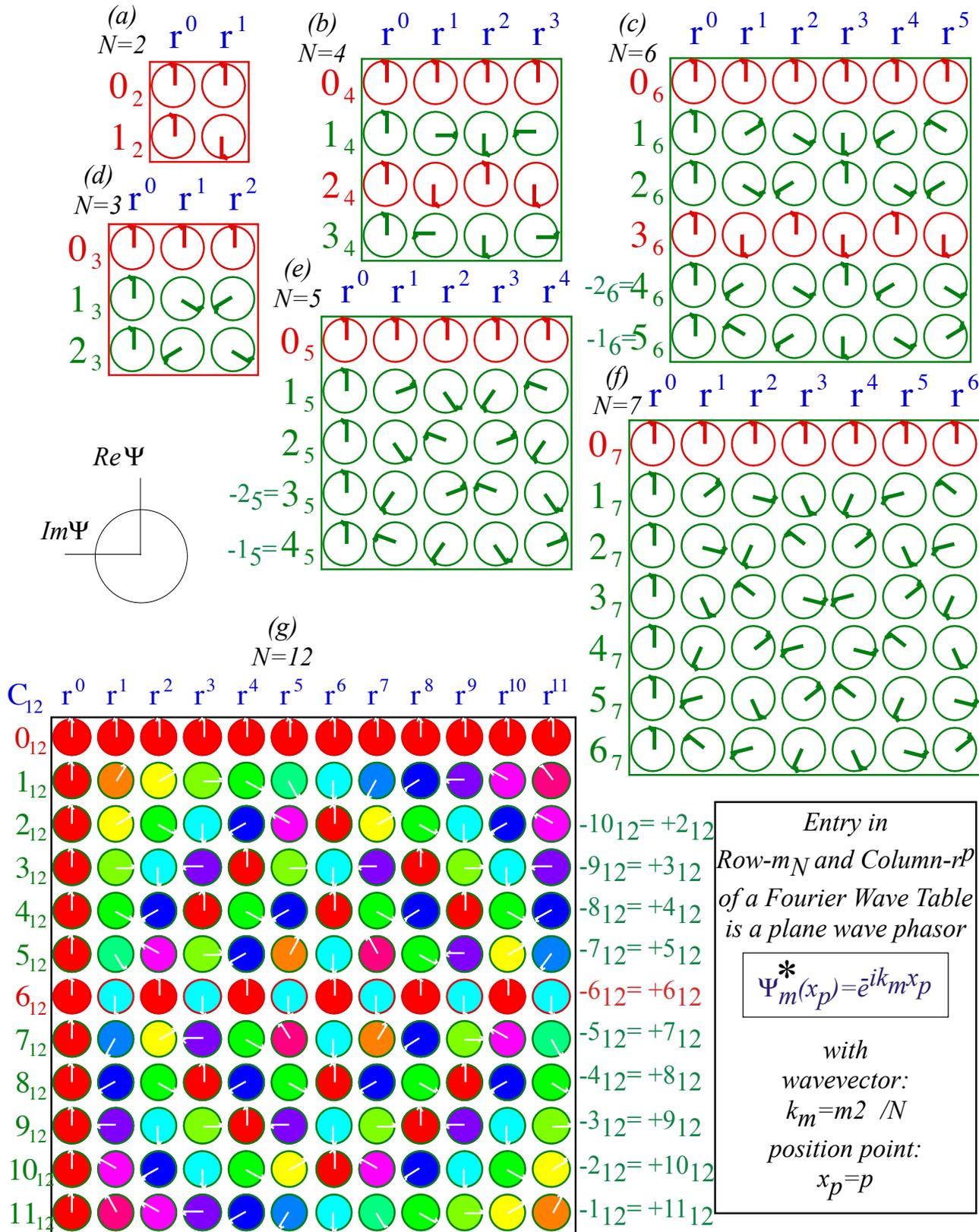

Fig. 2.5.6 Discrete wave phasor or Fourier transform tables for N=2,3,4,5,6,7, and 12.

(c) Wave structure and dynamics

When watching phasor waves in motion we are struck by the impression that some "spirit" is going through the phasors. (See *WaveIt* and *BohrIt* animations.) That, like many spooky notions, is an illusion because only the individual phasors determine the motion of their respective oscillator.

To honor our spooky illusion we construct what's called a *wavefunction*. We simply "fill in" the space between each x_p-phasor point $p=0,1,2...$ with the continuous *plane wave function* e^{ikx} of a continuous coordinate x. That is easy to since we are given discrete functions $\Psi_m(x_p)=e^{ik_m x_p}$ in Fig. 2.5.6 and it is easy to replace x_p with x and plot the resulting $\Psi_m(x)=e^{ik_m x}$. Wavevector k_m is still be discrete in order to fit an integral number m of wavelengths in the ring. But, as N becomes large, k_m becomes more continuous, too.

$$\Psi_m(x)=e^{ik_m x}=\cos k_m x+i\sin k_m x \quad \text{where:} \quad k_m=m\frac{2\pi}{N}. \tag{2.5.18a}$$

Fig. 2.5.7 shows the real part of the wave plotted darkly and the imaginary part shaded.

Distinguishing Ψ and Ψ^*: Conjugation and time reversal

Some symmetry conventions are used. The wave phasors plotted in Fig. 5.3 are for what's called the *conjugate* Ψ^* or *time-reversed-wave*. Its phasors run *backwards* or counter-clockwise like engineer phasors. Conjugation (*) reverses imaginary part ±sign.

$$\Psi_m^*(x)=e^{-ik_m x}=\cos k_m x-i\sin k_m x \quad \text{where:} \quad k_m=m\frac{2\pi}{N}. \tag{2.5.18b}$$

Wave tables with wavevector k_m or m-number as a row label must contain the conjugate $(e^{ikx})^*=e^{-ikx}$. Since we're plotting real Re Ψ in the vertical-up direction and Im Ψ in the horizontal-left direction, the act of conjugation *(*)* reflects the horizontal direction of phasor arrows. (Dirac's bra-ket notation is $\langle x|\Psi_m\rangle=\Psi_m(x)=\langle\Psi_m|x\rangle^*$ where "bras" or "row-vectors" imply a complex conjugating star *(*)*)

Ex.3.2.11 derives the sine-phase-lag rule: *A phasor leading its follower by $\Delta\phi$ feeds it in proportion to the sine of $\Delta\phi$*. Wave propagation is from leader to follower. Plane wave eigenvectors are eigenvectors of the shuffle-op r in (2.5.14) so each phasor leads one side by $\Delta\phi$ and a follows the other side by the same lag $-\Delta\phi$. Whatever is taken gets passed on with no chance to swallow and get fatter! Thus all phasors in a **K**-matrix eigenvector maintain area forever. Thus each $\Psi_m(x)$ is a *stationary state* or *eigenstate* wave. A real vs. imaginary mnemonic: *Imagination precedes reality by one quarter*. The imaginary wave (gray) always precedes the real one by exactly *1/4*-wavelength. ImΨ is the "*gonna'be*" and ReΨ "*is*."

Note that N-modular waves obey the base-N arithmetic. For example, the (*11*-mod-*12*) wave *(11₁₂)* is the same as a (*-1*-mod-*12*) wave *(-1₁₂)*. If we ignore the "spirit" wavefunction between the 12 points then *(11₁₂)=(-1₁₂)* wave has the exact shape of a *(+1₁₂)* wave going in the opposite direction as seen by closely examining Fig. 2.5.6(g). Wave *(10₁₂)=(-2₁₂)* and wave *(+2₁₂)* are similarly related, and so forth up to the wave *(6₁₂)=(-6₁₂)* which are identical standing waves known as Brillouin-band-boundary waves.

Standing waves are colored red while moving waves are colored green. (The international colors for *stop* and *go* are being used there and in preceding figures.) Recall that real number phase differences of $\Delta\phi=0$ or else $\Delta\phi=\pm\pi$ imply energy flow stops since then $sin\Delta\phi=0$. All other phases are complex and allow flow to go.
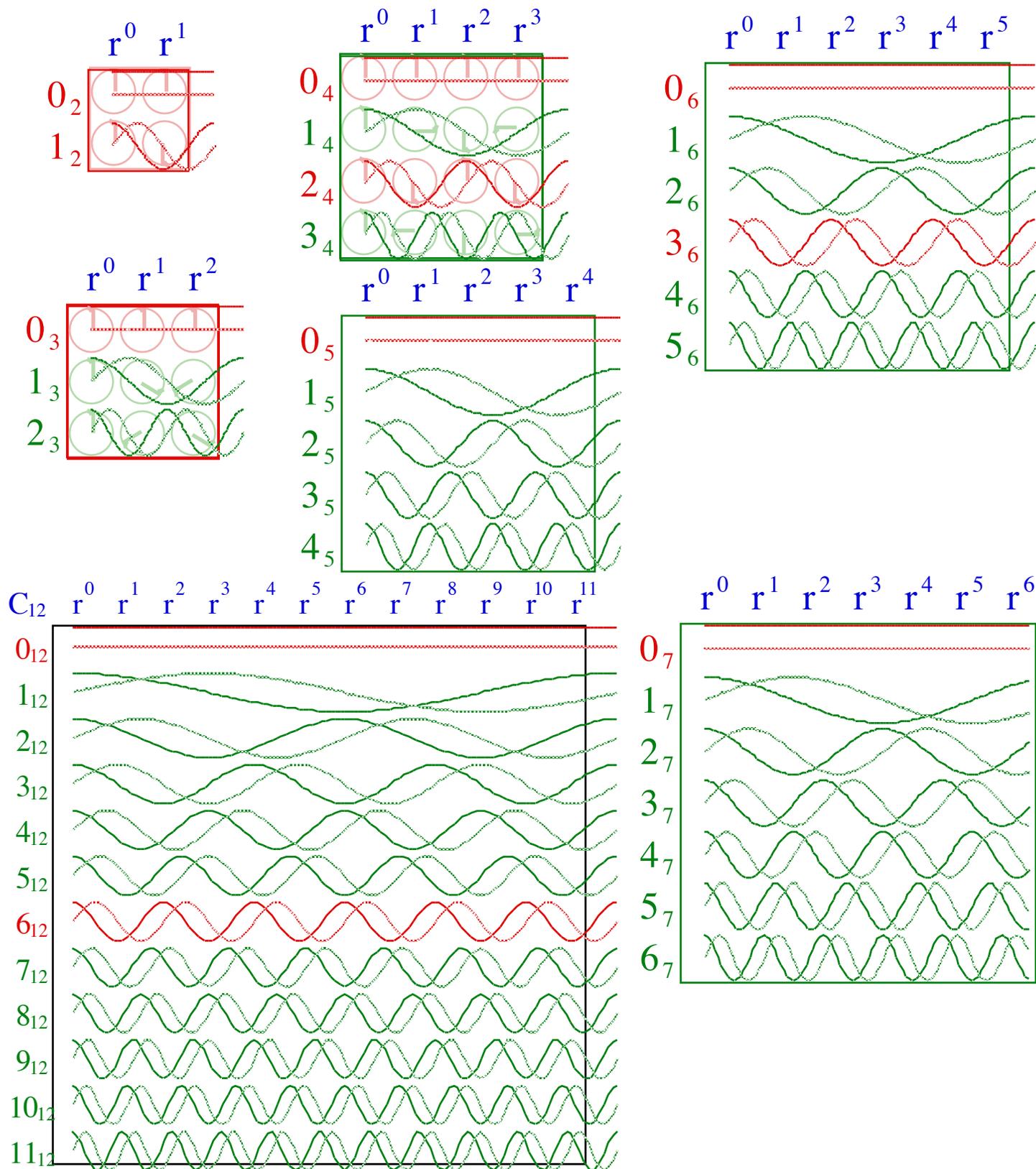
Fig. 2.5.7 Continuous "spirit" wavefunctions for N=2-7, and 12. NOTE:Gray ImΨ is for Ψ not Ψ.*

(d) Wave superposition

Suppose we add a $\Psi_{m=1}(x_p)$ wave to a $\Psi_{m=2}(x_p)$ wave of the same amplitude. The construction in Steps 1-5 of Fig. 2.5.8 does this phasor-by-phasor at time $t=0$, showing both their real and imaginary components. A vector sum is performed to obtain a resultant phasor at each of 12 points $x_0, x_1, x_2, \ldots x_{11}$, where starting point is $x_0=x_{12}$. The algebraic sum is done by an expo-sine-cosine identity ($e^{ia} + e^{ib} = e^{i\frac{a+b}{2}}\left(e^{i\frac{a-b}{2}} + e^{-i\frac{a-b}{2}} \right)$).

$$\Psi_{m=1}\left(x_p\right)+\Psi_{m'=2}\left(x_p\right)= e^{imp\frac{2\pi}{12}} + e^{im'p\frac{2\pi}{12}} = e^{ip\frac{m+m'}{2}\frac{\pi}{6}}\left(e^{ip\frac{m-m'}{2}\frac{\pi}{6}} + e^{-ip\frac{m-m'}{2}\frac{\pi}{6}} \right) = 2e^{ip\frac{m+m'}{2}\frac{\pi}{6}}\cos p\frac{m-m'}{12}\pi$$

$$\Psi_{m=1}\left(x_p\right)+\Psi_{m'=2}\left(x_p\right)= e^{ip\frac{\pi}{6}} + e^{i2p\frac{\pi}{6}} \quad = e^{ip\frac{1+2}{2}\frac{\pi}{6}}\left(e^{ip\frac{1-2}{2}\frac{\pi}{6}} + e^{-ip\frac{1-2}{2}\frac{\pi}{6}} \right) \qquad = 2e^{ip\frac{\pi}{4}}\cos\frac{p\pi}{12} \qquad (2.5.19)$$

The overall phase factor $e^{ip\frac{\pi}{4}} = e^{i\frac{3}{2}p\frac{2\pi}{12}}$ turns 1.5 times while the envelope factor $\cos\frac{p\pi}{12} = \cos\frac{1}{2}\frac{p2\pi}{12}$ does half a turn in the space between $p=0$ and $p=12$.

Fig. 2.5.8 reveals a beat that appears at first glance to be 100% complete, but the $\cos\frac{p\pi}{12}$ envelope is twisted π-out of phase at $p=12$, a kind of half-beat like the example in Fig. 2.5(a). The real wave *inside* the envelope does *1/2* phasor turn by $p=4$, which is *1/3* of the ring circumference from $p=0$ to $p=12$. So it's doing *3/2* turns per *12* units, but the twist of the envelope makes that look like two *full* turns.

Wave phase velocity

Each wave-k_m phasor turns clockwise with time in *Step 6* according to its frequency ω_m.

$$\Psi_m\left(x_p,t\right)= \Psi_m\left(x_p,0\right)e^{-i\omega_m t} = e^{ik_m x_p}e^{-i\omega_m t} = e^{i\left(k_m x_p - \omega_m t\right)} \qquad (2.5.20a)$$

The wave appears to move. The point where phase $k_m x_p - \omega_m t = 0$ moves at *phase velocity V_{phase}*.

$$V_{phase}\left(1\text{ plane wave}\right)= \frac{x_p}{t} = \frac{\omega_m}{k_m} \qquad (2.5.20b)$$

Phase velocity is *time wink rate over spatial kink setting*, $\underline{\omega}$ over $\underline{k}$. The wink rate ω_m is given in terms of kink setting or *wavevector $k_m=k_1 m$* by a dispersion function like (6.7). For low k_m, ω_m is linear: $\omega_m = C \cdot k_m$.

$$\omega_m = \sqrt{\frac{2k_{12} - 2k_{12}\cos k_m}{M}} = 2\sqrt{\frac{k_{12}}{M}}\sin 2k_m \approx Ck_m, \text{ where: } C=V_{phase} = 4\sqrt{\frac{k_{12}}{M}} \text{ for: } k_m = m\frac{2\pi}{N} << 1 \qquad (2.5.20c)$$

(Note: gravity g and $k = \frac{Mg}{\ell}$ are zero here.) Short waves, like dogs with short legs, must walk faster to keep up a speed C. If long wave-$k_{m=1}$ advances all its phasor by one tick, then twice-as-kinky and half-as-short wave-$k_{m=2}$ must do *two ticks* to keep up in *Step 6-8* of Fig. 2.5.8 and make the beat pattern move rigidly. Otherwise, wave patterns disperse as we'll see. That's why the *"winks-vs-kinks"* function $\omega_m(k_m)$ is called a *dispersion* function. It gives the phase and group velocities associated with any pair of frequencies as discussed in what follows.

Step-1 Construct 4 rows of 13 radius-2unit phasor circles with center-to-center distance of 5-units
(For sideways paper 5-units=1 inch. For normal vertical paper: 5-units=1/2 inch)

Label points p=0, 1, 2, 3, ….11, 12
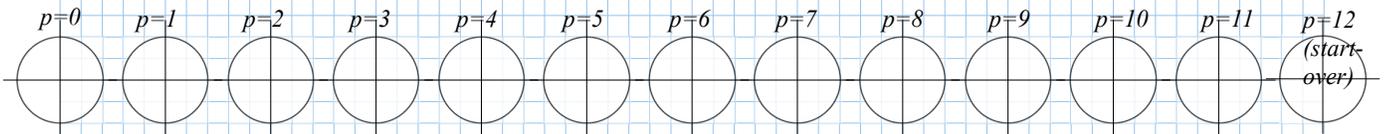
Step-2 Construct 12 equal time tics on first (p=0) and last (p=12). Connect them with <u>light</u> horizontal lines

Step-3 Construct and label the $m_{12}=1_{12}$ or k=1 wave by setting phasors back 1 hr. for each p to 0, -1, -2, -3, ...
Sketch real and imaginary "spirit" waves Re Ψ_m and Im Ψ_m   *(12, 11, 10, 9 ..)*
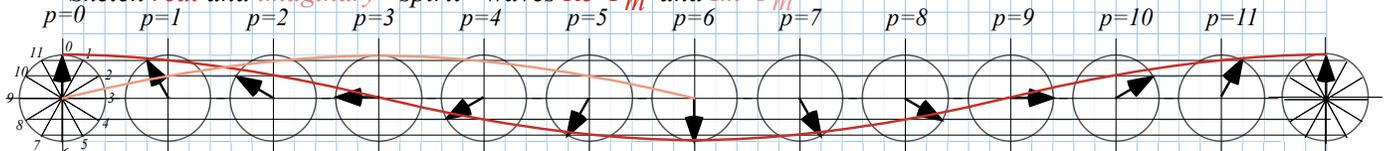
Step-4 Construct and label the $m_{12}=2_{12}$ or k=2 wave by setting phasors back 2 hr. for each p to 0, -2, -4, -6, ...
Sketch real and imaginary "spirit" waves Re Ψ_m and Im Ψ_m   *(12, 10, 8, 6 ..)*
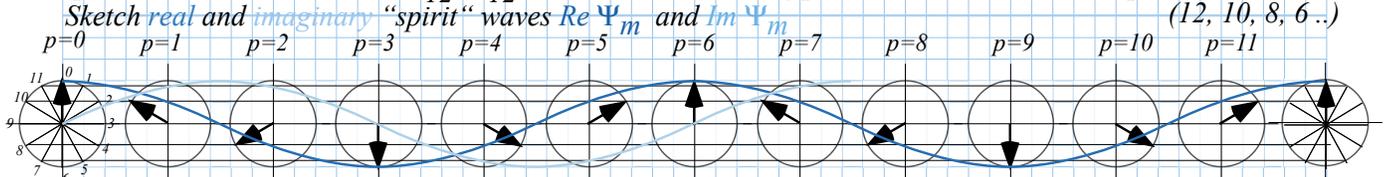
Step-5 Add phasors of k=1 wave to k=2 wave
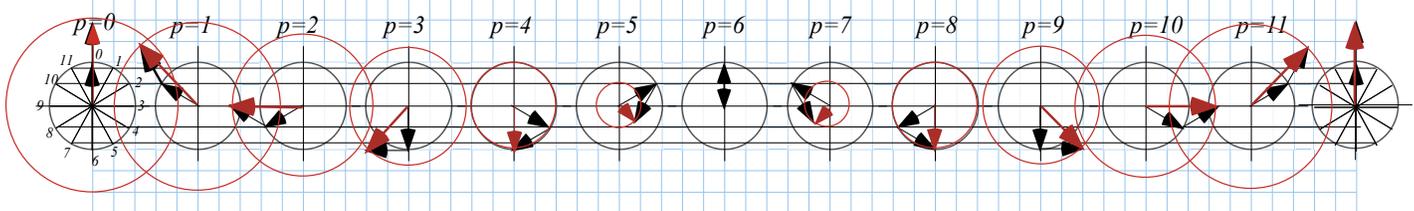
Step-6 Advanceall $m_{12}=1_{12}$ or k=1 phasors by 1 hr.
Sketch real and imaginary "spirit" waves Re Ψ_m and Im Ψ_m
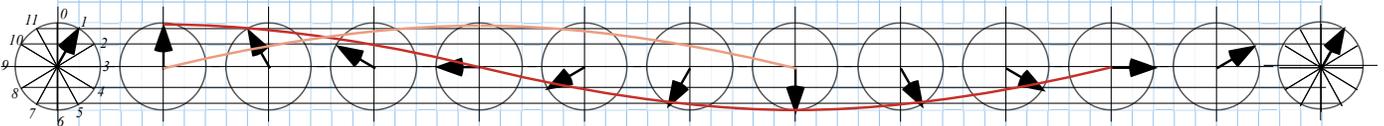
Step-7 Advance all $m_{12}=2_{12}$ or k=2 phasors by 2 hr.
Sketch real and imaginary "spirit" waves Re Ψ_m and Im Ψ_m
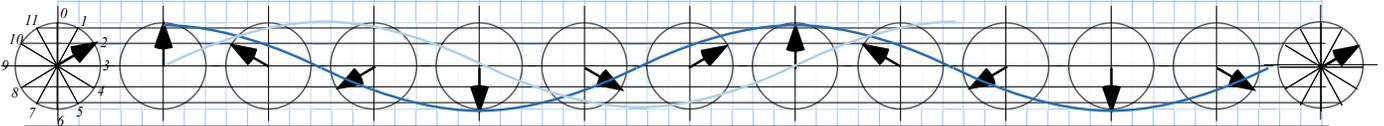
Step-8 Add phasors of k=1 wave to k=2 wave
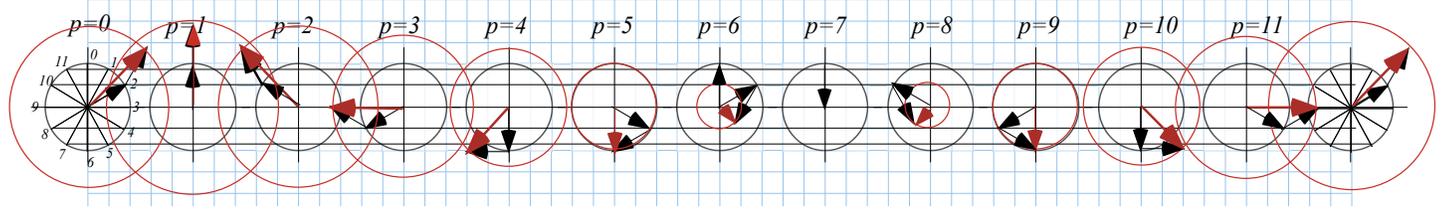
Fig. 2.5.8 Adding (m=1) and (m=2) waves. Step 1-5 is initial time t=0. Step 6-8 is later time t=1 tick.

Group velocity and mean phase velocity

A sum of two waves forms patterns that don't resemble either wave and the patterns may change or disperse over time. We factor their sum using $e^{ia} + e^{ia} = e^{i(a+b)/2}(e^{i(a-b)/2} + e^{-i(a-b)/2}) = 2e^{i(a+b)/2}\cos(\frac{a-b}{2})$.

$$\Psi_{k_m}\left(x_p,t\right) + \Psi_{k_n}\left(x_p,t\right) = e^{i\left(k_m x_p - \omega_m t\right)} + e^{i\left(k_n x_p - \omega_n t\right)} = 2e^{i\left(\frac{k_m+k_n}{2}x_p - \frac{\omega_m+\omega_n}{2}t\right)}\cos\left(\frac{k_m - k_n}{2}x_p - \frac{\omega_m - \omega_n}{2}t\right) \quad (2.5.21)$$

The sum wave has two velocities, one for the cosine envelope, and one for the exponential phase inside. Zeroing the *cos(.)* phase gives *exterior envelope velocity $V_{envelope}$* or *group velocity V_{group}*.

$$\left(\frac{k_m - k_n}{2}x_p - \frac{\omega_m - \omega_n}{2}t\right) = 0 \quad \text{implies: } x_p = \frac{\omega_m - \omega_n}{k_m - k_n}t \quad \text{or: } V_{envelope} = \frac{\omega_m - \omega_n}{k_m - k_n} = V_{group} \quad (2.5.22)$$

Zeroing the $e^{i(.)}$ phase gives an *interior wave velocity $V_{interior}$* or *mean phase velocity $V_{mean\ phase}$*.

$$\left(\frac{k_m + k_n}{2}x_p - \frac{\omega_m + \omega_n}{2}t\right) = 0 \quad \text{implies: } x_p = \frac{\omega_m + \omega_n}{k_m + k_n}t \quad \text{or: } V_{interior} = \frac{\omega_m + \omega_n}{k_m + k_n} = V_{mean\ phase} \quad (2.5.23)$$

A linear dispersion *($\omega_m = Ck_m$)* makes a sum wave move rigidly, that is, its interior and envelope wave go the same speed *C*. By (2.5.20c), individual wavespeed is *C*, too. *($\omega_m/k_m = C = const.$)*

$$V_{interior} = \frac{Ck_m + Ck_n}{k_m + k_n} = C = \frac{Ck_m - Ck_n}{k_m - k_n} = V_{envelope} \quad \text{if: } \omega_m = Ck_m \text{ for all } m. \quad (2.5.24)$$

For nonlinear dispersion, speed $V_{interior}$ of a wave's "guts" differs from speed $V_{envelope}$ of its "skin." (Imagine a slithering boa constrictor swallowing live rabbits that continuously hop along inside it!)

Absolute square $|\Psi|^2 = \Psi^*\Psi$ of equi-amplitude sum $\Psi = \psi_m + \psi_n$ (2.5.21) is just a cosine squared.

$$|\Psi|^2 = \left|e^{i\left(k_m x_p - \omega_m t\right)} + e^{i\left(k_n x_p - \omega_n t\right)}\right|^2 = \cos^2\left(\frac{k_m - k_n}{2}x_p - \frac{\omega_m - \omega_n}{2}t\right) \quad (2.5.25a)$$

The mean phase of $e^{i(.)}$ cancels $(e^{i(.)*}e^{i(.)} = e^{-i(.)}e^{i(.)} = 1)$ leaving envelope wave $|\Psi| = \sqrt{(\Psi^*\Psi)}$. Envelope $|\Psi|$ is more complicated for a sum of waves with unequal amplitudes $(A_m \neq A_n)$. (Recall cosine law.)

$$|\Psi| = \sqrt{\Psi^*\Psi} = \sqrt{\left|A_m e^{i\left(k_m x_p - \omega_m t\right)} + A_n e^{i\left(k_n x_p - \omega_n t\right)}\right|^2} = \sqrt{|A_m|^2 + |A_n|^2 + 2|A_m||A_n|\cos^2\left(\frac{k_m - k_n}{2}x_p - \frac{\omega_m - \omega_n}{2}t\right)} \quad (2.5.25b)$$

Both (2.5.25a) and (2.5.25b) have the same *cos(.)* and envelope velocity V_{group} but internal phase behavior is very different and "gallops" at a rate that depends on SWR. (The rabbits try to hop out of the boa!)

Fig. 2.5.9 plots archetypical dispersion functions $\omega(k_m)$. *Constant dispersion* $(\omega = K = Mg/l)$ describes uncoupled *($k_{12} = 0$)* pendulums. Weak coupling but no gravity *(g=0)* is approximated by *linear dispersion* *($\omega_m = Ck_m$)*(2.5.20c), and *quadratic dispersion* *($\omega_m = B + Ck_m^2$)* approximates weak coupling with gravity for low wavevector $k_m \ll \pi$. Next we will see how any *per-space-time* $\omega(k)$ dispersion graph is related to a *space-time x (t)* graph of paths of wave peaks and zeros.

Archetypical Examples of Dispersion Functions

(a) Constant dispersion   *(b) Linear dispersion*   *(c) Quadratic dispersion*   *(d) Phonon dispersion*   *(e) Exciton dispersion*
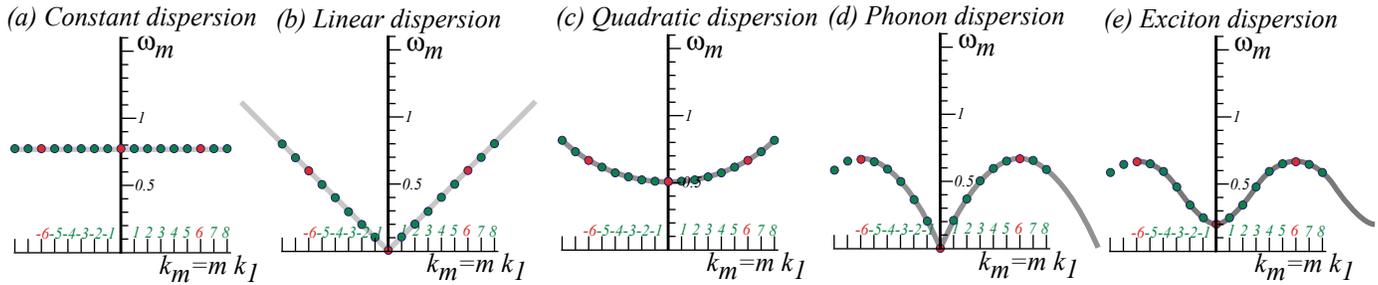
Applications:

Uncoupled pendulums	*Weakly coupled pendulums (No gravity)*	*Weakly coupled pendulums (With gravity)*	*Strongly coupled pendulums (No gravity)*	*Strongly coupled pendulums (With gravity)*
Movie marquis *Xmas lights*	*Light in vacuum (Exactly)* *Sound (Approximately)*	*Light in fiber (Approx)* *Non-relativistic Schrodinger matter wave*	*Acoustic mode in solids*	*Optical mode in solids* *Relativistic matter (If exact hyperbola)*

Reading Wave Velocity From Dispersion Function by (k,ω) Vectors

slope
$(\omega_{-5}-\omega_{-2})/(k_{-5}-k_{-2})$
is
(-5,-2)- group velocity

slope
$(\omega_{-5}+\omega_{-2})/(k_{-5}+k_{-2})$
is
(-5,-2)-
mean phase velocity

slope (ω_{-8}/k_{-8})
is (-8)-phase velocity

slope
$(\omega_8-\omega_3)/(k_8-k_3)$
is (8,3)- group velocity

slope
$(\omega_8+\omega_3)/(k_8+k_3)$
is (8,3)-mean phase velocity

slope (ω_7/k_7)
is (7)- phase velocity
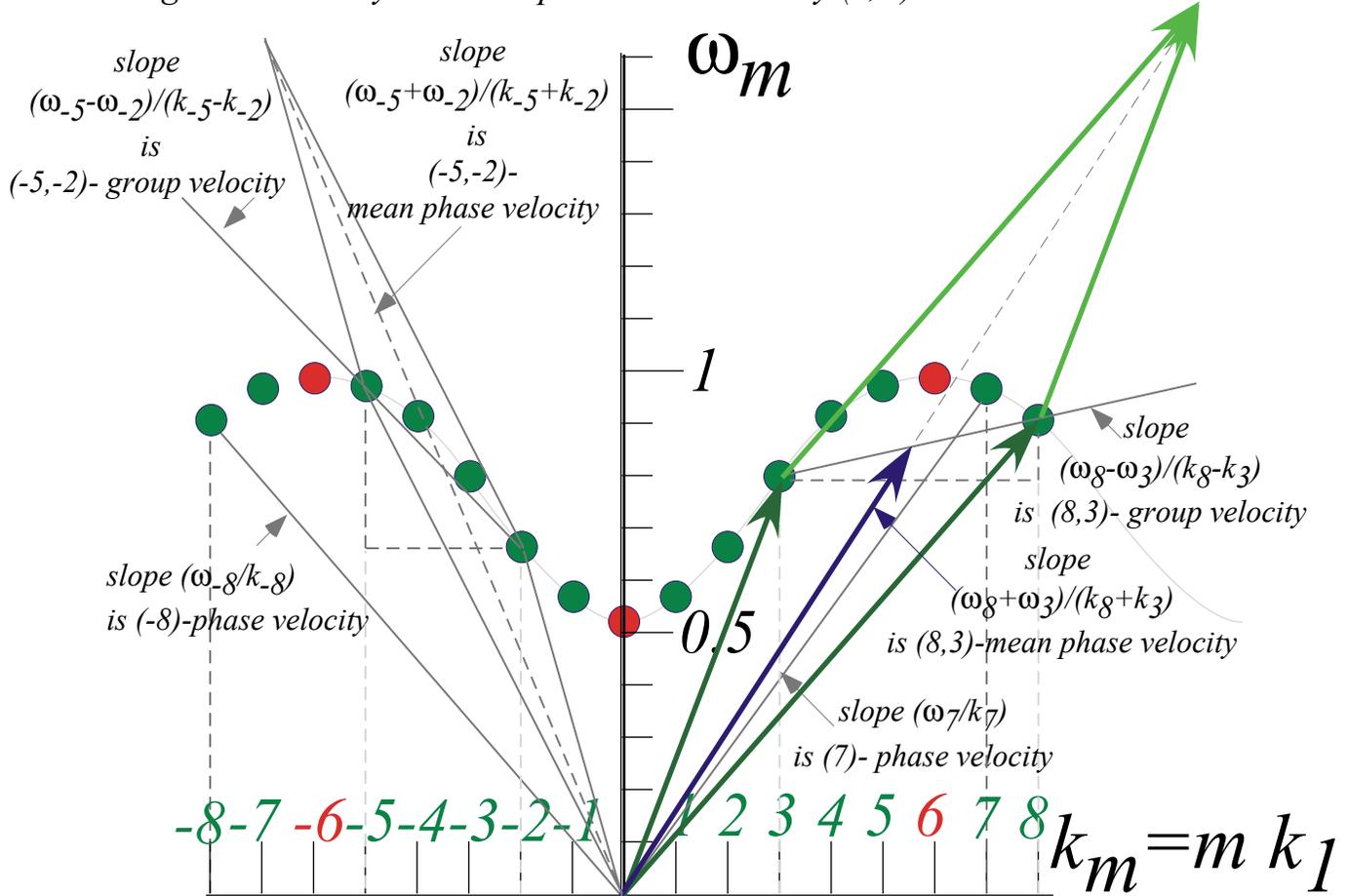
Fig. 2.5.9 Types of dispersion ω(k) functions and geometry of phase and group velocity.

Chapter 2.6 Coupled Oscillator Spectral Response: Green's Operators

(a) Multidimensional Green's operators

The normal coordinate eigenbasis gives decoupled equations (2.3.15b) of independent forced damped harmonic oscillators. The Lorentz-Green solutions (2.2.15) and (2.2.25) may be applied, in turn, to each normal coordinate equation.

$$\ddot{q}_{\varepsilon_j} + 2\Gamma_j \dot{q}_{\varepsilon_j} + \omega_0^2(\varepsilon_j) q_{\varepsilon_j}(t) = a_{\varepsilon_j}(t) \tag{2.6.1}$$

Here the normal coordinate acceleration stimuli are assumed to have the form:

$$a_{\varepsilon_j}(t) = \langle \varepsilon_j | a(t) \rangle = \sum_k \langle \varepsilon_j | k \rangle \langle k | a(t) \rangle = \sum_k \langle \varepsilon_j | k \rangle a_k(0) e^{-i\omega_s t} . \tag{2.6.2}$$

(Recall (2.3.15d).) The $a_k(0)$ are amplitudes of stimulus acceleration applied to k–th original coordinate x_k at frequency ω_s, and $\langle \varepsilon_j | k \rangle$ are components of the transformation from x_k to q_{ε_j}.

The general normal coordinate solutions follow from (2.2.25):

$$q_{\varepsilon_j}(t) = A_j e^{-\Gamma_j t} e^{-i\omega_{\Gamma_j} t} + G_{\omega_0(\varepsilon_j)}(\omega_s) a_{\varepsilon_j}(0) e^{-i\omega_s t} \tag{2.6.3a}$$

The amplitude A_j of the transient term depends on initial values $q_{\varepsilon_j}(0)$, and $\dot{q}_{\varepsilon_j}(0)$. Following (2.2.9) we define the damped angular frequencies. (Recall Exercise 2.2.9.)

$$\omega_{\Gamma_j} = \sqrt{\omega_0^2(\varepsilon_j) - \Gamma_j^2} \tag{2.6.3b}$$

The Lorentz-Green's function has the same form as (2.2.14).

$$G_{\omega_0(\varepsilon_j)}(\omega_s) = \frac{1}{\omega_0(\varepsilon_j)^2 - \omega_s^2 - i2\Gamma_j \omega_s} \tag{2.6.3c}$$

Generally, a stimulus of just one of the original coordinates x_k excites all the normal coordinates through the $\langle \varepsilon_j | k \rangle$ components in (2.6.2). This, in turn, means excitation of all $(x_1, x_2, \ldots)$ coordinates by stimulus of any one of them. However, stimulus of just one normal coordinates q_{ε_j} $(a_{\varepsilon_k}(0) = a\delta_{jk})$ leads to excitation of just that one coordinate.

(b) Abstract Green's operators

It is often possible to use spectral decomposition to solve abstract linear multidimensional equations such as, equation (2.3.10d) (which is repeated below) even when the impedance operators fail to commute.

$$\mathbf{L}|\ddot{q}\rangle + \mathbf{R}|\dot{q}\rangle + \mathbf{A}|q\rangle = |f(t)\rangle \tag{2.6.4}$$

By assuming a complex exponential solution and stimulus,

$$|q(t)\rangle = |q(0)\rangle e^{-i\omega t}, \quad |f(t)\rangle = |f(0)\rangle e^{-i\omega t} \tag{2.6.5}$$

one obtains an operator equation

$$\mathbf{F}(\omega)|q(0)\rangle e^{-i\omega t} = |f(0)\rangle e^{-i\omega t} \tag{2.6.6}$$

where a composite force matrix operator is defined by

$$\mathbf{F}(\omega) = -\omega^2 \mathbf{L} - i\omega \mathbf{R} + \mathbf{A} . \tag{2.6.7}$$

The spectral decomposition of $\mathbf{F}(\omega)$ for fixed ω may be used to solve (2.6.4). The eigenvalues $\phi_j(\omega)$ of $\mathbf{F}(\omega)$ are functions of frequency ω and may be complex.

$$\mathbf{F}(\omega)|\varepsilon_j(\omega)\rangle = \phi_j(\omega)|\varepsilon_j(\omega)\rangle \tag{2.6.8}$$

The eigenvectors $|\varepsilon_j(\omega)\rangle$ may also depend on ω .

Homogeneous or *particular transient solutions* $|\rho_j(\omega)\rangle$ are those for which the stimulus is zero. $(|f(0)\rangle = 0)$ These are eigenvectors for zero eigenvalues.

$$\mathbf{F}(\omega)|\rho_j(\omega)\rangle = 0 . \tag{2.6.9}$$

Solving the following gives ω values analogous to free damped frequency (2.2.9).

$$\phi_j(\omega) = 0 \tag{2.6.10}$$

Homogeneous eigenvectors $|\rho_j(\omega)\rangle$ describe how the unstimulated or 'free' system behaves.

Inhomogeneous or *response* solutions to (2.6.8) involve inversion of (2.6.6) to

$$|q(0)\rangle = \mathbf{G}(\omega_s)|f(0)\rangle \tag{2.6.11}$$

where the *Green's operator* is found by functional spectral decomposition to obtain the inverse $\mathbf{F}(\omega)^{-1}$ for a given stimulus frequency $\omega = \omega_s$.

$$\mathbf{G}(\omega_s) = \sum_{j=1} \frac{1}{\phi_j(\omega_s)} \mathbf{P}_j(\omega_s) . \tag{2.6.12}$$

Idempotent projectors $\mathbf{P}_j$ are found using (2.C.8). Again, they may depend on ω_s .

Example: Ion trap

A non-trivial example of the abstract Green's techniques is provided by linearized cyclotron trap equations.

$$\begin{pmatrix} m & 0 \\ 0 & m \end{pmatrix} \begin{pmatrix} \ddot{x}_1 \\ \ddot{x}_2 \end{pmatrix} + \begin{pmatrix} 0 & \beta \\ -\beta & 0 \end{pmatrix} \begin{pmatrix} \dot{x}_1 \\ \dot{x}_2 \end{pmatrix} + \begin{pmatrix} k_1 & 0 \\ 0 & k_2 \end{pmatrix} \begin{pmatrix} x_1 \\ x_2 \end{pmatrix} = \begin{pmatrix} f_1 \\ f_2 \end{pmatrix} . \tag{2.6.4}_{\text{Example}}$$

Here $\beta = |e\mathbf{B}|$ parametrizes a magnetic field force $e(\mathbf{v} \times \mathbf{B})$ due to a B–field normal to 1-2 axes while k_1 and k_2 represent the x_1 and x_2 harmonic force constants of a quadrupole trapping potential. This is a problem of one particle in two dimensions that has similar form to the preceding problems of two one-dimensional particles. One difference is that the **R**-matrix is *anti*-symmetric. The resulting $\mathbf{F}(\omega)$-matrix is:

$$\mathbf{F}(\omega) = -\omega^2 \mathbf{L} - i\omega \mathbf{R} + \mathbf{A} = \begin{pmatrix} -\omega^2 m + k_1 & -i\omega\beta \\ i\omega\beta & -\omega^2 m + k_2 \end{pmatrix} \tag{2.6.7}_{\text{Example}}$$

The homogeneous (stimulus-free) eigenvalue equation has the form:

$$
\begin{pmatrix} -\omega^2 m + k_1 & -i\omega\beta \\ i\omega\beta & -\omega^2 m + k_2 \end{pmatrix} \begin{pmatrix} x_1(0)e^{-i\omega t} \\ x_2(0)e^{-i\omega t} \end{pmatrix} = \begin{pmatrix} 0 \\ 0 \end{pmatrix}
\qquad (2.6.9)_{\text{Example}}
$$

Dividing by mass m and setting the eigenvalues of $\mathbf{F}(\omega)/m$ to zero gives the following equation.

$$
\frac{\phi(\omega)}{m} = -\omega^2 + \frac{k_1 + k_2}{2m} \pm \sqrt{\left(\frac{k_1 - k_2}{2m}\right)^2 + \left(\frac{\omega\beta}{m}\right)^2} = 0
\qquad (2.6.10)_{\text{Example}}
$$

Solving for ω gives two physically distinct values ω_+ and ω_- for the angular frequency.

$$
\omega_\pm = \sqrt{\frac{k_1 + k_2}{2m} + \frac{\gamma^2}{2} \pm \sqrt{\left(\frac{k_1 - k_2}{2m}\right)^2 + \gamma^2\left(\frac{k_1 + k_2}{2m}\right) + \frac{\gamma^4}{4}}}, \quad \text{where: } \gamma = \frac{\beta}{m}
\qquad (2.6.13)
$$

Here we denote the untrapped cyclotron angular frequency by $\gamma = \beta/m$.

If the trapping potential is isotropic $(k_1 = k = k_2)$ the $\omega_\pm$ are frequencies of trapped cyclotron orbits. The isotropic $\mathbf{F}(\omega)/m$ matrix is the following.

$$
\frac{\mathbf{F}(\omega)}{m} = \begin{pmatrix} -\omega^2 & 0 \\ 0 & -\omega^2 \end{pmatrix} + \frac{1}{m}\begin{pmatrix} k & -i\omega\beta \\ i\omega\beta & k \end{pmatrix}
\qquad (2.6.14)
$$

The eigenvector for the higher frequency ω_+ (including a time dependent phase factor) is

$$
\begin{pmatrix} x_1^+(0)e^{-i\omega_+ t} \\ x_2^+(0)e^{-i\omega_+ t} \end{pmatrix} = r(0)\begin{pmatrix} \dfrac{1}{\sqrt{2}} \\ \dfrac{i}{\sqrt{2}} \end{pmatrix}e^{-i\omega_+ t} = \begin{pmatrix} r(0)\cos\omega_+ t \\ r(0)\sin\omega_+ t \end{pmatrix} + (\text{imaginary parts}), \quad (2.6.15a)
$$

The eigenvalue (2.6.15b) and frequency (2.6.15c) come from (2.6.13).

$$
\frac{\phi(\omega_+)}{m} = -\omega_+^2 + \frac{k}{m} + \gamma\omega_+ = 0 \quad (2.6.15b) \qquad\qquad \omega_+ = \sqrt{\frac{k}{m} + \frac{\gamma^2}{2} + \sqrt{\gamma^2\frac{k}{m} + \frac{\gamma^4}{4}}} \quad (2.6.15c)
$$

The eigenvector for the lower frequency ω_- (with its slower phase factor) is

$$
\begin{pmatrix} x_1^-(0)e^{-i\omega_- t} \\ x_2^-(0)e^{-i\omega_- t} \end{pmatrix} = r(0)\begin{pmatrix} \dfrac{1}{\sqrt{2}} \\ \dfrac{-i}{\sqrt{2}} \end{pmatrix}e^{-i\omega_- t} = \begin{pmatrix} r(0)\cos\omega_- t \\ -r(0)\sin\omega_- t \end{pmatrix} + (\text{imaginary parts}), \qquad (2.6.16a)
$$

with eigenvalue (2.6.16b) and frequency (2.6.16c).

$$
\frac{\phi(\omega_-)}{m} = -\omega_-^2 + \frac{k}{m} - \gamma\omega_- = 0 \quad (2.6.16b) \qquad\qquad \omega_- = \sqrt{\frac{k}{m} + \frac{\gamma^2}{2} - \sqrt{\gamma^2\frac{k}{m} + \frac{\gamma^4}{4}}} \quad (2.6.16c)
$$

Note that for no **B**-field ($\gamma = 0$) we recover the trap frequency ($\omega_+ = \sqrt{\dfrac{k}{m}} = \omega_-$) and for no trap ($k = 0$) we recover the untrapped cyclotron frequency ($\omega_+ = \gamma$) and zero ($\omega_- = 0$). Note also, that in this example the eigenvectors, apart from their overall phase factors, are independent of the frequency.

The real parts of the eigenvectors give the orbit positions. The low (high) frequency orbits are clockwise (counter clockwise) circular orbits, respectively. Counter-clockwise circles of a given radius r are faster because

the $\mathbf{v}\times\mathbf{B}$ acceleration ($\gamma\omega_+ r$) is in the same center-pulling direction as the trapping force (kr) and together they oppose the centrifugal acceleration ($-\omega_+^2 r$). These are the three terms that sum to zero in (2.6.15). However, for clockwise circles the $\mathbf{v}\times\mathbf{B}$ acceleration ($-\gamma\omega_- r$) opposes the trapping force (kr) as seen in (2.6.14), and this reduces the orbit speed and frequency.

      The difference in frequency due to different orbit *handedness* or *orientation* (i.e., right-handed versus left-handed or clockwise versus counter-clockwise) is called *Zeeman splitting,* or *circular polarization* when it occurs in polarization optics. It is the effect of one important kind of symmetry breaking usually caused by *axial* vector fields like rotation or magnetic dipole fields.

      A different type of splitting occurs if an isotropic trapping potential is made anisotropic $k_1 \neq k_2$ and the

degenerate trap frequencies ($\omega_+ = \sqrt{\dfrac{k}{m}} = \omega_-$) split into normal mode frequencies. Now the difference in

frequency is due to orthogonal *direction* or *alignment* of the eigenvectors as in $|\varepsilon_1\rangle$ versus $|\varepsilon_2\rangle$ in Fig. 2.3.12. This is sometimes called *Dichroism* or *Stark* splitting, or *linear polarization* in optical models. It is generally caused by *polar* vector fields like electric dipole fields.

      If you have both types of effects at once the eigensolution orbits become *elliptical* with the ellipses becoming more and more eccentric as the polar fields dominate the axial fields. (See Exercise 2.6.6.)

      The Green's solution for the isotropic trapping potential orbits with stimuli $f_j = f_j(0)e^{-i\omega_s t}$ is the following:

$$\begin{pmatrix} q_1(0) \\ q_2(0) \end{pmatrix} e^{-i\omega_s t} = \mathbf{G}(\omega_s) \begin{pmatrix} f_1(0) \\ f_2(0) \end{pmatrix} e^{-i\omega_s t} \tag{2.6.11}_{\text{Example}}$$

where

$$\mathbf{G}(\omega_s) = \frac{1}{k+\omega_s\beta-\omega_s^2 m} \begin{pmatrix} \dfrac{1}{2} & \dfrac{-i}{2} \\ \dfrac{i}{2} & \dfrac{1}{2} \end{pmatrix} + \frac{1}{k-\omega_s\beta-\omega_s^2 m} \begin{pmatrix} \dfrac{1}{2} & \dfrac{i}{2} \\ \dfrac{-i}{2} & \dfrac{1}{2} \end{pmatrix} \tag{2.6.12}_{\text{Example}}$$

Notice that it blows up if stimulus frequency approaches one of the homogeneous eigenfrequencies. This would correspond to undamped *cyclotron resonance*.

Exercises for Ch. 5 Green's function spectral response

Chapter 2.7   Fourier Analysis of Polychromatic Stimuli

So far only a single or *monochromatic* stimulus of angular frequency ω_S represented by one complex phasor $a_S e^{-i\omega_S t}$ has been considered in equations of the form

$$\ddot{q}_\varepsilon + 2\Gamma_\varepsilon \dot{q}_\varepsilon + \omega_0^2(\varepsilon) q_\varepsilon(t) = a_\varepsilon(t) = a_\varepsilon(0) e^{-i\omega_S t} \tag{2.7.1}$$

The Lorentz-Green's function solution (2.2.25) contains two terms,

$$q_\varepsilon(t) = A_\varepsilon e^{-\Gamma_\varepsilon t} e^{-i\omega_\Gamma(\varepsilon) t} + G_{\omega_0(\varepsilon)}(\omega_S) a_\varepsilon(0) e^{-i\omega_S t} \tag{2.7.2a}$$

The first term is a transient at the oscillators own frequency

$$\omega_\Gamma(\varepsilon) = \sqrt{\omega_0^2(\varepsilon) - \Gamma_\varepsilon^2} \approx \omega_0(\varepsilon) \quad (\text{for } \Gamma_\varepsilon << \omega_0(\varepsilon)) \tag{2.7.2b}$$

with decaying amplitude (Its dying last breaths.) set by initial conditions, and the second is a steady lock-step response at the stimulus frequency ω_S with constant amplitude equal to the product of stimulus amplitude a_S and Green's frequency response function

$$G_{\omega_0(\varepsilon)}(\omega_S) = \frac{1}{\omega_0(\varepsilon)^2 - \omega_S^2 - i2\Gamma_\varepsilon \omega_S} \tag{2.7.2c}$$

Recall discussions around (2.3.15) and (2.6.3).

Now we extend the theory to multi-band or *polychromatic* stimuli that are composed of a *Fourier combination* of multiple stimulus frequencies ω_1, ω_2, ω_3, ...as follows.

$$\ddot{q} + 2\Gamma \dot{q} + \omega_0^2 q = a_1 e^{-i\omega_1 t} + a_2 e^{-i\omega_2 t} + a_3 e^{-i\omega_3 t} + ... \tag{2.7.3}$$

Because the equation is linear in coordinate q the solution is simply a sum of solutions (2.7.2)

$$q(t) = A e^{-\Gamma t} e^{-i\omega_\Gamma t} + G_{\omega_0}(\omega_1) a_1 e^{-i\omega_1 t} + G_{\omega_0}(\omega_2) a_2 e^{-i\omega_2 t} + G_{\omega_0}(\omega_3) a_3 e^{-i\omega_3 t} + ...$$

where the transient amplitude is set by initial values. (2.7.4)

$$A = q(0) - G_{\omega_0}(\omega_1) a_1 - G_{\omega_0}(\omega_2) a_2 - G_{\omega_0}(\omega_3) a_3 - ...$$

Because of high-frequency fall-off for the $G_{\omega_0}(\omega_S)$ function, the components with $\omega_S > \omega_0$ will be small compared to those below resonance (DC region). The only really significant contributions come from terms whose frequency falls in the resonance region. ($\omega_0 - \Gamma \le \omega_S \le \omega_0 + \Gamma$)

(a) Fourier harmonic series

Jean Baptiste Fourier first showed how any periodic function $a(t)$ that always repeats after time τ , can be expressed as a series of *harmonics* $\nu, 2\nu, 3\nu,$ ...of the *fundamental frequency* $\nu = 1/\tau$ or $\omega = 2\pi/\tau$ as follows

$$a(t) = ... + a_{-3} e^{i3\omega t} + a_{-2} e^{i2\omega t} + a_{-1} e^{i\omega t} + a_0 + a_1 e^{-i\omega t} + a_2 e^{-i2\omega t} + a_3 e^{-i3\omega t} + ...$$

or:
$$a(t) = \sum_{k=-\infty}^{\infty} a_k e^{-ik\omega t} \qquad (\omega = 2\pi/\tau) \tag{2.7.5a}$$

in terms of constant *Fourier coefficients* a_k given by the following single-period integrals

$$a_k = \frac{1}{\tau} \int_{-\tau/2}^{\tau/2} dt\, a(t) e^{ik\omega t} \qquad (\tau = 2\pi/\omega) \tag{2.7.5b}$$

The latter follows from the following elementary exponential integral

$$\int_{-\tau/2=-\pi/\omega}^{\tau/2=\pi/\omega} dt\, e^{i(j-k)\omega t} = \frac{e^{i(j-k)\omega t}}{i\omega(j-k)}\Bigg|_{-\pi/\omega}^{\pi/\omega} = \frac{e^{i(j-k)\pi} - e^{i(j-k)\pi}}{i\omega(j-k)} = \frac{2\sin\pi(j-k)}{\omega(j-k)}$$

$$= \left\{ \begin{array}{cc} 2\pi/\omega = \tau & \text{if } j=k \\ 0 & \text{if } j \neq k \end{array} \right\} = \tau\delta_k^j$$

(2.7.5c)

Given $a(t)$, this Fourier orthonormality relation yields the Fourier coefficients (2.7.5b) which can then be substituted into the Green's function sum to give the response (2.7.4) to $a(t)$. Consider a square wave of period τ shown in Fig. 2.7.1. The integral (2.7.5b) has three parts.

$$a_k = \frac{1}{\tau}\left(\int_{-\tau/2}^{-\tau/4} dt\, Ae^{ik\frac{2\pi}{\tau}t} + \int_{-\tau/4}^{\tau/4} dt\, Be^{ik\frac{2\pi}{\tau}t} + \int_{\tau/4}^{\tau/2} dt\, Ae^{ik\frac{2\pi}{\tau}t} \right)$$

$$= \frac{A\left(e^{-ik\pi/2} - e^{-ik\pi}\right)}{2\pi k} + \frac{B\left(e^{ik\pi/2} - e^{-ik\pi/2}\right)}{2\pi k} + \frac{A\left(e^{ik\pi} - e^{ik\pi/2}\right)}{2\pi k}$$

Fig. 2.7.1 Time plot of square wave and integrals that contribute to a_k coefficient.

The resulting Fourier coefficients are sketched below.

$$a_k = A\frac{\sin k\pi}{k\pi} + (B-A)\frac{\sin k\pi/2}{k\pi} = \left\{ \begin{array}{cccccc} k=0 & k=\pm 1 & & k=\pm 3 & & k=\pm 5 \\ \frac{A+B}{2}, & \frac{B-A}{\pi}, & k=\pm 2 \\ 0 \end{array}, & \frac{A-B}{3\pi}, & k=\pm 4 \\ 0 \end{array}, & \frac{B-A}{5\pi} \cdots \right.$$
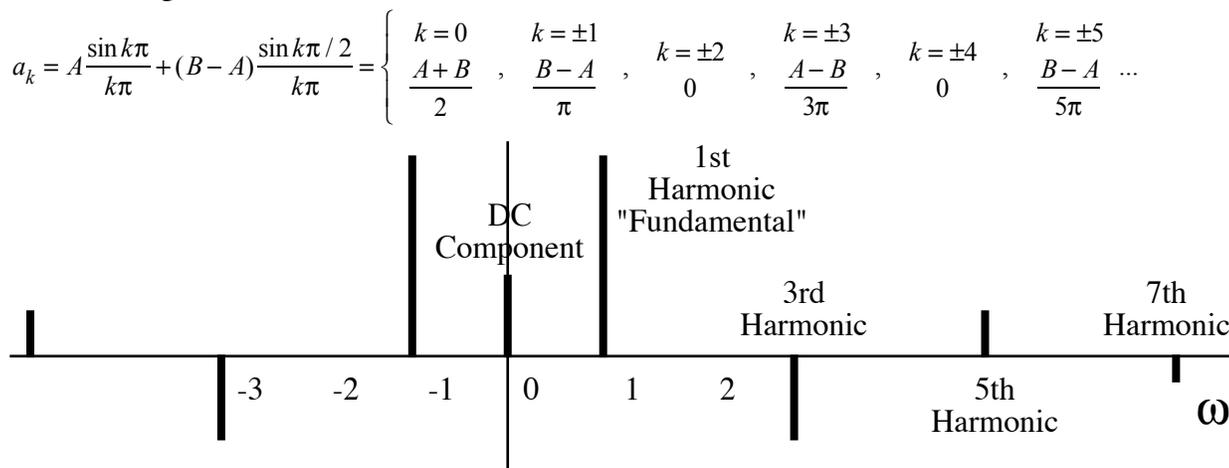
Fig. 2.7.2 Fourier frequency components of square wave

Note that even-k harmonics are zero except for the DC ($k=0$) one.

$$a(t) = \frac{B-A}{\pi}\left(e^{i\omega t} - \frac{e^{i3\omega t}}{3} + \frac{e^{i5\omega t}}{5} - \ldots\right) + \frac{A+B}{2} + \frac{B-A}{\pi}\left(e^{-i\omega t} - \frac{e^{-i3\omega t}}{3} + \frac{e^{-i5\omega t}}{5} - \ldots\right)$$

$$= \frac{A+B}{2} + 2\frac{B-A}{\pi}\left(\cos\omega t - \frac{\cos 3\omega t}{3} + \frac{\cos 5\omega t}{5} - \ldots\right)$$

This is a real function and therefore has both the positive and negative frequency components with exactly the same magnitudes. The response due to $\cos\omega t$ is exactly double that of $e^{-i\omega t}$. Complex analysis needs only the positive frequency (clockwise) phasor amplitudes a_k ($k \geq 0$) in (2.7.4).

Fourier series have a problem with vertical discontinuities such as the square wave jumps. Fig. 2.7.3 shows a 5-term (up to the k=9 harmonic), a 10-term (k=19), and a 20-term (k=39) series approximation to the square wave in Fig. 2.7.1.
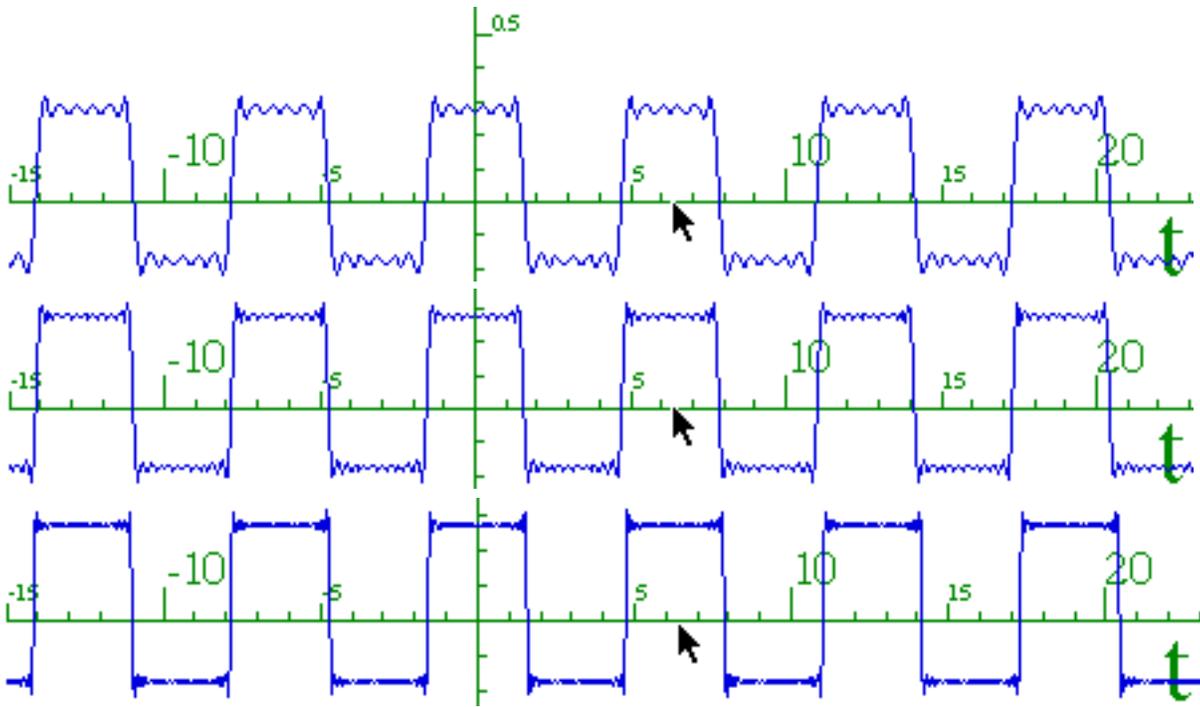
Fig. 2.7.3 Fourier series approximations to square wave stimulus up to k= 9, 19. and 39.

They all "overshoot" and "ring-down" then "ring-up" in between each jump. This is called *Gibbs phenomena*. Generally this phenomena or "fault" of Fourier analysis is not important since most oscillators can only "hear" the *k=1* or *k=3* harmonics. High frequency fall-off of response makes the oscillator "deaf" to high stimulus harmonics unless the stimulus fundamental is extremely low. Then the response is just that of a series of sudden origin shifts as shown in Fig. 2.7.4. Each square wave jump is followed by the normal decay of the oscillator around its new origin, but this has nothing to do with Gibb's "ring-down". The Gibb's "ring-up" seen in the stimulus approximation of Fig. 2.7.3 does not appear in the response. An oscillator cannot "predict" a future shift in origin.
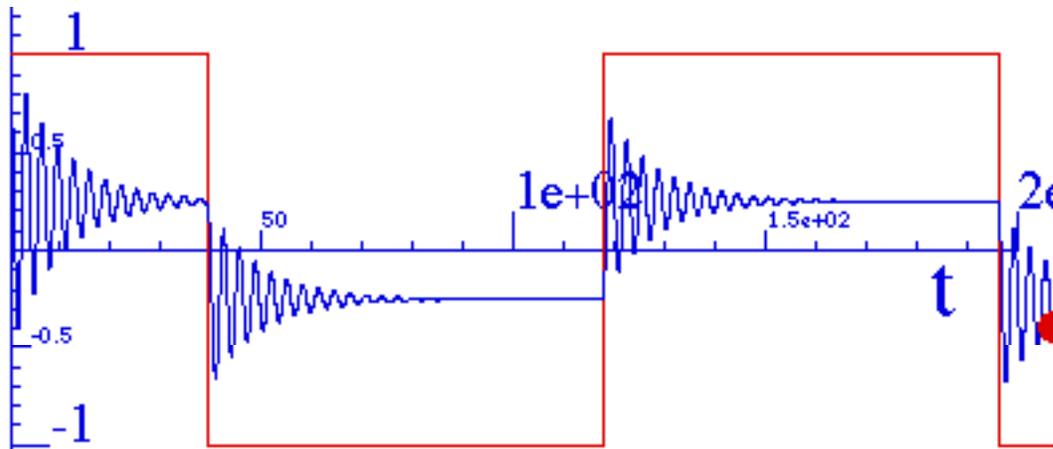
Fig. 2.7.4 Response of oscillator to low frequency square wave stimulus.

Gibb's phenomena are not an issue for continuous functions such as a saw-tooth wave. With only 2- and 5-term Fourier approximations, the saw-tooth stimulus shown in Fig. 2.7.5 is quite accurately represented.
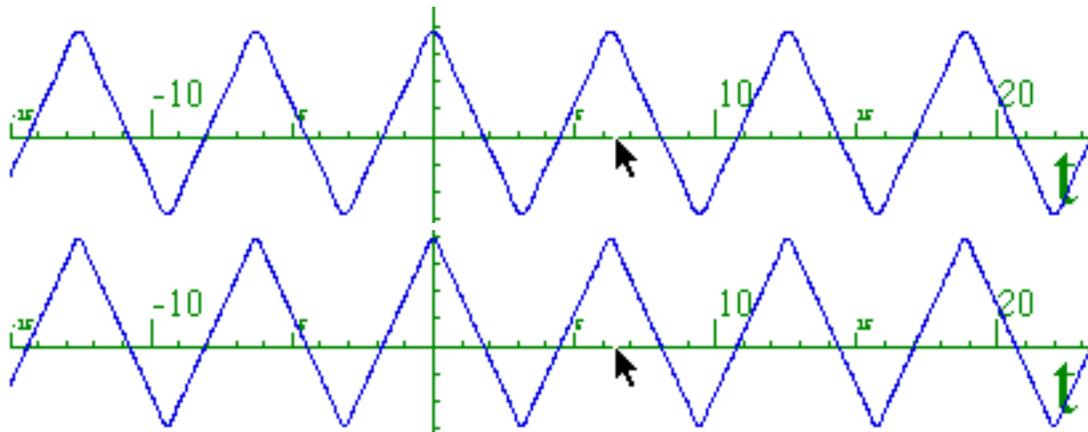
Fig. 2.7.5 Fourier series approximations to saw-tooth wave stimulus up to k= 3 and 9.

Nevertheless, an oscillator will be unable to respond faithfully to this unless the first one or two harmonic frequencies are in the DC region and well below resonance. If the fundamental is near or above the resonant frequency ω_0 of the oscillator, then it will be "deaf" to the harmonics and respond as though the saw-tooth was a pure cosine wave of the same frequency.

(b) Fourier integral transforms

Fourier also showed how <u>any</u> function, periodic or otherwise can be approximated by sines and cosines. Consider the fictitious function of time shown in Fig. 2.7.6 which is periodic for awhile, but like most of us, cannot maintain the pace forever and gets in trouble.
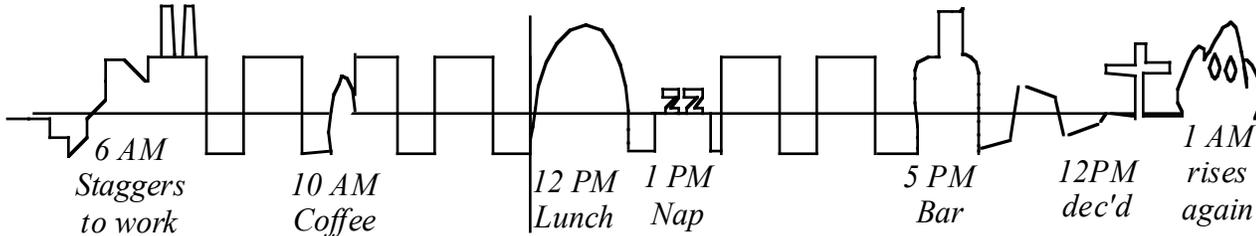
Fig. 2.7.6 A day in the life of a real function.

The trick is to let the fundamental period $(\tau = 2\pi / \omega)$ in (2.7.5) approach infinity, and in the series

$a(t) = \sum\limits_{k=-\infty}^{\infty} a_k e^{-ik\omega t}$, let the sum be an integral: $\sum\limits_{k=-\infty}^{\infty} = \sum\limits_{k=-\infty}^{\infty} \Delta k \rightarrow \int\limits_{-\infty}^{\infty} dk = \int\limits_{-\infty}^{\infty} d\omega \frac{\tau}{2\pi}$ and let frequency be

$$\omega = 2\pi k / \tau \tag{2.7.7}$$

that is, $k=0,\pm1,\pm2,...$ times the fundamental frequency

$$\omega_{Fundamental} = 2\pi / \tau \tag{2.7.8}$$

which approaches zero as τ approaches infinity. So does the incremental frequency interval

$$d\omega = \frac{2\pi}{\tau} dk \tag{2.7.9}$$

become infinitesimal while the sum increment is always one ($dk=1$) since k is an integer. Now k is very large for finite ω. So the Fourier series sum approaches a *Fourier frequency integral*

$$a(t) = \frac{1}{\sqrt{2\pi}} \int\limits_{-\infty}^{\infty} d\omega \, a(\omega) e^{-i\omega t} \tag{2.7.10a}$$

where we define the *Fourier amplitude* $a(\omega) \equiv a_k \tau / \sqrt{2\pi}$ given by a *Fourier time integral*

$$a(\omega) = \frac{1}{\sqrt{2\pi}} \int\limits_{-\infty}^{\infty} dt \, a(t) e^{i\omega t} \tag{2.7.10a}$$

that follows from (2.7.5b). This is copied below for comparison.

$$a_k = \frac{1}{\tau} \int\limits_{-\tau/2}^{\tau/2} dt \, a(t) e^{ik\omega t} = \frac{1}{\tau} \int\limits_{-\tau/2}^{\tau/2} dt \, a(t) e^{ik(2\pi/\tau)t} \tag{2.7.5b}_{copy}$$

Consider some examples for real functions like Fig. 2.7.7 below. For a single square hump the Fourier amplitude (2.7.10a) is given by the *elementary diffraction function*

$$a(\omega) = \frac{1}{\sqrt{2\pi}} \int\limits_{-T/4}^{T/4} dt \, Be^{-i\omega t} = B \frac{e^{-i\omega T/4} - e^{i\omega T/4}}{-i\omega\sqrt{2\pi}} = \frac{2B\sin(\omega T / 4)}{\omega\sqrt{2\pi}} \tag{2.7.11}$$

so called, because it is the first approximation to an optical diffraction pattern of a single square aperture. This is the *sin x/x* function plotted in Fig. 2.7.7.
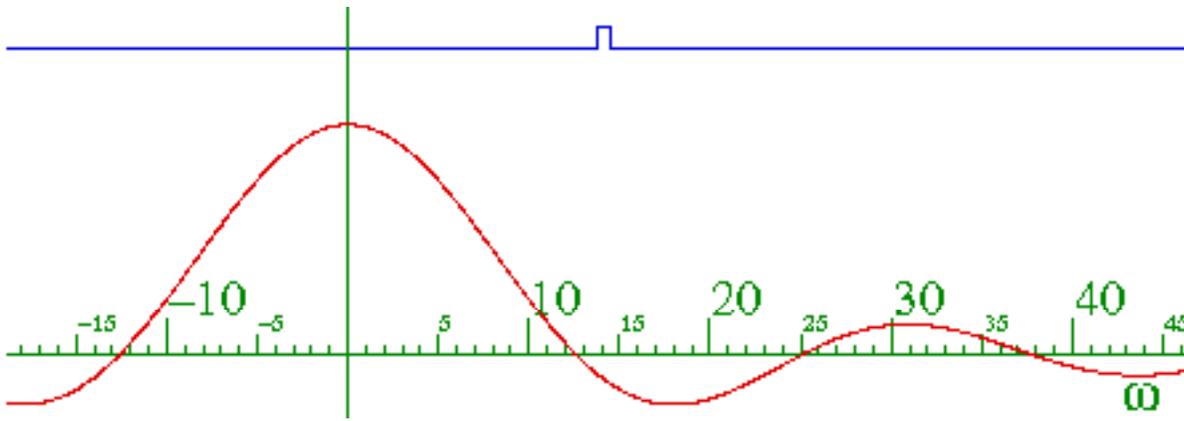
Fig. 2.7.7 Elementary diffraction function: Fourier transform of single half square wave.

The Fourier amplitude due to more and more square humps is a combination of finer and finer elementary diffraction patterns. Three half-humps gives the following which is plotted below.

$$a(\omega) = \frac{1}{\sqrt{2\pi}}\left[A\int_{-3T/4}^{-T/4} dt\, e^{-i\omega t} + B\int_{-T/4}^{T/4} dt\, e^{-i\omega t} + A\int_{T/4}^{3T/4} dt\, e^{-i\omega t}\right]$$

$$= A\frac{e^{i\omega T/4} - e^{3i\omega T/4}}{-i\omega\sqrt{2\pi}} + B\frac{e^{-i\omega T/4} - e^{i\omega T/4}}{-i\omega\sqrt{2\pi}} + A\frac{e^{-i3\omega T/4} - e^{-i\omega T/4}}{-i\omega\sqrt{2\pi}} \tag{2.7.12}$$

$$= \frac{2(B-A)\sin(\omega T/4)}{\omega\sqrt{2\pi}} + \frac{2A\sin(3\omega T/4)}{\omega\sqrt{2\pi}}$$
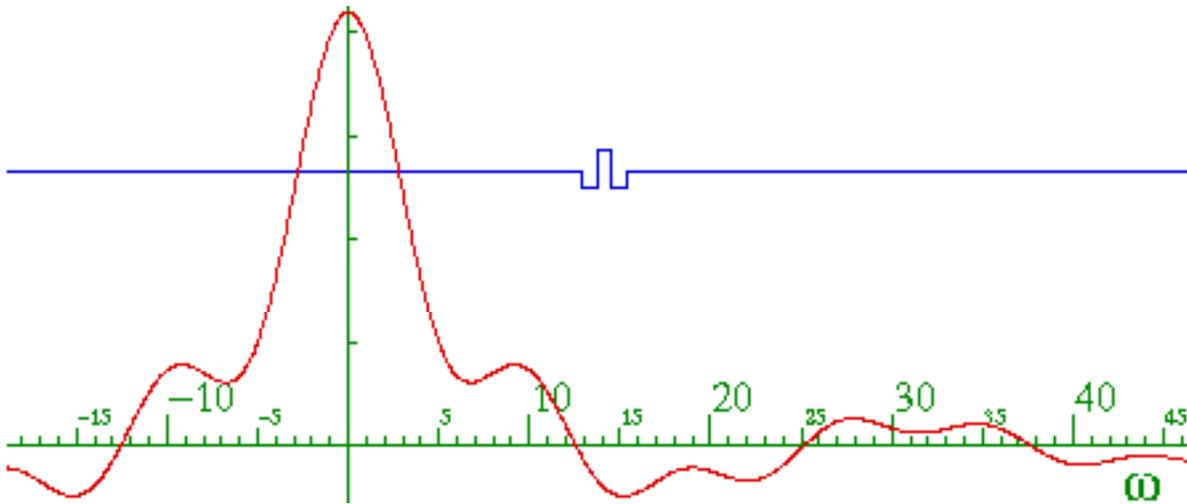
Fig. 2.7.8 Fourier transform of three half square waves.

The result which emerges after many humps is series of spikes corresponding to the Fourier series amplitudes in Fig. 2.7.1.
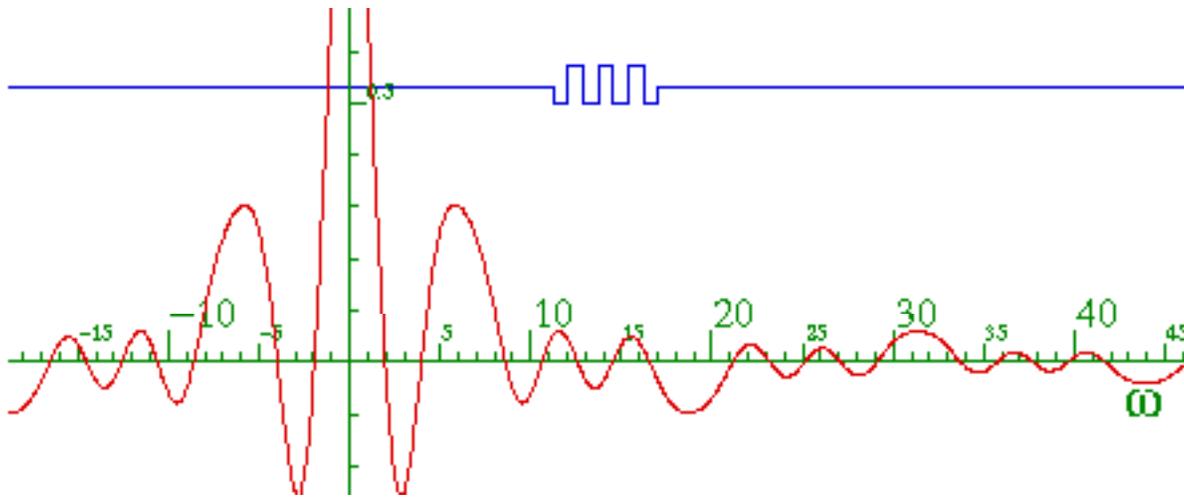
Fig. 2.7.9 Fourier transform of seven half square waves.
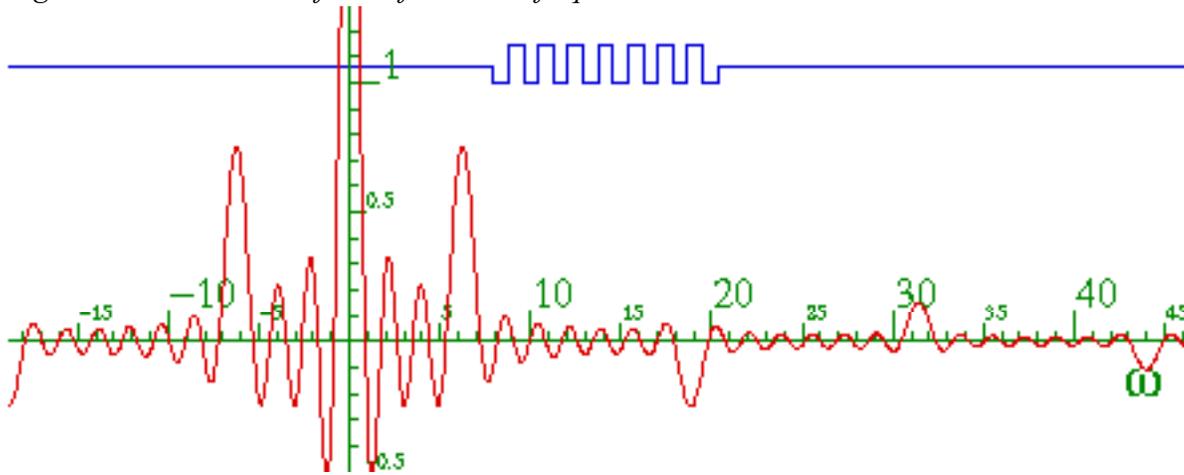
Fig. 2.7.10 Fourier transform of fifteen half square waves.
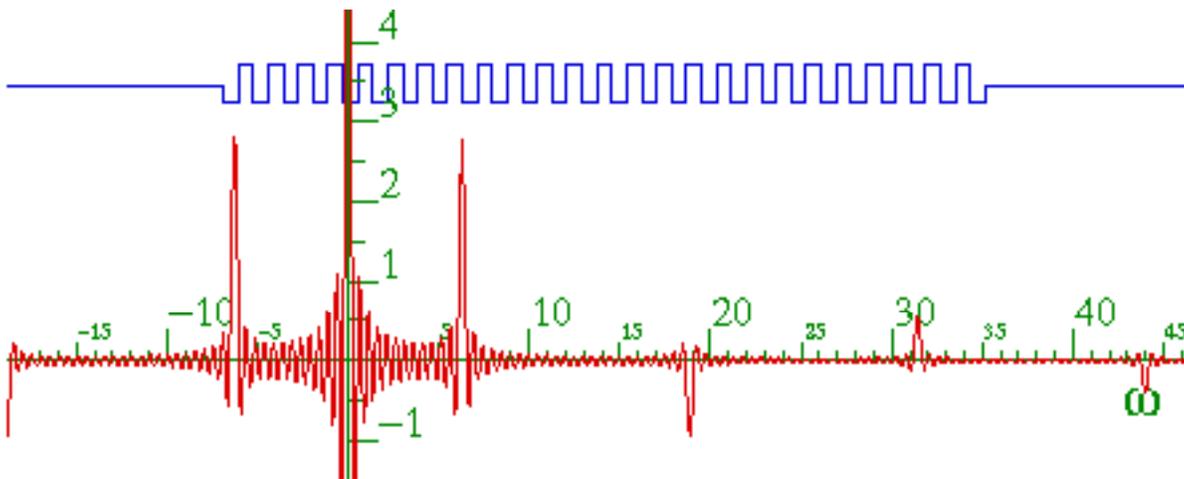
Fig. 2.7.11a Fourier transform of forty-nine half square waves.

Compare the DC peak of Fig. 2.7.11a above and Fig. 2.7.11b below that has two more squares in the finite square wave pulse train _f(t)_.
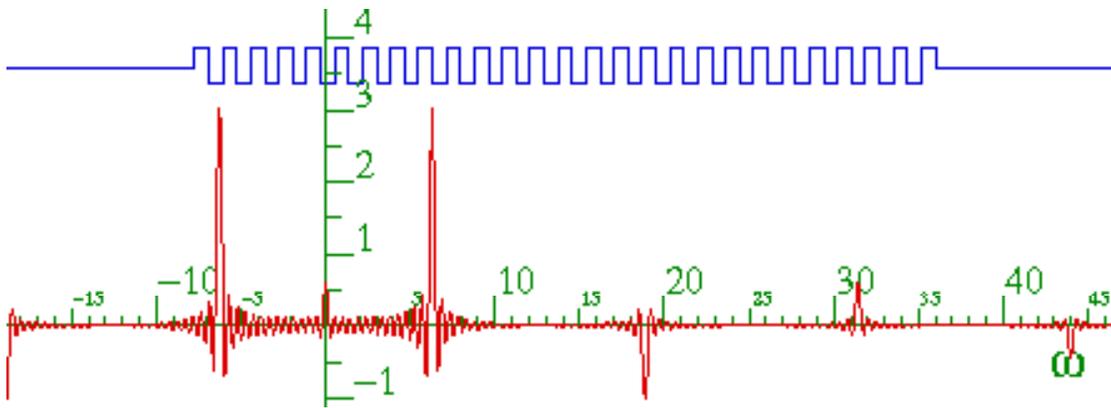
Fig. 2.7.11b Fourier transform of fifty one half square waves.

The "ringing" between the peaks is generally considered to be a nuisance. One way to damp it is to turn the square wave more gradually. Fig. 2.7.12 shows the Fourier transform of a wave that has been turned on and off by a Gaussian ($exp-(x/a)^2$). This *windowing* kills the ringing. The width of each peak varies inversely with the width a of the Gaussian window.
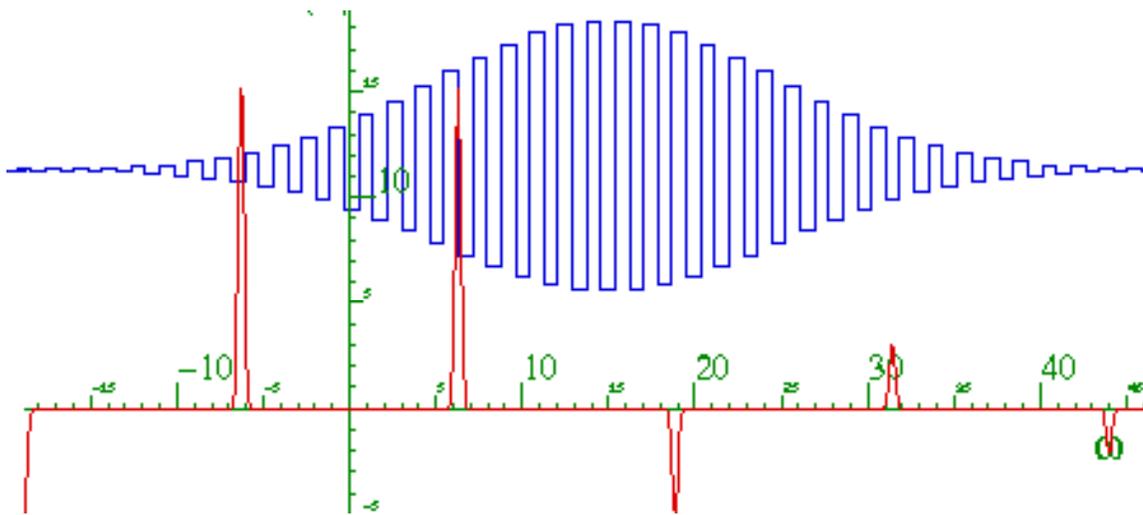
Fig. 2.7.12 Fourier transform of windowed square waves.

(c) Fourier analysis in Dirac notation

Fourier transforms and series are best analyzed using Dirac notation. One must get used to viewing functions like $a(t)$ as a list of bra-ket component $a(t)=\langle t|a\rangle$ of a vector $|a\rangle$ in basis $\{...|t\rangle, |t'\rangle, |t''\rangle, ...\}$ of time values. Fourier transform function $a(\omega)$ is a bra-ket component $a(\omega)=\langle\omega|a\rangle$ of the same vector $|a\rangle$ in basis $\{...|\omega\rangle, |\omega'\rangle, |\omega''\rangle, ...\}$ of frequency values. Fourier just transforms bases. In Dirac notation (2.7.10)

$$a(t)=\frac{1}{\sqrt{2\pi}}\int_{-\infty}^{\infty}d\omega\, a(\omega)e^{-i\omega t} \text{ becomes: } \langle t|a\rangle=\int_{-\infty}^{\infty}d\omega\,\langle t|\omega\rangle\langle\omega|a\rangle \quad \text{with: } \langle t|\omega\rangle=\frac{e^{-i\omega t}}{\sqrt{2\pi}}=\langle\omega|t\rangle* \qquad (2.7.13a)$$

Fourier transformation matrix component is $\langle t|\omega\rangle$. Its inverse is the conjugate.

$$a(\omega) = \frac{1}{\sqrt{2\pi}} \int_{-\infty}^{\infty} dt\, a(t) e^{i\omega t} \qquad \text{becomes:}\quad \langle \omega | a \rangle = \int_{-\infty}^{\infty} dt\, \langle \omega | t \rangle \langle t | a \rangle \qquad (2.7.13b)$$

The integrals are replaced by discrete sums for numerical purposes or when the variables can take on only discrete values as in (2.7.7). Then they identical to the Dirac transformations (2.A-5) in Appendix 2.A.

      The cool idea here is that an acceleration function or any function is an abstract "object" $|a\rangle$ that can be represented in the t-basis as $a(t)$ or in the ω-basis as $a(\omega)$ or in any ortho-complete basis. So any vector in the t-basis $\{...|t\rangle, |t'\rangle, |t''\rangle, ...\}$ is represented using the ω-basis $\{...|\omega\rangle, |\omega'\rangle, |\omega''\rangle, ...\}$, and *vice-versa*. Substituting $|\omega'\rangle$ for $|a\rangle$ in (2.7.13a) and $|t'\rangle$ for $|a\rangle$ in (2.7.13b) gives

$$\langle t | \omega' \rangle = \int_{-\infty}^{\infty} d\omega\, \langle t | \omega \rangle \langle \omega | \omega' \rangle \qquad\qquad\qquad \langle \omega | t' \rangle = \int_{-\infty}^{\infty} dt\, \langle \omega | t \rangle \langle t | t' \rangle$$

Moreover, this applies to any <u>combination</u> of t-bases, or <u>any</u> function $T(\omega)$ and vice-versa for any function $W(t)$.

$$T(\omega') = \int_{-\infty}^{\infty} dt\, T(\omega) \langle \omega | \omega' \rangle \qquad (2.7.14a) \qquad\qquad W(t') = \int_{-\infty}^{\infty} dt\, W(t) \langle t | t' \rangle \qquad (2.7.14b)$$

The functions $\langle \omega | \omega' \rangle$ or $\langle t | t' \rangle$ that satisfy these equations are called *Dirac delta functions.*

$$\delta(\omega - \omega') = \langle \omega | \omega' \rangle = \langle \omega' | \omega \rangle \qquad (2.7.15a) \qquad\qquad \delta(t - t') = \langle t | t' \rangle = \langle t' | t \rangle \qquad (2.7.15b)$$

By (2.7.13) they are

$$\delta(\omega - \omega') = \langle \omega | \omega' \rangle = \int_{-\infty}^{\infty} dt\, \langle \omega | t \rangle \langle t | \omega' \rangle \qquad\qquad \delta(t - t') = \langle t | t' \rangle = \int_{-\infty}^{\infty} d\omega\, \langle t | \omega \rangle \langle \omega | t' \rangle$$

$$= \int_{-\infty}^{\infty} dt\, \frac{e^{it(\omega - \omega')}}{2\pi} \qquad\qquad\qquad\qquad = \int_{-\infty}^{\infty} d\omega\, \frac{e^{-i\omega(t - t')}}{2\pi}$$

This is *Dirac orthonormality*; $\langle \omega | \omega' \rangle$ or $\langle t | t' \rangle$ are zero unless $\omega = \omega'$ or $t = t'$, respectively.

Then δ is infinite $(\delta(0) = \infty)$ but its <u>integral</u> is unity $(\int \delta(x)\, dx = 1)$ from (2.7.14) with $T = 1 = W$.

$$\int_{-\infty}^{\infty} d\omega\, \langle \omega | \omega' \rangle = \int_{-\infty}^{\infty} d\omega\, \delta(\omega - \omega') = 1 = \int_{-\infty}^{\infty} dt\, \delta(t - t') = \int_{-\infty}^{\infty} dt\, \langle t | t' \rangle \qquad (2.7.16a)$$

(c) Fourier-Green's operator analysis

The power of Dirac notation shows in the Fourier analysis of Green's operators. Dirac would write the forced-damped-harmonic oscillator equation (2.2.1)

$$D \cdot q = \frac{d^2 q(t)}{dt^2} + 2\Gamma \frac{dq(t)}{dt} + \omega_0^2 q(t) = a(t) \tag{2.7.17a}$$

as an abstract operator equation

$$\mathbf{D}|q\rangle = |a\rangle \tag{2.7.17b}$$

involving infinite dimensional ket coordinate vector $|q\rangle$ and ket stimulus vector $|a\rangle$. Similar notation would be used for the more complicated "ion-trap" equation (2.6.4):

$$\mathbf{L}|\ddot{q}(t)\rangle + \mathbf{R}|\dot{q}(t)\rangle + \mathbf{A}|q(t)\rangle = |f(t)\rangle \quad \text{becomes:} \quad \mathbf{F}|q\rangle = |f\rangle \tag{2.7.18}$$

Here the 2-dimensional $|q(t)\rangle$ vector is abstracted into the $2 \cdot \infty$ -dimensional $|q\rangle$ vector and the same for $|f(t)\rangle$ becoming $|f\rangle$.

The abstract definition of a Green's operator $\mathbf{G}$ is as simple as it is powerful. It is an inverse of $\mathbf{D}$, that is

$$\mathbf{G} \cdot \mathbf{D} = 1 = \mathbf{D} \cdot \mathbf{G} \tag{2.7.19}$$

so the solution to (2.7.17) results from operating on $\mathbf{D}|q\rangle = |a\rangle$ with $\mathbf{G}$.

$$\mathbf{G} \cdot \mathbf{D}|q\rangle = |q\rangle = \mathbf{G}|a\rangle \tag{2.7.20}$$

By representing these equations in bases $\{...|t\rangle, |t'\rangle, |t''\rangle, ...\}$ or $\{...|\omega\rangle, |\omega'\rangle, |\omega''\rangle, ...\}$ one quickly derives Fourier-Green solution formulas. This is summarized in Fig. 2.7.13.

First, the two representations of the equation of motion (2.7.17) are as follows.

$$\langle t|\mathbf{D}|q\rangle = \langle t|a\rangle = a(t) \qquad\qquad \langle \omega|\mathbf{D}|q\rangle = \langle \omega|a\rangle = a(\omega)$$
$$\int dt' \, \langle t|\mathbf{D}|t'\rangle\langle t'|q\rangle = \langle t|a\rangle = a(t) \qquad \int d\omega' \, \langle \omega|\mathbf{D}|\omega'\rangle\langle \omega'|q\rangle = \langle \omega|a\rangle = a(\omega)$$

$$(2.7.21a) \qquad\qquad\qquad\qquad\qquad (2.7.21b)$$

The *t*-representation matrix of $\mathbf{D}$ is a combination of a Dirac delta function and its derivatives.

$$\langle t|\mathbf{D}|t'\rangle = \frac{d^2\delta(t-t')}{dt'^2} + 2\Gamma\frac{d\delta(t-t')}{dt'} + \omega_0^2\delta(t-t') \tag{2.7.22}$$

The δ-time derivative is evaluated using integration by parts: $\int u \, dv = uv - \int v \, du$

$$\int_{-\infty}^{\infty} dt' \frac{d\delta(t-t')}{dt'} f(t') = -\int_{-\infty}^{\infty} dt \frac{d\delta(t-t')}{dt} f(t) = -\delta(t-t')f(t)\Big|_{-\infty}^{\infty} + \int_{-\infty}^{\infty} dt \, \delta(t-t')\frac{df(t)}{dt} = \frac{df(t')}{dt'} \tag{2.7.23}$$

A δ-time derivative amounts to a non-diagonal matrix. (It transforms $f(t)$ into $[f(t+dt)-f(t)]/dt$.)

On the other hand, the ω-representation of $\mathbf{D}$ is a diagonal matrix since the Fourier representation of the solution $q(\omega) = \langle \omega|q\rangle$ is an eigenfunction. (Recall (2.2.15).)

$$\langle \omega|\mathbf{D}|\omega'\rangle = \left(-\omega^2 - 2i\Gamma\omega + \omega_0^2\right)\delta(\omega-\omega')$$

$$\left(-\omega^2 - 2i\Gamma\omega + \omega_0^2\right)q(\omega) = a(\omega) \tag{2.7.24}$$

D|q⟩=|a⟩
Operator
D-Equation to solve

Represented
in
t-basis

Represented
in
ω-basis

⟨t|**D**|q⟩   =⟨t|a⟩=a(t)
∫dt′⟨t|**D**|t′⟩⟨t′|q⟩=⟨t|a⟩=a(t)

⟨ω|**D**|q⟩   =⟨ω|a⟩=a(ω)
∫dω′⟨ω|**D**|ω′⟩⟨ω′|q⟩=⟨ω|a⟩=a(ω)

∫dω⟨t|ω⟩⟨ω|a⟩=⟨t|a⟩=a(t)
$\int d\omega \frac{e^{-i\omega t}}{\sqrt{2}} a(\omega)=a(t)$
Inverse Fourier Transform

D·G=**1**=**G·D**
Definition of
Green's operator

∫dt⟨ω|t⟩⟨t|a⟩=⟨ω|a⟩=a(ω)
$\int dt \frac{e^{+i\omega t}}{\sqrt{2}} a(t)=a(\omega)$
Fourier Transform

⟨t|**D·G**|t′′⟩ =⟨t|**1**|t′′⟩=δ(t-t′′)
∫dt′⟨t|**D**|t′⟩⟨t′|**G**|t′′⟩   =δ(t-t′′)

⟨ω|**D·G**|ω′′⟩=⟨ω|**1**|ω′′⟩=δ(ω−ω′′)
∫dω′⟨ω|**D**|ω′⟩⟨ω′|**G**|ω′′⟩   =δ(ω−ω′′)

|q⟩=**G**|a⟩
Green's solution
*if **G** is diagonal*
in the ω-basis:
⟨ω|**G**|ω′⟩=*G(ω)*δ(ω−ω′)

⟨t|q⟩=⟨t|**G**|a⟩=∫dt′⟨t|**G**|t′⟩⟨t′|a⟩
q(t)=   =∫dt′ G(t,t′) a(t′)

⟨ω|q⟩=⟨ω|**G**|a⟩=∫dω′⟨ω|**G**|ω′⟩⟨ω′|a⟩
q(ω)=   = *G(ω)* a(ω)
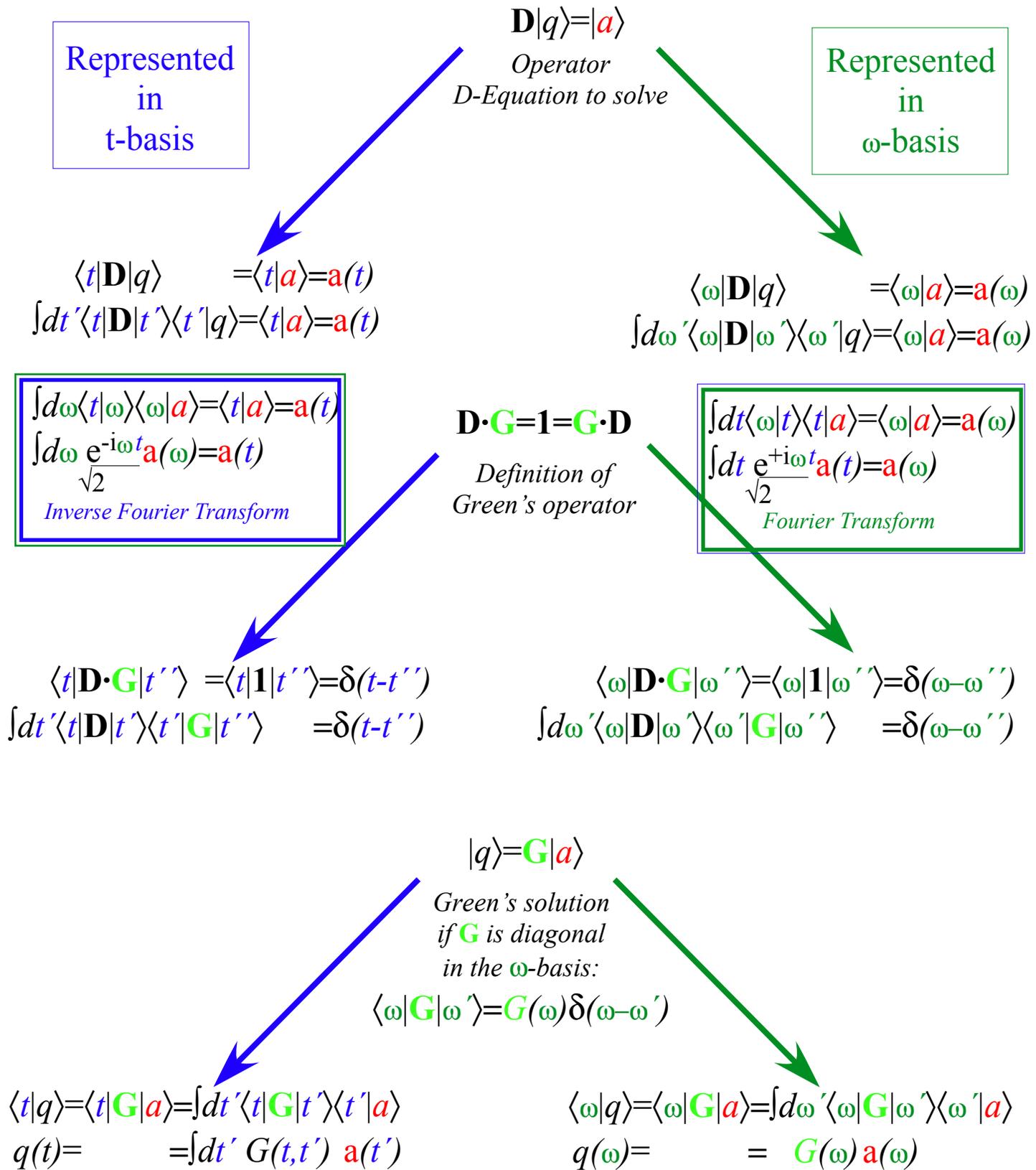
Fig. 2.7.13 Solving inhomogeneous equation in their time and frequency representations.

Next, the two representations of the inverse equation (2.7.19) are as follows.

$$\langle t|\mathbf{D}\cdot\mathbf{G}|t''\rangle = \langle t|\mathbf{1}|t''\rangle = \delta(t-t'')$$
$$\int dt'\langle t|\mathbf{D}|t'\rangle\langle t'|\mathbf{G}|t''\rangle = \delta(t-t'')$$

(2.7.25a)

$$\langle \omega|\mathbf{D}\cdot\mathbf{G}|\omega''\rangle = \langle \omega|\mathbf{1}|\omega''\rangle = \delta(\omega-\omega'')$$
$$\int d\omega'\langle \omega|\mathbf{D}|\omega'\rangle\langle \omega'|\mathbf{G}|\omega''\rangle = \delta(\omega-\omega'')$$

(2.7.25b)

The *t*-representation matrix of **G** is non-diagonal and called the *Green's time function G(t',t'')*.

$$G(t',t'') \equiv \langle t'|\mathbf{G}|t''\rangle$$

(2.7.26a)

Carrying out the matrix product integral (2.7.25a) gives the *Green's unit impulse equation*.

$$D\cdot G(t,t'') = \left[\frac{d^2}{dt^2} + 2\Gamma\frac{d}{dt} + \omega_0^2\right]G(t,t'') = \delta(t-t'')$$

(2.7.26b)

So, *G(t,t')* is the time response at time *t* due to a unit "hit" or impulse at time *t'* that adds unit velocity. For initial conditions $q(0)=0$ and $\dot{q}(0)=1$ the resulting Green's function is given below and plotted in Fig. 2.7.14.

$$G(t,0) = 0, \ \left(\text{for } t<0\right), \text{ and } G(t,0) = q(t) = \frac{e^{-\Gamma t}\sin(\omega_\Gamma t)}{\omega_\Gamma}, \ \left(\text{for } t>0\right)$$

(2.7.27)

$\omega_0=2\pi$

$\Gamma=0.5$
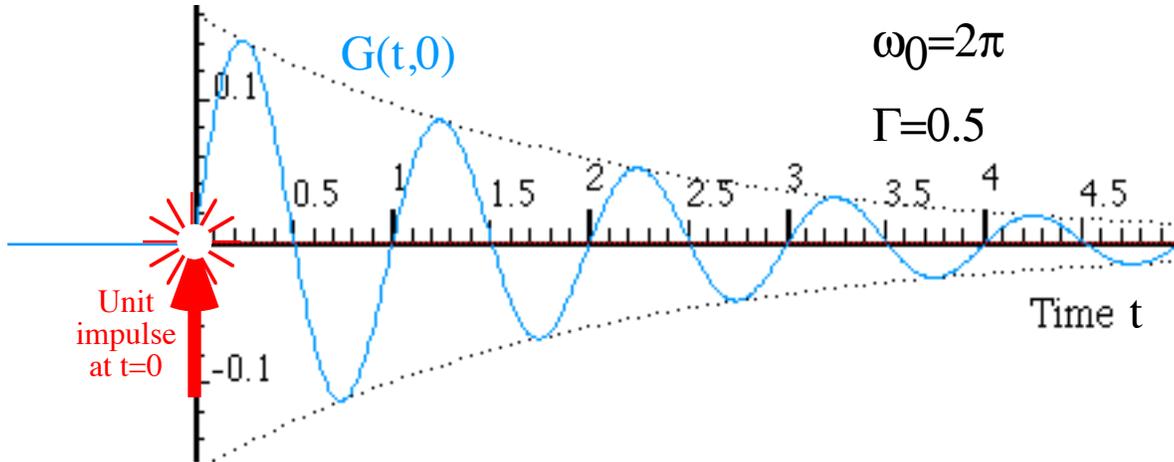
Fig. 2.7.14 Example of Green's time function G(t,0) .

Note that in Fig. 2.7.14 we have chosen the initial conditions of zero position and velocity before the unit impulse is delivered. This is not necessary. Any function $\phi(t)$ that satisfies the homogenous equation $D\cdot\phi(t) = 0$ can be added to *G(t,t'')* and it will still satisfy (2.7.26b).

The ω-representation of **G** is a diagonal matrix and (2.7.25b) yields the familiar *Green's frequency function G(ω)* first derived in (2.2.14).

$$\langle \omega|\mathbf{G}|\omega'\rangle = G(\omega)\delta(\omega-\omega') = \frac{\delta(\omega-\omega')}{\left(-\omega^2 - 2i\Gamma\omega + \omega_0^2\right)}$$

(2.7.28)

Finally, Green's solution (2.7.20) has the following two representations.

$$\langle t|q\rangle = \langle t|\mathbf{G}|a\rangle = \int dt'\langle t|\mathbf{G}|t'\rangle\langle t'|a\rangle$$
$$q(t) = \int dt' \, G(t,t')a(t')$$

(2.7.29a)

$$\langle \omega|q\rangle = \langle \omega|\mathbf{G}|a\rangle = \int d\omega'\langle \omega|\mathbf{G}|\omega'\rangle\langle \omega'|a\rangle$$
$$q(\omega) = G(\omega)a(\omega)$$

(2.7.29b)

Since **G** is not diagonal in the *t*-basis its transformation is an integral (sum) over *t'*. In the ω-basis **G** <u>is</u> diagonal so the transformation is reduced to a simple multiplication.

A change-of-basis transformation (See Appendix 3.B-6.) from the *t*-basis to the ω-basis gives the time Green's function in terms of the frequency Green's function.

$$G(t,t') \equiv \langle t|\mathbf{G}|t'\rangle = \int d\omega \int d\omega' \langle t|\omega\rangle\langle\omega|\mathbf{G}|\omega'\rangle\langle\omega'|t'\rangle$$

$$= \int d\omega \int d\omega' \frac{e^{-i\omega t}}{\sqrt{2\pi}} \langle\omega|\mathbf{G}|\omega'\rangle \frac{e^{i\omega' t'}}{\sqrt{2\pi}}$$

$$= \int d\omega \int d\omega' \frac{e^{-i(\omega t - \omega' t')}}{2\pi} G(\omega)\delta(\omega - \omega')$$

$$= \int d\omega \frac{e^{-i\omega(t-t')}}{2\pi} G(\omega)$$

This proves that the Green's time function is a function of only <u>one</u> time variable; the <u>difference</u> between stimulus time *t* and response time *t'*. This, with (2.7.29) is called the *convolution theorem*.

$$G(t,t') = G(t-t') = \frac{1}{2\pi}\int d\omega \, e^{-i\omega(t-t')} G(\omega) \tag{2.7.30}$$

G is still an operator even though it's behaving like a vector in this special case. However, its Fourier transform requires an extra √2π which a vector transform like (2.2.13) doesn't have.

A Green-Lorentz solution $|q\rangle = \mathbf{G}|a\rangle$ is not a unique solution to $\mathbf{D}|q\rangle = |a\rangle$ since any amount of a solution $|\phi\rangle$ to the homogenous equation $\mathbf{D}|\phi\rangle = \mathbf{0}$ can be added.

$$|\psi\rangle = |q\rangle + \alpha|\phi\rangle \quad \text{satisfies:} \ \mathbf{D}|\psi\rangle = |a\rangle \ , \ \text{if:} \ \mathbf{D}|q\rangle = |a\rangle \ , \ \text{and:} \ \mathbf{D}|\phi\rangle = \mathbf{0} \tag{2.7.31}$$

The $|\phi\rangle$ may be a transient which sets the intial conditions while the steady state Green's solution $|q\rangle$ responds only to the stimulus $|a\rangle$.

Exercises for Ch. 7 Fourier analysis

Chapter 2.8   Parametric Resonance

Here we consider a second and much more complex type of resonance; the so called *parametric resonance* in which the spring constant or inertial parameter of an oscillator is being stimulated as follows.

$$\ddot{x} + \left(\omega_0^2 + B\cos\left(\omega_s t\right)\right)x = 0 . \tag{2.8.1}$$

This is how quantum mechanical time evolution equations such as (2.4.1) are stimulated. Also, the quantum *Schrodinger wave equation* for a cosine potential has the same form

$$\frac{d^2\phi}{dx^2} + \left(E - V\cos(nx)\right)\phi = 0 \tag{2.8.2}$$

except a spatial independent variable x replaces time t. This kind of resonance is *nonlinear* and *multiplicative*, so if you double the amplitude B the solution may change in a very complicated way. Response is not simply proportional to stimulus as it is in linear resonance. Elementary Fourier and Green's function superposition techniques require linearity, too.

Let us consider a model in which both kinds of resonance can play a role. A simple pendulum with a oscillating support, such as is shown in Fig. 2.8.1, is such a model.
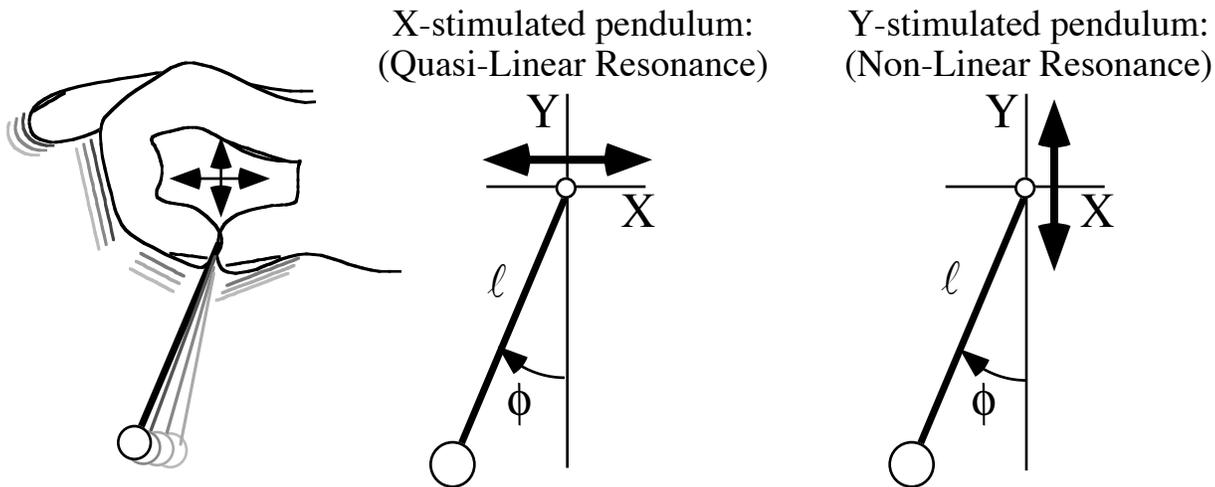
Fig. 2.8.1 Two cases for accelerated pendulum resonance .

The equations of motion can be derived quite easily by applying the *equivalence principle* to the accelerating frame which contains the pendulum support. According to this, it is only necessary to subtract the acceleration vector **a** of an oscillating frame from the usual vertical gravity acceleration vector **g** to obtain the effective gravity $\mathbf{g}^{eff}$ experienced by the pendulum.

$$\mathbf{g}^{eff} = \mathbf{g} - \mathbf{a}(t) = \begin{pmatrix} 0 \\ -g \end{pmatrix} - \begin{pmatrix} a_x(t) \\ a_y(t) \end{pmatrix} \tag{2.8.3a}$$

If the support is oscillating in the horizontal or x direction with angular frequency ω_x and in the vertical or y direction with angular frequency ω_x , then the acceleration vector is

$$\mathbf{a}(t) = \begin{pmatrix} a_x(t) \\ a_y(t) \end{pmatrix} = \begin{pmatrix} \ddot{X}^0 \\ \ddot{Y}^0 \end{pmatrix} = \begin{pmatrix} -\omega_x^2 A \cos(\omega_x t + \alpha) \\ -\omega_y^2 B \cos(\omega_y t + \beta) \end{pmatrix} \qquad (2.8.3b)$$

This gives the following effective gravity vector.

$$\mathbf{g}^{eff}(t) = \begin{pmatrix} g_x^{eff}(t) \\ g_y^{eff}(t) \end{pmatrix} = \begin{pmatrix} \omega_x^2 A \cos(\omega_x t + \alpha) \\ g + \omega_y^2 B \cos(\omega_y t + \beta) \end{pmatrix} \qquad (2.8.3b)$$

The general equation for the motion of a pendulum in such a $\mathbf{g}^{eff}$ field is the following.

$$\frac{d^2\phi}{dt^2} - \frac{g_x^{eff}}{\ell}\cos\phi + \frac{g_y^{eff}}{\ell}\sin\phi = 0 \qquad (2.8.4)$$

For small angles (*cos* $\phi\sim1$ and *sin* $\phi\sim\phi$) this reduces to

$$\frac{d^2\phi}{dt^2} + \frac{g_y^{eff}}{\ell}\phi = \frac{g_x^{eff}}{\ell} \qquad (2.8.5)$$

The two cases indicated in Fig. 2.8.1 are X-stimulation $\left(A \neq 0, \text{ and } B=0\right)$

$$\frac{d^2\phi}{dt^2} + \frac{g}{\ell}\phi = \frac{\omega_x^2 A}{\ell}\cos(\omega_x t + \alpha) \qquad (2.8.6)$$

and Y-stimulation $\left(A = 0, \text{ and } B \neq 0\right)$ (We take β=π here to get the same sign as (2.8.2).)

$$\frac{d^2\phi}{dt^2} + \left(\frac{g}{\ell} - \frac{\omega_y^2 B}{\ell}\cos(\omega_y t)\right)\phi = 0 \qquad (2.8.7)$$

An X-stimulated pendulum satisfies a linear resonance equation like (2.2.1) with no friction and acceleration stimulus of amplitude A_S acting on an oscillator of natural frequency $\omega_0 = \sqrt{g/\ell}$.

$$A_S = \frac{\omega_x^2 A}{\ell} \qquad (2.8.8a) \qquad\qquad\qquad \omega_0 = \sqrt{\frac{g}{\ell}} . \qquad (2.8.8b)$$

The Y-stimulated pendulum satisfies a Schrodinger's wave equation (2.8.2) if we relate the independent variables of time t for the pendulum to distance x for a Schrodinger wave by equating the arguments $\omega_y t$ of the cosine stimulus to nx of the Schrodinger cosine potential.

$$\omega_y t = nx, \quad \text{or:} \quad dt = \frac{n}{\omega_y}dx, \quad \text{and:} \quad dt^2 = \frac{n^2}{\omega_y^2}dx^2 . \qquad (2.8.9)$$

This converts the y-accelerated pendulum equation (2.8.7) to match a Schrodinger equation

$$\frac{d^2\phi}{dx^2} + \frac{n^2}{\omega_y^2}\left(\frac{g}{\ell} - \frac{\omega_y^2 B}{\ell}\cos(nx)\right)\phi = 0 = \frac{d^2\phi}{dx^2} + \left(\frac{n^2}{\omega_y^2}\frac{g}{\ell} - \frac{n^2 B}{\ell}\cos(nx)\right)\phi \qquad (2.8.10a)$$

where pendulum parameters g, ℓ, B, and ω_y match Shrodinger parameters E, V, and n through

$$E = \frac{n^2}{\omega_y^2}\frac{g}{\ell}, \qquad (2.8.10b) \qquad\qquad\qquad V = \frac{n^2 B}{\ell} . \qquad (2.8.10c)$$

The pendulum Y-stimulus frequency ω_y and amplitude B are as follows, where we set $g=1=\ell$.

$$\omega_y = n\sqrt{\frac{g}{E\ell}} = \frac{n}{\sqrt{E}} , \qquad (2.8.10d) \qquad\qquad\qquad\qquad B = \frac{V\ell}{n^2} = \frac{V}{n^2} \quad (2.8.10e)$$

The distinction between X-stimulated pendulum equation (2.8.6) and the Y-stimulated one (2.8.7) applies to the pendulum in Fig. 2.8.1 when it is near its lowest point (ϕ~0) where *cos ϕ~1* and *sin ϕ~ϕ* This distinction also applies when the pendulum is "up-side-down", that is, near its highest point *(ϕ~π)* where *cos ϕ ~ -1* and *sin ϕ ~ π−ϕ* . Then the equation is that of a hyperbolic (unstable) oscillator whose growth constant is oscillating. As we will see, oscillation can stabilize it

$$\frac{d^2\phi}{dt^2} - \left(\frac{g}{\ell} - \frac{\omega_y^2 B}{\ell}\cos(\omega_y t)\right)(\phi - \pi) = 0 , \quad \text{(where: } \phi \cong \pi) \qquad\qquad (2.8.10f)$$

As the pendulum moves away from either straight up or straight down, the two kinds of resonance get mixed up according to the general equation (2.8.5). In the trebuchet, the little ℓ-pendulum support moves in a big circle so it involves both kinds of acceleration to transfer energy from the big R-arm to the little throwing arm ℓ . So, the 10th century machine uses both kinds of resonance.

(a) Exploiting an analogy

The analogy between Schrodinger waves along a line *x* and pendulum vibrations versus time *t* is a powerful one because it makes one think critically and differently about either problem. Let us start with the simplest case when the Schrodinger potential *V* is zero and, by analogy, the pendulum Y-stimulus *B* is zero, too, according (2.8.10e). The two equations are eigen-equations

$$-\frac{d^2\phi}{dx^2} = E\phi \qquad\qquad (2.8.11a) \qquad\qquad\qquad\qquad -\frac{d^2\phi}{dt^2} = \omega_0^2\phi \qquad (2.8.11b)$$

The eigen-solutions are the familiar *Bohr orbitals* or, for the pendulum, the familiar phasor waves.

$$\langle x | M \rangle = \phi_M(x) = \frac{e^{\pm iMx}}{\sqrt{2\pi}}, \text{ where: } E = M^2 \quad (2.8.12a) \qquad \langle t | \omega \rangle = \phi_\omega(t) = \frac{e^{\pm i\omega_0 t}}{\sqrt{2\pi}}, \text{ where: } \omega_0 = \sqrt{\frac{g}{\ell}} \qquad (2.8.12b)$$

While it may not be an obvious step for the pendulum problem, the Bohr problem uses *periodic boundary conditions* by restricting *x* between *0* and *L* and demanding the wave solution and its first derivative are equal for the two end points. If we do the same for the pendulum we will be demanding that the time function repeat perfectly after a time *T*. This leads to *quantization conditions* for Bohr orbitals and restricts the allowed pendulum frequency to *harmonics* of a *fundamental frequency 2π/T*.

$$\phi(0) = \phi(L) \Rightarrow e^{iML} = 1, \text{ or: } M = \frac{2\pi m}{L} \qquad (2.8.13a) \qquad \phi(0) = \phi(T) \Rightarrow e^{i\omega_0 T} = 1, \text{ or: } \omega_0 = \frac{2\pi m}{T} \qquad (2.8.13b)$$

For Bohr orbitals the range limit *L* is 2π because *x* is a polar angle *x=θ* . To simplify notation we use this limit *L=2π=T* for both analogies. Then the allowed energies and frequencies are

$$E = m^2 = 0,1,4,9,16... \qquad (2.8.14a) \qquad \omega_0 = m = 0,\pm1,\pm2,\pm3,\pm4,... \qquad (2.8.14b)$$

The solution to the Schrodinger equation with non-zero V can be done using Fourier series. The equation (2.8.2) and its abstract form are

$$-\frac{d^2\phi}{dx^2} + V\cos(nx)\phi = E\phi , \qquad (\mathbf{D} + \mathbf{V})|\phi\rangle = E|\phi\rangle$$

It's Fourier representation is

$$\Sigma \langle j|(\mathbf{D}+\mathbf{V})|k\rangle\langle k|\phi\rangle = E\langle j|\phi\rangle \tag{2.8.15a}$$

where Fourier matrices are

$$\langle j|\mathbf{D}|k\rangle = j^2\delta_j^k, \tag{2.8.15b}$$

and, using (2.6.5c)

$$\langle j|\mathbf{V}|k\rangle = \int_0^{2\pi} dx \frac{e^{-ijx}}{\sqrt{2\pi}} V\cos(nx)\frac{e^{-ikx}}{\sqrt{2\pi}} = \int_0^{2\pi} dx \frac{e^{-i(j-k)x}}{2\pi} V\frac{e^{-inx}+e^{inx}}{2}$$

$$= \frac{V}{2}\left(\delta_j^{k+n}+\delta_j^{k-n}\right) \tag{2.8.15c}$$

(b) (n=2) Double-well potential and two-swing repeat

For example, consider a cosine potential $V\cos(2x)$ which has $n=2$ periods in the interval $L=2\pi$. Then the matrices by (2.8.15 b-c) break into two types;

$\langle j|(\mathbf{D}+\mathbf{V})|k\rangle =$ (for j and k even) $\langle j|(\mathbf{D}+\mathbf{V})|k\rangle =$ (for j and k odd)

$\cdots \; |-6\rangle,|-4\rangle,|-2\rangle, |0\rangle, |2\rangle, |4\rangle, |6\rangle,\cdots$ $\cdots \; |-7\rangle,|-5\rangle,|-3\rangle,|-1\rangle, |1\rangle, |3\rangle, |5\rangle,\cdots$

$$\begin{pmatrix} \ddots & & & & & & \\ & 6^2 & v & & & & \\ & v & 4^2 & v & & & \\ & & v & 2^2 & v & & \\ & & & v & 0 & v & \\ & & & & v & 2^2 & v \\ & & & & & v & 4^2 & v \\ & & & & & & v & 6^2 \\ & & & & & & & & \ddots \end{pmatrix}, \quad \begin{pmatrix} \ddots & & & & & & \\ & 7^2 & v & & & & \\ & v & 5^2 & v & & & \\ & & v & 3^2 & v & & \\ & & & v & 1^2 & v & \\ & & & & v & 1^2 & v \\ & & & & & v & 3^2 & v \\ & & & & & & v & 5^2 \\ & & & & & & & & \ddots \end{pmatrix}$$

where the off-diagonal matrix elements are by (2.8.10c):

$$v = \frac{V}{2} = \frac{2^2 B}{2\ell} = \frac{2B}{\ell} \tag{2.8.16}$$

The matrices go on forever in each direction. However, the lower eigenvalues E_j may be found by truncating them to 2-by-2 , or 3-by-3, ...or the 7-by-7 matrices shown in (2.8.16) if $v=V/2$ is small compared to the difference $j^2 - (j\pm 2)^2$ between the diagonal j^2 values. For example, if $v<<|3^2 - 1^2|$ then the following matrix approximates $E_{1\pm}$ near 1^2, that is, the lowest odd-k eigenvalues.

$$\begin{pmatrix} 1^2 & v \\ v & 1^2 \end{pmatrix} \tag{2.8.17a}$$

$$E_{1-} \sim 1^2 - v, \qquad\qquad E_{1+} \sim 1^2 + v. \tag{2.8.17b}$$

The closest even-k eigenvalues are obtained approximately from the eigenvalues of

$$\begin{pmatrix} 2^2 & v & 0 \\ v & 0 & v \\ 0 & v & 2^2 \end{pmatrix} \tag{2.8.18a}$$

$$E_0 \sim 0 - 2v^2/2^2+. , \qquad E_{2+} \sim 2^2 + 2v^2/2^2+.. , \qquad E_{2-} \sim 2^2 -.. \tag{2.8.18b}$$

as long as $v<<|4^2-2^2|$ allows neglect of the 4^2 rows. Approximate eigenvalues can be found by perturbation theory or continued fraction expansions, but direct numerical calculation is preferred if v is given. Then one takes as large a matrix (2.8.16) as needed to get a desired accuracy.

For example, the eigenvalues for *V=0.2* or *v=0.1* and *V=2.0* or *v=1.0* are listed below.

$V=0.2$ or $v=0.1$ $V=2.0$ or $v=1.0$

$E_0 =$	−0.0050
$E_{1-} =$	0.8988
$E_{1+} =$	1.0987
$E_{2-} =$	3.9992
$E_{2+} =$	4.0042
$E_{3-} =$	9.0006
$E_{3+} =$	9.0006

(2.8.19a)

$E_0 =$	−0.4551
$E_{1-} =$	−0.1102
$E_{1+} =$	1.8591
$E_{2-} =$	3.9170
$E_{2+} =$	4.3713
$E_{3-} =$	9.0477
$E_{3+} =$	9.0784

(2.8.19b)

Fig. 2.8.2 is a plot of some E_m-values versus the perturbation amplitude V or wiggle amplitude B.

$$B = V/n^2 = 2v/n^2 \qquad (2.8.20a)$$

Plugging each E_m-value into (2.8.10d-e) gives a corresponding Y-pendulum frequency $\omega_{y(m)}$.

$$\omega_{y(m)} = n/\sqrt{E} = 2/\sqrt{E_m} \qquad (2.8.20b)$$

(*V= 0.2 or B=0.05 and n=2*)   (*V= 2.0 or B=0.5 and n=2*)

$\omega_{y(0)} = 2/\sqrt{.0050}$	$= 28.2843$
$\omega_{y(1^-)} = 2/\sqrt{.8988}$	$= 2.10959$
$\omega_{y(1^+)} = 2/\sqrt{1.0987}$	$= 1.90805$
$\omega_{y(2^-)} = 2/\sqrt{3.9992}$	$= 1.00010$
$\omega_{y(2^+)} = 2/\sqrt{4.0042}$	$= 0.99948$

(2.8.20c)

$\omega_{y(0)} = 2/\sqrt{.4551}$	$= 2.9646$
$\omega_{y(1^-)} = 2/\sqrt{.1102}$	$= 6.02475$
$\omega_{y(1^+)} = 2/\sqrt{1.8591}$	$= 1.4668$
$\omega_{y(2^-)} = 2/\sqrt{3.9170}$	$= 1.0105$
$\omega_{y(2^+)} = 2/\sqrt{4.3713}$	$= 0.9566$

(2.8.20d)

The low amplitude oscillation (B *=0.05 or V=0.2)* has only one negative E_m-value while the high amplitude case (B *=0.5 or V=2.0)* has two negative E_m-values. According to (2.8.10f) negative E corresponds to "up-side-down" or unstable motion. Surprisingly, it is stabilized for certain ω_y.
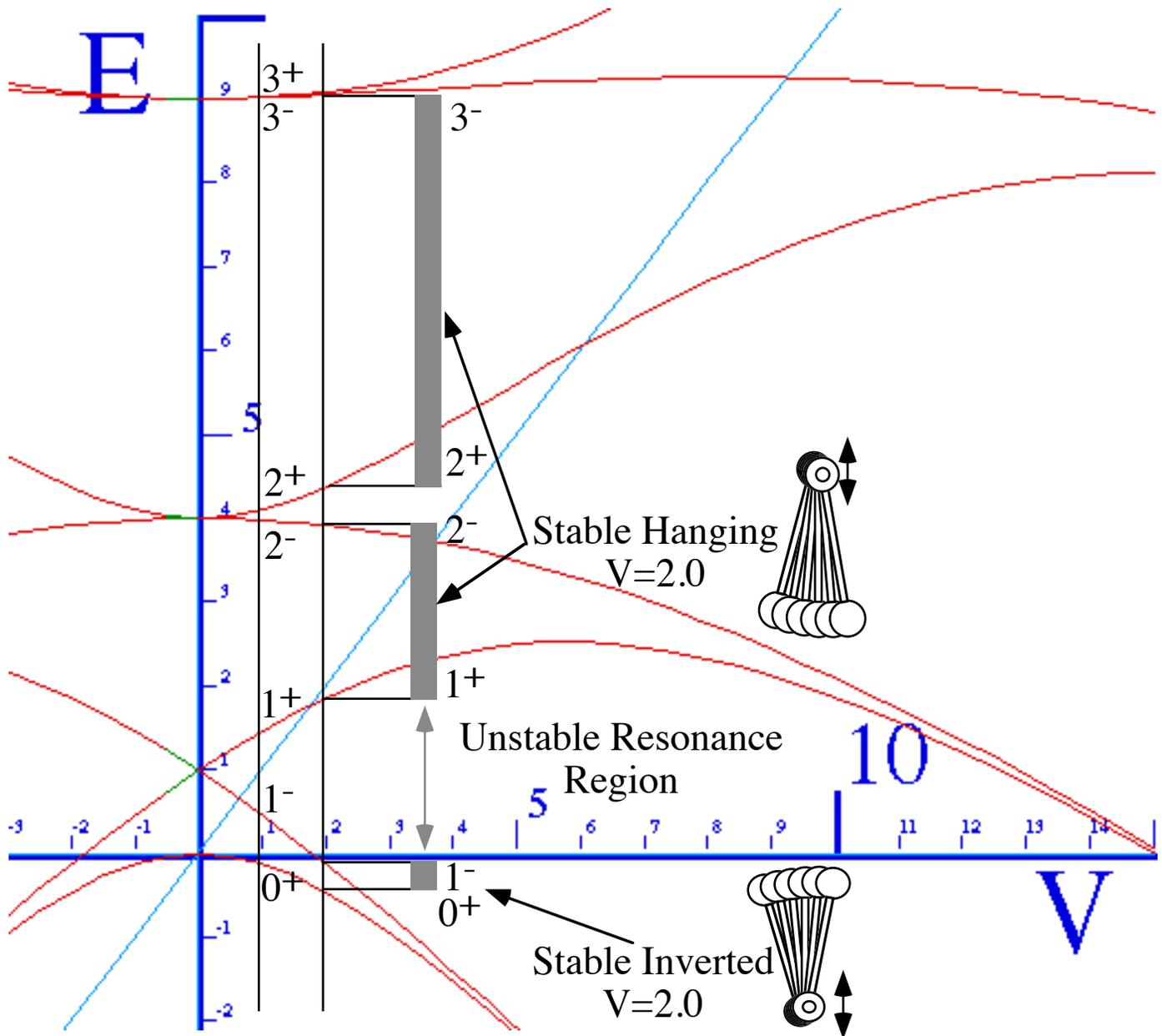
Fig. 2.8.2 E-Values versus perturbation amplitude V . Gray stability regions shown for V=2.0 .

        The lowest region of stability lies between the O$^+$ and 1$^-$ E-values. For perturbation amplitude V greater than V=1.8 these two E-values lie in the negative-E region and both motions correspond to inverted stability. Not until V becomes greater than 15 does another inverted stability region appear as the 1$^+$ and 2$^-$ E-values go negative. (See extreme right hand side of Fig. 2.8.2.)

The O$^+$ and 1$^-$ E-value motions (Y-stimulus frequency $\omega_{y(0+)}$ =2.9696 and $\omega_{y(1-)}$ =6.02475 from (2.8.20d).) are displayed in Fig. 2.8.3 a-b. Labels 1$^-$ (or O$^+$) signify that the pendulum crosses ϕ=0 exactly one (zero) time(s), respectively. The ±sign - (or +, respectively) refers to odd (or even) *parity* of $\phi(\tau)$ around a V-"hump" where the pendulum is feeling the *least* force.

(a)

O⁺ Mode

$B=0.5$

$\omega_y(0^+)=2.9646$

$\sin\phi(t)$

Y-perturbation
$V(t)=-B\omega_y^2\cos(\omega_y t)$

(b)

1⁻ Mode

$B=0.5$

$\omega_y(1^-)=6.02475$

$\sin\phi(t)$

Y-perturbation
$V(t)=-B\omega_y^2\cos(\omega_y t)$
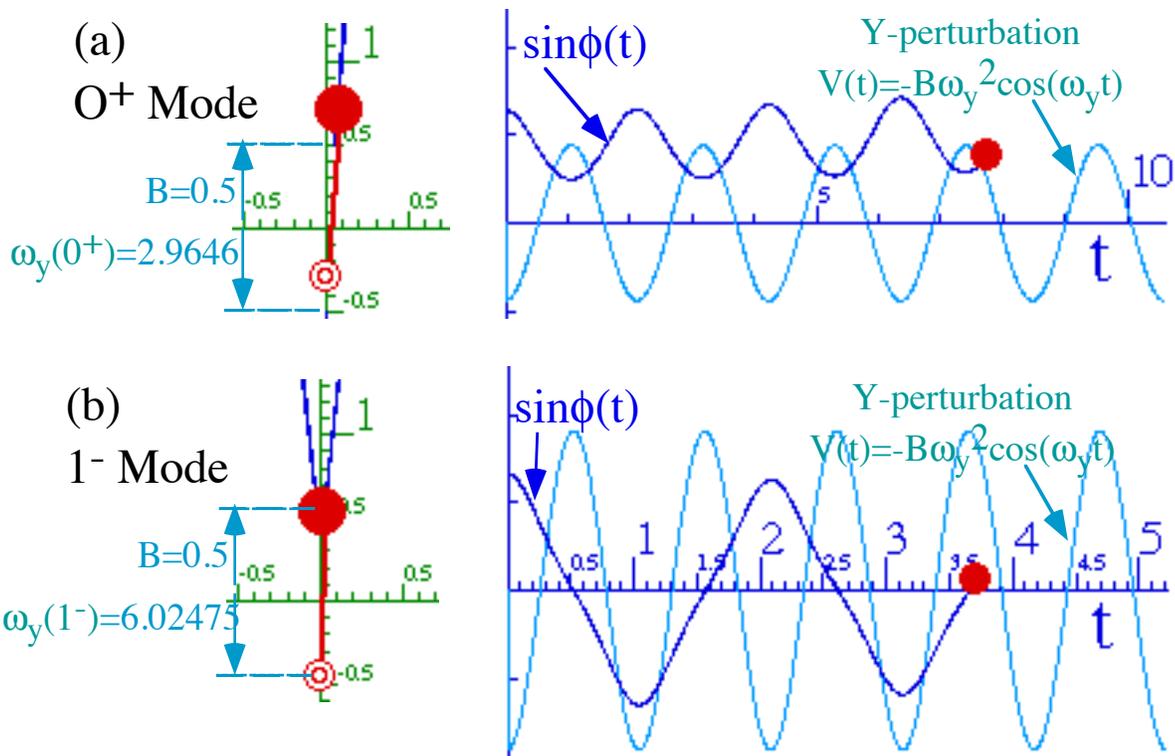
Fig. 2.8.3 Inverted Modes (a) Symmetric (one sided) 0⁺ mode, (b) Anti-symmetric 1⁻ mode .

The next two stable modes are the 1⁺ and 2⁻ *E*-modes shown in Fig. 2.8.4.

(a)

$B=0.5$

$\omega_y(1^+)=1.4668$

1⁺ Mode

$\sin\phi(t)$

Y-perturbation
$V(t)=-B\omega_y^2\cos(\omega_y t)$

(b)

$B=0.5$

$\omega_y(2^-)=1.01054$

2⁻ Mode

$\sin\phi(t)$

Y-perturbation
$V(t)=-B\omega_y^2\cos(\omega_y t)$
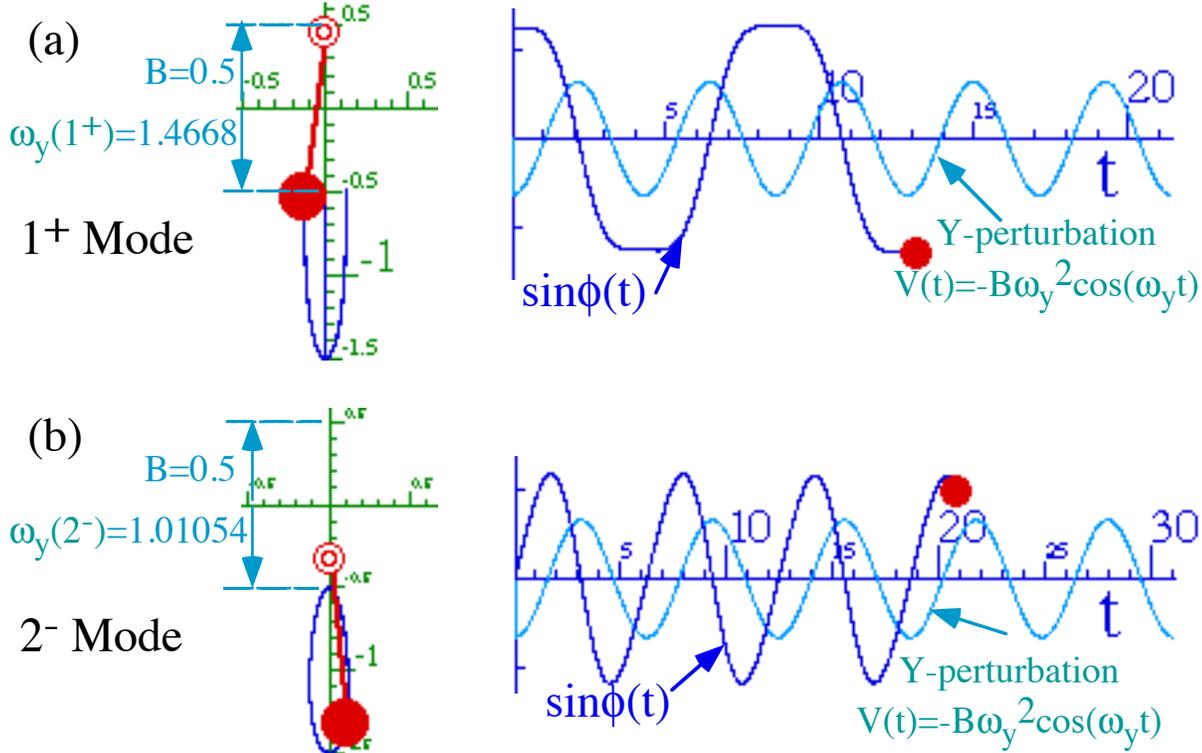
Fig. 2.8.4 Hanging Modes (a) Symmetric 1⁺ mode, (b) Anti-symmetric 2⁻ mode .
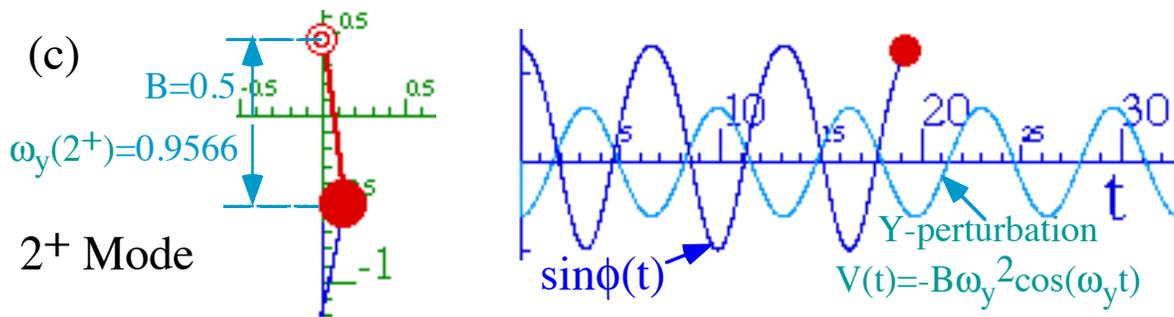
Fig. 2.8.5 symmetric 2^+ mode .

The 2^+ mode in Fig. 2.8.5 is very similar to the 2^- mode in the preceding Fig. 2.8.4(b). The latter 2^- wave is shifted relative to the stimulus by $\pi/2$, and therefore anti-symmetric with respect to the V-"humps." The 2^+ wave is symmetric laterally, but its vertical rise exceeds its vertical drop because the effective gravity is minimum when the pivot is at its high point ("top of roller-coaster effect") and maximum at its low point. (The Y-perturbation plot is effective gravity.)

This same "roller-coaster" makes the 2^- wave derivative steeper during the low (high-gravity) point than the high point. This effect is most pronounced in the 1^+ wave of Fig. 2.8.3b where the effective gravity is almost zero at the top so the wave becomes a horizontal straight line. This mode is very near the $E=V$ line in Fig. 2.8.2 , or by (2.8.10b-c), the $\omega_y^2 B=g$ line.

Most initial conditions lead to <u>in</u>stability for any of the frequency values in between those of 1- and 1+ modes, as in the example below. Now the pendulum thinks it's a trebuchet arm!
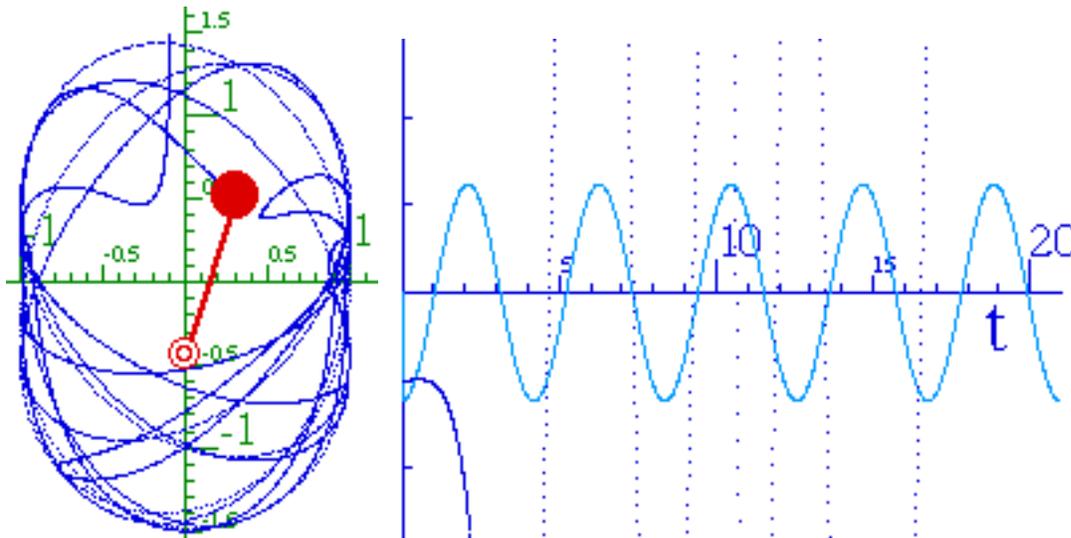

Fig. 2.8.6 Unstable Modes for frequency $\omega_y =1.5$.

Unstable resonance is virtually all that is possible for ω_y values between those of 1- and 1+ modes ($1.4668< \omega_y < 2.9647$) and above the 1- modes ($6.0248< \omega_y < \infty$). For amplitudes V less than ~1.8 there is a lower but no upper limit to the frequency which stabilizes an inverted pendulum.

For perturbations with greater amplitude the frequencies are generally smaller.Consider an ampplitude of $V=5.0$ or $B=1.25$.

$V=5.0$ or $v=2.5$		$(V=5.0$ or $B=2.5$ and $n=2)$		

$E_0 =$	-2.15308
$E_{1-} =$	-2.07633
$E_{1+} =$	2.49593
$E_{2-} =$	3.49247
$E_{2+} =$	5.61304
$E_{3-} =$	9.18571
$E_{3+} =$	9.61215

$\omega_{y(0)} = 2/\sqrt{2.15308}$	$=1.363013$
$\omega_{y(1^-)} = 2/\sqrt{2.07633}$	$=1.387975$
$\omega_{y(1^+)} = 2/\sqrt{2.49593}$	$=1.265942$
$\omega_{y(2^-)} = 2/\sqrt{3.49247}$	$=1.070196$
$\omega_{y(2^+)} = 2/\sqrt{5.61304}$	$=0.844172$

Now the difference between $sin\,\phi$ and ϕ is super critical. If they are not nearly the same magnitude the solution for the inverted cases may blow up as shown in Fig. 2.8.7a. Now the pendulum needs to "hug" the vertical axis during the period of high downward gravity (roller coaster at bottom) and only wander away from the axis a little when the effective gravity is pointing up. (Now the roller coaster is so fast that it feels several g's pulling up at the top.)
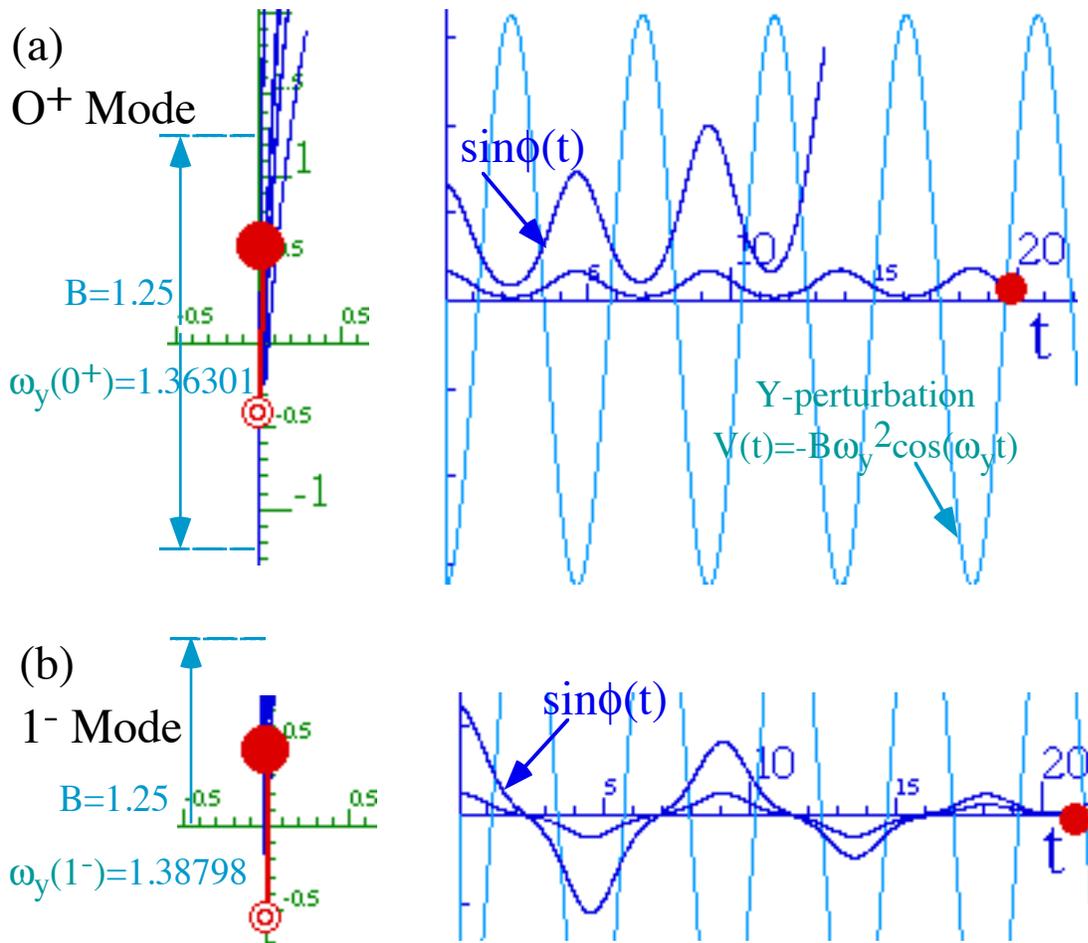

Fig. 2.8.7 Higher amplitude modes with inversion stability

For comparison with Figs. 2.8.4-5 the higher amplitude hanging modes are shown in Fig. 2.8.8 below. All are quite stable

(a) B=1.25 $\omega_y(1^+)=1.2659$

1^+ Mode

$\sin\phi(t)$

(b) B=1.25 $\omega_y(2^-)=1.0702$

2^- Mode

$\sin\phi(t)$

(c) B=1.25 $\omega_y(2^+)=0.8442$

2^+ Mode

$\sin\phi(t)$
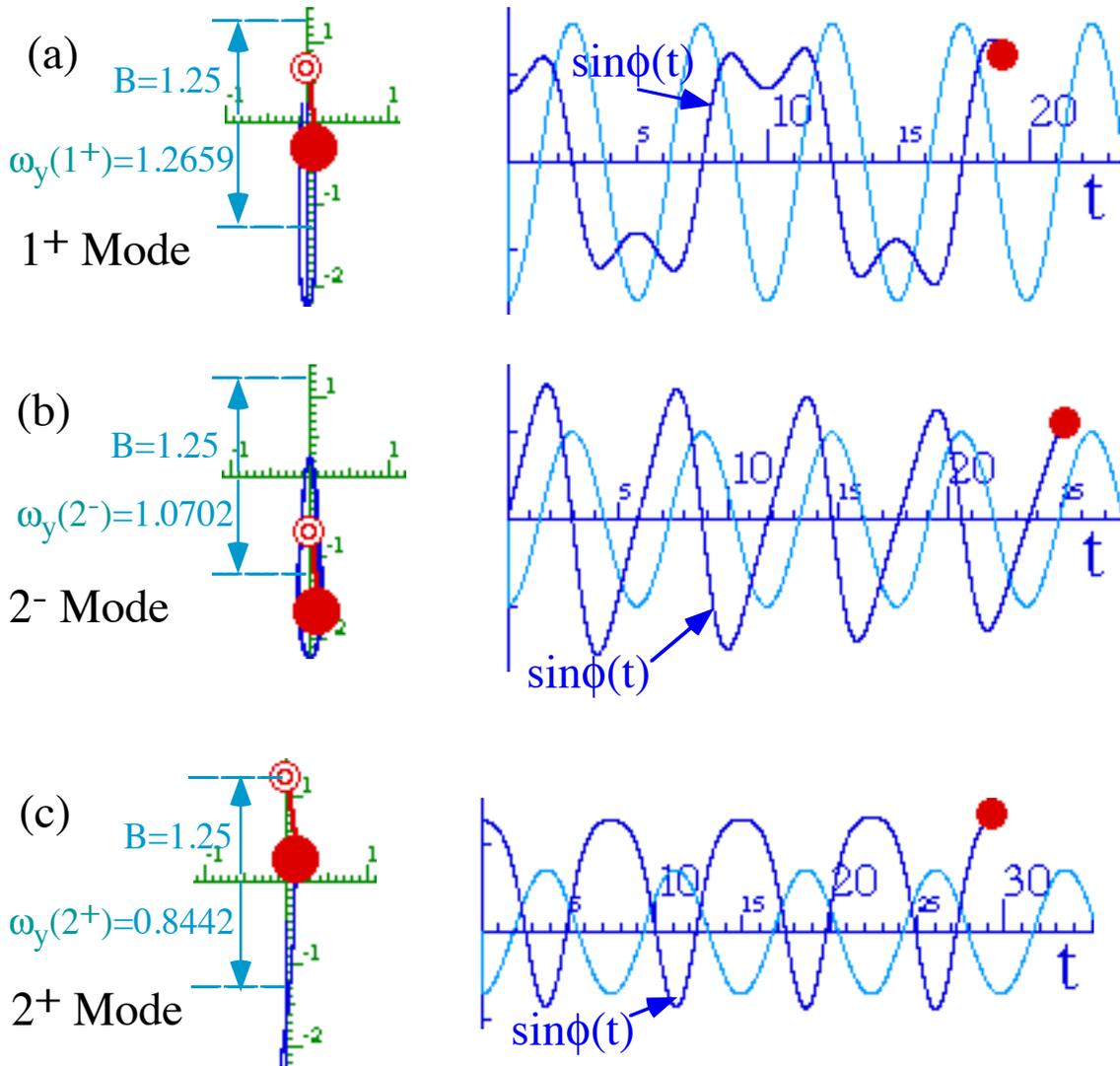
Fig. 2.8.8 Higher amplitude modes with hanging stability

The bands of *E*-values, such as the gray lines in Fig. 2.8.2, are all allowed and stable modes, too. Howver, only the values on the edges repeat after exactly n=2 periods of the stimulus. By picking a random value inside one of the gray regions, you will get a wave that tries to repeat after some random number, say 2.81 periods, or 3.11 periods, which means it won't really repeat at all. However, we can calculate how to make it repeat after any integral number n=2, 3, 4, ... of periods. This is left as a problem.

It is also possible to calculate all these modes for a non-sinusoidal periodic acceleration for which we know the Fourier series. (Another problem!)

Exercises for Ch. 8 Parametric resonance

Unit 2 Review Topics and Formulas

C_2	**1**	σ_B
1	**1**	σ_B
σ_B	σ_B	**1**

$$\begin{pmatrix} \langle 1|\mathbf{1}|1\rangle & \langle 1|\mathbf{1}|2\rangle \\ \langle 2|\mathbf{1}|1\rangle & \langle 2|\mathbf{1}|2\rangle \end{pmatrix} = \begin{pmatrix} 1 & 0 \\ 0 & 1 \end{pmatrix}, \quad \begin{pmatrix} \langle 1|\sigma_B|1\rangle & \langle 1|\sigma_B|2\rangle \\ \langle 2|\sigma_B|1\rangle & \langle 2|\sigma_B|2\rangle \end{pmatrix} = \begin{pmatrix} 0 & 1 \\ 1 & 0 \end{pmatrix}$$